A NEW PARADIGM FOR THE PERSONALIZED DELIVERY OF IODINATED CONTRAST MATERIAL AT CARDIOTHORACIC COMPUTED TOMOGRAPHY ANGIOGRAPHY

by

John F Kalafut

BSEE, University of Scranton, 1996

BS Physics, University of Scranton, 1997

MSEE, University of Pittsburgh, 2001

Submitted to the Graduate Faculty of

Swanson School of Engineering in partial fulfillment

of the requirements for the degree of

Doctor of Philosophy

University of Pittsburgh

2010

UNIVERSITY OF PITTSBURGH

SWANSON SCHOOL OF ENGINEERING

This dissertation was presented

by

John Francis Kalafut

It was defended on

June 25, 2010

and approved by

J.R. Boston, PhD, Professor Electrical and Computer Engineering Department

C.C. Li, PhD, Professor, Electrical and Computer Engineering Department

Z.H Mao, PhD, Assistant Professor, Electrical and Computer Engineering Department

M. Sun, PhD, Professor, Bioengineering and Electrical Engineering Department

K.T. Bae, MD PhD, Chair Radiology and Professor Bioengineering Departments

Dissertation Director: JR Boston, PhD, Professor, Electrical and Computer Engineering Department

A NEW PARADIGM FOR THE DELIVERY OF IODINATED CONTRAST MATERIAL AT CARDIOTHORACIC, COMPUTED TOMOGRAPHY ANGIOGRAPHY

John F Kalafut, PhD

University of Pittsburgh, 2010

In North America more than 40 million doses of iodinated X-Ray contrast medium are delivered to patients undergoing CT imaging every year. This particular pharmaceutical is necessary to enable Computed Tomography of soft tissue, tumors, and vasculature. Very few of the contrast enhanced procedures are performed with the dose of the drug tailored to the individual patient or procedure and nearly every patient receives the same dose of contrast material. This dissertation presents a methodology to allow the routine administration of a personalized dose of contrast material to generate contrast enhancement sufficient for diagnosis during cardiothoracic CT Angiography imaging. Parameter estimation of a patient specific model is performed using Maximum Likelihood Estimation (MLE) with data generated from the scanner during a pre-diagnostic "test" injection of contrast agent. A non-parametric system identification technique, using the truncated Singular Value Decomposition, is also developed for deriving a patient specific prediction of contrast enhancement. The MLE technique produces contrast enhancement predictions with less error than the tSVD method. It is also shown that the MLE method is less sensitive to data length and has greater noise immunity. A novel, patient-specific contrast protocol generation algorithm is also presented. It is based upon a constrained minimization (Sequential Quadratic Programming) that enforces constraints on the input parameters while minimizing the volume of contrast sufficient to achieve a prospectively chosen enhancement

target. A physiologically based pharmacokinetic (PBPK) numeric model is developed and used to validate the contrast prediction and protocol generation techniques. Finally, a novel, instrumented, flow phantom is developed and used to validate the identification and protocol generation techniques.

TABLE OF CONTENTS

PREFACE ..... **XVII**

1.0 INTRODUCTION **1**

2.0 BACKGROUND AND LITERATURE REVIEW **6**

2.1 X-RAY CONTRAST MEDIUM **6**

2.2 CONTRAST ENHANCED CT IMAGING **8**

2.2.1 Detailed Description of CTA Data Acquisition and Image Sets **11**

2.3 PHARMACOKINETIC DRUG MODELLING **17**

2.3.1 Physiologically Based Pharmacokinetic Modeling **19**

2.4 COMPUTER CONTROLLED INFUSION **21**

2.5 BAE'S PBPK MODEL OF CONTRAST MEDIA PROPOGATION **23**

2.6 BAE REDUCED ORDER PHARMACOKINETIC MODEL **27**

2.7 WADA AND WARD PBPK MODEL OF ALFENTANIL **30**

2.8 FLEISCHMANN AND HITTMAIR PATIENT SPECIFIC CONTRAST PROTOCOL COMPUTATION **33**

2.8.1 Fleischmann et al Clinical Results **36**

2.9 RELEVANT WORK BY THE AUTHOR **37**

2.10 CARDIAC OUTPUT ESTIMATION USING CT CONTRAST **39**

2.11 TRUNCATED SINGULAR VALUE DECOMPOSITION **41**

3.0 SPECIFIC AIMS OF THE RESEARCH 47

4.0 A NEW PATIENT SPECIFIC PHARMACOKINTEC MODEL 51

4.1 DESCRIPTION OF THE MODEL 51

4.1.1 Model Structure 53

4.1.1.1 Peripheral subsystem 55

4.1.1.2 Right Heart Subsystem 58

4.1.1.3 Lung Subsystem 58

4.1.1.4 Left Heart Subsystem 59

4.1.1.5 Body Subsystem 59

4.1.1.6 State Space Formulation 60

4.1.2 Parameter Selection 64

4.1.2.1 Cardiac Output and Central Blood Volume Estimators 64

4.1.2.2 Regional Blood Volume Estimates 66

4.2 SIMULATION METHODS AND RESULTS 68

4.2.1 Simulation results from the hybrid model 68

4.2.2 Comparison of results between the hybrid model and published Bae Data 73

4.3COMPARISON RESULTS TO BAE'S MODEL USING CLINICAL DATA 75

4.3.1 Clinical Data and Methods 76

4.3.2 Data Acquisition Methods 79

4.3.3 Simulations 80

4.3.4 Results 81

4.4 DISCUSSION 87

5.0 DATA DRIVEN CONTRAST MODEL IDENTIFICATION 89

5.1 PARAMETRIC (MODEL BASED) IDENTIFICATION 89

5.1.1 Model Based Methodological Background 90

5.1.2 Model Structure 93

5.1.3 Maximum Likelihood Estimator 101

5.1.3.1 Numerical Optimization Details 105

5.1.4 Parametric Estimator Evaluation Methods 107

5.1.4.1 Model-to-model Comparisons 109

5.1.4.2 Estimator Performance Using Hybrid Model Data 110

5.1.4.3 Estimator Performance Using Retrospective Data 112

5.1.5 Results 113

5.1.5.1 Estimator Performance using model to model comparisons 113

5.1.5.2 Hybrid Model Parameter Estimation Results 119

5.1.5.3 Maximum Likelihood Estimation Results with Clinical Data 125

5.2 NON-PARAMETRIC IDENTIFCATION 129

5.2.1 Truncated Singular Value Decomposition Methodology 130

5.2.2 Evaluation Methods 136

5.2.2.1 Hybrid Model Simulation Experiments 136

5.2.2.2 Clinical Data Experiments 137

5.2.3 Numerical Simulation Results 137

5.2.4 Clinical data results 141

5.3 DISCUSSION 144

6.0 PATIENT SPECIFIC CONTRAST PROTOCOL GENERATION 149

6.1 PROTCOL GENERATION ALGORITHM 149

6.1.1 Cost Function Formulation 153

6.1.1.1 Visualization of the cost function 156

6.1.2 Protocol Generation Algorithm 159

6.2 NUMERICAL EXPERIMENTS AND RESULTS 162

6.2.1 Comparison to Fleischmann and Hittmair 164

6.2.2 Hybrid PBPK Model Simulations and Results 170

6.3 DISCUSSION 176

7.0 CARDIOVASCULAR FLOW PHANTOM 178

7.1 BACKGROUND 178

7.2 PHANTOM TOPOLOGY/STRUCTURE 180

7.3 EXPERIMENTAL METHODS 185

7.3.1 Phantom Linearity Validation 185

7.3.2 Demonstration of equivalence between CT and nIR Injections 186

7.3.3 Contrast Enhancement Model Prediction Validation 188

7.3.4 Patient Specific Contrast Protocol Creation Validation 189

7.4 RESULTS 190

7.5 DISCUSSION 198

8.0 CONCLUSION 200

8.1 PROPOSED CLINICAL VALIDATION 202

8.2 ADDITIONAL APPLICATIONS 204

9.0 SPECIFIC CONTRIBUTIONS BY THE AUTHOR 206

APPENDIX A 208

APPENDIX B 210

APPENDIX C **214**

APPENDIX D **218**

APPENDIX E **222**

BIBLIOGRAPHY **226**

LIST OF TABLES

Table 1 Regional blood volume parameters used in the novel model simulation..... 66

Table 2 Transit delay parameters 67

Table 3 Summary demographic data Mean data are presented with standard deviations..... 77

Table 4 Relevant scan parameters from the clinical data set, first 20 subjects. 78

Table 5 Summary contrast protocol statistics from the clinical data set, first 20 subjects. 79

Table 6 Summary results of models compared against clinical data 85

Table 7 Upper and lower boundaries or constraints on the estimated parameters..... 106

Table 8 Parameter values used in the model-to-model simulations and comparisons..... 109

Table 9 Summary of parameter bias for θ_{He2D}. 115

Table 10 Summary of parameter bias for θ_{He1D}. 115

Table 11 Summary of parameter estimation variance for He2D 116

Table 12 Summary of parameter estimation variance for the He1D system 116

Table 13 Summary results comparing the MLE and hybrid model results from Chapter 4 127

Table 14 Non-parametric estimation algorithm 133

Table 15 Simulation analysis results from determining the tSVD truncation index..... 136

Table 16 Protocol Generation Algorithm..... 161

Table 17 Summary results from protocol generation experiments. 176

Table 18 Phantom settings during the protocol generation validation experiments – set 1..... 190

Table 19 Results from the experiments in set 1. 195

Table 20 General algorithm for predicting enhancement using MLE 209

LIST OF FIGURES

Figure 1 Example thoracic CTA data set. 2

Figure 2 Pictorial demonstrating the temporal relationships among scanner, injection system . .. 4

Figure 3 Example of a typical, CT enhancement curve 10

Figure 4 Detailed schematic of a contrast enhanced CTA imaging procedure..... 13

Figure 5 Example CTA data set 16

Figure 6 A 2-compartment PK model with Central and Peripheral compartments. 17

Figure 7 Example of a PBPK model structure, adapted from [25]. 21

Figure 8 Bae's representation of a blood vessel. 24

Figure 9 Bae's model of the diffusion of contrast medium in organs. 25

Figure 10 Bae et al.'s simplified circulatory model. 28

Figure 11 Topology of the Wada and Ward PK model. 31

Figure 12 Example Picard plot using clinical data. 45

Figure 13 Example "L-curve" constructed with a clinical data set. 46

Figure 14 Model structure of the new PK model 53

Figure 15 All-integrator view of the physiologic based pharmacokinetic model 63

Figure 16: Simulated contrast enhancements for a normal subject. 69

Figure 17 Simulated peak aortic enhancements and times to peak aortic enhancement 71

Figure 18 Simulation results demonstrating the ability to simulate the effect of saline 72

Figure 19 Comparison of data reported by Bae et al. to the new model output. 75

Figure 20 Subject 1's contrast enhancement profile extracted from the descending aorta. 80

Figure 21 Subject 11clinical data and predictions from models 82

Figure 22 Model predictions compared to clinical data for subject 6 and subject 8. 84

Figure 23 Box-and-whisker plots of the summary results 86

Figure 24 Scatter plots of the simulation tests 87

Figure 25 An axial CT image acquired from a test bolus scan procedure. 91

Figure 26 Time enhancement curve generated from a patient 92

Figure 27 Reduced hybrid model structure used for parameter estimation 94

Figure 28 Reformulated right heart and peripheral compartments (He1) model structure 95

Figure 29 Reformulated left heart and lung compartment (He2) model structure 98

Figure 30 Block diagram of the discrete model 101

Figure 31 Contour plots of the J_{LH} cost-function for parameter pairs for the He2D subsystem.118

Figure 32 Contour plots showing projection of the J_{RH} cost function 119

Figure 33 Hybrid model simulation for a diagnostic injection. 120

Figure 34 Results from the hybrid model simulation set using MLE 121

Figure 35 Simulation results using the MLE methodology from hybrid model data. 122

Figure 36 Results demonstrating the impact of reduced length test bolus and noise 124

Figure 37 Performance metrics of the MLE methodology using the clinical data set. 126

Figure 38 MLE prediction results using clinical data for (a) subject 6 and (b) subject 8. 128

Figure 39 Box-and-whisker plots for predicted enhancements using the hybrid model 129

Figure 40 Solution for the impulse response, h_{sys}, using subject 7 data and least squares 131

Figure 41 Estimated impulse response for subject 7 data using the tSVD method 132

Figure 42 Performance metrics for the tSVD estimating left-heart enhancement 138

Figure 43 Hybrid model simulation results comparing the performance of MLE and tSVD ... 139

Figure 44 Simulation results for test bolus length of 35 seconds with varying AWGN 140

Figure 45 Results from the two estimation methodologies using the clinical data set 142

Figure 46 Box and whisker plots comparing the two estimation techniques 143

Figure 47 Test bolus for Subject 15 in the clinical data set. 146

Figure 48 Depiction of the desired outcome from individualized protocol generation. 152

Figure 49 3D surface plots of the proposed cost function 157

Figure 50 2D Contour plots of cost function for subject 6 simulated data 158

Figure 51 Sample test bolus response measured in the descending aorta as presented in [9] ... 164

Figure 52 Computed injection protocols using the Fourier deconvolution method from [9].... 167

Figure 53 Predicted and desired enhancement levels generated with the injection protocols . 168

Figure 54 Comparative result between desired enhancement and the predicted enhancement 169

Figure 55 Illustration of protocol generation validation experiments..... 172

Figure 56 Hybrid model simulation result using Subject 8 data and generated protocol 173

Figure 57 Enhancement values greater than the 350 HU target 174

Figure 58 Enhancement values greater than the 250 HU target 175

Figure 59 Picture of the cardiovascular phantom system 181

Figure 60 CT cross section of the phantom showing the anatomical regions of interest. 182

Figure 61 Topology of the cardiovascular phantom. 183

Figure 62 Plot displaying additive linearity response of phantom 191

Figure 63 Plot of the mean (solid line) and curves from three separate injections of nIR 192

Figure 64 Plot of mean response from three injections of nIR dye to CT results 193

Figure 65 Results of phantom experiments using tSVD method toenhancement. 194

Figure 66 Predicted and measured TECs for experiments 1-3 196

Figure 67 Predicted and measured TECs for experiments 4-6. 197

Figure 68 Hybrid model outputs and Bae model outputs for subjects one through nine. 211

Figure 69 Hybrid model outputs and Bae model outputs subjects 10 through 18. 212

Figure 70 Hybrid model outputs and Bae model outputs for subjects 19 and 20. 213

Figure 71 Predicted (subjects 1-9) contrast enhancement 215

Figure 72 Predicted (subjects 10-18) contrast enhancement 216

Figure 73 Predicted contrast (subjects 19 and 20) enhancement 217

Figure 74 Predicted contrast (subjects 1 and 9) enhancement 219

Figure 75 Predicted contrast (subjects 10 and 18) enhancement 220

Figure 76 Predicted contrast (subjects 19 and 20) enhancement 221

Figure 77 Clinical data - Time Enhancement Curves for subjects one through nine 223

Figure 78 Clinical data - Time Enhancement Curves for subjects 10 through 18 224

Figure 79 Clinical data - Time Enhancement Curves for subjects 19 and 20 225

PREFACE

I give sincere thanks and appreciation to the members of my committee: Drs. Li, Sun, Mao, Bae, and Boston. I am very fortunate to have on my committee one of the pioneers of optimal contrast enhanced CT imaging and one of the most creative thinkers in medical imaging research, Dr KT Bae.

To my advisor, Dr Boston, I am grateful beyond words for the support, guidance, patience and understanding you have provided to me over the past ten years. I have learned many skills from you that make be a better engineer and a researcher. I thank you for persevering with me as I made an unorthodox ascent through my doctoral candidacy.

To my employer, MEDRAD Inc., I am extremely grateful. I owe tremendous gratitude and respect to my management team, Joe Havrilla and Don DeLauder. I appreciate the opportunities you have afforded me and the patience, commitment and motivation you have shown me to complete this work. I also thank John Friel, for his encouragement and for providing the corporate environment that allowed me to pursue this work. For my parents I am thankful for you efforts, during my formative years, to instill in me an appreciation for education, and a desire to learn.

To my beautiful children, Sydney and Simon – I miss the hours at night and the weekends we didn't get to spend together as I completed this work. The miracles that you are, though, motivated me throughout this journey. Finally, to my wonderful wife Charlotte – thank you. Thank you for pushing me, for consoling me when I lost heart, for understanding the hours of work that kept me away from the family, for keeping me on track and for all you do to brighten my life. I dedicate this work to you.

Finally, Ad Majorem Dei Gloriam!

1.0 INTRODUCTION

The administration of iodinated contrast agent has become a routine and necessary component of most Computed Tomography (CT) X-Ray imaging procedures. In 2009 alone, there were nearly 40 million contrast enhanced CT procedures performed worldwide. Although X-Ray contrast agents have been used on humans for nearly a hundred years, only in the past twenty years have microprocessor controlled injection systems been introduced that make possible rapid bolus injections of the contrast agent (up to 10 ml/s) into a patient's peripheral venous blood stream prior to and during CT examination. Typical clinical protocols call for the delivery of between 60 - 170 ml of contrast agent at injection rates varying from 2 to 7 ml/s [1].

The volume of contrast to be injected, the flow rate of injection, the ideal concentration of iodine in the bolus, and the time delay between injection and commencement of the scan is mostly determined by empirical experience and clinical judgments [2]. Modern contrast injection systems have open-loop control architectures, and published approaches [3-10] to quantitatively model the contrast injection process have generally not been incorporated into clinical practice due to the practical complexities these techniques introduce.

CT X-Ray scanners produce high-resolution 2D and 3D images of anatomy in multiple imaging planes. Despite the high spatial resolution generated by CT, exogenous intravenous contrast agents provide better image contrast. Recent advances in multi-detector or multi-slice CT (MDCT or MSCT) scanner technology facilitate the acquisition of sub-millimeter resolution

images in seconds [2]. A typical image created by contrast enhanced CT is shown in **Figure 1**. A 3D reconstruction was applied to the raw, axial CT data acquired after the injection of 85 ml of contrast material and the image data were acquired in 2.5 seconds (Definition FLASH, Siemens Healthcare, Malvern PA). The full extent of the thoracic and abdominal aorta is visualized in this image along with other details like surgical sutures, some coronary artery segments, and an implanted pain pump.

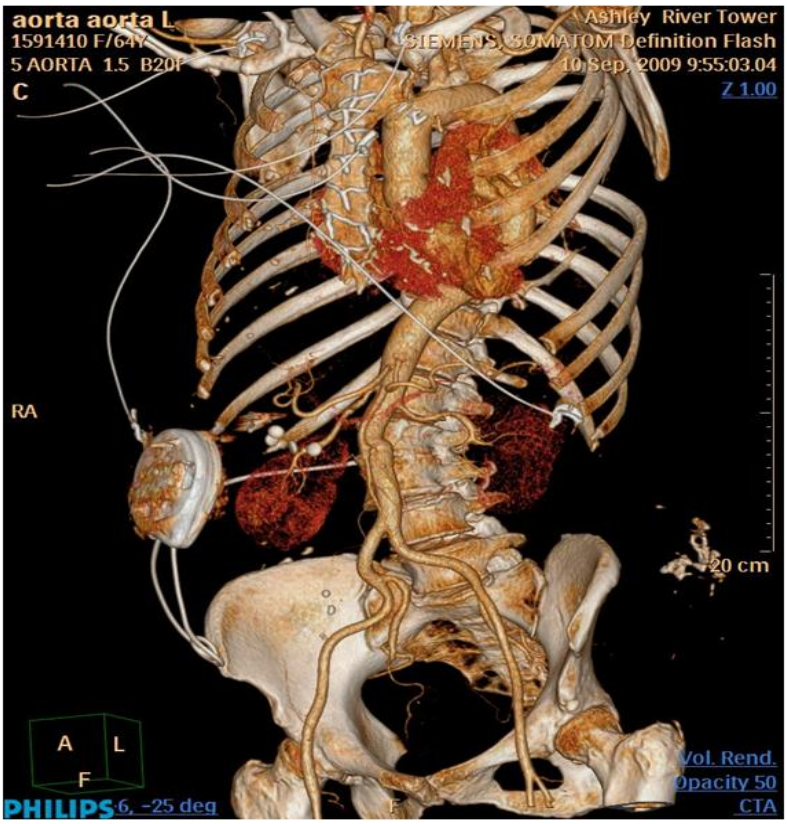

Figure 1 Example thoracic CTA data set. A 3D reconstruction was performed on CT data acquired after the injection of 85 ml of contrast material at 5 ml/s. The scan data was acquired in 2.5 seconds. Visible in the image are prior surgical repairs to the aorta and an implanted drug pump.

Whereas faster acquisition times reduce the total volume of contrast agent needed to enhance an anatomical region, the contrast must be injected at a faster rate, resulting in a challenge for the scanner operator to ensure optimal scan timing because the injection of the drug occurs over a very short duration. The most useful diagnostic image is generated during peak plasma or tissue concentration of the contrast media. The magnitude of the peak enhancement and the time to reach a maximum are variable across patients and are affected by cardiovascular properties of the patient and the intrinsic pharmacokinetics of the contrast agent [4].

Because quick image acquisition times mandate faster injection rates for visualization of arteries, the need exists to match scan interval to the peak enhancement of the vessels. The imaging of arteries with CT is known as CT Angiography (CTA). Miscalculating the contrast arrival and the subsequent scan acquisition may result in poor vessel opacification and a potential misdiagnosis. A poor image due to improper technique may also require a repeated procedure that unnecessarily increases a patient's exposure to ionizing radiation.

Figure 2 illustrates the relationship among the contrast agent injector, the drug's propagation and the scanner acquisition. For this case, the scan starts at the first vertical line, marked with the letter A. This time also corresponds to the scan delay. A representation of the contrast media delivery is on the middle axis, while the image acquisition is depicted on the top axis. The time difference between the end of the contrast material administration and the beginning of the scan is the contrast arrival time, or the time needed for the contrast material to migrate into the vascular territory of interest. Finally, the bottom axis represents the plasma concentration of the contrast material in the vascular territory of interest. The contrast enhancement of the image is linearly related to the plasma concentration of the contrast material.

An ideal scanning procedure uses a minimal amount of contrast material and ensures scanning during the period of maximal plasma contrast concentration/image contrast enhancement.

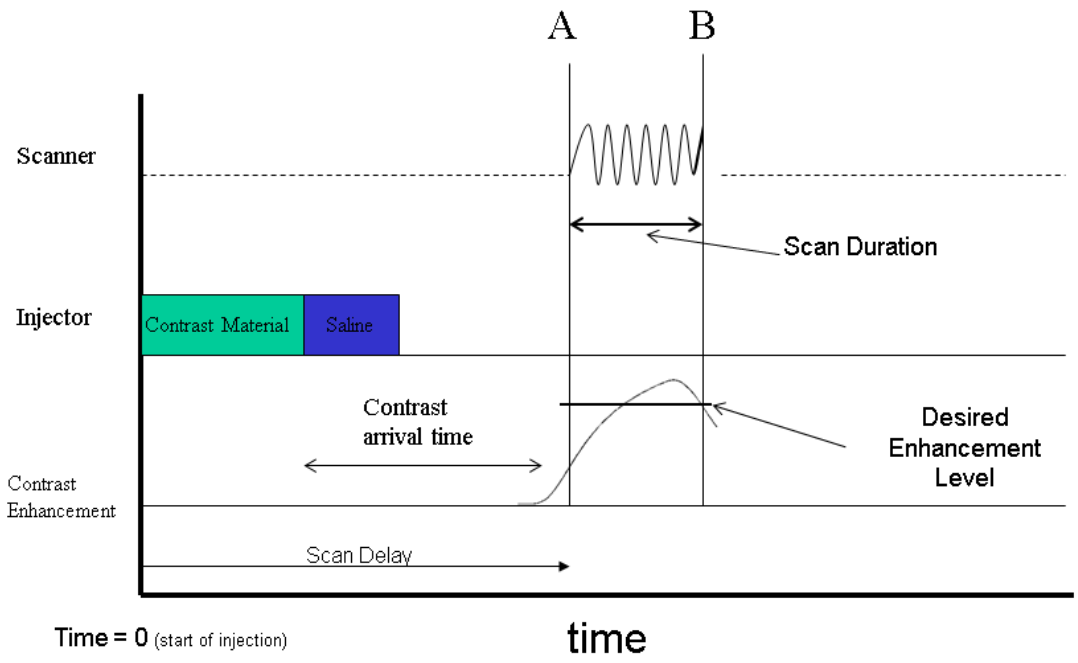

Figure 2 Pictorial demonstrating the temporal relationships among scanner, injection system and *in vivo* contrast enhancement profile.

The existing methods for administering X-Ray contrast agent during CTA can be improved by generating and fitting patient-specific models of contrast dynamics with image data provided by the scanner and processed by the injection system. This dissertation presents a modeling and identification strategy that can be used to create patient-specific injection protocols. The algorithm results in optimized contrast injection protocols and ideal MSCT scan

timing for an individual patient. Optimized dosing, in this context, is defined to be the minimally sufficient volume of contrast material to enable reliable contrast enhancement (as specified by the clinician) of cardiothoracic arterial structures.

Reducing the total volume of contrast fluid is especially desirable in patients with compromised renal function. The paradigm presented here considers the constraints of the injection system (ie: volumetric flow rates, pressures, scan times, contrast concentration) and of the patient's cardiovascular system, a consideration not formally made in previously published work. The initial clinical application for this research is thoracic CT Angiography because of the technical challenges inherent to the procedure, the growth of the procedure, and the valuable clinical information made available by consistent and repeatable examinations. The methods proposed here for optimal, diagnostic CT angiography of thoracic structures can also be applied to other anatomical regions of the body and also for other diagnostic imaging modalities requiring exogenous contrast material.

2.0 BACKGROUND AND LITERATURE REVIEW

This chapter is a summary of relevant research, including brief reviews of X-Ray contrast, the practice of Contrast Enhanced CT angiography imaging, and pharmacokinetic modeling. Whereas a survey of the CT imaging literature reveals numerous approaches for the creation of ideal contrast injection protocols (see reviews in [1, 11]), Fleischmann [9] and Bae [6] are the most sophisticated techniques for computing patient specific contrast administration protocols. Bae's work is particularly noteworthy because it establishes a quantitative modeling framework (enhancing Blomley/Dawson and Krause) that serves as a means to generate patient-specific delivery protocols. Fleishmann and Bae's works are the precursors to the work presented here and therefore are described in detail.

2.1 X-RAY CONTRAST MEDIUM

Soft tissues and vasculature show poor contrast in CT images due to their low X-Ray absorption. The solution to imaging these structures is to introduce an intravascular agent that absorbs or scatters X-rays. In the 1920s, chemists synthesized water soluble mixtures of iodine that could be tolerated by mammalian physiology [12]. The organic chemistry was perfected by the 1950's, and physicians began to safely administer iodinated contrast pharmaceuticals via centrally inserted catheters, which enabled X-Ray imaging of the vascular system.

The iodinated agents were introduced via a hand syringe. Handheld delivery is suboptimal because the necessary force to push contrast through small catheters into the central circulation exceeds the force that can be produced by hand. The automated "power" injector, which could be remotely triggered, allowed the physician to distance himself from the X-Ray source and could generate sufficient hydrodynamic force while providing repeatable procedures. The power injector is routinely used in the millions of catheterization procedures performed each year.

The intensity of an X-Ray image with contrast agent is directly proportional to the concentration of iodine in the vessel or organ's blood plasma, the electron configuration of iodine, and the excitation energy of the X-Ray photons as determined by the voltage applied across the X-Ray tube. The concentration of iodine in an X-Ray contrast agent is expressed in units of mg iodine per ml of fluid. Iodinated contrast agent is hyperosmolar in solution.

Hounsfield Units are dimensionless units that normalize CT scan values across scanner types. The units reflect the attenuation values in the path of the X-Rays. A measurement of zero Hounsfield units is the attenuation of X-Rays when passing through water. The attenuation of air is calibrated to –1000 HU. Bone is measured at 1000 HU and is typically the upper end of the HU scale, although modern CT scanners report HU values up to 3000 HU. The HU is defined as

$$\mathrm{HU} = \frac{\mu_{\text{tissue}} - \mu_{H_2 0}}{\mu_{H_2 0}} \cdot 1000 \tag{2.1}$$

where μ's are the mass attenuation coefficient of material measured by X-Ray attenuation.

2.2 CONTRAST ENHANCED CT IMAGING

During Computed Tomography Angiography (CTA) procedures, the imaging of the vessels should coincide with the maximum concentration of contrast material. To ensure the rapid accumulation of contrast in the vessels, CT power injectors deliver contrast at volumetric flow rates of 4 ml/s and greater. The rapid injection ensures a sufficient volume of contrast material is present during the "first pass" of drug through the arterial system from the peripheral, venous injection site.

Because contrast enhancement is related to the amount of iodine and its mass flux in a volume within an anatomical territory of interest, radiologists can modify the contrast volume and delivery flow rate to maximize image enhancement. The volume injected is regulated by a servo system controlling the linear displacement of a plunger sliding inside a large syringe containing the contrast agent. Contrast agent is injected into the patient at a programmed flow rate. Contrast enhancement in vessels is greatest when the contrast is delivered to the heart via the peripheral venous system at a high flow rate [13]. The fast injection of viscous contrast agent through the small tubing and catheter creates large pressures in the syringe (25 - 325 psi), patient connector tubing, and peripheral catheter. The polymer syringes and disposable tubing set cannot support large pressures (> 500 psi) for sustained periods and the pressure generated in the syringe is typically limited to 325 psi.. Sometimes the pressure limit is reduced for patients with difficult intravenous access or with compromised veins.

Contrast medium injected into the peripheral venous circulation drains into the heart. The heart then delivers the agent throughout the body. Contrast agent migrates from the central blood volume (within blood vessels) into parenchyma and tissue due to the concentration gradients across capillaries. Contrast medium is hyperosmolar and so plasma is "pulled" into the

intravascular space to balance osmotic pressures. The extravasation of contrast media into the tissue space and dilution in the bloodstream must be recognized when attempting to predict peak enhancement in an artery or organ.

The diffusion of the contrast agent and the recirculation of the agent cause an asymmetrically peaked CTA enhancement curve (see Figure 3) for long duration contrast injections. Patients with diseased cardiovascular systems may exhibit CT enhancement peaks that are low in amplitude and excessively dispersed. Decreased vascular opacification can result in a misdiagnosis by the radiologist. Because there is no feedback to the injection system regarding the behavior of the contrast *in vivo*, large inter-individual differences in contrast enhancement result in some patients receiving more contrast than needed to obtain an adequate diagnosis [14].

An injection of saline following the main bolus of contrast material is a standard technique for CTA procedures. The extra saline, typically injected at the same flow rate as the contrast material, ensures that contrast material is not left in the syringe and tubing set of the injection system and helps to maintain the momentum of the main bolus of contrast as it migrates through the peripheral venous circulation [15]. The saline phase has been demonstrated to increase the peak aortic enhancement from 5% to 10% as compared to injections without a saline phase [16]. Lee et al [17] investigated the impact on contrast enhancement in the aorta and pulmonary artery when a saline flush or "chase" phase followed a bolus of contrast material using a canine model. They followed the contrast phase with no saline, saline injected at the same flow rate as the contrast bolus, and saline injected at half the flow rate of the contrast bolus.

The enhancement profiles in the experimental groups using the saline phase (or "flush" as it is sometimes called) had greater peak enhancements and later peak enhancement times than the protocol group in which no saline flush was used.

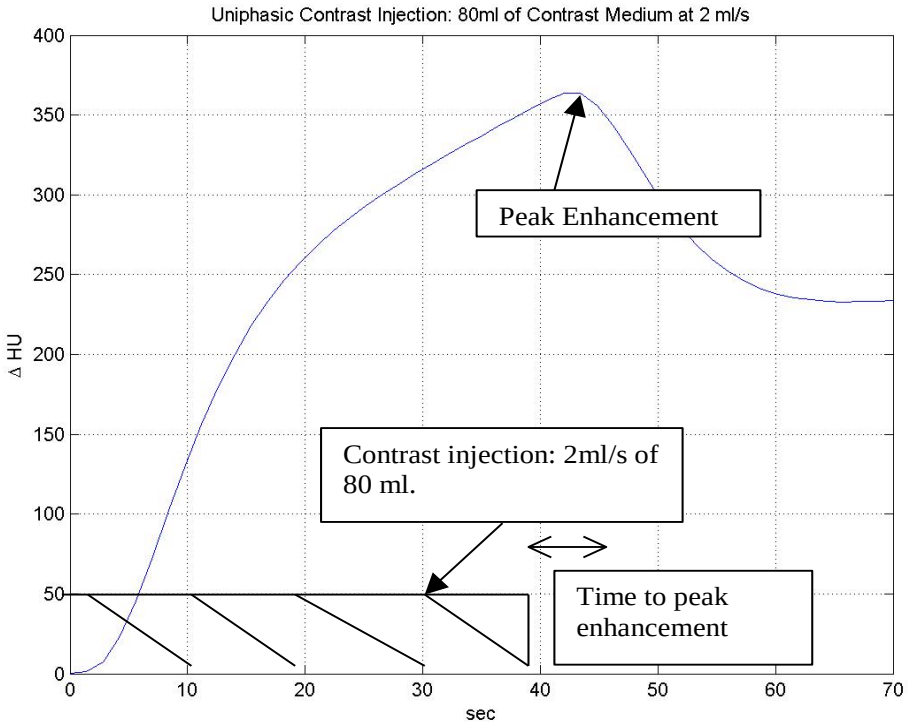

Figure 3 Example of a typical, CT enhancement curve generated from an uniphasic injection of contrast medium. This curve exhibits the typical peak associated with CT images of blood vessels. The y-axis represents Hounsfield units.

2.2.1 Detailed Description of CTA Data Acquisition and Image Sets

There are three standard techniques for determining an appropriate CT scan delay [14, 18], or the time from commencement of the contrast injection to the start of the scan acquisition. These methods are:

- use of a fixed delay for each patient
- base the scan delay on the peak of a small "timing" or "test" bolus of contrast – the timing bolus technique
- use of bolus "tracking" software integrated into the scanner – the bolus tracking technique.

The fixed scan delay for every patient is the least desirable method, especially for cardio-thoracic CTA, because of large hemodynamic differences among patients. Most radiologists, therefore, compute a scan delay based on the time to peak of a small timing/identification bolus (similar injection as proposed in this research) or use the bolus tracking method.

A drawback to the timing bolus technique is that the time of peak contrast enhancement for a timing (or test) bolus is not the same as the time of peak enhancement for a full diagnostic bolus. Radiologists apply empirically derived rules, such as adding 4 or 5 seconds to the test bolus peak, to determine the scan delay [18]. Assuming linearity of the system, one could compute an estimate of the time to peak of an arbitrary injection if the entire timing bolus enhancement curve were available [19], but this is not done in practice due to the current data exchange limitation between scanners and injection systems.

The bolus tracking technique, a software feature commonly available on all commercial CT scanners, consists of a low level scan of a region of interest during the contrast injection. Once the enhancement in a chosen vessel exceeds a certain threshold, the scanner positions the

patient for the diagnostic scan. Some methodological issues prohibit bolus tracking from working ideally for all patients. The most notable drawback of bolus tracking is that choosing the proper enhancement level for the threshold is arbitrary and varies among clinicians. Additionally, there are unknown (to the clinician) latencies in the processing of the scan information, positioning of the patient, and initiation of the diagnostic scan. These indeterminate delays can make the scan timing less than ideal.

Knowledge of the specific patient's physiologic status and how it influences the contrast agent is difficult, if not impossible, for the clinician to assess before delivering the agent. Some clinical procedures suggest the modulation of the flow rate or the volume based upon patient weight or other habitus index [20, 21]. Whereas these techniques do show promise in reducing some of the uncertainty associated with image quality and contrast medium dosage, they are not robust and also cannot aid in finding the ideal scan times [22].

For patient specific contrast protocol calculation, the timing bolus technique is preferred because the data provide a representation of the cardiovascular and contrast dynamics. To better understand the imaging techniques used in this research, a more detailed explanation of the contrast enhanced imaging procedure (assuming a timing or “test” bolus is used for timing and/or identification of the patient) is presented. An illustration of an entire imaging procedure is presented to aid comprehension in Figure 4, which is an elaboration of the process depicted in Figure 2.

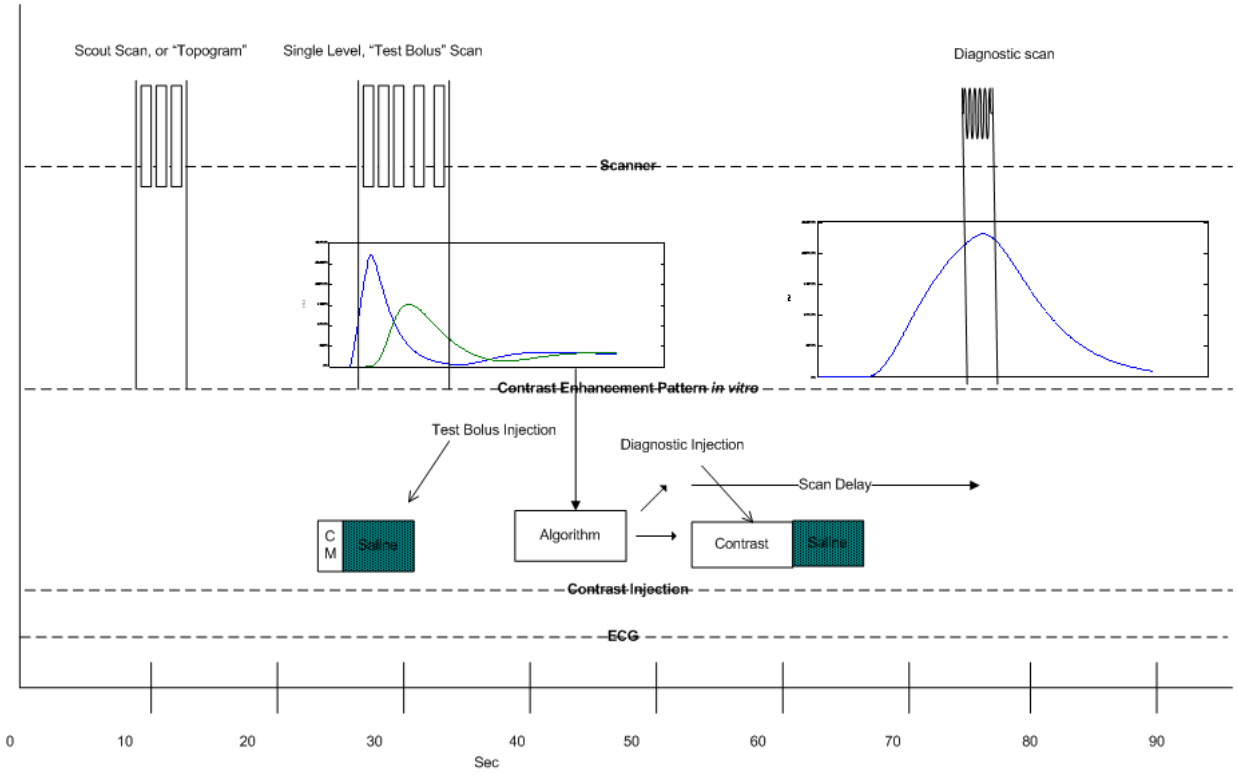

Figure 4 Detailed schematic of a contrast enhanced CTA imaging procedure

In **Figure 4**, the origin of the time axis coincides to when the patient is positioned on the table and the scanner is initialized. The scanner axis contains three distinct imaging operations: a scout scan or topogram, a test (or timing) bolus scan, and the diagnostic scan. The topogram is a low-level scan used in planning the procedure. Both the topogram and test bolus scans are acquired with the patient stationary in relationship to the gantry (the gantry contains the X-Ray source and the detectors). This type of scan is referred to as a "single level" scan. It is important to appreciate that the diagnostic scan (typically) is acquired in a helical, or spiral, fashion. The patient is moved continuously through the opening in the scanner and the gantry rotates around the patient as she is moved linearly through the scanner. For most cardio-thoracic CTA studies, the patient's ECG signal is acquired simultaneously.

Modern CT detectors are 4-16 cm in width and are composed of multiple rows. As the patient moves through the bore of the scanner, the X-Ray fan beam passes through the patient and is intercepted by the detector array. Because the patient is continuously moving through the scanner, not every detector row receives a normal projection of X-Ray photons. Reconstruction algorithms on the scanner interpolate the "missing" data on each detector and reconstruct axial slices. Because of this helical acquisition mode, the diagnostic scan in **Figure 4** is indicated with a wavy line, a different representation from the other, stationary scans. It is important to recognize that diagnostic CT data sets acquired in a helical mode are therefore a function of space and time. A convention in medical imaging is to label the spatial direction along the scanner bore – or the direction that the patient moves - as the z-axis.

When the timing bolus is administered, the contrast injector infuses a small bolus of contrast followed by saline. The scanner then starts acquiring data in a single-level mode four to 10 seconds after the start of contrast injection. The scanner operator processes the single-level scan series and constructs Time Enhancement Curves (TECs) on the relevant vascular anatomy. The resulting curve presents a dynamic view of the contrast bolus as it passes through the anatomy. Features of the TECs are used to plan the diagnostic scan contrast and scan protocols. Most commonly, the scan delay is computed from the peak contrast enhancement of the TEC acquired in the test bolus series.

Because the contrast bolus propagates to the vascular region in a finite amount of time, the diagnostic scan must be delayed an appropriate amount to allow the bolus to appear in the territory of interest. In **Figure 4**, the diagnostic scan contrast protocol is injected and the helical acquisition starts in a time defined by the "scan delay". One goal of optimized protocol construction is to time the helical acquisition to ensure the maximum of the contrast

enhancement concentration in the territory of interest (refer to **Figure 4**). When the scan delay time elapses, the scanner is triggered and the patient is moved through the scanner as the data are acquired.

Depending upon the clinical indications and site preferences, the reconstruction software generates multiple views of the data. The patient's ECG signal is used by the scanner's reconstruction software to generate data free of motion artifact. Most commonly for CTA procedures, "thin" slice axial images are generated by the scanner software. Because the spatial resolution between the slices can be less than one millimeter, these thin slices may be used to construct views of the data from different angles (multi-planar reformatting MPR).

An example of MPR imagery is given in **Figure 5**. The top row of the figure shows, from left to right, axial, sagital and coronal views of the data. The bottom row depicts the enhancement profile of the contrast in the descending aorta from the top of the image set to the bottom. In this example, the scanner was configured such that each of the axial images was reconstructed with a .375 mm separation. There were 477 axial images in the data set. The blocked regions on the axis indicate the data reconstructed at each diastolic portion of the patient's cardiac cycle (~75% of the R-R interval – these blocks, therefore are roughly 1 second apart at a 60 bpm heart rate). Because the data in each block were reconstructed at the same point relative to the cardiac cycle, the contrast data in that block are averaged together to present a temporal and spatial evolution of the contrast bolus in the aorta independent of changes related to the beating heart.

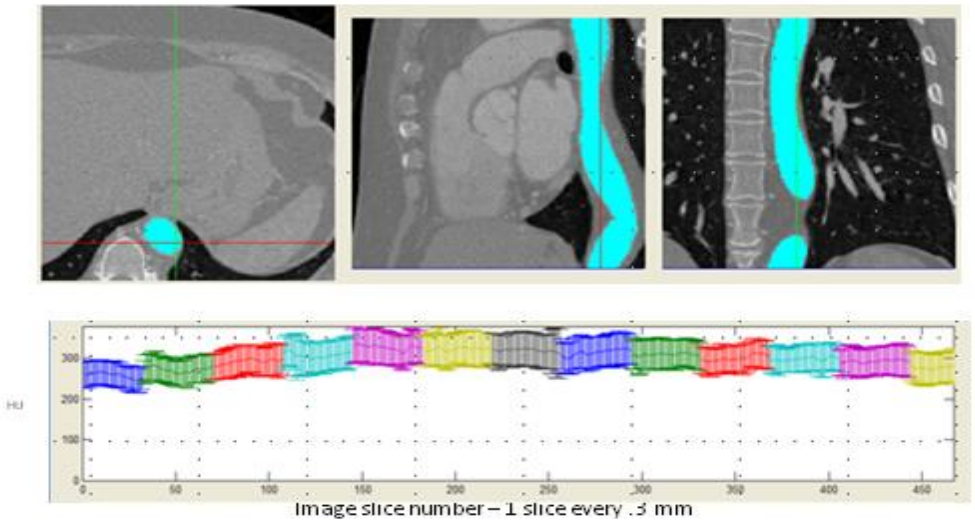

Figure 5 Example CTA data set (top – the shaded structure is the descending aorta) and contrast enhancement values derived from the aorta (bottom). The colored blocks indicate that the multiple slices within that block were acquired at one time instance.[1]

The methodology just described is used to compare numerical techniques developed in subsequent sections of this dissertation. An implicit assumption for the applicability of this method is that the propagation velocity of the contrast media and blood mixture is greater than the time necessary to acquire the imaging data with the scanner. This is a valid assumption because the typical linear velocity of blood and contrast ejected from the Left Ventricle is 50-70 cm/sec and the patient is moved through the scanner (a limiting factor in acquiring the image data during a helical acquisition) at speeds typically between 1-2 cm/sec.

[1] MATLAB software and GUI developed by CA Kemper PhD, MEDRAD Innovations

2.3 PHARMACOKINETIC DRUG MODELLING

Pharmacokinetics (PK) is the study of drug distribution throughout an organism, the absorption of the drug in various tissues and the excretion of the drug through metabolic and/or excretory processes. It is contrasted with pharmacodynamics, the study of a drug's impact or effect on the organism. A common technique in pharmacokinetics is to model the transport and distribution of drug by dividing the physiology into several "compartments" in which conservation of mass is enforced. The rate-transfer among the components parameterizes the model. These compartments don't necessarily have a 1-1 relationship with an anatomical section of the organism but, rather, are useful mathematical structures for describing the distribution of drug. An example of a typical structure, a 2 compartment PK model, is shown in Figure 6.

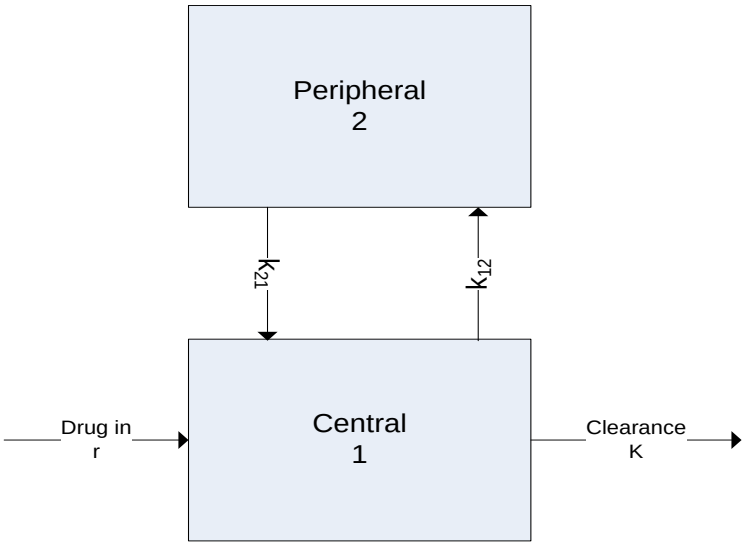

Figure 6 A 2-compartment PK model with Central and Peripheral compartments. The parameters r, k_{12}, k_{21}, and K are all mass rate transfer coefficients with units of time^{-1}.

The two compartments in Figure 6 are not meant to represent the actual central and peripheral circulatory systems of an organism. Rather, they provide a means to accommodate dynamics apparent in dose response data. The drug input is the infusion or adsorption mass rate of drug into the system. The clearance, K, represents the excretion of drug from the system – typically via urine or hepatic processes. The transfer coefficients between the 2 compartments introduce into the model a means of modeling non-instantaneous distribution of drug throughout the body. With mass (x_i) being the independent parameter, the coupled set of first order differential equations describing Figure 6 is:

$$\frac{dx_1}{dt} = r - K - k_{12}x_1 + k_{21}x_2$$
$$\frac{dx_2}{dt} = k_{12}x_1 - k_{21}x_2 \qquad (2.2)$$

The concentration of the drug in either compartment can be found by dividing the mass by an apparent volume (sometimes called a distribution volume), V_i which has no direct physiologic meaning. An estimate of plasma concentration in compartment 1:

$$C_p = \frac{x_1}{V_1} \qquad (2.3)$$

Numerical fitting of dose-response data, blood plasma measurements made after the administration of varying doses of a drug either to an animal or human, yields the rate transfer coefficients. The majority of pharmacokinetic models assume the system is linear and time

invariant. The parameters of the models are usually based on population statistics acquired from drug plasma measurements in many animals or subjects acquired during the drug's development.

2.3.1 Physiologically Based Pharmacokinetic Modeling

An alternative approach to classical, pharmacokinetic modeling in which the structure of the model is dictated primarily by mathematical convenience is physiologically based pharmacokinetic modeling (PBPK). It is a modeling approach that considers relevant physiology and function when determining the model structure. A review of the PBPK principles and clinical and pharmacology applications is presented in [23], and a recent text by Reddy and Yang [24] describes the history and development of the field. It is interesting to note that the first efforts to quantify and predict drug distribution were made using the PBPK paradigm. The non-existence at that time of numerical methods made solving the coupled systems of differential equations over many time-steps nearly impossible. Thus, the classical one and two compartment approaches to fitting plasma concentration measurements became ascendant until the early 1980s.

In a PBPK model, the body is separated into a number of interconnected compartments corresponding to anatomical regions. Each compartment is parameterized (volume, blood flow, perfusion) based on physiologic and anatomic considerations of the organism, and each connected by vascular compartments that facilitate the convective transport of the species to and away from the compartment. An advantage of this approach is the ability to scale the model across species without changing the structure of the model. Fitting experimental data to a very large PBPK model can be computationally expensive and difficult, however. To overcome data

fitting challenges, modelers typically attempt to construct a model with the fewest compartments necessary while still maintaining physiologic and anatomic fidelity [24].

An example of a typical, whole body PBPK model (adopted from [25]) is presented in **Figure 7**.The mathematical basis of the PBPK model is mass-conservation among the various compartments. The convective transport of blood is denoted by the variable *Q* in the figure. There is a volume of blood in each compartment of the model and the blood volume is typically divided among the interstitial territory of the organ (V_i), the vascular territory of the organ (V_v), and the cellular sub-compartment (V_c). Within each compartment, the drug concentration is annotated by C_i and the mass is the product of volume and concentration. The mass flux of the species into an organ must equal the mass flux leaving the organ and is defined as the product of blood flow Q and concentration C. Further elaboration of the concepts and nomenclature are given in the next section, where a PBPK model of X-Ray contrast media propagation is discussed (Section 2.5).

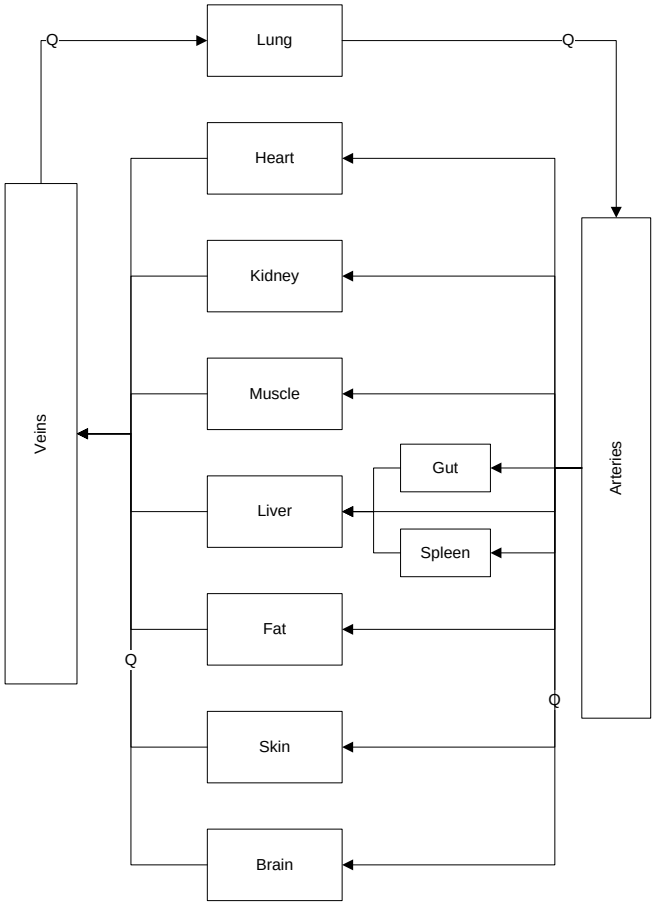

Figure 7 Example of a PBPK model structure, adapted from [25]. Q represents blood flow through the vasculature connecting each region of the body.

2.4 COMPUTER CONTROLLED INFUSION

A large body of published literature exists related to optimal or predicative control of infusion pumps for administering chemotherapeutic, analgesic, and anesthetic agents. Representative publications are Rao [26], Held and Roy [27], and Jacobs [28]. In these works, a one or two compartment PK model described and subsequently predicted the drug distribution. The most

refined Computer Controlled Infusion (CCI) or Target Controlled Infusion (TCI) work was performed with the intent of controlling the delivery of propofol [29]. A commercial product, the *Diprifusor* was developed and distributed by Astra-Zeneca Inc. in the late 1990's based on this work.

The X-Ray contrast delivery problem is different from similar ones in the Computer Controlled Infusion (CCI) literature because the delivery rate of the contrast is fast and of short duration (bolus delivery). While published CCI studies modeled drug pharmacokinetics in an effort to devise optimal injection routes, the infusion rates were very low relative to those used during contrast medium delivery (ml/min compared to ml/s). Furthermore, the infusions last minutes or hours, allowing for the potential update of model parameters based on previous control moves. Because the volume of administered contrast is typically between 60-150 ml, and the intravenous space volume from the injection site through the heart and pulmonary circulation is about 400-500 ml, once the contrast medium bolus enters the cardiac circulation, further control of the propagation of the contrast agent is not feasible. Control schemes to improve the delivery of these diagnostic agents (and potentially therapeutic agents) must decide the best trajectory before the agent is delivered to the patient.

Model Predictive Control (MPC) techniques can be applied in CCI applications to identify the model dynamics once the injection has started – observing the actual scan enhancement values during the administration of the contrast, comparing them to an underlying model and updating the model parameters as a function of prediction error. A recent study by Gentilini et al.[30] proposed a model predictive control approach for controlling the plasma concentration of the opiate alfentanil with a computer controlled infusion pump. They used a 3-compartment PK model to predict the distribution of opiate in a human. The controller relied

upon an observer to estimate plasma concentrations of the drug based on measurements of mean arterial pressure and the PK model running in parallel with data acquisition..

Krause proposed a PK multi-compartmental model describing the distribution of X-Ray contrast medium [31]. Krause fit the results of plasma concentration data, as measured by periodic blood withdrawal, to simple kinetic models and produced dynamic curves of contrast medium propagation and the time to reach steady state in the human circulation. A particular emphasis was placed on studying the contrast behavior in the time-frame typical of liver CT scans, 40-80 seconds after the time period of interest during cardiac CT.

Ledzewicz and Schattler considered the treatment of certain cancers via intravenous chemotherapy in a minimum-fuel context [32]. They used a two-compartment pharmacokinetic model to describe the action of the chemotoxic agents. The authors demonstrated that the optimal controls are bang-bang with respect to the dosing of the drug. A distinction, however, between this work and the contrast delivery problem is that contrast delivery for CTA is a one-bolus delivery problem opposed to a slow infusion of drug over time. Furthermore, the introduction of "gaps" in the bolus of contrast agent will present as un-enhanced regions in the imagery.

2.5 BAE'S PBPK MODEL OF CONTRAST MEDIA PROPOGATION

Bae et al. used the PBPK framework to model and ultimately control the propagation of X-Ray contrast media [5]. Bae treated the concentration of the intravenous contrast injection as the input function to a whole-body PBPK model with two main components in the model – the blood vessels and organs.

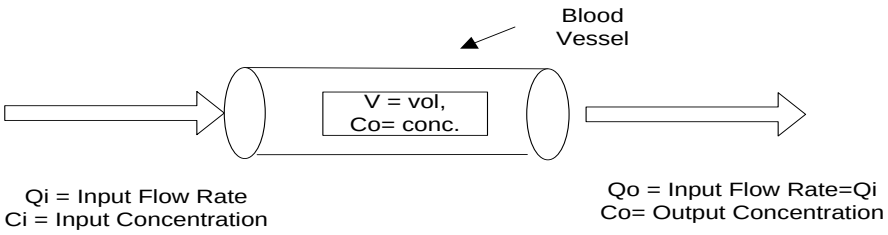

Figure 8 Bae's representation of a blood vessel. It is assumed that the volume of the component is fixed, the vessel is a rigid tube (no compliance), the flow is non-pulsatile and the compartment is well-mixed.

Bae modeled the blood vessels as rigid tubes with a mass flow rate entering the vessel equal to that leaving, pictorially demonstrated in **Figure 8**. He also assumed that the blood and contrast instantaneously and uniformly mix within the vessel. Contrast concentration follows first-order kinetics as the bolus propagates through the vasculature. The differential equation describing the mass balance on the concentration of Iodine in the vessel is given by the Fick principle:

$$V\frac{dC_o(t)}{dt} = Q_i C_i - Q_o C_o(t) \tag{2.4}$$

where V is the volume of the vessel, Q_i and Q_o are the mass flow rates at the entrance and exit of the vessel (usually, assumed to be equal), C_i is the input concentration (assumed constant) and

C_o is the output concentration. The differential equation can be solved for output concentration, where T_{inj} marks the end of the injection.

$$C_O(t) = \begin{cases} \frac{Q_i}{Q_o} C_i \left(1 - e^{\frac{-Q_o}{V} t} \right), t \le T_{inj} \\ C_o(T_{inj}) e^{\frac{-Q_o}{V} t}, t > T_{Inj} \end{cases} \quad (2.5)$$

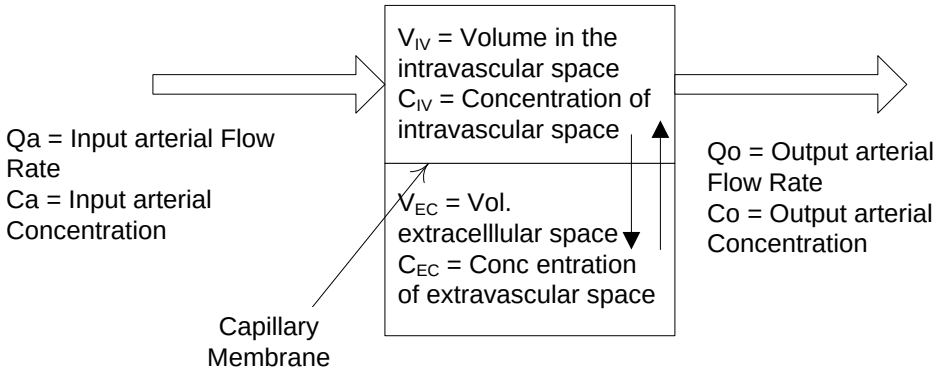

Figure 9 Bae's model of the diffusion of contrast medium in organs of the mammalian system.

The organs were modeled as multi-compartment structures with intravascular and extravascular compartments. A graphical depiction of the organ model is shown in **Figure 9**. The intravascular region consists of the plasma compartment of the blood while the extravascular

component represents the permeable tissue of an organ separated from the intravascular domain by the capillary endothelial membrane.

Fick's Law of Diffusion modeled the diffusion of contrast medium across the capillary membrane separating the intra and extravascular spaces. The Fick principle, applied across the membrane is stated as:

$$\frac{dM}{dt} = DS\frac{C_i - C_o}{\Delta x} \tag{2.6}$$

where M is the mass of a species, D is the diffusion coefficient, S is the surface area between the two compartments, and Δx is the membrane thickness. For thin membranes, one may include D and Δx in the permeability, P, of the membrane. Thus, equation (2.6) may be rewritten as:

$$\frac{dM}{dt} = PS\ C_i - C_o \tag{2.7}$$

The values of P and S must be approximated, however, because there is no direct means of measuring the surface area of the membranes for all the capillary beds of the model's organ compartments. The permeability of these membranes is also dependent on a number of factors, including the flow rate of blood through the compartment and the concentration of the species within the compartment. Bae assumed a flow-limited regime and set the PS term proportional to the local flow rate of blood through the region.

Equations (2.6) and (2.7) were coupled and applied to ten major organs and the contrast propagation in organ compartments was modeled as:

$$V_{IV}\frac{dC_{IV}(t)}{dt} = Q\ C_a(t) - C_{IV}(t)\ - PS\ C_{IV}(t) - C_{EC}(t)$$
$$V_{EC}\frac{dC_{EC}(t)}{dt} = PS\ C_{IV}(t) - C_{EC}(t\ ) \qquad (2.8)$$

Subscript notation in equation (2.8) is described in Figure 9. Because contrast material does not penetrate the intracellular space of the blood cells, the intracellular compartment was omitted from the model and equation (2.8). Excretion of contrast agent occurs via glomerular filtration and was fixed at 19% of the renal arterial blood flow in the model. A total of 104-coupled differential equations were solved and the predicted arterial concentration was compared to empirical data collected from 25 human volunteers who received chest CT scans.

The anatomical volumes of the vessels and organs were obtained from published data. The authors claim "good" agreement between the averaged empirical and simulated enhancement results with the mean percent difference in maximum aortic enhancement of 7.4% and in maximum liver enhancement of 4.8%. The variation in time to maximum enhancement between experimental data and simulation predictions was measured as 11.6% in the aorta and 12.7% in the liver.

2.6 BAE REDUCED ORDER PHARMACOKINETIC MODEL

Bae recognized the practical limitations of the full-body model, namely that the use of the model in clinical practice would require the entry of many constants and the estimation of cardiac

output. He subsequently simplified the global circulatory model to make it more amenable for clinical use.

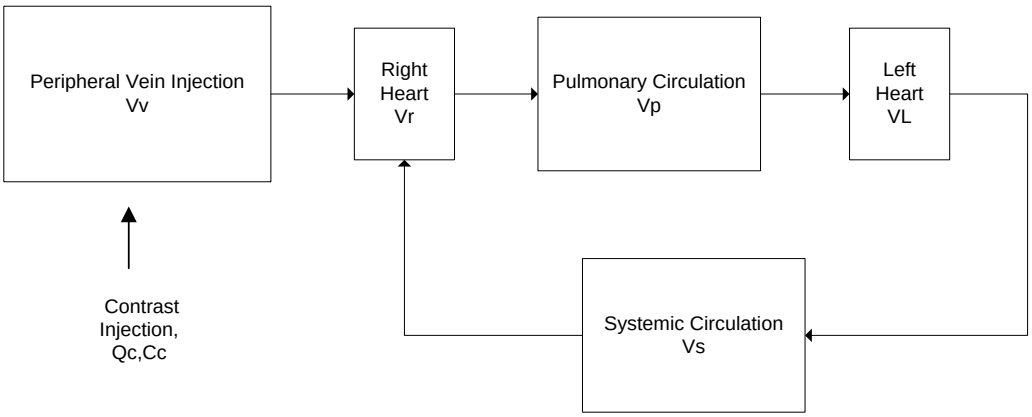

Figure 10 Bae et al.'s simplified circulatory model. This model was used to compute the input (contrast injection) that would produce an uniform contrast enhancement in the aorta (output of Left Heart).

Bae et al. simplified the circulatory system into five sections: the right heart, the pulmonary circulation, the left heart, peripheral venous circulation, and the systemic circulation, as depicted in Figure 10. The set of equations describing the dynamics of the contrast medium is given in equation (2.9), and the initial conditions for all concentration parameters are 0 at time 0. It was assumed, during contrast injection, that the volumetric flow rates (Q terms) are equal. There was no consideration given for pulsatile flow or local vessel compliance changes. In [3], Bae solved for the input function ($Q_cC_c(t)$) in the coupled differential equation system (equation (2.9)) that would produce an uniform, flat contrast enhancement at the aorta (C_L).

$$
\begin{aligned}
V_v \frac{dC_v(t)}{dt} &= Q_c C_c(t) - Q_v C_v(t) \\
V_r \frac{dC_r(t)}{dt} &= Q_v C_v(t) + Q_s C_s(t) - Q_r C_r(t) \\
V_p \frac{dC_p(t)}{dt} &= Q_r C_r(t) - Q_L C_p(t) \\
V_L \frac{dC_L(t)}{dt} &= Q_p C_p(t) - Q_L C_L(t) \\
V_s \frac{dC_s(t)}{dt} &= Q_L C_L(t) - Q_L C_s(t)
\end{aligned}
\tag{2.9}
$$

Bae showed that by injecting contrast into the venous system as an exponential function of time, the resulting contrast enhancement in the left heart compartment was uniform over a time period:

$$
Q_c(t) = (\alpha) e^{\frac{-Q_c}{V_{(v+r+p+L)}}}
\tag{2.10}
$$

with α being the initial injection rate. The model predictions compared well with enhancement data generated from a porcine model[4] .

In [33], Bae and colleagues applied the injection profile in equation (2.10) to pigs and reported the results as "good uniform enhancement of the aorta" and that the empirical and simulation results were in good agreement. Bae subsequently reported results on a sample of patients undergoing standard CTA exams [7] in which there was uniform enhancement in the abdominal aorta.

2.7 WADA AND WARD PBPK MODEL OF ALFENTANIL

Wada and Ward [34, 35] derived a PBPK model similar to the Bae model and applied it for regulating the plasma concentration of anesthetic (the opioid alfentanil). Their model included the recirculation effect of drug through the blood stream, which was modeled as explicit transport delays. The state-space model of the drug and patient explicitly considered the injection delay and delay through the cardiopulmonary circuit as well. The transport of the pharmaceutical was approximated as plug flow for the larger vessels of the cardiovascular system and implies that the amount of time for a bolus of fluid to traverse the administration route is t=Q/V, with Q representing the volumetric flow rate of the blood and V is the blood volume between the injection site and the measurement location. The volumetric flow rate and concentration of the drug are treated as separate elements of mass flux throughout the model, $J_i=Q_iC_i$ with Q the volumetric flow rate and C the concentration of the drug.

Cardiopulmonary parameters were fit with a weighted sum of squares technique using experimental data from blood measurements. Blood plasma values 60 seconds post injection of the drug were used to fit the parameters of the model. Data collected after 60 seconds were used to validate the fitted models. Wada and Ward reported prediction errors of less than 5%. Parameter estimation was performed using the Nelder-Mead Simplex algorithm [34].

The estimated cardiopulmonary parameters were: the blood volume of the left heart, the blood volume of the right heart, the blood volume of the lung, and the transfer coefficients of drug through the pulmonary capillary endothelium. Other parameters in the model, like cardiac output and the total volume of fluid in the system, were based on average human values (5.5

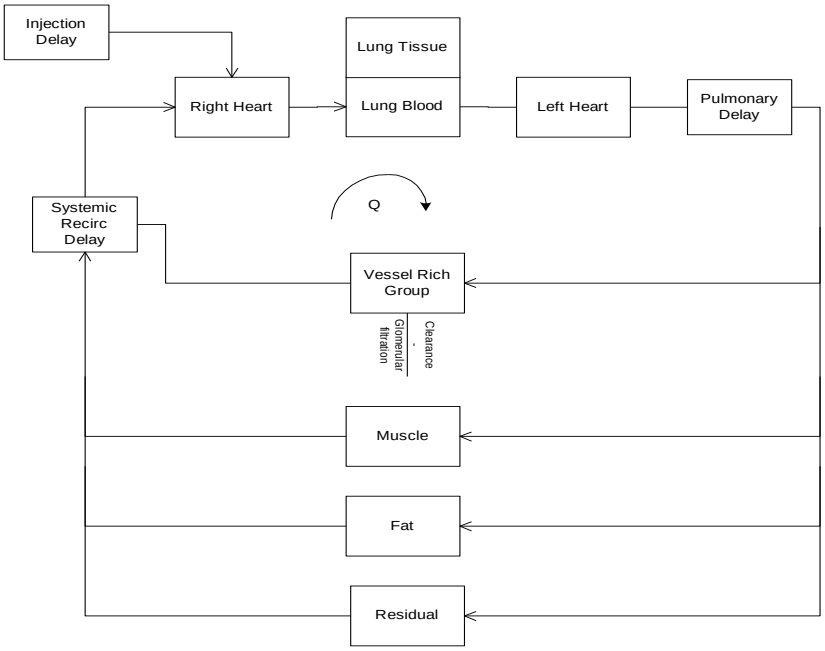

Figure 11 Topology of the Wada and Ward PK model. The Vessel Rich Group represents organs with many blood vessels in which drug is more likely to diffuse from the intravascular compartment.

L/min cardiac output and 14.9 L of residual fluid volume). The resulting prediction of drug concentration in the plasma agreed well with the sampled data. Wada and Ward [35] also applied their pharmacokinetic (PK) model to control multiple effects of anesthetic drugs. Their control scheme required an anesthesiologist to set the allowable side-effect levels (expressed as a plasma concentration).

A representation of the model structure is illustrated in Figure 11 and is the basis for a novel pharmacokinetic model describing contrast medium propagation developed in Chapter 4. Two primary compartment types - Tissue and Blood denoted by subscript "T" and "B" respectively – are used to construct the global model. Blood compartments are pure vascular

regions, while Tissue compartments are extracellular tissue spaces. It is possible that the drug can be irreversibly cleared from the Tissue compartment.

Conservation of mass applied to any subsystem in Figure 11 yields:

$$\begin{aligned} \dot{x}_B &= -\left(\frac{Q_{out}}{V_B} - k_{BT} \right) x_B + k_{TB} x_T + Q_{in} c_{in} \\ \dot{x}_T &= k_{BT} x_B - \left(\frac{Cl}{V_T} + k_{TB} \right) x_T \\ c_{out} &= \frac{1}{\rho V_B} x_B \end{aligned} \tag{2.11}$$

where the subscripts $_{B,T}$ represent the blood and tissue compartments respectively. The rate transfer coefficient k_{BT} is the rate at which the drug diffuses from the blood to the tissue compartment and k_{TB} is the rate of movement from the tissue compartment back to the blood compartment. The variable *Q* is the volumetric flow rate of the blood/drug mixture through a vascular compartment and *C* is the concentration of contrast medium entering or leaving a compartment. Drug concentration is mass divided by the estimated total volume of blood in the compartment. Wada and Ward scaled the apparent volume of the compartments by an estimated hematocrit value of the blood, ρ.

2.8 FLEISCHMANN AND HITTMAIR PATIENT SPECIFIC CONTRAST PROTOCOL COMPUTATION

Fleischman and Hittmair approached the problem of computing an injection profile that produces a uniform contrast enhancement in the aorta by treating the patient's circulatory system as a single input single output (SISO) linear, time-invariant "black box". The input to the system is the contrast injection profile and the output is the enhancement profile at the aorta as measured by the CT scanner. The transfer function of the system (vasculature) was acquired by applying a short duration contrast bolus (a "test bolus") of volume 16 ml at 4 ml/s and the resulting contrast enhancement curve from the scan data was the system output signal.Fleischmann and Hittmair used Fourier methods to perform the deconvolution necessary to estimate the patient/drug transfer function. If $u_t(n)$ is the discrete-time test bolus(units ml/s), $y_t(n)$ is the discrete-time signal representing the response of the patient and drug as measured by the scanner (Hounsfield Units). Assuming the contrast media and vascular system behave as a linear time invariant system, the estimated system impulse response was found by deconvolution:

$$\hat{h}(n) = y_t(n) \otimes^{-1} u_t(n) \tag{2.12}$$

In the Z-domain, the deconvolution operation, $\otimes^{-1}$,is a spectral division:

$$\hat{h}(n) = Z^{-1}\{H(z)\} = Z^{-1}\{\frac{Y_t(z)}{U_t(z)}\} \tag{2.13}$$

where Z^{-1} represents the inverse z-transform operator. Discrete-time operations were performed because the patient response signal, $y_t(n)$ was sampled every 1 or 2 seconds by the CT scanner. Contrast enhancement was measured by applying circular Regions Of Interest (ROI) over the abdominal aorta proximal to the iliac arteries.

To reduce the influence of high frequency noise (assumed to be non-physiological), Fleischmann and Hittmair filtered the output spectrum by multiplication with an exponential kernel (m is a scaling factor):

$$Y_t(k)' = Y_t(k) \cdot e^{-\frac{m}{k}} \tag{2.14}$$

Because the zero or small values in the denominator of equation (2.13) can cause numerical instabilities, they ensured H(k) was zero when $U_t(k)$ was zero by multiplying the filtered output spectrum by a masking signum function, sgn(x) defined as:

$$\operatorname{sgn}(x) = \begin{cases} -1 \text{ if } x < 0 \\ 0 \text{ if } x = 0 \\ 1 \text{ if } x > 0 \end{cases} \tag{2.15}$$

. The estimated transfer function of the patient/drug system was:

$$\hat{H}(k) = \frac{Y_t(k)' \cdot T_f(k)}{U_t(k)'} \tag{2.16}$$

with:

$$T_f(k) = \mathrm{sgn}(|U_t(k)|) \tag{2.17}$$

the signum masking function preventing the transfer function estimate from growing unbounded.

Their goal was to determine the input necessary to give a desired enhancement response during a diagnostic CT scan. The ideal contrast input function was computed by:

$$U_d(k) = \frac{Y_d(k)}{|\hat{H}(k)|} \tag{2.18}$$

An inverse, discrete Fourier Transform of equation (2.18) determined the input function necessary to achieve the desired enhancement level in time.

In general, the raw, computed input function is not realizable because negative flow rates were generated and the flow rates often exceeded 8 ml/s. Flow rates are limited by clinical and system constraints to 6-7 ml/s due to material strength limits of the syringe, tubing and catheters. The pressure generated in the system is a function of contrast medium viscosity, catheter gauge (or inner diameter), tubing length and diameter, and patient's vascular status. Therefore, many radiologists reduce the maximum flow rate for a patient depending on the condition of the vascular access site, the patient's health status, or confidence of the clinician administering the drug. To produce realizable injection profiles, Fleischmann and Hittmair applied a heuristic to the contrast injection protocol that prevented negative flow rates and rounded the continuously varying function so that a contrast injection system could realize the injection. No explicit

algorithm describing the truncation, however, was described in [9] or [36] although some MATHEMATICA code was included in [8].

2.8.1 Fleischmann et al Clinical Results

Fleischmann tested the algorithm described in [9] by applying the computed "optimal" injection profiles to a group of 16 patients undergoing CT angiography suspected of abdominal aneurysms. A control group of 16 patients undergoing the CT scans (abdominal aortic imaging) were administered contrast agent with a standard, uniphasic protocol (120 ml of contrast at one flow rate, 4ml/s) [36]. Time enhancement curves were generated from the axial, CT data sets for each patient in the 2 cohorts. ROIs were drawn in the abdominal aorta every 2 cm by a radiologist to construct the time enhancement curves. Variability in a subject's contrast enhancement was measured by the standard deviation of the enhancement signal throughout the scan duration.

Contrast enhancement variability within the group receiving injection protocols computed via Fourier deconvolution was significantly smaller than that of the control group ($p < .001$, two tailed t-test), suggesting that the computed contrast injection profile produced more uniform contrast enhancement. A statistically significant difference between the control and deconvolution groups' mean enhancement was not found, however. Fleischmann et al. concluded that the patient-specific, optimized input functions resulted in a reduction of enhancement variability for individual subjects (low intra-subject variability), but did not reduce inter-subject variability.

Hittmair and Fleischmann conducted a subsequent investigation similar to that in [36] , but added a group with central venous injections [37]. The results suggested that a more uniform and less variable contrast enhancement can be achieved when the contrast medium is injected via a central venous catheter directly into the right heart. Those findings suggest that dispersion effects of the peripheral venous system and contrast migrating into ancillary arm veins from the injection site to the right heart contributed to the variability in their results. The administration of a large volume of saline after the injection of contrast can aid in pushing the contrast consistently into the right heart and so the introduction of this saline push capability in standard contrast delivery systems should reduce some of the inter-subject variability reported in their work.

An important consideration not made in Fleischmann or Bae is that the maximum, deliverable flow rate is dictated by hydraulic constraints, namely the viscosity of the drug solution and the inner diameter (gauge) of the catheter that provides vascular access. These factors limit the useable flow rates for contrast medium to 6-7 ml/s for most clinical situations. Furthermore, the radiologist may decide to lower the flow rate when a patient having a compromised vascular system is scanned. An optimal, patient specific contrast medium delivery algorithm should consider these constraints when computing an injection trajectory.

2.9 RELEVANT WORK BY THE AUTHOR

Numburi et al. [38, 39] presented clinical validation of the Fleishcmann/Hittmair algorithm with a 16-slice MSCT scanner. The results were in accordance with Fleischmann's – the enhancement

profiles were more uniform, but there was large variability among patients in how well the model predicted enhancement.

Kalafut developed a set of algorithmic rules commercialized as MEDRAD's Stellant ™ P3T™ Cardiac software [40] . The principles applied in the algorithm were similar to those suggested by Awai et al.[8] in that the injection duration is a function of scan duration and the injection volume is scaled to body weight [40]. Clinical validation of the approach was presented in [41].

The software validated in [41] adapted the iodine delivery rate (gI/s) based upon a non-linear relationship between patient weight, scan duration and concentration of the contrast material. Numerical simulations using the pharmacokinetic model of Bae et al.[6] refined the relationship between iodine administration rate and patient weight. The scan procedure information, patient characteristics and data from a test-bolus injection were used to compute patient specific scan delays. With knowledge of scan delay and scan duration, further refinements and customizations of the contrast protocol were made. For example, because the algorithm knew the scan's end-time, the contrast injection was forced to finish several seconds prior to the completion of scan acquisition, ensuring the maximum utilization of the contrast material. The algorithmic approach and software is a first step towards robust, optimal contrast protocol generation in the clinic.

In [42], Kalafut et al. presented an identification and contrast protocol generation technique that fit a 1-compartment PK model to enhancement data generated from test bolus injections. Specifically, the times to maximum contrast enhancement and the maximum magnitude of contrast enhancements in the pulmonary artery and ascending aorta were inputs to the algorithm. The algorithm allowed the radiologist to set desired contrast enhancement targets

in the left heart structures. A direct-search optimization computed the flow rate and injection duration for the diagnostic contrast bolus. Seventy subjects undergoing cardiac CTA were included in a test of the injection scheme. The injection protocols resulted in the desired contrast enhancement in all segments of the coronary anatomy and used 18 ml (mean) less contrast than a retrospective control group. The main limitation to this algorithm was that it only considered a few discrete points on the test bolus enhancement curves.

2.10 CARDIAC OUTPUT ESTIMATION USING CT CONTRAST

Many studies have been published describing the use of tracers for identifying quantitative processes in metabolic systems. Of relevance to the research presented in this document is work using X-ray contrast medium as a tracer or indicator. Indicator-dilution techniques introduce an exogenous tracer into a flow system. By measuring the concentration of indicator (or dye) present in the system at a moment in time and comparing it to the amount injected into the inlet side of the system, estimates of flow field parameters can be extracted. A standard assumption in these techniques is that the indicator instantaneously mixes in the system, mass is conserved, and the concentration response is linear.

The Stewart-Hamilton equation states that a measure of the cardiac output from a mammalian heart is the quotient of an injected indicator's mass and the area under the curve of the indicator's concentration measurement:

$$CO = \frac{Mass}{AreaUnderCurve} = \frac{Mass_{indicator}}{\int_0^{\infty} c(t)dt} \tag{2.19}$$

Mahnken et al. conducted a feasibility study for determining cardiac output using X-Ray contrast medium as an indicator and a Multi-Detector CT scanner as a measurement device with 25 patients undergoing cardiac CTA [43]. Mahnken and colleagues injected each subject with 20 ml of non-ionic contrast medium followed by a saline chaser of 30 ml. Dynamic CT images (axial images were taken at one level of the thorax, and only at that level) were recorded in the ascending aorta for 38 seconds. The resulting time-density curves (Hounsfield units vs time) were fit to a gamma-variate function to correct for recirculation of contrast medium. Recirculated contrast manifests as an elevated baseline after the initial peak enhancement, and fitting the data to a gamma-function removes the excess signal after the peak enhancement.

After fitting the CT enhancement data to the gamma function, Mahnken computed the cardiac output for each subject using the Stewart-Hamilton equation as presented in equation (2.19). The Stewart-Hamilton derived cardiac output was compared to the cardiac output determined by calculating the stroke volume of the heart via volumetric analysis of the left ventricle using image data. Cardiac output was determined by multiplying the stroke volume by the averaged heart rate of the subject. Estimated cardiac output computed with both methods correlated well, with a Pearson's correlation coefficient of .87.

Mahnken and colleague also compared the test bolus analysis technique for cardiac output determination with the thermal dilution technique (the "gold" standard for invasive measurement of cardiac output) using Bland-Altman analysis and present animal results having

5-10% standard error between the CT image data derived cardiac output measurement. and the catheter measurements[44]

2.11 TRUNCATED SINGULAR VALUE DECOMPOSITION

Ostergaard et al. applied Fourier deconvolution and other deconvolution approaches to extracting the "residue" function, or impulse response of brain tissue between a feeding artery and a draining vein for assessment of ischemic stroke in Contrast Enhanced (CE) MRI perfusion [45]. Whereas the MRI perfusion application is different from the current problem, it has similarities to the contrast medium/patient identification problem in that measurements are made of a physiologic blood flow system using intravascular agents. Therefore similar noise processes would be expected. Ostergaard discovered that truncated Singular Value Decomposition (tSVD) was the most robust method for solving the tissue impulse response inverse problem, even when the SNR was < 10 [46]. Recently, Koh et al. [47] also demonstrated the robustness of tSVD in MR perfusion assessment using a novel technique to choose the Singular Value Decomposition's truncation index.

The goal of the tSVD (as is other deconvolution techniques) is to estimate **h**, given a noisy **y** measurement vector and a **U** matrix constructed from input samples, **u**.

$$\mathbf{y} = h * u + \varepsilon = \mathbf{H} \cdot \mathbf{U} + \varepsilon \tag{2.20}$$

and ε is assumed to be an iid random process. Before solving for **h**, **H** is decomposed into singular vectors (left **U** and right **V)** and a singular value matrix (Σ) via singular value decomposition:

$$\mathbf{H} = \mathbf{U}\Sigma\mathbf{V}^{T} = \sum_{i=1}^{n} u_i \sigma_i v_i^{T} \tag{2.21}$$

where Σ is a square matrix with the nonnegative singular values of **H** on the diagonal. A solution for **h** can be found by algebraic manipulation if **H** from equation (2.21) is inserted into equation (2.20). An obvious solution for **h** is:

$$\mathbf{h} = \mathbf{U}\Sigma\mathbf{V}^{T\ -1}\mathbf{y} \tag{2.22}$$

Small singular values, however, can amplify the noise present in the measurement vector. To limit the effect of noise, the rank of the equations can be reduced by ignoring singular values Σ greater than a threshold value. The solution vector for **h** is:

$$h_k = \sum_{i=1}^{k} \frac{u_i y_i}{\sigma_i} v_i \tag{2.23}$$

The rationale for proper selection of the truncation index, *k,* for a given problem must be considered, however. tSVD is a regularization technique - a nonparametric approach to solving ill-conditioned inverse problems in which one makes a tradeoff between data fitting and

smoothness of the solution. A standard regularization technique is Tikhonov's regularization that solves the following minimization problem (assuming the standard notation of a linear system **Ax=b)**:

$$\min \ \left\|\mathbf{A}x-\mathbf{b}\right\|_2^2+\lambda^2\left\|x\right\|_2^2 \tag{2.24}$$

where λ is the regularization parameter that weights the solution norm $\left\|x\right\|_2^2$ versus the residual norm $\left\|\mathbf{A}x-\mathbf{b}\right\|_2^2$. Hansen [48]demonstrated the connection between Tikhonov regularization and tSVD and how the solution of equation (2.24) can be expressed in terms of the SVD:

$$x_\lambda=\sum_{i=1}^{n}\left(\frac{\sigma_i^2}{\sigma_i^2+\lambda^2}\right)\frac{u_i\mathbf{y}}{\sigma_i}v_i \tag{2.25}$$

where σ_i are singular values, and λ is the regularization parameter. The first term in the summation is known as the Tikhonov filter factor. If the truncation index, k, from the tSVD is known, then the regularization parameter is $\lambda=\sigma_k$ where σ_k is the singular value at index *k*.

The L-curve is a log-log plot (Figure 13 is an example) of the solution norm versus the residual norm for various values of the regularization parameter. The (index) point of maximum curvature on the L-curve is used as the estimate of optimal trade-off between solution and residual errors. A drawback to this technique, however, is that sometimes a corner point is obscured by noise.

Koh et al. present an automated technique for finding the truncation index for the tSVD (and thus the regularization parameter $\lambda = \sigma_k$) by fitting piecewise linear curves to a log plot of the SVD's Fourier coefficients ($\left|u_i^T \mathbf{y}\right|$)versus the index of singular values. The log plot representation of the Fourier coefficients is called a Picard plot. In the presence of noise, the log of the Fourier coefficients in a Picard plot tend to monotonically decrease to a point at which the slope of the line decreases and begins to level-off (see the example in Figure 12). The index of the inflection or transition point, then, is the truncation index for the tSVD. The singular value at the index is used in the Tikhonov filter factor. Koh et al. determined the transition point by fitting two different linear models to the data in the Picard plot and using a sum of squared error criterion to determine the transition point.

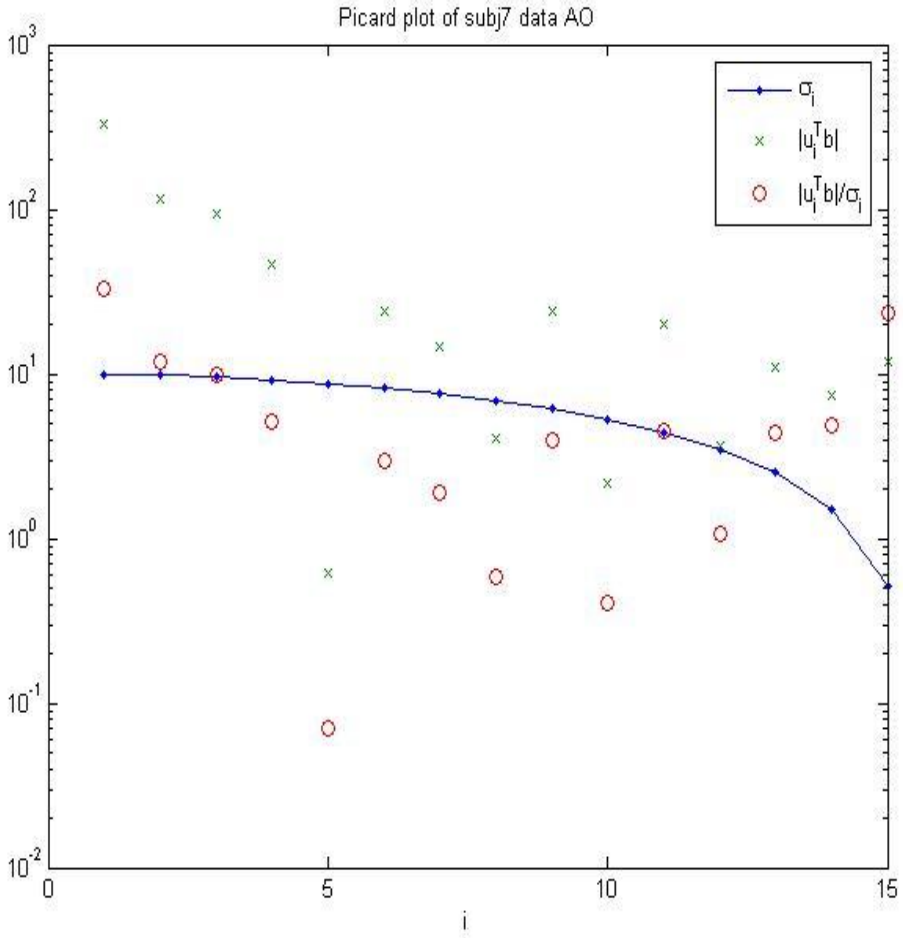

Figure 12 Example Picard plot using clinical data. The x axis is index value and the y-axis is a log transform of the Fourier coefficients $|u_i b|$ The singular values are plotted with diamonds and connected with a solid line.

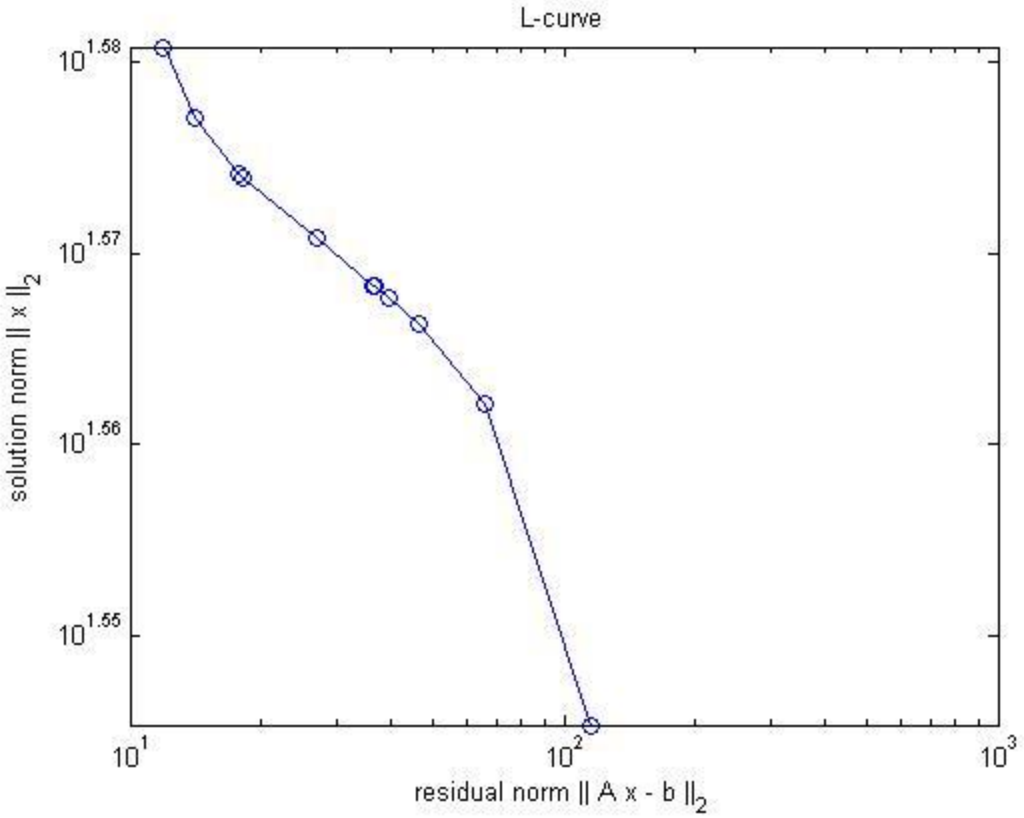

Figure 13 Example "L-curve" constructed with a clinical data set.

3.0 SPECIFIC AIMS OF THE RESEARCH

The primary goal of this research is the generation of methodology for infusing X-Ray contrast medium tailored to an individual patient's physiology, the pharmacokinetics of the drug, and the requirements of the contrast enhanced, imaging procedure. The infusion generation algorithm must also be cognizant of constraints pertinent to the patient's intravenous access and the desire to use the minimum contrast agent sufficient to achieve image contrast enhancement. The specific aims of this dissertation are:

1) **To develop a new, physiologic based pharmacokinetic model of contrast propagation.** The model will improve upon the work of Bae and Krause [6] [31] by incorporating explicit transport delays in its formulation, by including a non-linear saturation in the input, by including the saline flush effect on the contrast propagation, and by using fewer states than Bae's full body model. This new model will be used in developing and validating a new infusion paradigm in which a data-driven model will predict a patient's response to contrast agent. Potentially, the new model may be used in predicting the behavior of other radiological pharmaceuticals (future work). The new model structure will be simulated with parameters used by Bae et al in [6]. The predicted enhancements in the Left Heart compartment for the new PBPK model will be compared to those made by the Bae model. It is expected that the *de novo* technique presented here will match those of the Bae full body

model. Finally, retrospective clinical imaging data will be used to compare the performance of the new model with the Bae model.

2) **To develop and test system identification techniques for the contrast/human system based on individual scan data.** Two classes of identification schemes will be explored and developed. Both strategies are predicated on an identification operation; the drug/patient system is perturbed with a small infusion of drug and the response is recorded with the imaging system. In both instances, a discrete time realization of the system model must be generated.

    a) **Model based (or parametric)** The model based identification strategy will perform a maximum-likelihood parameter estimation to fit parameters to a Physiologic Based Pharmacokinetic (PBPK) model describing the dynamics of the drug in an individual patient's cardiovascular system. The identified LTI model will be used in the subsequently developed patient-specific infusion strategy.

    b) **Model Independent (or non-parametric)** The model independent identification strategy will generate a non-parametric estimate of the drug/patient system by solving an inverse problem using the truncated Singular Value Decomposition (tSVD) deconvolution technique.

3) **To develop and implement a rational technique for computing individual, optimal contrast protocols based on an identified model (using scan data) for a subject** - A constrained optimization will be performed to compute a minumum volume of drug necessary to achieve contrast enhancement above a clinically significant threshold (e.g. >= 300 HU) in the cardiovascular anatomy throughout

the duration of a diagnostic CT scan. The physical constraints of the injection, drug and patient system will be explicitly enforced. In addition to non-negative injection flow rates, the maximum injection flow rate will be set according to the radiologist's preference or from recognition of the pressure to flow-rate relationship inherent in the injection system's fluid path (ie: the higher a flow rate, more pressure is generated in the syringe and fluid path). Furthermore, the maximum volume of contrast fluid that can be delivered to the patient will be adjustable. With the constraints enforced, the algorithm will compute the maximum contrast enhancement achievable for a specific patient, drug formulation, and injection system configuration. The ability to prospectively obtain a patient specific enhancement bound by constraints differs from and improves upon the Fleischmann and Hittmair approach [9].

4) **To create a novel, CT compatible, cardiovascular flow phantom system for repeated scanning and validation of the developed identification and protocol generation strategies.** The developed contrast protocol computation methods will be implemented and targeted to a prototype drug delivery system. The delivery system will deliver contrast medium into a realistic, cardiopulmonary mock-flow loop. The flow loop will provide pulsatile flow of a blood emulant, into which contrast agent will be injected. Obviously, repeated injections and scanning of human patients is not possible. Likewise, it is desirable to minimize or eliminate the amount of animal testing needed to validate the new contrast delivery paradigm. This realistic, cardiovascular flow phantom will enable repeated experiments for validation of the resulting models, identification and optimization methods. The

dynamics of the flow loop and kinetics of the drug will allow for realistic simulation of the injected contrast media's intravascular transport and distribution. Laboratory sensors and contrast emulant will be calibrated against results acquired with a CT scanner.

4.0 A NEW PATIENT SPECIFIC PHARMACOKINTEC MODEL

A physiologically based, pharmacokinetic (PBPK) model is developed combing elements of Bae's [6] [3] and Wada's [34] models. The new formulation incorporates parameterized transport delays of the contrast material from the injection site into the central circulation, models the effect of a saline "push" after the infusion of the main bolus of diagnostic contrast material, and is formulated so that the model can be discretized (when linearized and time-varying terms are adjusted) for use as a plant model in future research investigating model predictive control techniques. The model shares a similar structure to the Bae reduced model, however, but differs in that it includes a saturating non linearity on the input function and a time-varying formulation of the peripheral vascular compartment. In subsequent chapters, the model is used to develop and test patient-specific identification schemes.

4.1 DESCRIPTION OF THE MODEL

In Bae's models, there is no consideration for implementation of the PK models in a controller framework. When converting the differential equation system of (2.9) into a state-space form, the rank of the resulting state matrix (**A**) is less than the order of the system because of the number of free parameters in the system formulation. This rank deficiency manifests itself as a singularity when attempting to invert the matrix and is problematic for digital representation of

the system for prediction and control. The Bae models do not address transport delays of the contrast material directly, but model the transport delay by introducing multiple, in series sub-compartments throughout the cardiopulmonary model. The multiple sub-compartments provide a propagation delay in the simulated output because the new phase response of the system is different (additive) due to the additional compartments. The introduction of the multiple compartments is somewhat arbitrary, albeit based on physical insight of the vascular system. For example, the lung compartment is divided into 30 sub-compartments because of the contrast bolus dispersion and delay through the cardiopulmonary system.

To overcome the mathematical difficulties intrinsic to the Bae models, a modeling approach similar to that of Wada and Ward [34] (see Section 2.7) is taken. The Wada and Ward model can be transformed into the discrete-time domain and allows for the explicit introduction of transport delays in the drug dynamics (ie: propagation time of contrast through the pulmonary vasculature). A PBPK strategy is adopted in which consideration is given to describing the distribution of drug in the vascular structures throughout the body because the focus is for predicting enhancement during the arterial phase of contrast distribution. Because the model developed here combines the topology of the Wada and Ward model with the parameterization of the Bae contrast model, it will be referred to as the "hybrid" model. In addition to incorporating explicit transport delays into the model structure and a saturating non-linearity in the input compartment, the new hybrid model also allows for the simulation of saline injection after the main contrast bolus. The Bae model does not model the effects of the saline flush on *in vivo* contrast enhancement.

4.1.1 Model Structure

The compartments of the new contrast media model are shown in **Figure 14**.

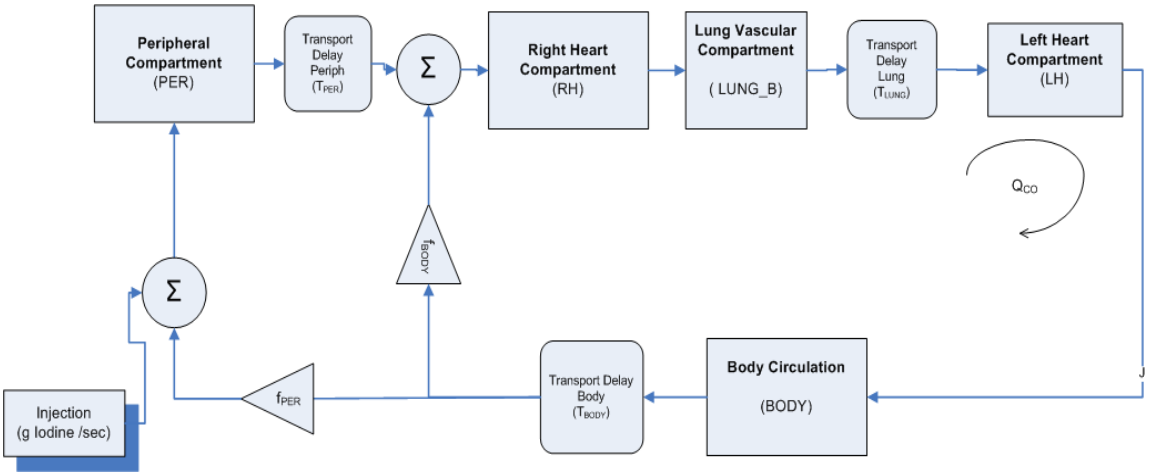

Figure 14 Model structure of the new PK model describing contrast medium propagation.

Each subsystem in the model represents an anatomical region of the body. As described in Chpater 2, subsystems in PBPK models are split into three compartments – the intracellular, extracellular and intravascular spaces (see Figure 9). Contrast material does not enter the intracellular space and so it is ignored in PBPK models of contrast medium propagation. The notation used by Wada is adopted (see section 2.7) throughout the development below.

The state variable, *x*, for the hybrid PBPK model is the mass of the contrast medium in a compartment (x_i). The volumetric flow rate of blood/contrast in an i^{th} compartment is denoted by Q_i, and volumes are denoted by the variable V_i. The clearance of contrast medium from a subsystem, *Cl*, occurs via an irreversible process. Extraction of contrast medium occurs via glomerular filtration through the kidneys.

Because this model is intended for studying and predicting the distribution of contrast medium during CT angiography, quantifying the blood plasma concentration during the first-pass of the agent into the body is of primary concern and there is less interest in describing the absorption and distribution of the contrast material as it diffuses through systemic organs and parenchyma, with the exception of the lung subsystem. The model only considers the vascular compartments of the peripheral veins, the right and left heart, and the systemic circulation.

The mass "flux" (J) in or out of a compartment of the model is:

$$J_i = \frac{Q_i}{V_i} x_i \tag{4.1}$$

where *Q* is the volumetric flow rate and *V* is the apparent volume of the compartment. The flow fractions, f_{BODY}, and f_{PER} scale the cardiac output through the respective body segments. A summation of the flow fractions must equal the cardiac output, Q_{CO}: $f_{PER}Q_{CO} + f_{BODY}Q_{CO} = Q_{CO}$. For vascular compartments in this model, the apparent volume is the intravascular blood volume. Application of mass balance in the subsystems of the model results in the following global expression for the subsystems in **Figure 14**, Peripheral, Lung, Right Heart, Left Heart, and Body (i = 1:5)

$$\dot{x}_i \;\; t \;\; = \left[\left(\frac{-Q_i + Q_{exog}}{V_i} \right) x_i(t) + k_{ji} x_j(t) - k_{ij} x_i(t) \right] + 1 \cdot \left(\left(\sum_{j=1}^{N} y_{i-j}(t) \right) + u_{exog}(t) \right)$$

$$y_i(t) = \frac{Q_i}{V_i} x_i \tag{4.2}$$

where $u_{exog}(t)$ is the exogenous administration of contrast medium. It is non-zero only in the peripheral compartment and is defined by:

$$u_{exog}(t) \equiv C_{inj}(t) \cdot Q_{inj}(t) \tag{4.3}$$

because the administration flow rate, $Q_{inj}(t)$, or the concentration of the administered contrast agent, $C_{inj}(t)$, can be varied as a function of time. The product of volumetric flow rate and contrast concentration is termed the iodine administration rate. Predictions of concentration in the various compartments of the model are made by dividing the state-variable (mass units) by the effective blood volume in the respective compartment.

4.1.1.1 Peripheral subsystem Contrast agent is injected into a peripheral vein in the left or right arm of a human. The endogenous flow rate of blood draining through the peripheral veins in the arm ranges from 2- 4 ml/s [6]. The flow rates typical with CTA examinations are greater than the endogenous flow rate of blood draining through the peripheral veins. In the model, therefore, the injection of contrast into the peripheral veins results in an additive contribution to the endogenous flow rate through the veins, which was also a consideration made by Bae in [4]. Mathematically, the peripheral venous subsystem is a linear time-varying formulation of mass balance in the peripheral subsystem due to the injection of the contrast:

$$\dot{x}_{PER}(t) = \frac{-\,Q_{PER}(t)}{V_{PER}} x_{PER}(t) + u_{exog}(t) + y_{BODY}(t - T_{BODY}) f_{PER}$$

with

$$Q_{PER}(t) = Q_{PER\_END} + Q_{inj}(t) \tag{4.4}$$

where Q_{PER_END} is the endogenous flow rate of blood through the peripheral vein and T_{BODY} is the transport delay of contrast recirculating through the entire body back through the peripheral veins. The general solution to (4.4) is:

$$x_{PER}(t) = \int_0^t u_{exog}(\tau) e^{V_{PER}\int_0^t \frac{1}{Q_{PER}(x)}dx} d\tau e^{\int_0^t \frac{-V_{PER}}{Q_{PER}(\tau)}d\tau} \tag{4.5}$$

To avoid formulating a time-varying model, (4.4) can be rewritten considering that after the injection, $Q_{PER}(t) = Q_{PER\_END}$ and that during the injection the flow rate is the sum of $Q_{PER\_END}+Q_{Inj}$. The transport delays introduced by the circulatory system are denoted by T_{PER} and T_{BODY} and represent the output delays of the contrast agent from the peripheral and body subsystems. The time delays can be constants or functions of the volume and flow rate of blood in the respective systems. Details concerning the time delays are discussed in section 4.1.2. In the subsequent development, T_{inj} represents the duration of the contrast injection.

Under these assumptions, the peripheral subsystem dynamics can be expressed in standard LTI, state-space formulation as:

$$\left.\begin{aligned} \dot{x}_{PER}(t) &= \frac{-Q_{PER\_END}+Q_{inj}}{V_{PER}}x_{PER}(t)+u_{exog}(t-T_{PER})+y_{BODY}(t-T_{BODY})\cdot f_{PER} \\ y_{PER}(t) &= \frac{Q_{PER\_END}+Q_{inj}}{V}x_{PER}(t) \end{aligned}\right\} \text{for } t \le T_{inj}$$

$$\left.\begin{aligned} \dot{x}_{PER}(t) &= \frac{-Q_{PER\_END}}{V_{PER}}x_{PER}(t)+u_{exog}(t-T_{PER})+y_{BODY}(t-T_{BODY})\cdot f_{PER} \\ y_{PER}(t) &= \frac{Q_{PER\_END}}{V}x_{PER}(t) \end{aligned}\right\} \text{for } t > T_{inj} \qquad (4.6)$$

where $y_{PER}(t)$ is the mass flux (units gI/s) of contrast exiting the peripheral subsystem. The concentration in the peripheral subsystem is $x_{PER}(t)$ divided by the blood volume in the peripheral veins.

A saturating behavior affects the injection flow rate into the peripheral compartment. Empirical evidence suggests that injections greater than 8-10 ml/s saturate because of the compliant nature of the peripheral veins or because of reflux of contrast through the right atrium into the inferior vena cava [10]. The most general description of the peripheral compartment dynamics, therefore is:

$$\begin{aligned} \dot{x}_{PER}(t) &= \frac{-Q_{PER}(t)}{V_{PER}}x_{PER}(t)+u_{exog}(t-T_{PER})+y_{BODY}\ \ t-T_{BODY}\ \ f_{PER} \\ y_{PER}(t) &= \frac{Q_{PER}(t)}{V_{PER}(t)}x_{PER}(t) \end{aligned} \qquad (4.7)$$

where the non-linear exogenous input function is a function of both flow rate and time:

$$\begin{aligned} u_{exog}(Q_{inj}, t) &= Q_{inj}(t) \cdot C_{inj}(t) \quad Q_{inj}(t) \le 8[ml/s] \\ u_{exog}(Q_{inj}, t) &= 8 \cdot C_{inj}(t) \quad\quad Q_{inj}(t) > 8[ml/s] \end{aligned} \tag{4.8}$$

4.1.1.2 Right Heart Subsystem Conservation of mass applied to the Right Heart subsystem in Figure 14 is:

$$\begin{aligned} \dot{x}_{RH}(t) &= \frac{-Q_{CO}}{V_{RH}} x_{RH}(t) + y_{PER}(t - T_{PER}) + y_{BODY}(t - T_{BODY}) f_{BODY} \\ y_{RH}(t) &= \frac{Q_{CO}}{V_{RH}} x_{RH}(t) \end{aligned} \tag{4.9}$$

4.1.1.3 Lung Subsystem The lung subsystem differs from the pure vascular subsystems in that the role of permeability between the capillary bed and the lungs is modeled. Consideration of the tissue compartment is made for completeness and for anticipated future work in which the effect of recirculation and accumulation of contrast in tissue will be of interest.

$$\begin{aligned} \dot{\mathbf{x}}_{\mathbf{LUNG}}(t) &= \begin{pmatrix} \frac{-Q_{CO}}{V_{LUNG\_B}} & -k_{LUNG\_BT} \\ k_{LUNG\_BT} & -k_{LUNG\_TB} + CL_{LUNG\_T} \end{pmatrix} \mathbf{x}_{\mathbf{LUNG}}(t) + y_{RH}(t) \\ y_{LUNG}(t) &= \left[\frac{Q_{CO}}{V_{LUNG\_B}} \right] \mathbf{x}_{\mathbf{LUNG}}(t) \end{aligned} \tag{4.10}$$

where Q_{CO} is the cardiac output, k_{LUNG_BT} is the rate transfer coefficient of contrast from the blood compartment into the tissue compartment, k_{LUNG_TB} is the rate transfer coefficient from the tissue compartment back into the blood compartment, and CL_{LUNG_T} represents an irreversible clearance term out of the tissue compartment.

4.1.1.4 Left Heart Subsystem The delay of contrast through the pulmonary vasculature is modeled as an input delay term in the dynamics of the Left Heart subsystem:

$$\begin{aligned} \dot{x}_{LH}(t) &= \frac{-Q_{CO}}{V_{LH}} x_{LH}(t) + y_{LUNG}(t - T_{LUNG}) \\ y_{LH}(t) &= \frac{Q_{CO}}{V_{LH}} x_{LH}(t) \end{aligned} \tag{4.11}$$

and $y_{LUNG}(t)$ is the mass flux of contrast exiting the Lung subsystem. T_{LUNG} is the delay time of the bolus travelling through the pulmonary vasculature. It can be a scalar constant or a function of the cardiac output and blood volume in the lung.

4.1.1.5 Body Subsystem First-pass distribution and propagation of the contrast bolus is of primary interest for CT angiography applications. Because the organs, muscle, and fat compartments affect the distribution of the contrast after several recirculation times, they are not considered in the current model description. Bae [4, 16] and others combined the systemic circulation into one, large vascular compartment and is modeled in that fashion here.

$$\dot{x}_{BODY}(t) = \frac{-Q_{CO}}{V_{BODY}} x_{LH}(t) + y_{LH}(t)$$
$$y_{BODY}(t) = \frac{Q_{CO}}{V_{BODY}} x_{BODY}(t) \tag{4.12}$$

4.1.1.6 State Space Formulation A unified formulation of the model, combining Equations (4.4) through (4.12) is now given to ease implementation in numerical simulations. For notational convenience and to ensure that transport delays only appear as input and output delays, an augmented state vector comprised of state variables for each of the sections of the model is defined. The Right Heart, Lung and Left Heart subsystems are combined into a Cardiopulmonary (CP) state vector:

$$\mathbf{x_{Aug}} = [x_{PER}\ \mathbf{x_{CP}}\ x_{BODY}] \tag{4.13}$$

where the Cardiopulmonary (CP) state vector consists of the Right Heart, Lung and Left Heart state variables:

$$\mathbf{x_{CP}} = [x_{RH}\ x_{LUNG}\ x_{LH}] \tag{4.14}$$

The total system is expressed as:

$$
\begin{aligned}
\dot{x}_{PER} &= A_{PER}x_{PER} + \mathbf{B}_{PER}\mathbf{u}_{PER} \\
y_{PER}(t) &= C_{PER}x_{PER}(t) \\
\dot{\mathbf{x}}_{\mathbf{CP}} &= \mathbf{A}_{\mathbf{CP}}\mathbf{x}_{\mathbf{CP}} + \mathbf{B}_{\mathbf{CP}}(y_{PER}(t) + y_{BODY}(t - T_{BODY})) \\
y_{CP}(t) &= \mathbf{C}_{\mathbf{CP}}\mathbf{x}_{\mathbf{CP}}(t) \\
\dot{x}_{BODY} &= A_{BODY}x_{BODY} + B_{BODY}y_{CP}(t - T_{LUNG}) \\
y_{CP}(t) &= C_{BODY}x_{BODY}
\end{aligned}
\tag{4.15}
$$

The input vector to the peripheral subsystem is composed of the exogenous contrast media injection through a peripheral vein and the recirculated contrast from the body subsystem:

$$
\mathbf{u}_{PER} = \begin{bmatrix} \varphi(u_{exog}(t - T_{PER})) & y_{BODY}(t - T_{BODY})f_{PER} \end{bmatrix}
\tag{4.16}
$$

The blood-plasma concentration of the contrast in the body subsystem is scaled by a flow fraction, f_{PER}. The scalar function, $\varphi(u_{exog})$ in (4.16) defines the saturating non-linear behavior of the venous system between the injection site and the right heart described in (4.8).

$$
\varphi(u_{exog}) = \begin{cases} u_{exog}(Q_{inj}, t) = Q_{inj}(t) \cdot C_{inj}(t) & Q_{inj}(t) \le 8[ml/s] \\ u_{exog}(Q_{inj}, t) = 8 \cdot C_{inj}(t) & Q_{inj}(t) > 8[ml/s] \end{cases}
\tag{4.17}
$$

The state matrices are:

$$
A_{PER} = \frac{-Q_{PER}(t)}{V_{PER}}
\tag{4.18}
$$

$$\mathbf{A}_{CP} = \begin{bmatrix} \frac{-Q_{CO}}{V_{RH}} & 0 & 0 & 0 \\ \frac{Q_{CO}}{V_{RH}} & \frac{-Q_{CO}}{V_{LUNG\_B}} & -k_{LUNG\_BT} & 0 \\ 0 & k_{LTB} & -k_{LUNG\_TB} + Cl_{LT} & 0 \\ 0 & \frac{Q_{CO}}{V_{LUNG\_B}} & 0 & \frac{-Q_{CO}}{V_{LH}} \end{bmatrix} \tag{4.19}$$

$$A_{BODY} = \frac{-Q_{CO}}{V_{BODY}} \tag{4.20}$$

where the time varying flow through the peripheral circulation, $Q_{PER}(t)$ is defined in (4.4). The control (B's) and output (C's) are presented below, followed by an all-integrator view of the model in **Figure 15**.

$$\mathbf{B}_{PER} = \begin{bmatrix} 1 & 1 \end{bmatrix}^T \tag{4.21}$$

$$\mathbf{B}_{CP} = \begin{bmatrix} 1 & 0 & 0 & 0 \end{bmatrix}^T \tag{4.22}$$

$$B_{BODY} = 1 \tag{4.23}$$

$$C_{PER} = \left[\frac{Q_{PER}(t)}{V_{PER}} \right] \tag{4.24}$$

$$\mathbf{C}_{CP} = \begin{bmatrix} 0 & 0 & 0 & \frac{Q_{CO}}{V_{LH}} \end{bmatrix} \tag{4.25}$$

$$C_{BODY} = \left[\frac{Q_{CO}}{V_{BODY}} \right] \tag{4.26}$$

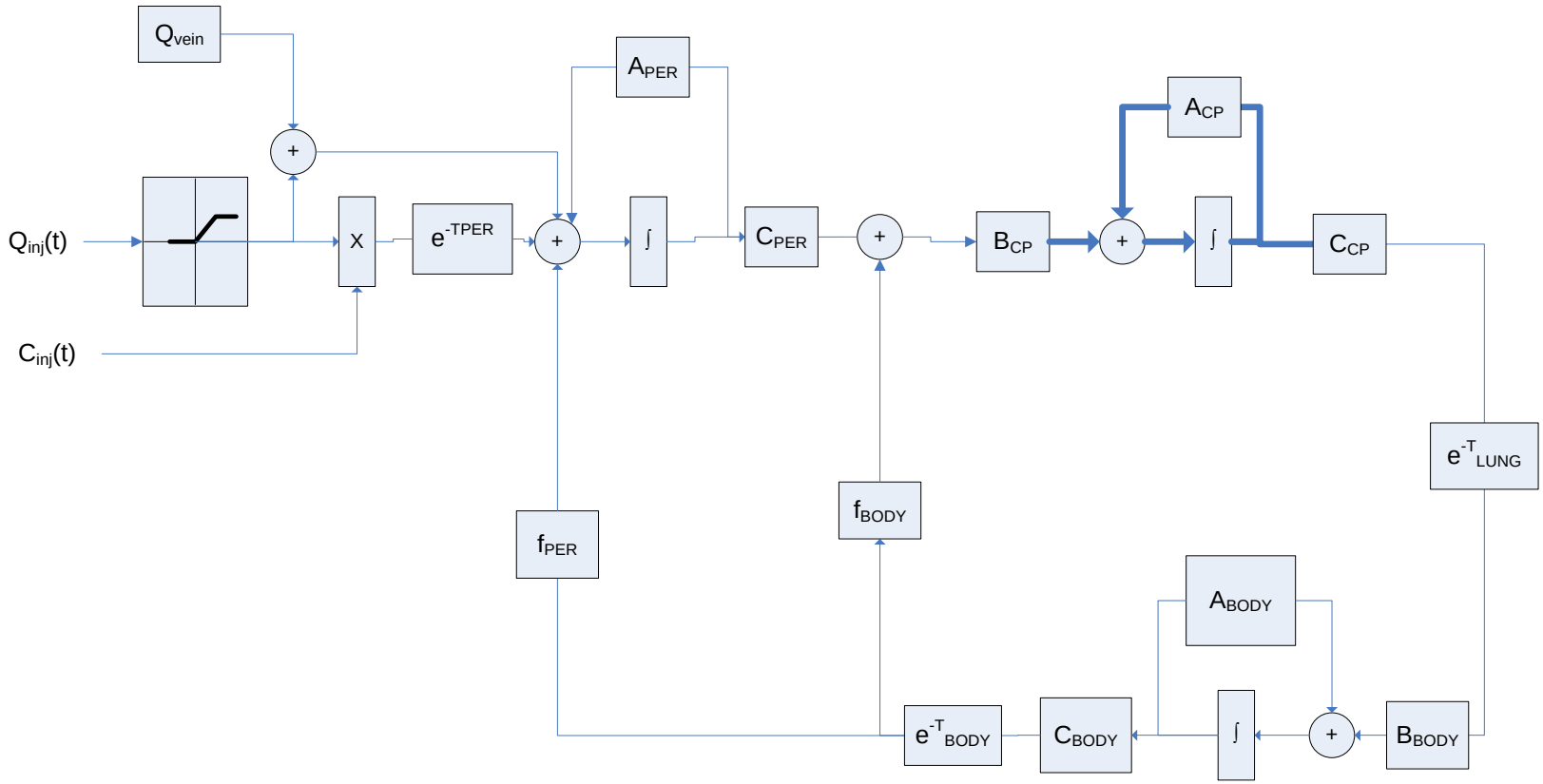

Figure 15 All-integrator view of the physiologic based pharmacokinetic model developed in this section. The thick lines in the "CP" section denotes vector quantities. The matrix values in the figure are those defined in equations (4.18) through (4.26).

4.1.2 Parameter Selection

In choosing model parameter values for numerical simulations, a balance between fidelity and realizability must be made. It is difficult to deduce parameter values for each sub-compartment which match the true, physiological parameters for an individual. The direction taken in this work follows that of Bae [6, 33] and Wada and Ward [34]– reliance upon standard, physiologic "look up" tables and relationships determined via regression analyses on population data. In Chapter 5, PBPK model identification methods using test bolus enhancement data from patients are developed. The simulations performed in this chapter use parameter values based solely on demographic data (height, weight, sex, age) and procedure specific values such as flow rate, volume and concentration of the contrast material.

4.1.2.1 Cardiac Output and Central Blood Volume Estimators Bae et al. used Guyton's [49] regression formulae, corrected for age, to estimate cardiac output and blood volume. The cardiac output estimation method of Bae is adopted here and provides the cardiac output estimation when the hybrid model is simulated. The estimator is:

$$\hat{CO}(h, w, a) = 36.36 \cdot h^{.725} \cdot w^{.425} \quad 1 - .005 \quad a - 30 \tag{4.27}$$

where the parameters *h*,*w*, and *a* are height [inches], weight [lbs] and age [years]. The central blood volume estimator in the model is, likewise, derived from a published regression formula and is a function of height, weight, and sex. The estimated blood volume for males is:

$$\hat{BV}(h,w) = 33.164 \cdot h^{.725} \cdot w^{.425} - 1229 \tag{4.28}$$

and for females:

$$\hat{BV}(h,w) = 34.850 \cdot h^{.725} \cdot w^{.425} - 1954 \tag{4.29}$$

.

4.1.2.2 Regional Blood Volume Estimates The regional blood volume parameters throughout the hybrid model must equal the total blood volume estimated by equation (4.28) or(4.29). With the exception of the peripheral compartment, the volumetric flow rate of blood through the model is the cardiac output computed by equation (4.27). Blood volumes in the different sub-systems are also set according to the relationships used by Bae et al [6], with one modification. Instead of setting the Left Heart blood volume to 3.6% of the total blood volume as by Bae et al., an additional 100 ml of blood is added in the hybrid PBPK model so as to include the ascending aorta in the computations. The procedure for configuring the blood volumes for a given subject is to compute an estimate of cardiac output and blood volume using height, weight, age and sex. The regional blood volumes are then computed using the relationships in Table 1.

Table 1 Regional blood volume parameters used in the model simulation

Parameter	Value [Units]
V_{PER}	.08*BV(*h,w,sex*)[ml]
V_{RH}	.036*BV(*h,w,sex)[ml]*
V_{LB}	.088*BV(*h,w,sex*)[ml]
V_{LH}	.056*BV(*h,w,sex*)[ml]
V_{SYS}	.848*BV(*h,w,sex*)[ml]

Additional model parameters include the rate transfer coefficients between the lung, blood and tissue compartments and contrast clearance from the central blood compartment. Because extraction of contrast material from the blood supply and tissue compartments occurs minutes after bolus injection, clearance terms (C_{LUNG_T}) are set to zero. Likewise, on the first

pass of contrast material, there is little passage of contrast material through the pulmonary capillary bed, and subsequent accumulation into the tissue is minimal. The pulmonary transfer rate constants are therefore set to zero. Bae et al. made a similar assumption in their reduced-order model in [33] in which the pulmonary compartment is purely vascular and consists of many sub-compartments to model the transport of contrast through phase delays.

The final parameters considered are the contrast bolus propagation delays through the peripheral venous circulation (T_{PER}), the propagation time through the pulmonary system (T_{LUNG}), and the recirculation delay of a bolus throughout the entire circulatory system (T_{BODY}).

The system recirculation delay is held constant at 30 seconds, as used by Wada and Ward [34]. Consideration of per-patient values, however, is made for the other two propagation delays. T_{PER} is a function of the blood volume in the peripheral venous sub-system and the sum of injection rate and endogenous venous flow. Likewise, the propagation delay through the pulmonary compartment is a function of the pulmonary blood volume and the estimated cardiac output for each subject. The transit delays used in the model are given in Table 2.

Table 2 Transit delay parameters

Parameter	**Value [Units]**
T_{PER}	$\frac{\left(\frac{V_{PER}}{2}\right)}{Q_{vein}+Q_{Inj}}$ [sec]
T_{LUNG}	$\frac{V_{LUNG\_B}}{Q_{CO}}$ [sec]
T_{BODY}	30 [sec]

4.2 SIMULATION METHODS AND RESULTS

Performance of the model as a function of various parameters and inputs is presented in the following sections and compared to predictions by the Bae model (both published and resulting from an implementation of the model in Simulink). The hybrid model's ability to predict contrast enhancement in a human data set is described section 4.3 and is also compared to Bae model predictions.

4.2.1 Simulation results from the hybrid model

This section presents the results of experiments in which injection parameters and model parameters were varied to demonstrate the model's ability to mimic known behaviors of contrast dynamics. Simulations demonstrating the model's ability to reproduce the effect of varied cardiac output on contrast enhancement were conducted. The saturating behavior of contrast enhancement as injection rates increase was demonstrated via simulation of the model as were the effects of saline flush after the contrast medium injection.

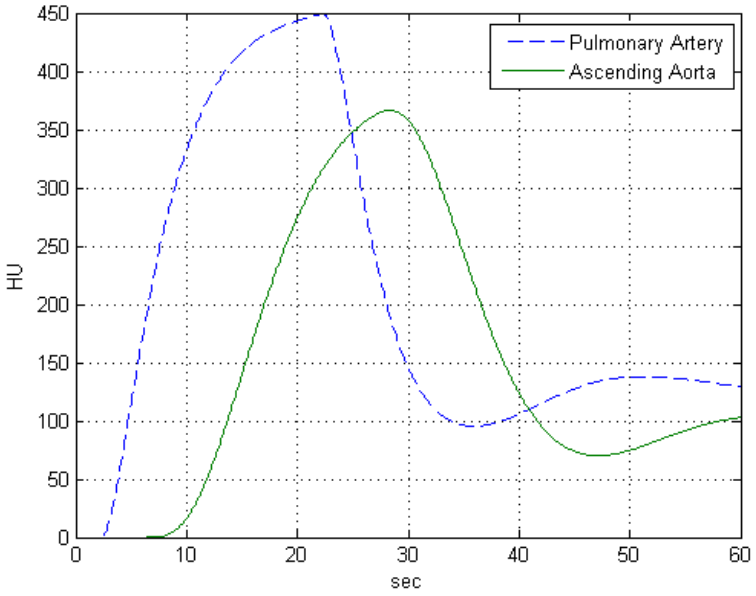

Figure 16: Simulated contrast enhancements for a normal subject.

Figure 16 presents simulated contrast enhancement in the pulmonary artery and ascending aorta for a virtual patient with nominal attributes. The model was implemented and simulated in MATLAB (R2008b). The patient parameters for this example were, weight=170 lbs, height = 68 in, sex=Male, age = 35 years. Using equation (4.27), the estimated cardiac output was 6.60 L/min. The injection protocol consisted of contrast with 370 mgI/ml concentration contrast agent, injected at a volumetric flow rate ($Q_{inj}(t)$) of 5 ml/s for 20 seconds (volume = 100 ml). Following the contrast injection, a 30 ml volume of saline was injected at 5 ml/s for 6 seconds. Note the enhancement in the ascending aorta peaks 5-6 seconds after maximum enhancement in the pulmonary artery as expected. Likewise, the enhancement level in the ascending aorta compartment is ~100 HU below that in the pulmonary artery as expected because the bolus was diluted between the pulmonary trunk and the ascending aorta. One can appreciate the systemic recirculation of the contrast material by noting the secondary contrast

enhancement peak in the pulmonary artery at 50 seconds and the appearance in the ascending aorta of a secondary peak near 60 seconds.

Another series of simulations was conducted in which contrast injection parameters were held constant across a set of simulated patient parameters to demonstrate the model's ability to replicate the influence of cardiac output on contrast enhancement. The injection parameters were: 370 mgI/ml concentration contrast injected at 5 ml/s for 10 seconds (volume = 50 ml) followed by a saline flush phase of 30 ml at 5 ml/s. The cardiac output of the simulated patient was adjusted from a low value (3 L/min) to a high value (8 L/min) in 1 L/min increments. This experiment assumed that the cardiac output can be manipulated independently of the blood volume. The blood volume for the patient was held constant for each of the cardiac output values (using the same parameters as in the previous experiment: a 170 lb, 68 inch, 35 year old male). A shorter injection duration than in the previous example was used to avoid any recirculation phenomena at the low cardiac output values.

The peak contrast enhancement level in the ascending aorta and the time of maximum contrast enhancement were recorded and are graphically presented in **Figure 17**. We expect to find that as the cardiac output increases, the arrival time of the contrast bolus in a vascular territory decreases. Likewise, as the cardiac output increases, we expect the contrast enhancement in the vascular structure to decrease as demonstrated theoretically and empirically by Bae and others [4, 10, 50].

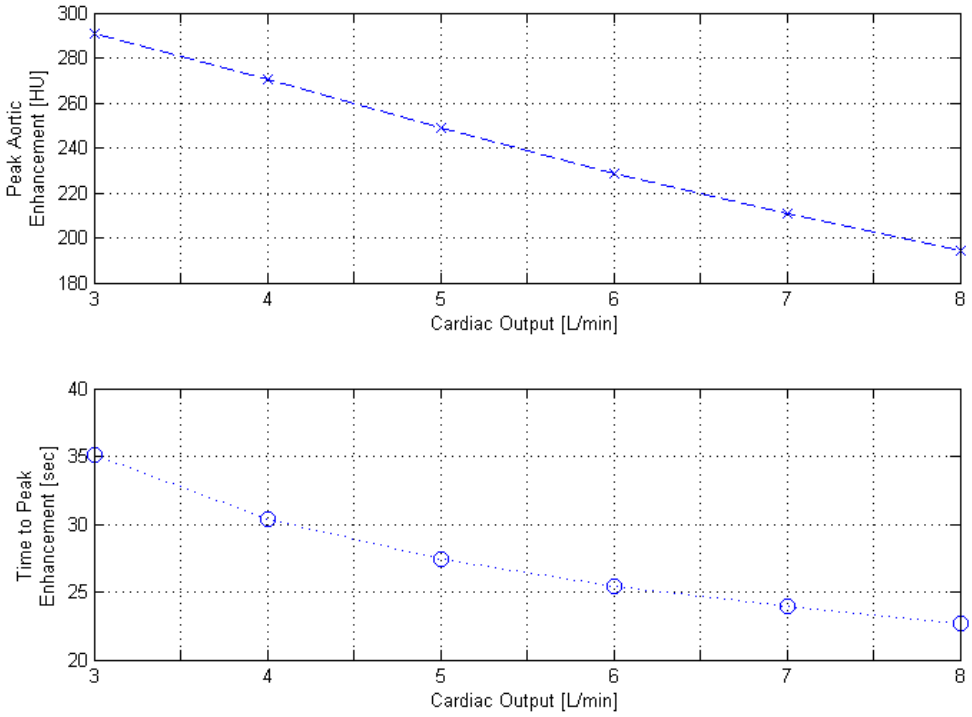

Figure 17 Simulated peak aortic enhancements and times to peak aortic enhancement plotted as functions of cardiac output in the hybrid model

The hybrid model was also simulated in MATLAB/Simulink using a virtual, 35 year old male, 68 inches tall and weighing 170 lbs. with three different injection protocols of 5 ml/s of 370 mgI/ml contrast for 10 seconds (volume = 50 ml), followed by a saline chaser at 5ml/s over 6 seconds (volume = 30 ml), a saline chaser at a flow rate of 2.5 ml/s over 6 seconds (volume = 15 ml), or no saline chaser. The resulting time enhancement curves are shown in **Figure 18**. The simulations demonstrated a 14% increase in peak aortic enhancement for the protocol in which a saline flush was injected at the same flow rate of the contrast bolus. The time to peak enhancement was also delayed by 0.8 seconds. For the injection in which the saline was injected at half the flow rate of the contrast bolus, the increase in peak enhancement was 7% greater than

when no saline flush was administered. The peak enhancement time was increased by 0.6 seconds. These results cannot be replicated with the Bae models because these models are not formulated (as published) to allow consideration of the effects of a saline chaser after the administration of the contrast bolus. The results demonstrated qualitative agreement of the model response with results demonstrated by Lee [17] and others in animal models and humans.

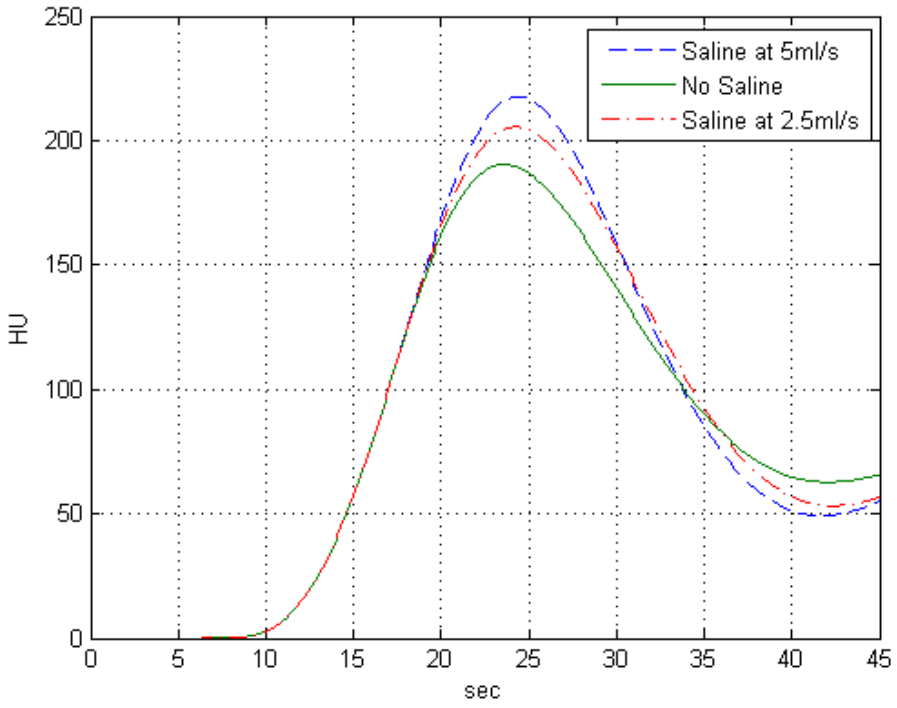

Figure 18 Simulation results demonstrating the model's ability to simulate the effect of saline flusi injections.

4.2.2 Comparison of results between the hybrid model and published Bae Data

Concordance between the hybrid model results and Bae models is now presented. Aggregate data from a test cohort published by Bae et al in [6] facilitated the performance comparison. The patients were enrolled into three groups based on contrast injection protocol. There were three contrast protocols used in the study: a biphasic low-flow rate protocol, a uniphasic low-flow rate protocol, and a uniphasic high-flow rate protocol. A saline flush phase was not used in any of the groups because the technique was not widely practiced when the study was performed (1997).

The data from the uniphasic, high-flow rate cohort were used for evaluating the hybrid model. In that group, the mean body weight of the 27 subjects was 177 lb and the range of values was 44.1 to 135.0 lbs. The contrast protocol consisted of injecting 320 mgI/ml contrast at 5.0 ml/s for 25 seconds (volume = 125 ml). The heights, sex and age composition of the subject sample were not reported, but the authors used an average height of 68 inches and male sex when simulating their model. Single level scanning was performed on each of the subjects at the mid-abdominal aorta every 15 seconds for 120 seconds, and then once every 60 seconds up to 300 seconds. TECs were created by the investigators after placing a $1cm^2$ ROI on the abdominal aorta at the celiac axis and another one on the liver parenchyma.

The hybrid model was executed in MATLAB/Simulink. Because the empirical results were collected to 300 seconds, the contrast has sufficient time to recirculate through the vascular system. Clearance terms were added into the model to ensure adequate downslope/recirculation dynamics in the TECs. A typical Glomerular Filtration Rate (GFR) was set in the simulation of the Bae model (nominally 50-70 ml/min) as a clearance term set to 19% of the blood's volumetric flow-rate in the simulated renal artery.

The new model does not contain a kidney compartment and the mechanism to mimic clearance is through the lung compartment. In the simulation comparing the published Bae empirical data, a blood-tissue transfer coefficient (k_{LUNG_BT}) of .08 sec^{-1} and a compartment clearance value (CL_{LUNG_T}) of .1 sec was used to approximate a 60 ml/min clearance rate because no meaningful physiologic process for this problem has a time scale shorter than 1 second. Too short a time step results in an inefficient simulation because excess time is taken to deliver equivalent results to what would be obtained with a longer time step. Simulations conducted at times steps of .01 and .001 revealed no difference in predicted enhancements.

Hybrid model simulation results using the aggregate patient data from the Bae study are shown in **Figure 19** alongside the results from the aggregate enhancement data. Simulations were performed with a fixed-step solver (Runge-Kutta) and a step-time of .1 seconds. The enhancement data were down-sampled for a better visual comparison to the empirical data.

The average peak enhancement of the high-flow rate group in [6] was reported as 313.7 HU and the new model generated an aortic enhancement curve with a peak enhancement of 317.3 HU, a percent difference of 1.15%. The Bae full-body model generated an enhancement curve with a peak enhancement of 321.3 HU, a percent difference of 2.42%. The time to peak enhancement predicted by the model was 31 seconds, the time to peak enhancement predicted by the Bae full-body model was 31 seconds, and the empirical data had an average peak enhancement time of 32 seconds.

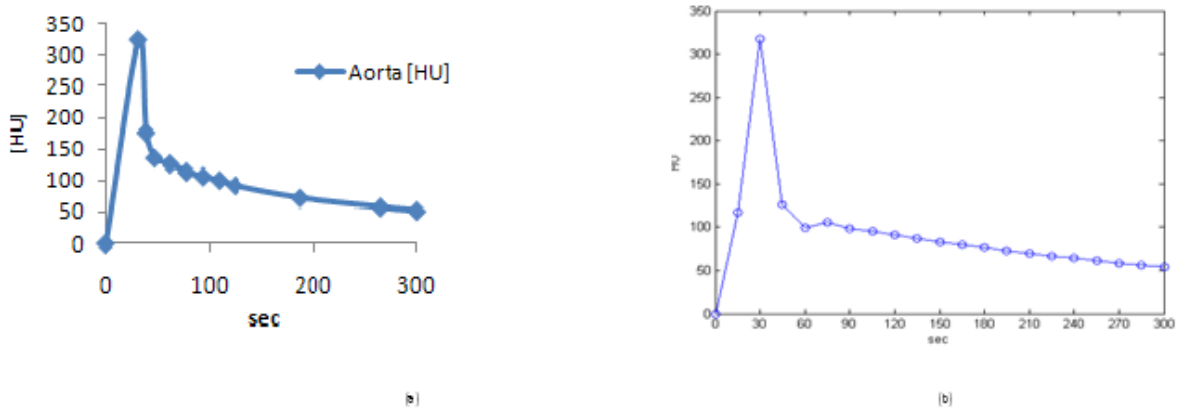

Figure 19 Comparison of data reported by Bae et al. to the hybrid model output. (a) figure 6a in [6] from the patient group using a 5 ml/s injection (b) predicted output from the new model in the abdominal aorta using the same contrast protocol and patient demographics as for the data in the empirical study.

4.3 COMPARISON RESULTS TO BAE'S MODEL USING CLINICAL DATA

The validation results presented in [6] did not assess the model's utility in simulating individual contrast enhancement profiles. To determine the ability of the Bae full-body model and the hybrid model to predict individual contrast enhancement profiles, simulations using individual patient attributes (height, weight, age, sex) from a CTA imaging clinical trial were performed. The corresponding enhancement profiles from those patients' imaging data were then used to compare the outputs of the two models.

Three metrics were used to evaluate the predictive ability of both models – the Root Mean Square Error (RMSE), the Percent Difference in Maximum Enhancement (PDME), and a metric described in [6] as the "Enhancement Difference Index (EDI)"(the sum of the difference between the simulated and empiric enhancement curves, obtained from the clinical imaging data set, divided by the empirical data's area under the curve:

$$\mathrm{EDI} = \frac{\sum_{i=1}^{N} \left| \mathrm{AUC}_{\mathrm{Sim}} - \mathrm{AUC}_{\mathrm{Emp}} \right|}{\mathrm{AUC}_{\mathrm{Emp}}} \tag{4.30}$$

where the subscripts "Sim" and "Emp" stand for the simulated response data and the empiric data respectively.

4.3.1 Clinical Data and Methods

A CT angiography data set collected at the Medical University of South Carolina was used to compare the performance of the hybrid model and the Bae full body model. The study was a HIPAA compliant, prospective study (sponsored and funded by MEDRAD Inc.) approved by the local Institutional Review Board. The study's objective was to evaluate a patient-specific, optimized contrast delivery algorithm using features of timing bolus scans at the level of the pulmonary trunk. Seventy subjects undergoing routine coronary CTA (cCTA) were enrolled in the study. Due to incomplete axial CT data set storage and transfer, data from only 20 of the

subjects could be used in the comparison tests presented here. The performance of the personalized delivery algorithm have been reported in [42] and also in [51].

The demographics of the 20 subjects used in this analysis are summarized in

Table 3. The average weight in this sample was average for adults in the United States [52] and the average age is representative of the population typically indicated for cCTA.

Table 3 Summary demographic data. Mean data are presented with standard deviations.

Parameter	*mean*	*min*	*max*	*median*
Weight [lbs]	196.7 +/-57.3	110	290	184
Height [in]	68.1 +/-44.3	61	76	68
Age [yrs]	60.1+/10.2	37	74	60.5
Heart Rate [bpm]	65.6+/-8.47	50	81	64.5
Freq. Male	11			

All subjects in the study were scanned with a Dual Source CT scanner (Definition DS, Siemens Medical, Malvern PA) using standard scan parameters (details in the Appendix). All subjects were administered a 20 ml test bolus of 300 mgI/ml contrast material followed by a 30 ml saline flush at a flow rate of 5ml/s. The timing bolus scan was started approximately (variation due to scanner software) 5 seconds after the start of contrast injection, and single-level scans were acquired every 2 seconds until approximately 5 seconds after the peak enhancement in the ascending aorta. The scanner operator used discretion in stopping the data acquisition to reduce undue radiation exposure to the subject and a consistent length of acquisition data was not obtained.

TECs were created by the scanner software based on ROIs drawn in the pulmonary trunk and ascending aorta by the scanner operator. The times to peak and peak enhancements in those two areas were used by the investigational software to compute a patient-specific contrast flow rate, volume, contrast/saline admixture, and a personalized scan delay for the diagnostic CT scan. Summary procedure specific results are presented in **Table 4** and **Table 5**. Many factors influence the scan duration of a CTA examination including scanner settings, patient heart rate, and the length of anatomy being imaged. Recall that the scan delay in this data set was computed by the investigational software described in [42].

The contrast protocol computed by the investigational software consisted of 3 phases – a contrast only portion, a contrast and saline admixture phase, and finally a saline only "flush" phase. The volume reported in **Table 5** for phase 2 refers to the volume of contrast in the phase while the phase 3 volume is the amount of saline delivered in the flush. Because the contrast was diluted in phase 2, the concentration reported in **Table 5** is not the concentration of the stock solution (300 mgI/ml).

Table 4 Relevant scan parameters from the clinical data set, 20 subjects. Mean values are given with standard deviations.

Parameter	*mean*	*min*	*max*	*median*
Scan Duration [sec]	10.3+/-2.59	4.3	16	18
Scan Delay [sec]	18+/-3.9	11.2	27	18

Table 5 Summary contrast protocol statistics from the clinical data set, first 20 subjects. Values are mean +/- standard deviation.

	Flow Rate [ml/s]	*Volume [ml]*	*Concentration [mgI/ml]*
Phase 1	4.18+/-.88	74+/-12.7	300
Phase 2	4.18+/-.88	3.01+/-3.72	69+/-65.4
Phase 3	4.18+/-.88	30	0

4.3.2 Data Acquisition Methods

A semi-automated segmentation software tool developed for other research tasks was used to extract time enhancement data from the 20 subject imaging sets (the helical imaging data are from the diagnostic scans) as presented in section 2.2.1. Each axial CT image was separated by .375 mm. The time between blocks of acquisition data (see **Figure 5**) varied between .75 and 1second. An example data set is presented (subject 1) in **Figure 20**. The scan delay for this particular acquisition was 23 seconds and thus the time axis begins at 23 seconds. Because the enhancement data are a function of time and space, the corresponding spatial dimension across the data set is superimposed on the figure's x-axis. Because the hybrid model generates predictions with respect to time in discrete "compartments", the comparisons employed here will be with the temporal view of the image data extracted from the aortas of the 20 subjects.

To determine the relationship between HU value and blood-plasma concentration of the contrast material, an experiment with diluted amounts of contrast material was performed on the scanner prior to the clinical study. Diluted contrast material was placed into radio-opaque containers and scanner using the same parameters used during the clinical trial. The conversion factor between HU and mgI/ml was computed, by linear regression, to be 27.1HU/(mgI/ml). This

constant was used in the hybrid model and Bae model simulations to convert the plasma concentration of iodine to HU.

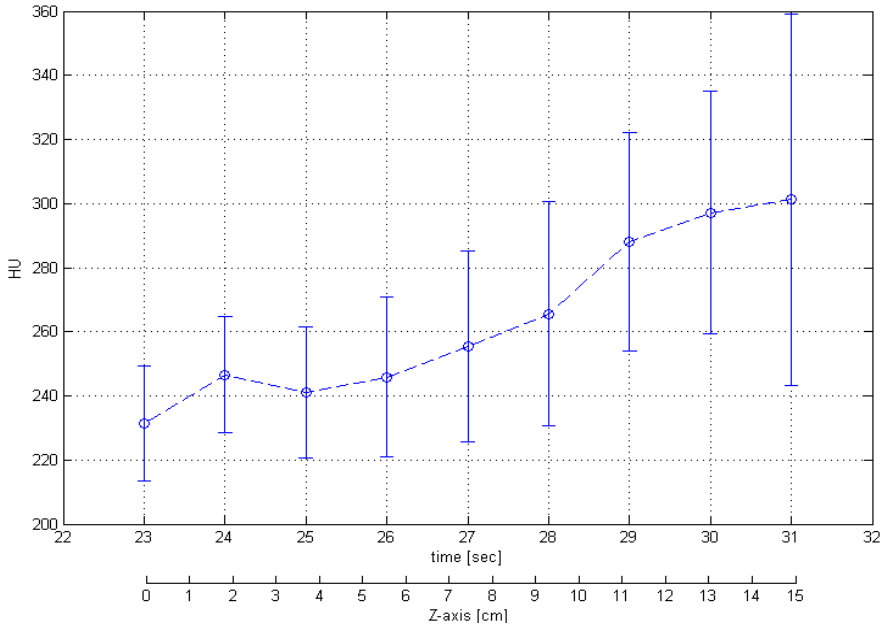

Figure 20 Subject 1's contrast enhancement profile extracted from the descending aorta. Error bars indicated the standard deviation of contrast enhancement at each measurement location.

4.3.3 Simulations

An implementation of the Bae full-body PK model was made in MATLAB/Simulink to provide a comparison of the hybrid model's performance using the clinical imaging data. The parameters for the model described in [6] and further elaborated in [53] were used in configuring the model. A fixed-time step solver (Runge-Kutta) executed the model every .1 seconds. Individual subject

demographic data (height, weight, sex, and age) were computed using equations (4.27), and equations (4.28) and (4.29) were used to compute the cardiac output and total central blood volume estimates for each simulated subject. Because the Bae model, as published, does not allow for modeling a saline flush phase, the contrast protocols used in simulating the model only included contrast. The conversion factor of 27.1 HU/(mgI/ml) converted blood-plasma concentrations to HU values.

The hybrid model was simulated using the parameters and methods presented in section 4.1.2. As with the Bae model, subject demographic data and the relationships defined in equations (4.27), (4.28) and (4.29) provided the values for cardiac output and blood volume. The parameter values in **Table 1-3** were used to configure the model. MATLAB/Simulink (R2008b) was used to simulate the model for each patient using the clinical data for patient parameters and the diagnostic phase contrast injection protocol, including the saline flush phase. As with the Bae model, the conversion factor of 27.1 HU/(mgI/ml) converted plasma concentrations to HU values.

Predicted HU values for each subject were downsampled to match the temporal resolution of the enhancement curves from the imaging data (1 sec/sample). Only the portions of the predicted enhancement curves spanning the time segment of the imaging data were used in computing the comparison metrics (MSE, PDME, EDI).

4.3.4 Results

All 20 sets of demographic, procedure, and imaging data were sufficient to allow simulations of the models and to allow computation of the metrics. An example simulation output using subject

11's demographic and procedure data is plotted with the contrast enhancement profile from the imaging data in Figure 21. The error bars on each imaging data point are the standard deviations of the contrast enhancement as determined by analysis of all the pixels in the aorta at each acquisition location. Contributing to the noise at each point is intrinsic imaging noise in the CT scanner, contrast flow dynamics, image processing mechanisms, and motion of the structure. The results for all 20 simulations using the hybrid and Bae models, superimposed over the clinical scan enhancement data, are presented in Appendix B

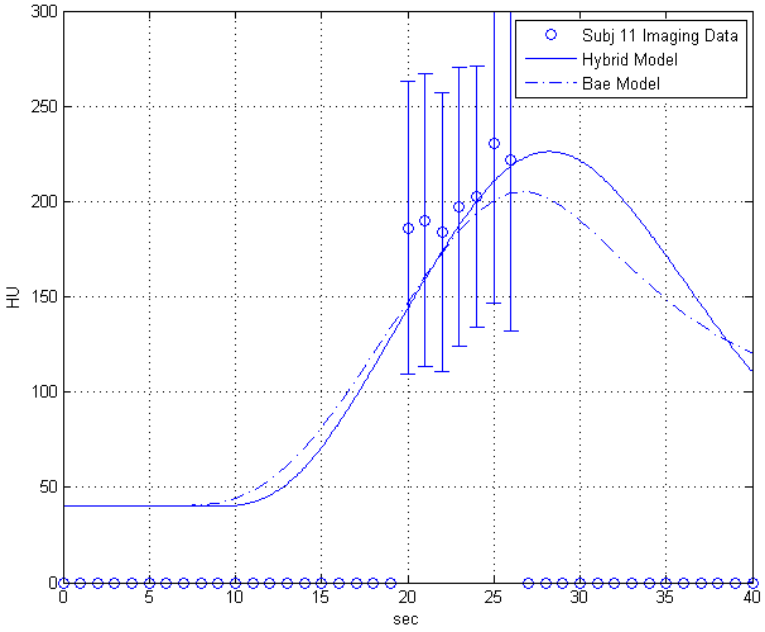

Figure 21 Subject 11 clinical imaging data, hybrid model simulation prediction and Bae model predictions

The hybrid model using data from subject 11 a 60 year old female weighing 280 lbs with a height of 68 inches, generated an enhancement curve matching favorably – RMSE of 15 HU -

to the enhancement curve acquired from the aortic imaging data for that patient. The results for this patient are displayed because the predicted enhancement curves matched very favorably to the measured data and also because heavier patients present challenges to conventional contrast dosing protocols. A total of 61 ml of 300 mgI/ml contrast was delivered at 4.1 ml/ and the scan duration was 11 seconds.

The Bae model produced an adequate enhancement curve but undershoots the empirical data by 20-40 HU. The hybrid model predicted a higher peak enhancement value than the Bae model. Linear extrapolation of the clinical data suggests the actual (assuming the ability to measure the contrast enhancement *in vivo* in the aorta for 10-20 more seconds) peak enhancement value should be greater than the Bae model would suggest, in agreement with the hybrid model prediction.

Examples comparing enhancement predictions from the models and the two sets of imaging data are given in **Figure 22** for cases that did not match well. The first comparison is for Subject 6, who was a 37 year old female, weighing 110 lb at a height of 61 inches with a heart rate of 80 bpm. Seventy seven ml of 300 mgI/ml contrast material was delivered at a flow rate of 5.9 ml/s for a scan that lasted 9 seconds. Subject 8 was a 53 year old male, weighing 223 lbs at a height of 70 inches. His heart rate averaged 58 bpm. Seventy four ml of 300 mgI/ml contrast was injected at 4.1 ml/s and his scan duration was 12 seconds.

Neither the Bae model nor the hybrid model predicts a contrast enhancement profile that matches the empirical data adequately .For Subject 6, both the Bae and hybrid models predict enhancement maxima 200 HU less than the empirical data. For Subject 8, the hybrid model predicts a maximum enhancement 79 HU less than the empirical data's maximum. The Bae maximum prediction was 111 HU less than the empirical data's maximum.

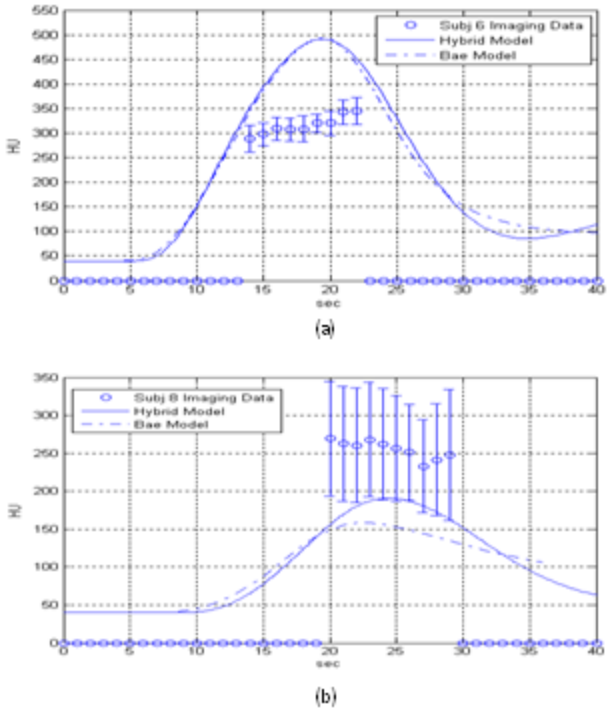

Figure 22 Model predictions compared to clinical data for (a) subject 6 and (b) subject 8. Subject 6 was a 47 year old, 110 lb female while patient 8 was a 53 year old, 246 lb male.

Statistical results comparing the predictions of the hybrid and the Bae models are presented in tables and plots below. For each subject, the same patient and procedure data were used in both models. In each instance, the model's enhancement outputs for the aortic compartment were compared to the imaging data set. Simulation data segments starting at the time point corresponding to the scan delay and lasting until the scan was completed were included in the computations of Root Mean Square Error and the Enhancement Difference Index. Tabulated results are presented in **Table 6**. Although the three comparison metrics are smaller for the hybrid model simulation, Mann-Whitney U tests do not reveal significant differences

between the medians for all measures (RMSE - U=455,p=.229; PDME - U=445,p=.351; EDI - U=470,p=.064).

Table 6 Summary results of models compared against clinical data

	Bae Model Results					Hybrid Model Results				
metrics	*mean*	*stdev*	*min*	*max*	*median*	*mean*	*stdev*	*min*	*max*	*median*
RMSE [HU]	50.5	28.9	17.1	134.1	40.6	41.9	29.8	12.2	142.3	37.3
PDME [%]	18.5	11.7	3.7	42.9	15.7	14.6	10.2	0.8	42.1	14.5
EDI [%]	16.0	11.1	1.7	42.7	14.0	10.8	11.0	2.1	45.8	5.3

Box-and-whisker plots for the three comparison tests reveal the skewed distribution of the data and the equivalence of medians. The box-and-whisker plots in **Figure 23** are drawn with whiskers extending to the data point 1.5 times the Interquartile Range (IQR) greater or less than the median. Crosses in **Figure 23** indicate outliners that are data points greater than 1.5*IQR away from the median.

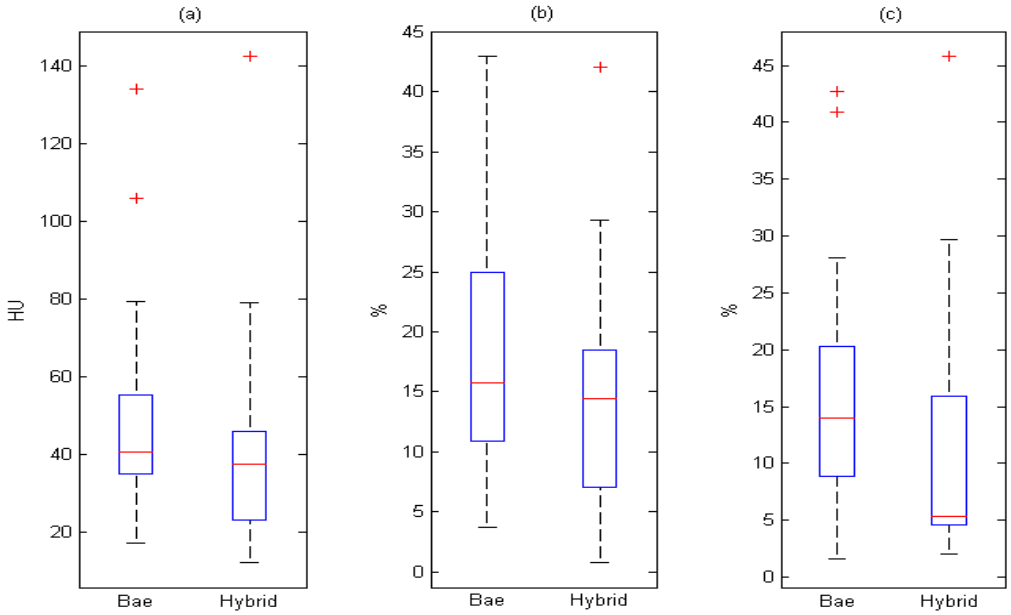

Figure 23 Box-and-whisker plots of the summary results for (a) RMSE (b) PDME and (c) EDI.

Another visualization of the data is given as a series of bar plots in **Figure 24**. Visual inspection of the charts reveals the results for subjects 6,8,12,16 and 19 show the greatest variation in simulation performance. The hybrid model predictions for subjects 15-20 show slightly better agreement with the clinical data than the Bae data. The hybrid model generated lower RMSE values in 14 of the 20 subjects, lower PDME results in 13 of the 20 subjects, and lower EDI in 17 of the 20 subjects.

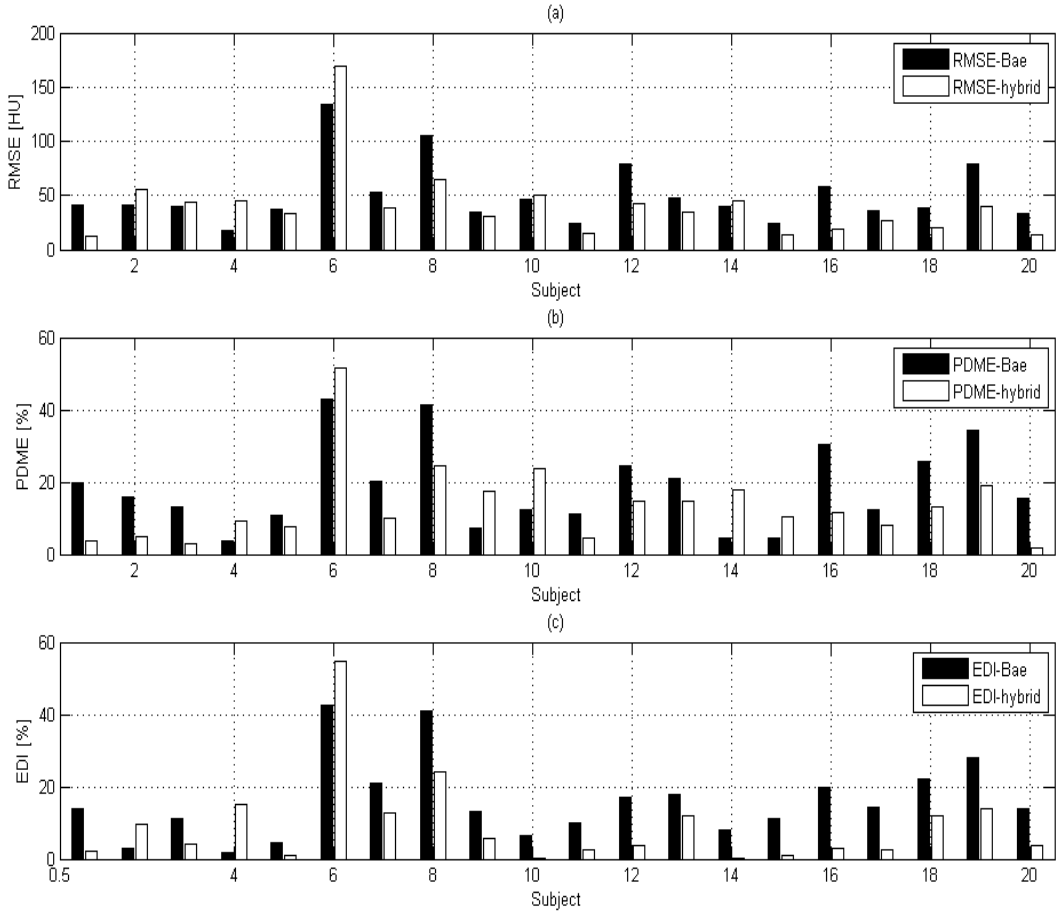

Figure 24 Scatter plots of the simulation tests (x- = Bae model, o-- = hybrid model) – (a) RMSE (b) PDME (c) EDI

4.4 DISCUSSION

In this chapter, a new physiologic-based pharmacokinetic model (a hybrid) describing contrast medium propagation was developed. In comparison to the published, full-body physiologic-based pharmacokinetic of Bae et al., the hybrid model has a reduced order, is discretizable,

explicitly models contrast propagation delays, models the effects of saline flush injections routinely performed during CTA procedures, and models the time-varying effects of blood-plasma/contrast interactions in the peripheral venous circulation. A comparison of the model's output to clinical data published by Bae et al in [6] shows favorable agreement. Further comparison of the hybrid model with contrast enhancement profiles derived from helical CTA data revealed close agreement with the Bae model and, in many instances, a better ability to fit the clinical data.

The hybrid model is used in subsequent chapters to test methods to identify models from test bolus data sets. In the methods developed, reduction strategies will be employed, rather than attempting to fit all the parameters of the hybrid model. This model reduction is done to reduce the computation burden and reliability of the numerical predictions. It is expected that by making use of identification data (ie: test bolus scan TECs) and individually identified models, the RMSE and EDI for subjects with the highest values, subjects 6,8 and 10 in particular, should improve.

5.0 DATA DRIVEN CONTRAST MODEL IDENTIFICATION

This chapter presents techniques for developing patient-specific predictions of contrast enhancement using contrast enhancement data derived from a test bolus injection. Two techniques were evaluated, one assuming a model structure and another using a non-parametric "black box" approach. In the model-based approach, the order of the pharmacokinetic model developed in Chapter 4.0 was reduced slightly by considering a subset of the physiologic compartments and to ease the computational burden when identifying the model parameters and to overcome the challenges of modeling time varying systems. Furthermore,sub-systems were decoupled during the parameter estimation to further aid the numerical fitting process.

5.1 PARAMETRIC (MODEL BASED) IDENTIFICATION

An approach for identifying and constructing a data-dependent, patient specific contrast propagation model with a decoupled and reduced-form of the hybrid PBPK model is developed in this section. Model parameters are estimated after acquisition of two CT time-enhancement curves (sequential low-level CT scans at the level of the pulmonary trunk) resulting from the injection of a small "identification" bolus of contrast medium (10-20 ml).

This section presents an overview of the methodology for extracting the identification data, a description of the model structure used for parameter estimation, and the methodology employed for generating the parameter estimate. An evaluation of the estimation technique with two data sets is given. The first data set was created with the hybrid model developed in Chapter 4, and the second validation data set consisted of retrospective imaging data from a clinical trial.

5.1.1 Model Based Methodological Background

Contrast agent is infused into the peripheral circulatory system, typically via intravascular access in a forearm vein or in the antecubital fossa. Several seconds later, the bolus of contrast arrives in the right heart. Next, the right ventricle pushes the contrast bolus through the pulmonary circulation. At this point, the transport of the contrast bolus is dominated by central circulatory parameters, namely the cardiac output. Between 6 and 20 seconds later, the contrast arrives in the left side of the heart and is ejected by the left ventricle into the main arterial and coronary vasculature. By positioning an axial CT acquisition at the level of the pulmonary trunk and acquiring CT images at that level every *n* seconds, a numerical and graphical depiction of the contrast's transport is generated.

Figure 25 presents an axial "slice" of cross-sectional image data acquired from a patient undergoing CT Angiography. A small test bolus of contrast (20 ml of 350 mgI/ml) was injected peripherally and scans were taken at the level of the pulmonary trunk every 2 seconds. As contrast flows through the anatomy, image enhancement or brightness in vascular structures increases. Upon acquisition of the axial images, the scanner or off-line processing software performs a surface integration within the Regions of Interest (ROI's) on each image and plots the

averaged attenuation value with respect to time. Standard clinical practice is to start the acquisition 5-10 seconds after the start of contrast injection and to acquire images for 20-30 seconds at a standard tube voltage (120 kV) but at a low tube current-time product (10-30 mAs).

Typical Time Enhancement Curves (TEC) for a human subject are shown in **Figure 26**. A region of interest (ROI) marker is placed over the subject's pulmonary artery trunk and the ascending aorta as demonstrated in **Figure 25**.

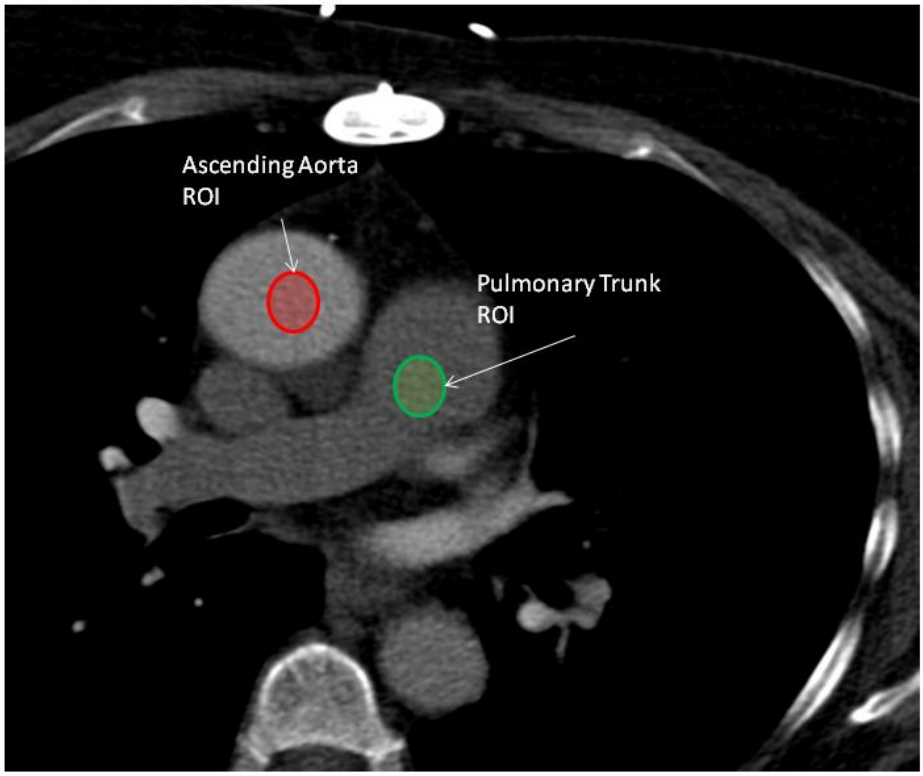

Figure 25 An axial CT image acquired from a test bolus scan procedure.

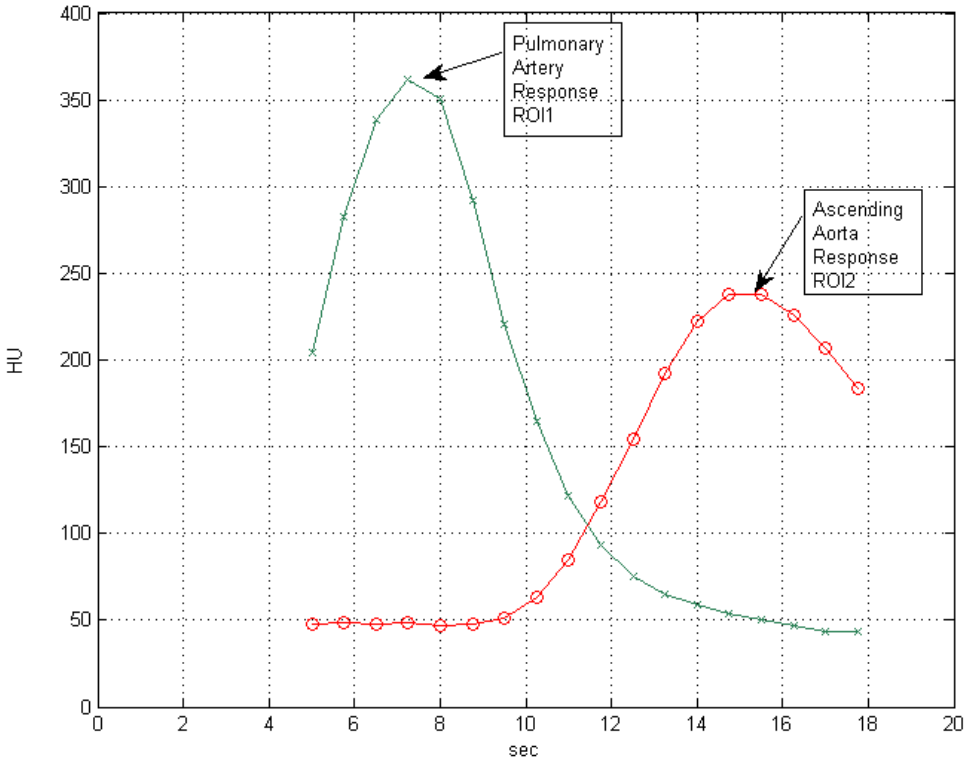

Figure 26 Time enhancement curve generated from a patient after analysis of the test bolus scan arising from a test bolus contrast injection (data set from Figure 25).

5.1.2 Model Structure

An attempt to fit all the parameters of the hybrid model using the limited length of data available from test bolus TECs was not made. Rather, a model reduction strategy was employed where the most relevant compartments of the hybrid model are considered during the first-pass of the contrast agent – the peripheral venous compartment, the right heart compartment, the lung compartment and the left heart/aortic compartment. This approach is justified by recognition that CTA imaging is performed during the first-pass of the contrast material and is typically ended 30 seconds after the initiation of contrast injection due to the short scan acquisition time of the scanner. There are also intrinsic challenges to statistical identification techniques when feedback is present in the system [54]. Contrast recirculation would be considered a type of feedback in the hybrid model.

Figure 27 is an illustration of the hybrid model subsystems used for parameter estimation. The PER and RH compartments are collapsed into one transfer function, He1, where the contrast injection infusion is the input function $u_{inj}(n)$ and the measured TEC (ROI1 in **Figure 26**) in the pulmonary trunk, $y_{RH}(n)$, is the output signal. $y_{RH}(n)$ is converted to blood plasma concentration using a scaling coefficient dependent on the scanner configuration and determined via calibration. Because linearity is assumed throughout the model, the transport delay describing the propagation delay of the contrast bolus from the injection site to the pulmonary artery can be positioned anywhere within the He1 block. Likewise, the LUNG_B and LH subsystems are combined into one subsystem with transfer function He2. The input function for the He2 block is $y_{RH}(n)$ and the output signal is the measured concentration TEC $y_{LH}(n)$ derived from the ROI (ROI2 in **Figure 26**) placed in the aorta during a test bolus scan.

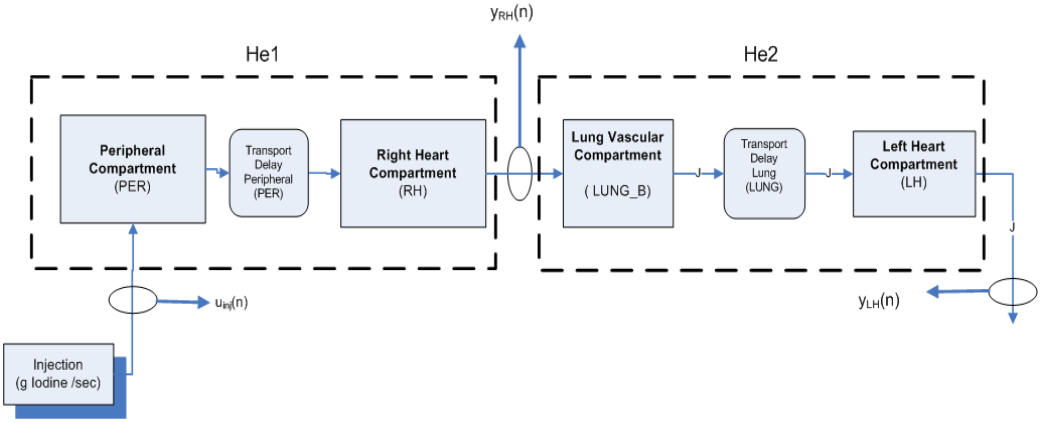

Figure 27 Reduced hybrid model structure used for parameter estimation with test bolus scan data. The dashed lines represent the model subsystems combined for model identification.

By performing the parameter estimation in two distinct operations, computational complexity is reduced. In addition to reducing computational complexity, a theoretical reduction in parameter variance can be realized [54] when fewer parameters are identified using input/output data. Furthermore, a reduction in the total number of parameters identified with a pair of input/output data help prevent overfitting.

Including only the RH and PER compartments, in the HE1 system, during preliminary parameter estimation resulted in non-convergence and poor fitting of experimental data. Increasing the order of the He1 system by introducing an "intermediate" compartment between the peripheral vein compartment and the right heart compartment resulted in convergence of the parameter estimators. This intermediate compartment also provides a means to model the effects of the injection flow rate within the peripheral compartment because the mass flux between the peripheral compartments is driven by a new volumetric flow rate term, Q_{PER} that is neither the

injection flow rate nor the flow rate of blood entering the right heart. The model structure is presented in **Figure 28** which shows $u_{inj}(t)$, the contrast bolus injection into a peripheral vein, and $y_{RH}(t)$, a TEC measured in the pulmonary artery (and converted to concentration units from HU).

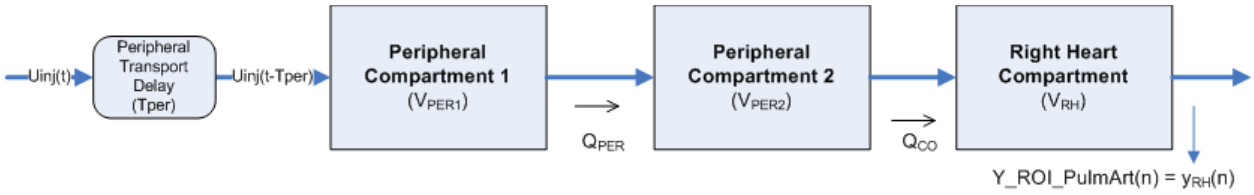

Figure 28 Reformulated right heart and peripheral compartments (He1) model structure for use in the parameter estimation. The mass flow rate terms, Q_{PER} and Q_{CO} transport contrast from peripheral compartment one to two and from peripheral compartment two into the right heart.

The continuous time state-space formulation for He1 is:

$$\mathbf{A}_{He1} = \begin{bmatrix} \frac{-Q_{PER}}{V_{PER1}} & 0 & 0 \\ \frac{Q_{PER}}{V_{PER1}} & \frac{-Q_{CO}}{V_{PER2}} & 0 \\ 0 & \frac{Q_{CO}}{V_{PER2}} & \frac{-Q_{CO}}{V_{RH}} \end{bmatrix}$$

$$\mathbf{B}_{He1} = \begin{bmatrix} 1 & 0 & 0 \end{bmatrix}^T \qquad (5.1)$$

$$\mathbf{C}_{He1} = \begin{bmatrix} 0 & 0 & \frac{1}{V_{RH}} \end{bmatrix}$$

$$\mathbf{D}_{He1} = [0]$$

$$\dot{\mathbf{x}}_{He1}(t) = \mathbf{A}_{He1}\mathbf{x}_{He1} + \mathbf{B}_{He1}u_{inj}(t - T_{PER})$$
$$y_{He1}(t) = \mathbf{C}_{He1}\mathbf{x}_{He1}(t) \tag{5.2}$$

and recalling that $y_{He1}(t) = y_{RH}(t)$ when measured data are available from CT data collected in a Right Heart structure, such as the pulmonary artery. The predicted output for the system has units of concentration, which is from the governing equations of Chapter 4 in which the model outputs had units of mass flux. The transport delay of the contrast through the peripheral venous circulation is T_{PER}. The input function in (5.2) is parameterized by the administration flow rate (Q_{inj}) , the concentration of the test bolus (C_{inj}), and the contrast bolus duration T_{DUR}:

$$u_{inj}(t) = Q_{inj}(t)C_{inj}\ u(t) - u(t - T_{DUR}) \tag{5.3}$$

where u(t) is the unit-step function.

The contrast injection flow rate (Q_{inj}) is omitted in the formulation of (5.1) because it is assumed that the identification data set is acquired when a saline bolus flush follows the test bolus contrast volume. A saline infusion following the test bolus maintains the flow rate in the peripheral compartments (Q_{PER}) for a duration of 10-14 seconds (the volume of contrast and saline divided by the flow rate). A typical diagnostic bolus has duration of 10-14 seconds (contrast) so the assumption is that the peripheral flow rate during the diagnostic injection will be the same as during the test bolus injection.

Because the CT data are acquired by single-level scanning at discrete time steps, the models used in the identification step were discretized. Discretization of the continuous state-

space system defined in (5.1) was obtained by a standard transformation of Linear System Theory:

$$\mathbf{A}_{He1D} = e^{\mathbf{A}_{He1}\Delta}$$
$$\mathbf{B}_{He1D} = \int_{\tau=0}^{\Delta} e^{\mathbf{A}_{He1}\tau}\mathbf{B}_{He1}\,d\tau \tag{5.4}$$

The subscript "D" refers to the discretized state-space matrix form and Δ is the sampling interval defined by the time between single-level scans. This approach yields the following state-space matrices:

$$\mathbf{A}_{He1D} = \begin{bmatrix} e^{\frac{-Q_{PER}}{V_{PER1}}\Delta} & 1 & 1 \\ e^{\frac{Q_{PER}}{V_{PER1}}\Delta} & e^{\frac{-Q_{CO}}{V_{PER2}}\Delta} & 1 \\ 1 & e^{\frac{Q_{CO}}{V_{PER2}}\Delta} & e^{\frac{-Q_{CO}}{V_{RH}}\Delta} \end{bmatrix}$$

$$\mathbf{B}_{He1D} = \begin{bmatrix} -\frac{V_{PER1}}{Q_{PER}}\left(e^{-\frac{Q_{PER}}{V_{PER1}}\Delta} - 1\right) \\ \frac{V_{PER1}}{Q_{PER}}\left(e^{\frac{Q_{PER}}{V_{PER1}}\Delta} - 1\right) \\ 0 \end{bmatrix}$$

$$\mathbf{C}_{He1D} = \begin{bmatrix} 0 & 0 & \frac{1}{V_{RH}} \end{bmatrix}$$

$$\mathbf{D}_{He1D} = [0] \tag{5.5}$$

The second sub-system of the model is a combination of the Lung and Left-Heart compartments, denoted as He2 in **Figure 27**. Because first-pass circulatory effects dominate when predicting contrast enhancement for CT Angiography, the transport of contrast from the vascular region to lung tissue is ignored. As in the derivations of the hybrid model, the propagation delay of contrast material through the cardiopulmonary circuit is lumped into a transport delay, $T_{LUNG.}$ A graphical depiction of the isolated He2 sub-system is presented in **Figure 29**.

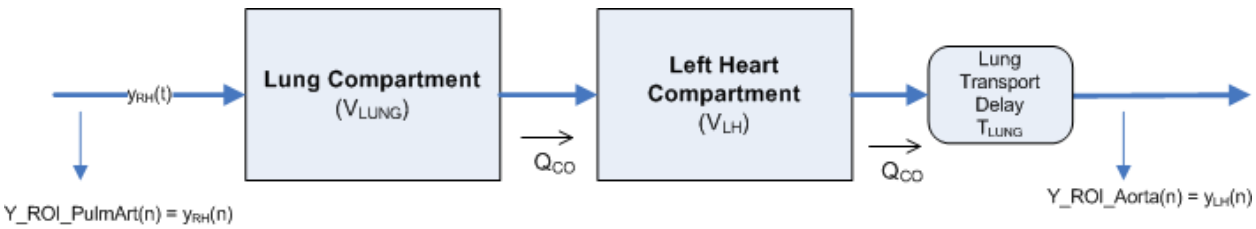

Figure 29 Reformulated left heart and lung compartment (He2) model structure for use in the parameter estimation. The cardiac output (Q_{CO}) transports the contrast bolus from the Lung compartment to the Left Heart compartment.

The continuous time state-space dynamics for He2 are:

$$\begin{aligned}
\mathbf{A}_{He2} &= \begin{bmatrix} \frac{-Q_{CO}}{V_{LUNG}} & 0 \\ \frac{Q_{CO}}{V_{LUNG}} & \frac{-Q_{CO}}{V_{LH}} \end{bmatrix} \\
\mathbf{B}_{He2} &= \begin{bmatrix} Q_{CO} & 0 \end{bmatrix}^{T} \\
\mathbf{C}_{He2} &= \begin{bmatrix} 0 & \frac{1}{V_{LH}} \end{bmatrix} \\
\mathbf{D}_{He2} &= [0]
\end{aligned} \tag{5.6}$$

$$\begin{aligned}
\dot{\mathbf{x}}_{He2}(t) &= \mathbf{A}_{He2}\mathbf{x}_{He2} + \mathbf{B}_{He2}y_{RH}(t - T_{LUNG}) \\
y_{He2}(t) &= \mathbf{C}_{He2}\mathbf{x}_{He2}(t)
\end{aligned} \tag{5.7}$$

and $y_{He2}(t)=y_{LH}(t)$ when TEC data are available from a left heart structure, such as the ascending aorta. Applying (5.4) to the system equations results in the discrete-time representation for the A and B matrices (the C and D matrices are equivalent to the continuous-time version), with Δ representing the sampling time:

$$\mathbf{A}_{\text{He2D}} = \begin{bmatrix} e^{-\frac{Q_{CO}}{V_{LH}}\Delta} & 1 \\ e^{\frac{Q_{CO}}{V_{LUNG}}\Delta} & e^{-\frac{Q_{CO}}{V_{LH}}} \end{bmatrix}$$

$$\mathbf{B}_{\text{He2D}} = \begin{bmatrix} -V_{LH}\left(e^{-\frac{Q_{CO}}{V_{LH}}\Delta}+1\right) \\ V_{L}\left(e^{\frac{Q_{CO}}{V_{LUNG}}\Delta}-1\right) \end{bmatrix} \tag{5.8}$$

$$\mathbf{C}_{\text{He2D}} = \begin{bmatrix} 0 & \frac{1}{V_{LH}} \end{bmatrix}$$

$$\mathbf{D}_{\text{He2D}} = [0]$$

The two discrete systems serve as the basis for the data-driven parameter estimation technique developed herein. Input to the first discrete system (He1D) is a sampled injection input signal, $u_{inj}(n)$ (discrete version of (5.3)) and the output is the TEC measured in the pulmonary trunk, $y_{RH}(n)$ (ROI1 in **Figure 26**). The input to the second discrete system, He2D, is $y_{RH}(n)$ and the output vector is the TEC measured from the Ascending Aorta, $y_{LH}(n)$ (ROI2 in **Figure 26**). **Figure 30** presents a block-diagram view of the two discrete systems and the respective inputs and outputs for the systems. The two, discrete, state-space systems used in the parameter estimation are:

$$\begin{aligned} \dot{\mathbf{x}}_{\text{He1D}}(n) &= \mathbf{A}_{\text{He1D}}\mathbf{x}_{\text{He1D}} + \mathbf{B}_{\text{He1D}}u_{inj}(n - T_{PER}) \\ \hat{y}_{RH}(n) &= \mathbf{C}_{\text{He1D}}\mathbf{x}_{\text{He1D}}(n) \end{aligned} \tag{5.9}$$

$$\begin{aligned} \dot{\mathbf{x}}_{\text{He2D}}(n) &= \mathbf{A}_{\text{He2D}}\mathbf{x}_{\text{He2D}} + \mathbf{B}_{\text{He2D}}y_{RH}(n - T_{LUNG}) \\ \hat{y}_{LH}(n) &= \mathbf{C}_{\text{He2D}}\mathbf{x}_{\text{He2D}}(n) \end{aligned} \tag{5.10}$$

The parameters to be estimated in the first system, He1D, are: V_{PER1},V_{PER2},V_{RH},Q_{PER},Q_{CO}, and the transport delay T_{PER}. Parameters to be estimated in the second system are: V_{LH}, V_{LUNG}, Q_{CO}, and the transport delay through the pulmonary system T_{LUNG}.

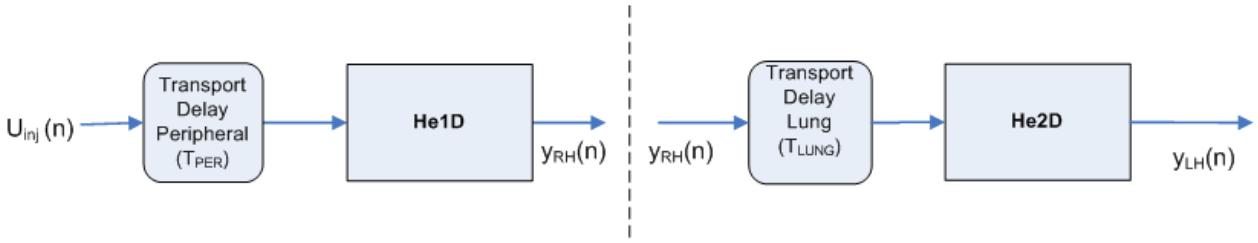

Figure 30 Block diagram of the discrete model used for identifying parameters with a maximum likelihood estimator.

5.1.3 Maximum Likelihood Estimator

In this section, the methodology for identifying the parameters of a patient-specific, reduced-order, hybrid pharmacokinetic model is presented. The approach presented here differs from the parameter estimation and individual pharmacokinetic model generation presented in Chapter 4.0 because the identification data is derived from scan data acquired after the injection of a small bolus of contrast material into a patient.

Parameter estimation occurs in two distinct steps. By using two measured signals, y_{RH}(n) and y_{LH}(n), and estimating the two systems serially, the convergence time, computation burden and parameter variability are reduced because fewer parameters need to be identified in one

single identification step by numerical optimization. For example, instead of estimating 10 parameters with the sampled test bolus enhancement data, six parameters are identified in He1D using the known input function, $u_{inj}(n)$ and the output signal $y_{RH}(n)$ (which might only have 10 data points) and then only 4 parameters for He2D are identified in another separate parameter estimation step (using $y_{RH}(n)$ and $y_{LH}(n)$ as input/output data).

First, the "He2" system is parameterized using the scan data from a test bolus injection and the resulting TECs measured in the pulmonary artery and the ascending aorta – $y_{RH}(n)$ and $y_{LH}(n)$. Next, the "He1" system is parameterized using the signals $u_{inj}(n)$ and $y_{RH}(n)$, the input injection function and the TEC measured in the pulmonary artery. After estimating the parameters, an individual model for that patient is constructed using equations (5.9) and (5.10). Goodness-of-fit is determined by comparing the predicted enhancement in the ascending aorta (with a test bolus injection) against the measured data.

Because a large number of noise sources influence the measurement process, including the Zero-Order sampling process, it is assumed the errors are normally distributed throughout the system. With the assumption of Gaussian distributed error and independent noise processes, Maximum Likelihood Estimation (MLE) can be used for estimating the unknown model parameters[54]. The cost function used in the MLE when estimating the parameters of He1D and He2D is the sum of squared differences between the measured test bolus TEC data $y_{RH}(n)$ and $y_{LH}(n)$ and the estimated test bolus response in those structures, $y_{RH}(n)$ and $y_{LH}(n)$:

$$\theta_{He1D} = \arg\min_{\theta_{He1D}} \frac{1}{2\sigma^2_{meas}} \sum_{i=1}^{N} \left[y_{RH}(i) - y_{RH}(\hat{\theta}_{He1D}, i) \right]^2 \tag{5.11}$$

$$\theta_{He2D} = \arg\min_{\theta_{He2D}} \frac{1}{2\sigma^2_{meas}} \sum_{i=1}^{N} \left(y_{LH}(i) - y_{LH}(\hat{\theta}_{He2D}, i) \right)^2 \tag{5.12}$$

where the parameter estimate vectors ("hat" notation, ^, signifies estimated parameters):

$$\begin{aligned} \theta_{He1D} &= \begin{bmatrix} V_{PER1} & V_{PER2} & V_{RH} & Q_{PER} & Q_{COr} & T_{PER} \end{bmatrix}^T \\ \theta_{He2D} &= \begin{bmatrix} V_{LUNG} & V_{LH} & Q_{CO} & T_{LUNG} \end{bmatrix}^T \end{aligned} \tag{5.13}$$

recognizing that maximum likelihood estimation is equivalent to least squares fitting when the noise processes are Gaussian [54]. The variance term, σ^2_{meas} in (5.11) and (5.12) does not enter into the cost function and may be estimated post-hoc, based on noise estimates from the measured TECs. In the summations of (5.11) and (5.12), *N* is the number of TEC samples available from the test bolus enhancement data, and the index variable, *i*, ranges across the discrete-time samples.

In matrix notation, the problem is stated as minimizing the sum of squares of residuals through a function of the estimated parameters:

$$J_{RH}(\theta_{He1D}) = \left\| \mathbf{r}_{RH} \quad \theta_{He1D} \right\|^2 = \left\| \mathbf{y}_{RH} - \mathbf{f}_{RH}(\theta_{He1D}) \right\|^2 \tag{5.14}$$

$$J_{LH}(\theta_{He2D}) = \left\| \mathbf{r}_{LH} \quad \theta_{He2D} \right\|^2 = \left\| \mathbf{y}_{LH} - \mathbf{f}(\theta_{He2D}) \right\|^2 \tag{5.15}$$

where $\mathbf{f}(\theta_i)$ are *n*-vectors that estimate the LH and RH signals given the p-value parameter estimates θ_{He1D} and θ_{He2D} (p=6 and p=4) and inputs. The vectors $\mathbf{r}_{RH}(\theta_{He1D})$ and $\mathbf{r}_{LH}(\theta_{He2D})$ are the residuals for the estimates of the He1D and He2D systems:

$$\mathbf{r}_{RH}\ \theta_{He1D} = \mathbf{y}_{RH} - \mathbf{C}_{He1D} \cdot \mathbf{x}_{He1D} + \eta(n) \tag{5.16}$$

$$\mathbf{r}_{LH}\ \theta_{He2D} = \mathbf{y}_{LH} - \mathbf{C}_{He2D} \cdot \mathbf{x}_{He2D} + \eta(n) \tag{5.17}$$

with $\eta(n)$ representing the model and measurement uncertainty.

The *n* x *p* Jacobian matrices, $\mathbf{V}_{RH}\ \theta_{He1D}$ and $\mathbf{V}_{LH}\ \theta_{He2D}$ are constructed from the first derivatives of the residual vectors with respect to the parameter vectors. Note that bold **V** notation is used for the Jacobians while V (non-bold) is used for volume. The i^{th} and j^{th} elements of the Jacobian matrices are:

$$V^{RH}{}_{i,j} = \frac{\partial r_i}{\partial \theta^{RH}{}_j} = \frac{\partial\ y_{RH}(i) - \mathbf{C}_{He1D} x_i^{RH}}{\partial \theta_j^{RH}} \tag{5.18}$$

$$V_{i,j}^{LH} = \frac{\partial r_i^{LH}}{\partial \theta_j^{LH}} = \frac{\partial\ y_{LH}(i) - \mathbf{C}_{He2D} x_i^{LH}}{\partial \theta_j^{LH}} \tag{5.19}$$

The maximum likelihood estimates of the parameter vectors are normally distributed with covariance of $\sum = \sigma^2\ \mathbf{V}^T\mathbf{V}^{-1}$ where the estimators of variance are [55]:

$$\sigma_{RH}^{2} = \frac{J_{RH}\ \boldsymbol{\theta}_{RH}}{n-p}$$

$$\sigma_{LH}^{2} = \frac{J_{LH}\ \boldsymbol{\theta}_{LH}}{n-p} \tag{5.20}$$

The variance of the parameter estimates can also be expressed as the inverse of the Fisher Information Matrix (the inverse of the Hessian), which is often accessible from numerical computing packages such as MATLAB's optimization toolbox.

An approximate expression for the parameter bias, that is the difference between the estimated and the true parameter, can be expressed in terms of the Jacobian matrices:

$$E\ \theta - \theta\ \approx\ \mathbf{V}^{T}\mathbf{V}^{\ -1}\mathbf{V}^{T}\mathbf{d} \tag{5.21}$$

where $\mathbf{d} = \frac{\sigma^2}{2}$ trace $\mathbf{V}^{T}\mathbf{V}^{\ -1}\mathbf{H}^{\ T}$ where **H** is the *p* x *p* Hessian matrix (derivative of the Jacobian).

5.1.3.1 Numerical Optimization Details Because the model, as defined by (5.9) and (5.10), is non-linear in the parameters the minimization of the cost functions is a non-linear Least Squares (NLS) problem. There are numerous iterative techniques for solving NLS problems. An optimization scheme for this problem needs to provide non-negativity constraints on the parameters. Also, it is reasonable to enforce physiologic bounds on the parameter estimates.

Because the problem is a constrained minimization, line-search techniques like Gauss-Newton, simplex or hybrid techniques like the classic Levenberg-Marquardt are not applicable. For this reason, a subspace trust-region method, based on an interior-reflective Newton method as implemented in the MATLAB Optimization toolbox (nonlinsq), was used to estimate the parameter vectors in (5.13). The algorithm computes an approximate solution at each iteration of the solver using a Precondition Conjugate Gradient (PCG) technique. Finite difference approximations were used to construct the Jacobian and Hessian matrices during the solution process.

In the experiments described below, the minimizations were run with convergence criteria of 10^{-5} on the cost function evaluation and a tolerance of 10^{-5} on the parameters. A maximum number of function evaluations of 400 was set and the maximum number of iterations at each solution step allowed was 500. The parameter bounds for θ_{He1D} and θ_{He2D} used in the experiments are presented in **Table 7**.

Table 7 Upper and lower boundaries or constraints on the estimated parameters

θ_{He1D}			θ_{He2D}		
Parameter	***Lower Bound***	***Upper Bound***	***Parameter***	***Lower Bound***	***Upper Bound***
V_{RH} [ml]	30	400	V_{LH} [ml]	50	400
V_{PER1} [ml]	10	90	V_{LUNG} [ml]	250	825
V_{PER2} [ml]	10	200	Q_{CO} [ml/s]	30	200
T_{PER} [sec]	1	5	T_{LUNG} [sec]	1	8
Q_{PER} [ml/s]	1	80			
Q_{COr} [ml/s]	30	170			

The parameters were initialized, prior to starting the estimation, at 50% midpoints of the upper and lower parameter bounds. To investigate the sensitivity of the solver to initial condition selection, five solver runs were executed per parameter estimation. The initialization vector with the best-fit output curve was selected as the starting estimate. The estimated output vector for the He1D system, $\hat{y}_{RH}(n)$, was used as the input to He2D system when performing forward predictions of contrast enhancement. A detailed description of the parameter estimation methodology is included in Appendix A.

5.1.4 Parametric Estimator Evaluation Methods

To demonstrate the effectiveness of the parameter estimation technique, three distinct experiments were conducted. The first two experiments used synthetic data to determine properties of the estimator (bias, variance) and it's robustness to truncated input/output data and variations in temporal sampling of the data. Retrospective clinical data were then used to determine the estimator's performance in predicting aortic contrast enhancement in human subjects based on timing bolus scan TECs measured in the pulmonary trunk and the ascending aorta. A table is provided to aid the reader in navigating the methods and corresponding results sections for this section.

Description	Method Section	Results Section
Analysis of the estimator performance – bias and variance analyses • The reduced-order model is the source of comparison data	Section 5.1.4.1, Page 109	Section 5.1.5.1, page 113
Effect of the test bolus enhancement data length and noise on estimator performance. • The hybrid PBPK model is the source of comparison data	Section 5.1.4.2, page 110	Section 5.1.5.2, page 119
Performance of the estimator using clinical imaging data	Section 5.1.4.3, page 112	Section 5.1.5.3, page 125

5.1.4.1 Model-to-model Comparisons To characterize the estimator, a synthetic data set was created using the system defined by (5.9) and (5.10), the same equations used by the estimator. The hybrid model, therefore, did not generate the data used in these experiments. The intent of this methodology was to isolate the performance of the estimator independent of the measurement data. This type of comparison has been termed a "model-to-model" comparison in the literature [56, 57] and is useful for studying the behavior of an estimator independent of other factors such as model accuracy, sampling noise and variability in noise processes. The model-to-model terminology indicates that the same model used for estimating the parameters generated the data. It is also useful for visualizing the solution space and assessing the performance of the estimators because the "true" parameters, θ_{HeiD}^{true} for i=1,2 are known. A data set was computed using the parameter values specified in Table 8.

Table 8 Parameter values used in the model-to-model simulations and comparisons.

θ_{He1D}^{true}		θ_{He2D}^{true}	
Parameter	***Value***	***Parameter***	***Value***
V_{RH} [ml]	200	V_{LH} [ml]	325
V_{PER1} [ml]	30	V_{L} [ml]	310
V_{PER2} [ml]	100	Q_{CO} [ml/s]	90
T_{PER} [sec]	2	T_{LUNG} [sec]	3
Q_{PER} [ml/s]	4		
Q_{COr} [ml/s]	80		

The input function, $u_{inj}(t)$ (5.3) was parameterized by contrast concentration of 370 mgI/ml (C_{inj}) for a duration 5 seconds (T_{DUR}), at a flow rate of 5 ml/s (Q_{inj}). Simulations were

performed in MATLAB using a time-step of .10 sec/sample. The simulated TECs were downsampled at rates of 1 sec/sample, 2 sec/sample and 5 sec/sample to mimic the effect of sampling on the TECs by the CT scanner,.

Simulations were also performed with the "true" parameters corrupted with synthetic measurement noise (AWGN) having standard deviations of 0, 1 and 2 HU ($\eta(n)$ in (5.16) and (5.17) to develop estimates of bias and variance. For every combination of noise level and sample time, 30 parameter estimations were performed. For each simulation run, the initial parameter estimates were varied by 25% of the nominal values. Five parameter estimates were computed and the best set of parameters was determined by choosing the set which generated the minimum residual Mean Square Error between the predicted enhancement curve from the parameter estimation and that generated by the model, $\hat{y}_{RH}^{Test}(n), \hat{y}_{LH}^{Test}(n)$.

Finally, noise-free simulations were performed with true parameter values varied by +/- 20% in 2% increments to generate graphical illustrations of the cost functions $J_{RH}(\boldsymbol{\theta_{He1D}})$, and $J_{LH}(\boldsymbol{\theta_{He2D}})$. These simulations also allow for analysis of the sensitivity of the estimator to initial condition selection. Five simulations using with the initial conditions randomly varied within 25% of the values in **Table 8** were executed. The Root Mean Square Error between the predicted test bolus and the simulated test bolus enhancement for each set of initial conditions were recorded and analyzed.

5.1.4.2 Estimator Performance Using Hybrid Model Data This section presents the methods for determining the estimator's performance in the presence of noise and sensitivity to truncated test bolus enhancement data. The hybrid model was simulated using the parameters and methods presented in section 4.1.2. Simulated subject demographic data and the relationships defined in

equations (4.27), (4.28) and (4.29) provided the values for cardiac output and blood volume. The parameter values in Table 1-3 configured the model. MATLAB/Simulink (R2008b) was used to simulate the model for each patient using the clinical data for patient parameters and the diagnostic phase contrast injection protocol, including the saline flush phase. The same parameter set was used to create synthetic, discrete test bolus data $y_{RH}^{Test,H}(n)$ and $y_{LH}^{Test,H}(n)$ ((4.9) and (4.11)) where the superscript (Test,H) denotes a simulated test bolus injection response created from the hybrid model. The patient demographics used for simulations in 4.3 parameterized the model system (4.15). A fixed flow rate and contrast volume injection signal (uDiag(n)) was delivered to each simulated "subject" to generate a simulated enhancement curve $y_{LH}^{Diag,H}(n)$.The injection protocol, $u_{Diag}(n)$, was parameterized with the following values: Qinj = 5ml/s, Cinj = 350 mgI/ml, for 15 seconds followed by a saline phase at a flow rate of 5ml/s and duration of 8 seconds.

Parameter estimation was performed with Gaussian noise vectors with standard deviations of: .1, .25, .5, 1.0, 2.0, 5.0, 10, and 20 HU added to the hybrid model test bolus data. Performance of the predicted enhancement against the "true" enhancement as simulated by the hybrid-model for the twenty data sets were assessed using the metrics developed in 4.0 - RMSE, Percent Difference in Max Enhancement (PDME), and Enhancement Difference Index (EDI).

It is common practice for the technologist performing the study to stop data collection from a test bolus scan shortly after the peak contrast enhancement. Reasons for stopping the data acquisition include concern of excess radiation exposure to the patient and a desire to make the study time short. Because the test bolus data record may contain only a few samples of data after

peak enhancement, patient-specific contrast delivery algorithms must function in the presence of truncated data sets.

Experiments were conducted with truncated test bolus data vectors created with the simulated hybrid model to determine the effect of truncated test bolus scan data on the MLE parameter estimator. The vectors were truncated at durations of 20, 25, 30, and 35 seconds with no additive noise present. Next, simulated test bolus TECS were truncated at 25 and 35 seconds and noise was added. The AWGN were created with standard deviations of .1, .25, .5, 1.0, 2.0, 5.0, 10, and 20 HU. In all cases, the first data points of $y_{RH}^{Test,H}(n)$ and $y_{LH}^{Test,H}(n)$ were 5 seconds after the start of injection. The truncation times of 25 and 35 were chosen as specific test points because a 25 second acquisition duration can be expected in clinical practice and 35 seconds ensures the capture of the contrast peak and a number of samples after the peak in the left heart compartment for most procedures.

5.1.4.3 Estimator Performance Using Retrospectively Gathered Clinical Data The estimator performance was assessed against clinical data collected during an IRB approved clinical trial at the Medical University of South Carolina (Somatom Definition DS, Siemens Healthcare Malvern PA). The data set and methods used to collect the data are described in 4.3.2. The test bolus TECs collected during the clinical trial were used to derive parameter estimates and the semi-automated aortic contrast enhancement data were used to compare the estimator's predicted output, identical to the methods in 4.3.2.

During the clinical trial, scanner operators acquired the test bolus scan data by placing ROIs on the pulmonary trunk and the ascending aorta. Data collection started at 5 seconds after the injection of contrast started. Single-level scan acquisition was stopped by the operator two to

four seconds after the peak of contrast enhancement in the ascending aorta was observed. The scanner software then processed the data and created TECs which were exported to data files and saved. Diagnostic scan enhancement profile data was extracted as in Chapter 4.3.2.

An outline of the experimental methodology is:

1. Extract test-bolus TEC data
2. Perform parametric estimation using MLE technique
3. Generate predicted contrast enhancement using the diagnostic injection protocol from the clinical data set and the identified parameters from step 2
4. Extract the enhancement curve from the clinical data set
5. Compare the predicted contrast enhancement against the clinical data (from the scan delay to the end of the scan acquisition)

Predicted outputs from the data-drive estimator were compared to the actual, clinical data using RMSE, PDME, and EDI.

5.1.5 Results

All simulations and analyses were conducted with MATLAB (r2008b), the Optimization Toolbox (v4.1) and Simulink (v7.2).

5.1.5.1 Estimator Performance using model to model comparisons The results from the model-model simulation are presented in Table 9 through Table 12. The resulting mean estimator bias for each parameter in the cardiopulmonary system, He2D, is listed in Table 9. The goodness

of fit criteria used to gauge the performance of the estimators is the Mean Square Error between the predicted $\hat{y}_{LH}(n)$ and estimated y_{LH}. The mean of MSE across the 30 simulations (and the square root of the MSE) are tabulated in addition to the percent bias for each parameter. Bias results for the He1D subsystem parameter estimation are summarized in Table 10.

Parameter estimation bias increased independently of the additive noise in the He2D subsystem, except for the Qco and TLUNG parameters at sampling periods of .5 and 1 sec/sample. The MSE of the fit appears to be independent of the sampling period because it increases similarly as a function of the noise sigma for all three sample periods. Parameter estimation bias increased in the He1D subsystem when data sampling periods exceeded one sec/sample. The MSE of the residual between the estimator's prediction and the true values increased as the noise contribution increased and for sampling periods greater than 1 sec/sample. Variance of the parameter estimates for both systems are shown in Table 11 and Table 12. Parameter estimation variance was the largest, for all sampling times, when the standard deviation of the noise contribution was 2 HU. The variance of the transport delay parameter, TLung, was the largest among all the parameters.

Table 9 Summary of parameter bias for θ_{He2D}. Values are percent bias from the nominal values. MSE is the Mean Square Error of the residual error for the estimated and actual enhancement signal, y_{LH}

Ts	σ_{HU}	V_{LH}	V_{LUNG}	Q_{CO}	T_{LUNG}	MSE
0.5	0	-2.2	9.6	3.7	-8.1	0.0
	1	-6.6	11.6	2.5	-7.2	1.0
	2	-10.5	18.1	4.3	-5.7	4.2
1	0	-5.1	8.2	1.7	-15.9	0.0
	1	-4.5	14.3	5.2	-15.4	1.0
	2	-9.2	23.0	7.0	-14.3	4.1
2	0	-14.9	18.4	2.9	-29.8	0.0
	1	-13.7	16.7	2.8	-29.2	1.0
	2	-17.3	32.2	9.9	-25.6	3.7

Table 10 Summary of parameter bias for θ_{He1D}. Values are percent bias from the nominal values. MSE is the Mean Square Error of the residual error for the estimated and actual enhancement signal, y_{RH}

Ts	σ_{HU}	V_{RH}	V_{PER1}	V_{PER2}	T_{PER}	Q_{PER}	Q_{COr}	MSE
0.5	0	0.0	3.0	12.5	-0.4	0.4	10.0	0.0
	1	-10.2	2.1	22.8	-0.4	0.3	9.9	1.0
	2	-4.4	3.1	19.1	-0.4	0.4	10.1	3.8
1	0	0.0	2.7	12.5	-0.9	0.4	10.0	0.0
	1	-4.5	2.3	17.4	-0.9	0.3	10.0	1.0
	2	-4.5	1.3	16.2	-0.9	0.2	10.1	3.7
2	0	35.1	1.9	-90.0	-1.0	0.3	10.7	2.4
	1	34.9	3.3	-90.0	-1.0	0.5	10.6	3.4
	2	38.1	3.3	-90.0	-1.0	0.5	10.8	5.3

Table 11 Summary of parameter estimation variance for He2D

Ts	σ_{HU}	V_{LH}	V_{LUNG}	Q_{CO}	T_{LUNG}
0.5	0	4.14E-07	4.01E-07	2.02E-05	4.92E-03
	1	2.01E-02	1.88E-02	9.50E-01	2.30E+02
	2	3.38E-04	3.08E-04	1.55E-02	3.79E+00
1	0	4.20E-06	4.01E-06	2.02E-04	4.69E-02
	1	9.80E-03	9.02E-03	4.56E-01	1.14E+02
	2	1.52E-04	1.35E-04	6.92E-03	1.84E+00
2	0	4.87E-05	4.23E-05	2.16E-03	5.16E-01
	1	5.25E-03	4.67E-03	2.34E-01	5.61E+01
	2	7.00E-05	5.80E-05	2.88E-03	8.32E-01

Table 12 Summary of parameter estimation variance for the He1D system

Ts	σ_{HU}	V_{RH}	V_{PER1}	V_{PER2}	T_{PER}	Q_{PER}	Q_{COr}
0.5	0	6.23E-12	1.06E-09	7.83E-12	7.58E-08	5.96E-08	3.56E-10
	1	3.83E-03	6.26E-01	4.55E-03	4.51E+01	3.55E+01	2.13E-01
	2	5.85E-05	8.95E-03	7.09E-05	7.00E-01	4.99E-01	3.29E-03
1	0	3.50E-11	5.50E-09	4.39E-11	4.25E-07	3.09E-07	2.00E-09
	1	1.88E-03	3.04E-01	2.32E-03	2.26E+01	1.70E+01	1.06E-01
	2	2.83E-05	4.87E-03	3.47E-05	3.39E-01	2.71E-01	1.57E-03
2	0	2.22E-03	3.94E-01	3.59E-03	2.97E+01	2.19E+01	1.21E-01
	1	3.14E-03	5.16E-01	5.08E-03	4.20E+01	2.87E+01	1.71E-01
	2	1.87E-05	3.08E-03	3.05E-05	2.52E-01	1.70E-01	1.02E-03

Contour plots of the noise-free cost-functions for the left heart and right heart estimators ((5.14) and (5.15)) were created for a range of parameters and are shown in **Figure 31** and **Figure 32**. In each plot, two parameters were varied about a nominal value while the other parameters in the model were fixed. The resulting plots are 2D projections of the *n*-space hyperplanes defining the parameter space over the specified range. When the ellipsoids near the minimum of the solution space are elongated, this gives an indication that numerical solvers could have trouble converging on the true minimum and increased variance. The contour plots do display single minima. Many of the parameter pairs exhibit long and narrow ellipses near the minimum – in particular the V_{LH}, V_{LUNG} pair for the He2D subsystem.

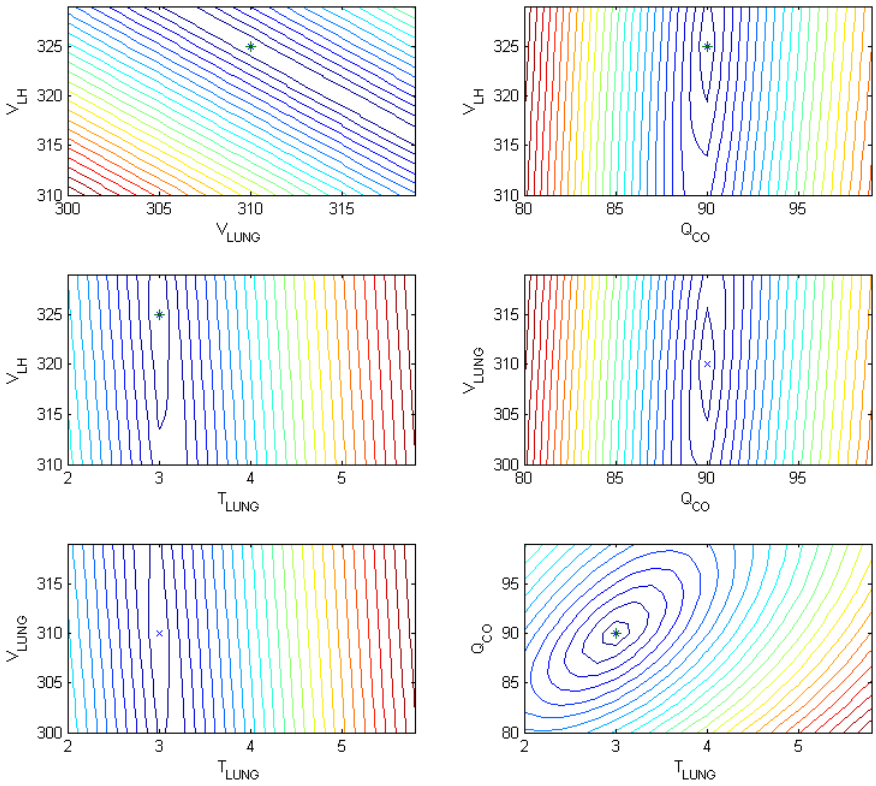

Figure 31 Contour plots of the J_{LH} cost-function for parameter pairs for the He2D subsystem.

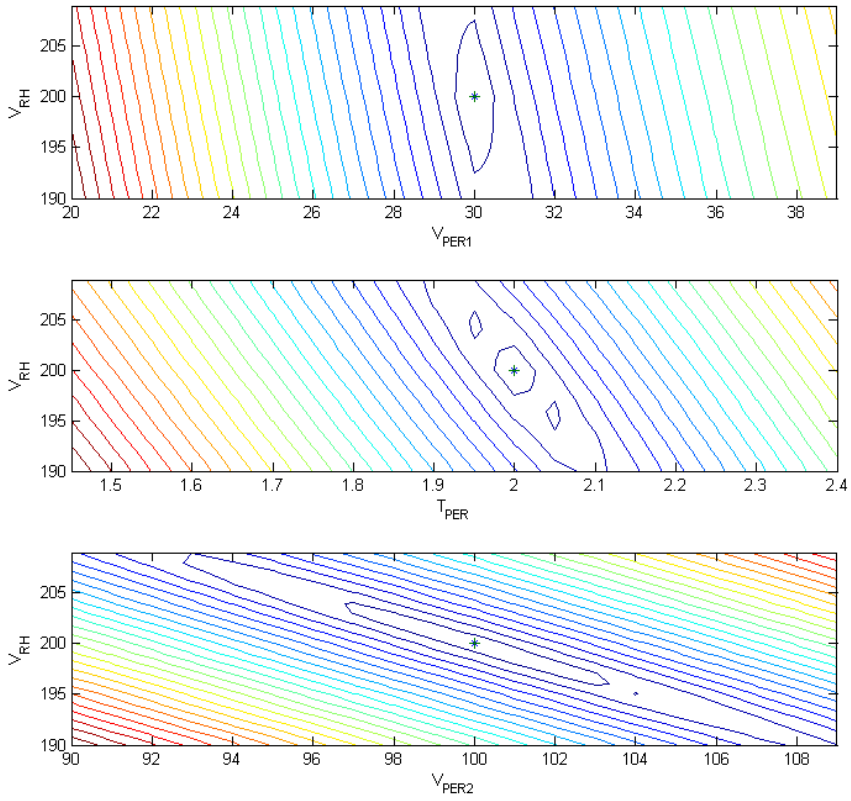

Figure 32 Contour plots showing projection of the J_{RH} cost function as a function of parameter pairs.

5.1.5.2 Hybrid Model Parameter Estimation Results Results from parameter estimation experiments using the hybrid model as the source of enhancement data for 20 subjects are presented in this section. In all 20 subjects, test bolus enhancement data were generated in the left and right heart compartments of the hybrid model using an input injection of 20 ml, 350 mgI/ml concentration contrast injected at 5 ml/s followed by 40 ml of saline. AWGN (standard

deviation = 2.5 HU) was added to the simulations response vectors and the test bolus enhancement signals were truncated at 35 seconds.

The diagnostic injection for the simulated data set was a 75 ml bolus of 350 mgI/ml at 5 ml/s and followed by 40 ml of saline at 5 ml/s. Only data between the scan delay and the end of the scan were used in the comparisons between the estimated and simulated data (the scan delay and scan duration for each subject came from the clinical data set) as illustrated in **Figure 33**. For all subjects, the data points between the two vertical lines were included in the computations of RMSE, PDME, and EDI as defined in (4.30).

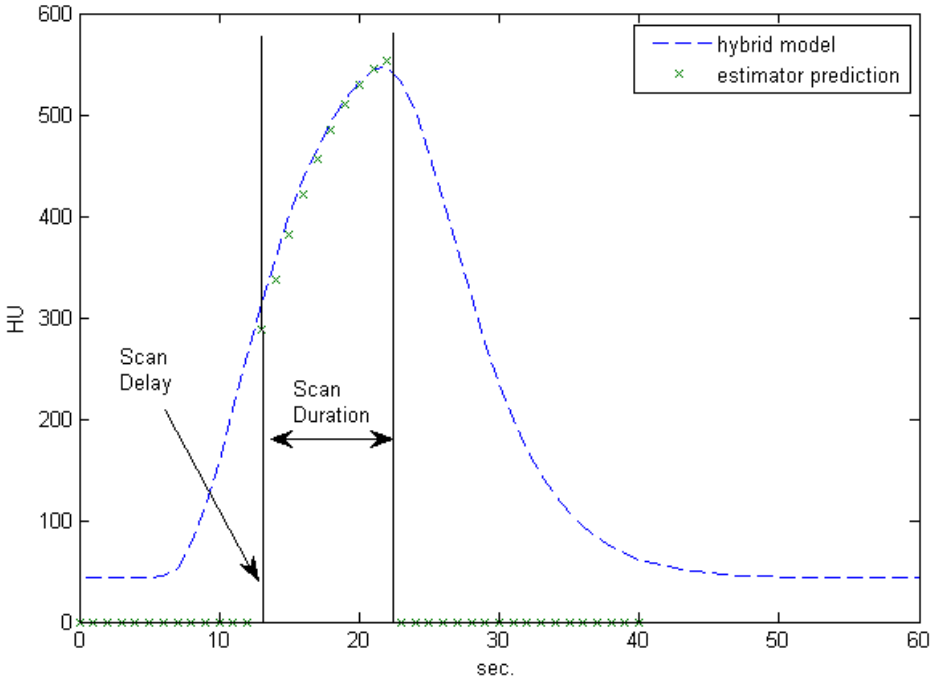

Figure 33 Hybrid model simulation for a diagnostic injection, using Subject 6 data, and estimated enhancement curve using the MLE methodology. The scan delay and scan duration values were extracted from the clinical data set for subject 6 as well.

The mean Root Mean Square Error between the simulated and estimated response was 7.78 +/- 4.40 HU. The average maximum percent difference between maximum enhancement (PDME) for both curves across the 20 subjects was 1.29 +/- 1.12%, and the mean Enhancement Difference Index was 1.57+/- 1.16%.

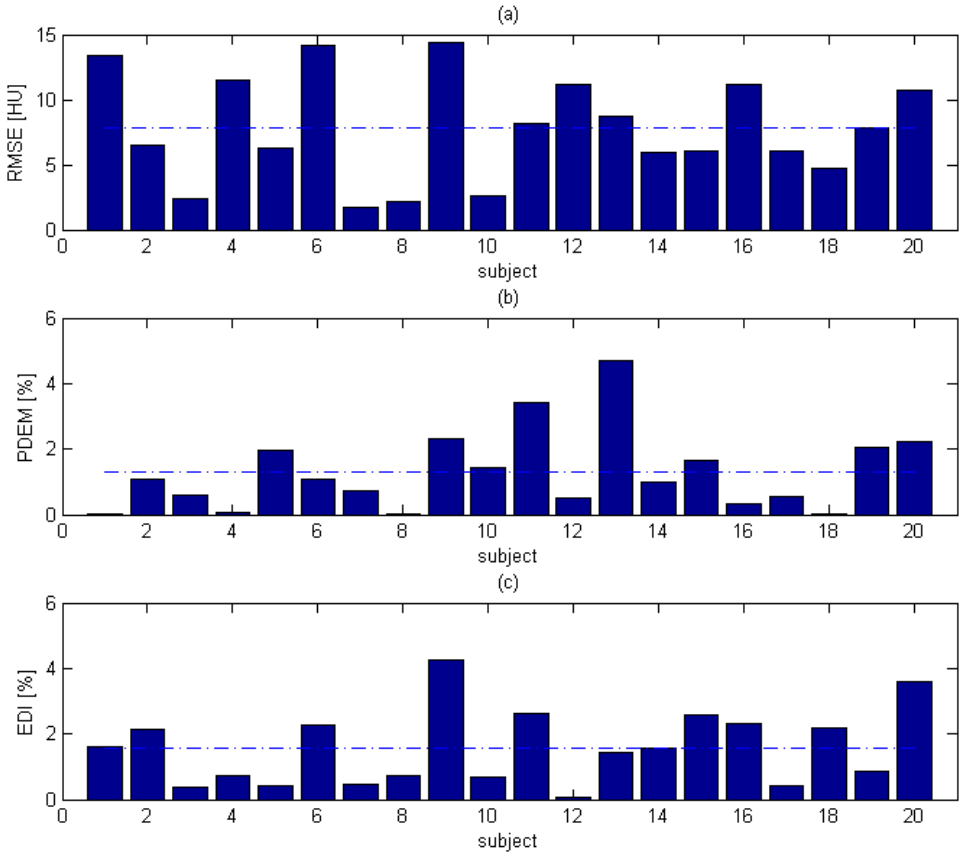

Figure 34 Results from the hybrid model simulation set using the Maximum Likelihood Estimator. a) Root Mean Square Error between 20 patients simulated with the hybrid model and the predicted enhancement b) The Predicted Difference Maximum Enhancement between the

simulated hybrid model data and the estimated response c) Enhancement Difference Index results. Dashed lines represent the mean value for each data set.

The impact of test bolus data length and additive noise on the estimator's performance are shown in **Figure 35.** Hybrid model simulations of the twenty subjects in the clinical set were performed using the same diagnostic injection for all subjects (75 ml of 350 mgI/ml concentration contrast at 5 ml/s followed by 40 ml of saline).

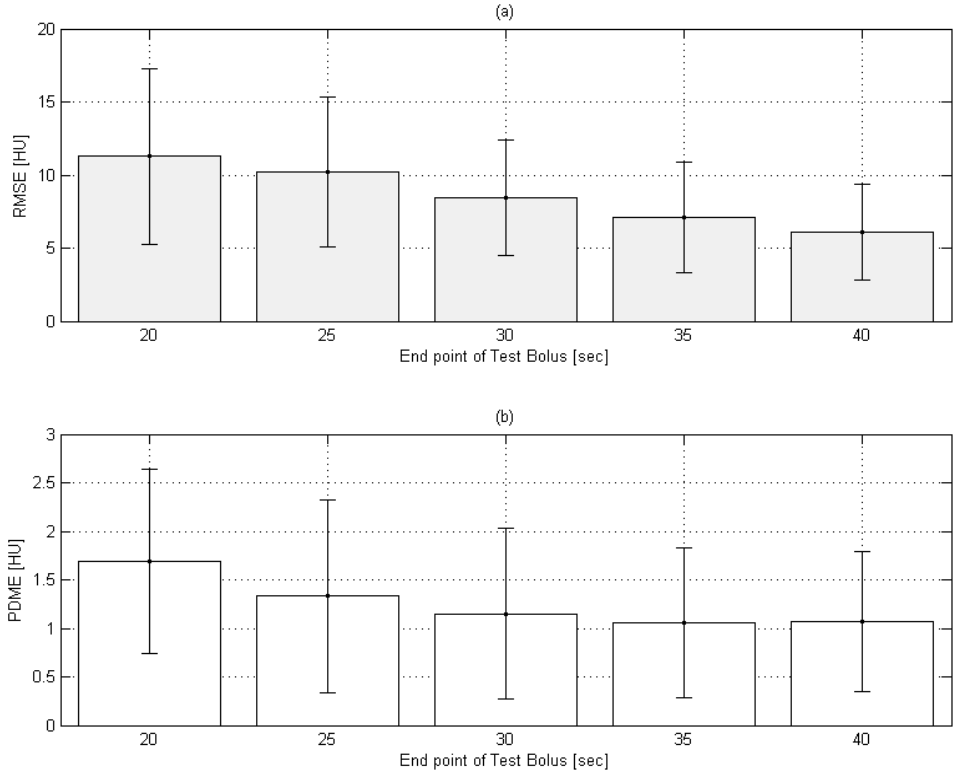

Figure 35 Simulation results using the MLE methodology from hybrid model data (mean of 20 subjects). Error bars indicate one standard deviation of the mean. a) Root Mean Square Error (RMSE) between simulation and predicted enhancements b) Percent Difference Maximum Enhancement (PDME) between simulation and predicted enhancement data.

In the experiments that generated **Figure 35**, the additive noise was zero. As the test bolus data vector decreased, the RMSE and PDME increased. It is not expected that scanner operators will acquire test bolus data many seconds after the appearance of the peak contrast opacification due to increased patient radiation exposure. Typical peak times in the ascending aorta from a test bolus injection are 17 to 24 seconds. The mean time to peak in the simulation cohort was 21.1+/- 2.1 seconds. When the test bolus curves were truncated at 20 seconds, the peak enhancement was missing in most instances. Despite this fact, the estimator was still able to generate estimates of the system dynamics with 12 HU RMS error.

Shown in Figure 36 is the performance of the estimator when additive noise between .1 and 20 HU is added to test bolus enhancement data truncated at 25 and 35 seconds. There is a consistent separation of approximately 3 HU for RMSE and there is less RMSE for longer test bolus enhancement curves. Prediction of maximum contrast enhancement is less sensitive to the length of test bolus measurement data vector. Typical noise on clinical test bolus enhancement data ranges between 2 and 10 HU. The difference in PDME between 25 and 35 second test bolus vectors is less than .5%. Both comparison metrics remain constant until the additive noise sigma exceeds 2 HU. Then the errors increase linearly.

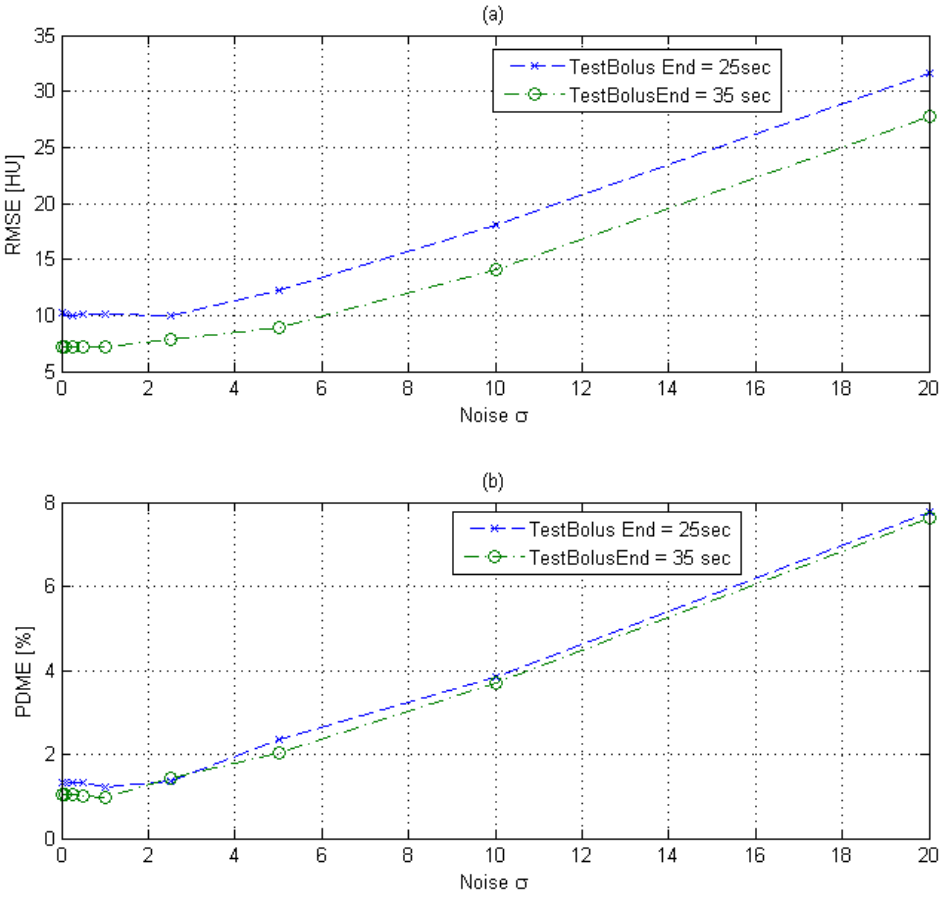

Figure 36 Results demonstrating the impact of reduced length test bolus for identification and noise contribution on estimator performance a) RMSE between hybrid model simulation outputs and the estimator's predictions for test bolus data ending at 25 and 35 seconds b) PDME between the hybrid model simulation outputs and estimator's predictions for test bolus data truncated at 25 and 35 seconds.

5.1.5.3 Maximum Likelihood Estimation Results with Clinical Data This section presents the ability of the estimator to predict contrast enhancement using the retrospective clinical data set. For each subject, the test bolus TEC data measured in the pulmonary trunk and the ascending aorta were used as inputs to the MLE algorithm. Comparisons between the estimated model (based on the MLE fitting) and the diagnostic scan contrast enhancement in the aorta were made. The injection protocol and scan parameters from the clinical data set were used in making the comparisons and only data points between the scan delay and the end of the scan were included in the computation of RMSE, PDME and EDI (as demonstrated with **Figure** 33).

Figure 37 presents the results for all 20 subjects estimated using the test bolus data and the MLE technique. The horizontal, dashed lines indicate the sample mean for each performance metric. Subjects seven, nine and fifteen have the largest errors across all three categories. Numerical results from the analysis using the MLE are in **Table 13** along with the prediction results (from Chapter 4) when using the hybrid model parameterized with only subject demographic data. The MLE method resulted in lower mean RMSE, PDME and EDI (PDME was significantly different, $p<.05$) , a smaller range of data for all 3 metrics, and lower valued standard deviations. The maximum RMSE for the hybrid simulation was 142.3 HU while the RMSE was 70.5 HU using MLE. Plots for all 20 subjects and the clinical enhancement data are presented in Appendix C.

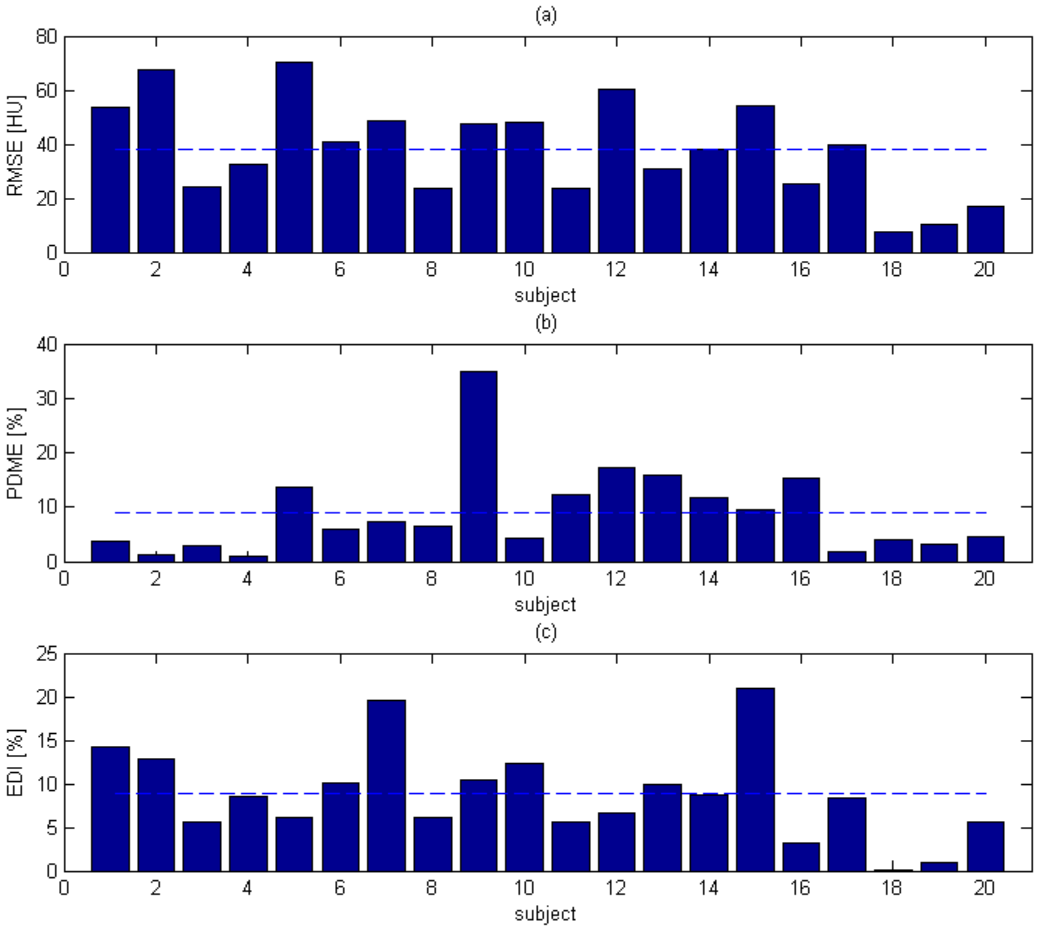

Figure 37 Performance metrics of the MLE methodology using the clinical data set. Dashed horizontal lines indicate mean value.

Table 13 Summary results comparing the MLE and hybrid model prediction results from Chapter 4

	MLE Prediction Results					Hybrid Model Results				
metrics	*mean*	*stdev*	*min*	*max*	*median*	*mean*	*stdev*	*min*	*max*	*median*
RMSE [HU]	38.2	18.1	7.3	70.5	38.7	41.9	29.8	12.2	142.3	37.3
PDME [%]	8.9	8.1	1.0	35.0	6.3	14.6	10.2	0.8	42.1	14.5
EDI [%]	8.8	5.4	0.1	21.0	8.4	10.8	11.0	2.1	45.8	5.3

Figure 38 plots the predicted contrast enhancement and diagnostic contrast enhancement for two subjects (6 and 8). The predicted enhancements for these patients using the hybrid model were presented in **Figure 22** (Chapter 4, page 84). Their prediction performance was the worst among all 20 subjects. Using the test bolus TEC from the clinical data and the MLE methodology, better contrast enhancement prediction was achieved for these two subjects (RMSE of 39 HU vs. 160 HU for subject 6 and 21 HU vs. 57 HU for subject 8 – MLE and hybrid results).

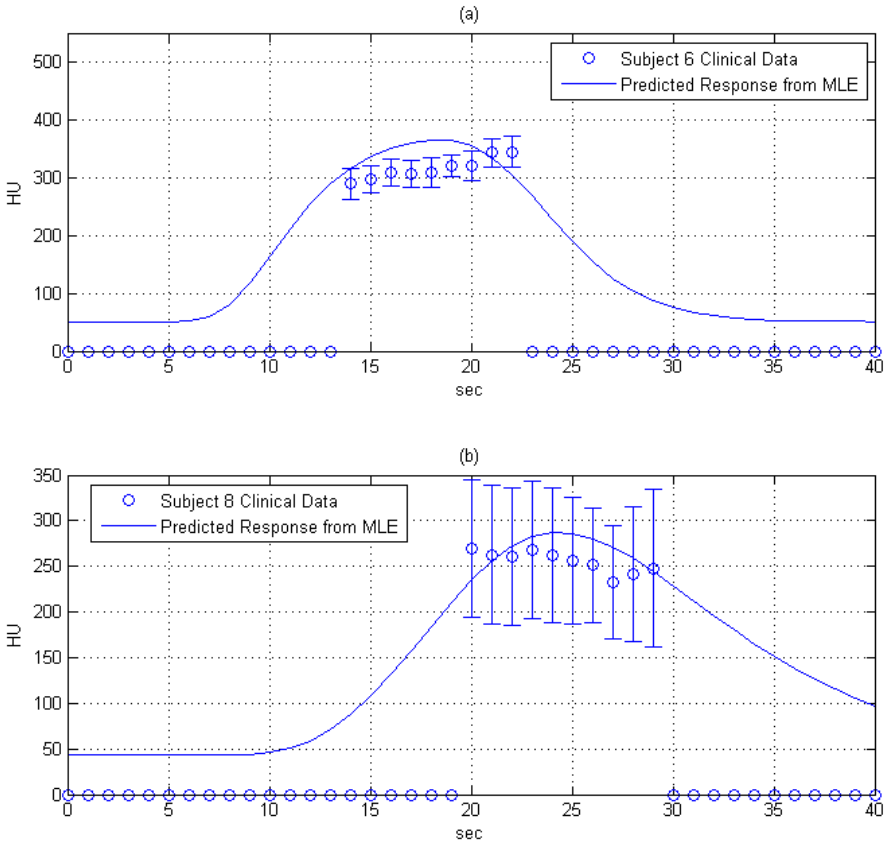

Figure 38 MLE prediction results using clinical data for (a) subject 6 and (b) subject 8. Error bars indicate plus/minus one standard deviation of the mean, as measured in the aorta at the particular z-axis location.

Figure 39 presents box-whisker plots graphically comparing the results from the hybrid model and MLE across the 20 subjects. The horizontal line in each box indicates the median data value and the edges of the vertical boxes indicate 1st and 3rd quartile of data.

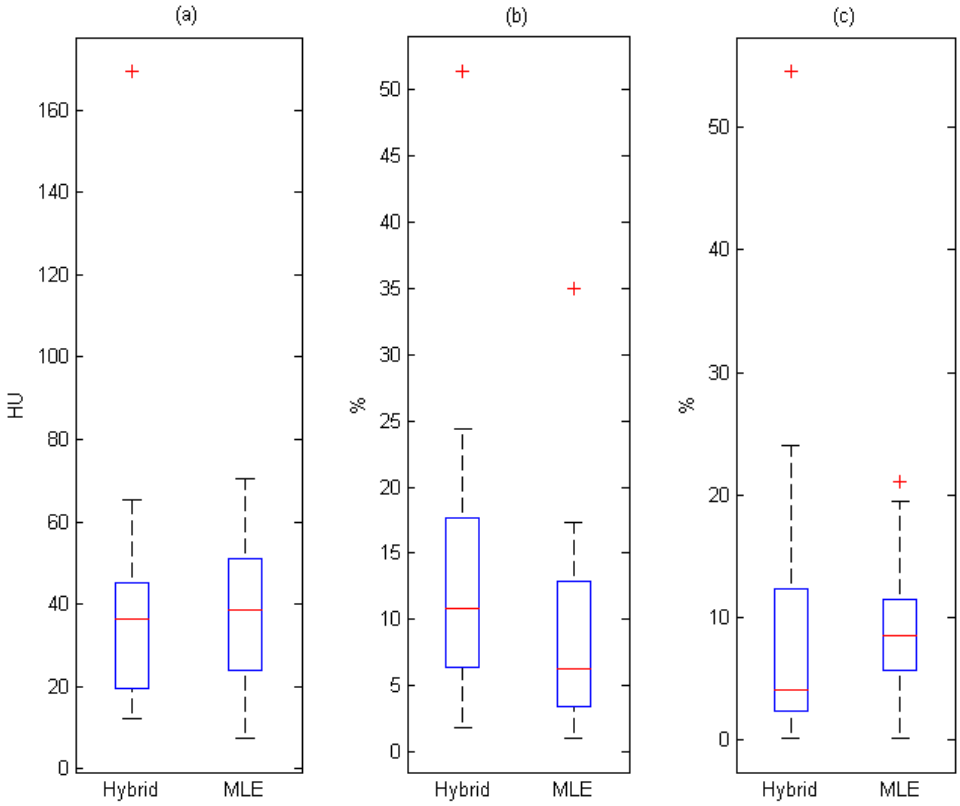

Figure 39 Box-and-whisker plots for results of predicted enhancements using the hybrid model (Hybrid) and the MLE methodology (MLE) to predict contrast enhancement in the clinical data set . (a) RMSE (b) PDME (c) EDI

5.2 NON-PARAMETRIC IDENTIFCATION

In this section, the methodology and results (simulation and clinical data) for a non-parametric identification technique for prediction of contrast enhancement using the test-bolus paradigm are presented. A truncated Singular Value Decomposition method is introduced, it's performance on

simulation and retrospective clinical data are presented and a comparison to the MLE methodology is presented.

5.2.1 Truncated Singular Value Decomposition Methodology

In section 5.1, a parametric identification methodology was developed for estimating and predicting contrast enhancement on an individual basis using test-bolus enhancement data to parameterize a reduced-order pharmacokinetic model. In this section, a non-parametric (or model-independent) approach is developed that is also dependent on data from a test-bolus injection and scan, but only requires data from one scan location. In this research, the ascending aorta is used as the scan location. One advantage of a non-parametric approach is that assumptions, such as the model structure and order, are not required. The assumption that the underlying system dynamics can be modeled as a LTI system is made, however.

The non-parametric methodology poses the contrast enhancement problem as an inverse problem in which the output (image data from the ascending aorta upon administration of a test-bolus) and the input (test bolus Iodine administration profile) are known. A regularization method, the truncated Singular Value Decomposition (tSVD) presented in Section 2.11 is used to estimate the impulse response (or residue function) of the drug and cardiopulmonary system. A truncation index that adapts to measurement noise and that balances residual error and solution error must be selected for the tSVD to produce the desired results. As discussed in section (2.23), the adaptive truncation index and the tSVD is more robust to data variation than the Fleischmann/Hittmair Fourier deconvolution methodology because in that approach only a low pass filter with a fixed cutoff frequency was used.

The necessity for a regularization technique, like tSVD, when creating predictive contrast enhancement techniques is demonstrated with an example. An estimated impulse response, $\mathbf{h_{sys}}$, for Subject 7 in the clinical data set (test bolus TEC data) was generated by using standard linear least squares (MATLAB's matrix left division operator). The enhancement dynamics were defined by the matrix product of the impulse response and a lower triangular, Toeplitz matrix formed from the input function(2.20): $\mathbf{y_{LH}=U_{inj}h_{sys}}$. **Figure 40** plots a linear least squares solution for $\mathbf{h_{sys}}$, using the clinical enhancement data from the left heart generated from a test bolus injected at 5 ml/s for 20 seconds (350 mgI/ml concentration contrast). Clearly evident are the oscillations introduced by the measurement noise. The linear least squares method inability to filter the noise prohibits the robust estimation of the system impulse response.

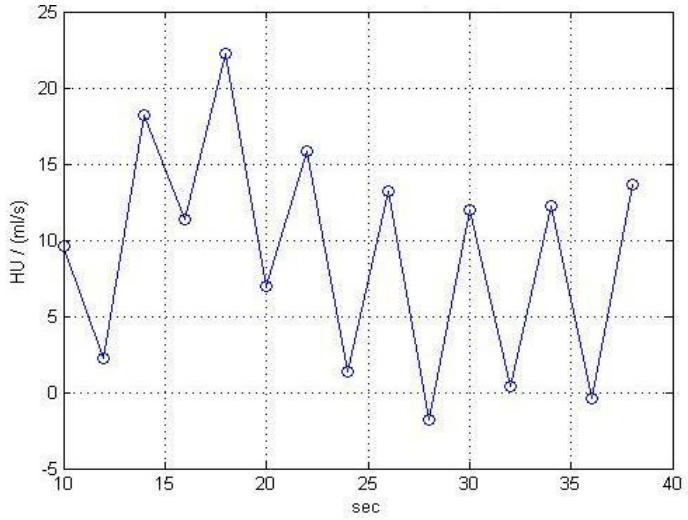

Figure 40 Solution for the impulse response, h_{sys}, using subject 7 data and matrix division (least squares solution)

Contrasted with the impulse response estimate using simple Least Squares is the plot in **Figure 41** which is an estimated impulse response for Subject 7 using the tSVD methodology developed in this section. The detailed algorithm for creating a contrast enhancement prediction using the tSVD is presented below in Table 14.

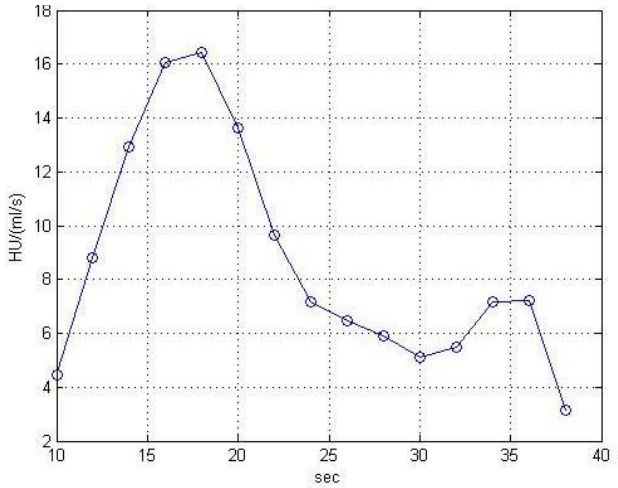

Figure 41 Estimated impulse response for subject 7 data using the tSVD method

.

Table 14 Non-parametric estimation algorithm

1. Acquire and process test-bolus enhancement data from the Left Heart compartment (ie: Ascending Aorta), $y_{LH}^{Test}(n)$ generated by a test-bolus injection, $u_{inj}(n)$.
2. Define the system in matrix notation as in (2.20): $\mathbf{y}_{Test} = \mathbf{H} \cdot \mathbf{U}_{Test}$
   a. Construct a Toeplitz Matrix $\mathbf{U_{temp}}$ from the scalar input function, $u_{Test}(n) = Q_{inj}C_{inj}[u(n)-u(n-N_{inj})]$where Q_{inj}, C_{inj}, and N_{inj} are the flow rate, concentration and duration of the test bolus injection.
   b. $\mathbf{U_{Test}}$ is the lower triangular portion of $\mathbf{U_{temp}}$
3. $\mathbf{H} = \mathbf{U}_{Test}^{-1} \cdot \mathbf{y_{Test}}$
4. Decompose $\mathbf{U_{Test}}$ into its singular vectors (**U, V)** and singular value matrix (**Σ**) by the Singular Value Decomposition:
   a. $\mathbf{H} = \mathbf{U\Sigma V}^{T\ -1}\mathbf{y}_{Test}$
5. The columns of **H** are (per (2.23)):
   a. $\mathbf{h}_k = \sum_{i=1}^{k} \frac{u_i y}{\sigma_i} v_i$
6. Determine the system impulse response estimate, $\mathbf{h_{sys}}$, by selection of an optimal truncation index, *k*. Select *k* by the method of:
   a. Piecewise linear-fit method Koh et al [47]
   b. Adaptive pruning method of Hansen et al [58]
7. Compute RMSE between $\hat{\mathbf{y}}_{Test} = \mathbf{h}_{sys} \cdot \mathbf{u}_{Test}$ and $\mathbf{y_{Test}}$
8. Compute estimate of diagnostic enhancement $\hat{\mathbf{y}}_{Diag} = \mathbf{h}_{sys} \cdot \mathbf{u}_{Diag}$ for an arbitrary injection input, $\mathbf{u_{Diag}}=Q_{Diag}C_{Diag}[u(n) - u(n-N_{Diag})]$

Two approaches for selecting the truncation index, *k*, in the singular value decomposition were investigated and implemented – the linear piece-wise fit method of Koh et al [47] and the adaptive pruning L-curve criterion of Hansen et al.[58]. The truncated singular value decomposition method provided in the Regularization toolbox [59], freely distributed on the Internet, (tsvd.m*)* was used to create impulse response estimates.

As presented in section 2.11, the Koh method computes the truncation index by approximating the Picard plot with a piece-wise, linear function. A Picard plot is a log plot of the Fourier coefficients against an index variable ranging over the length of the data samples in the observation vector, $\mathbf{y}_{LH}^{Test}$. The system of linear equations for the problem is:

$$\mathbf{U}_{inj} \cdot \mathbf{h}_{sys} = \mathbf{y}_{LH}^{Test} \tag{5.22}$$

which is similar to the standard notation of Ax=b for a linear system. The Fourier coefficients are the absolute values of the product of the left singular vectors (columns of the left singular matrix from a singular value decomposition) and the observation vector $\left|u_i{}^T \mathbf{y}_{Test}\right|$. The coefficients for the approximation to the Picard plot were determined by solving:

$$\beta_{lsq} = \frac{\mathbf{X}^T\mathbf{Y}}{\mathbf{X}^T\mathbf{X}} \tag{5.23}$$

where **Y** is the vector of Fourier coefficients, $\left|u_i{}^T \mathbf{y}_{Test}\right|$. The **X** matrix was formulated as described in section 2.11. MATLAB's internal matrix multiplication and inversion utilities were used to solve (5.23). Finally, a vector consisting of the sum of squared errors, SSE indexed by *k*, was constructed:

$$SSE_k = \left(Y - \mathbf{X}\beta_{lsq}\right)^T \left(Y - \mathbf{X}\beta_{lsq}\right) \tag{5.24}$$

Per Koh's algorithm, the optimal truncation index was selected as the index belonging to the element of the SSE array with the smallest value.

The adaptive pruning algorithm for determining the truncation index is described fully in [58]. In summary, the technique constructs a discrete L-curve, which is simply a plot of the solution norm $\left\|h_{sys}\right\|_2^2$ versus the residual norms $\left\|\mathbf{U}h_{sys} - \mathbf{y}_{Test}\right\|_2^2$. The Hensen adaptive pruning algorithm searches for the L-curve's corner by systematically removing points from the discrete L-curve in two stages. The corner function in Hansen's Regularization Toolbox implements the pruning algorithm, and it was used to compute the truncation index, *k* [59].

Simulations of the hybrid model were used to determine the preferred methodology to compute the truncation index. The same twenty subjects simulated in section 5.1.4.2 were simulated, using a fixed flow rate and volume of contrast (5ml/s of 350 mgI/ml contrast for 4 seconds) as the injection for all the simulations. Two simulation runs were completed. The first used the L-curve adaptive pruning algorithm to determine the optimal truncation index for the tSVD and the second used the Koh method to select the truncation index. A comparison of RMSEs between the two methodologies was performed to determine the preferred method.

Mean values for the three performance metrics, RMSE, PDME and EDI across the 20 subjects are given in Table 15. The Koh method produces predicted enhancement with 11% less RMS error, 22% less maximum difference error, and 10% less average EDI percentage. Also, the resulting impulse responses and reconstructed test bolus curves were smoother when the Koh technique computed the truncation index. Also, the Koh method computed lower valued

truncation indices than the adaptive pruning algorithm for this problem. The Koh method was selected, based on these results, for the subsequent experimentation.

Table 15 Simulation analysis results comparing the two methods of determining the tSVD truncation index

Truncation Method	Mean RMSE [HU]	Mean PDME [%]	Mean EDI [%]
Adaptive Pruning [58]	7.9	2.2	1.9
Koh [47]	7.0	1.7	1.7

5.2.2 Evaluation Methods

One set of experiments used the hybrid PBPK model to generate enhancement data and was conducted to determine the performance of the non-parametric estimator in the presence of additive noise and with truncated test bolus measurement vectors. Next, retrospective clinical data (the same set as used with the parametric MLE technique described in Section 5.1) were used to ascertain the performance of the non-parametric technique with human subject data. The performance metrics were then compared to those from the parametric method in Section 5.1.

5.2.2.1 Hybrid Model Simulation Experiments Once again, a set of 20 subjects were numerically simulated using the hybrid PBPK model and the patient demographics from the clinical data set using the same methodology as in section 5.1.4.2 . Only the test bolus response

in the left heart compartment, $y_{LH}^{Test}(n)$, was used in generating the non-parametric estimate of the system. The block of 20 subjects had AWGN added to the test bolus data (0,.1,.25,.5,1,2,5,10,20 HU). The impact of the test bolus vector on performance was investigated by performing simulations with variable length test bolus enhancement data.

5.2.2.2 Clinical Data Experiments Experiments using the retrospective clinical data set were conducted, again using the methods of Section 5.1.4.3. The same performance metrics, RMSE, PDME and EDI, were used to describe the performance of the estimation and prediction technique. Comparison to the results using the MLE methodology was also conducted.

5.2.3 Numerical Simulation Results

Presented here are the results of the tSVD methodology tested with simulated data and clinical imaging data. The mean RMSE, PDME and EDI results for all 20 subjects using tSVD to predict contrast enhancement using simulated data from hybrid model simulation are presented in Figure 42. Comparisons were made between the simulated and predicted enhancement in the left heart compartment when the same diagnostic injection protocol was delivered to all 20 simulated patients. These results are comparable to those in **Figure 34** where the MLE method estimated the contrast enhancement for these 20 subjects. The RMSE (mean +/- standard deviation) between the enhancement values was 7.3+/-5.1 HU, the PDME was 1.8+/-1.3%, and EDI was

1.6+/-1.3%. Using the MLE with these same data resulted in RMSE, PDME, and EDI of 7.78+/-4.40HU , 1.29+/-1.1%, and 1.57+/-1.2% (see **Figure 34**).

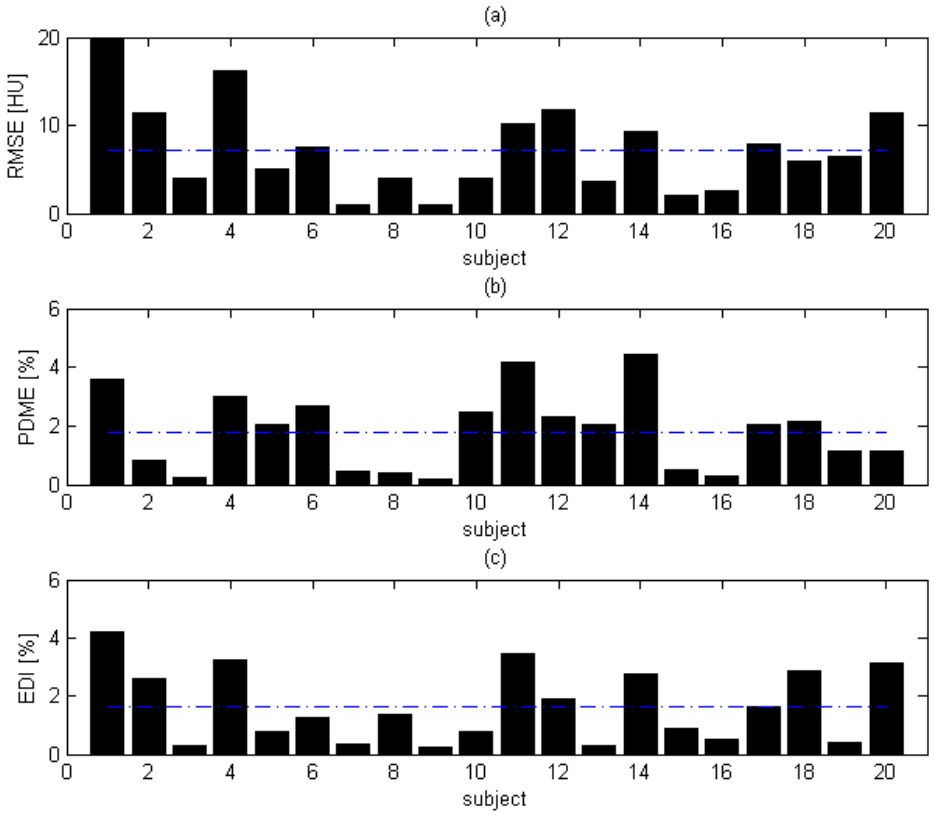

Figure 42 Performance metrics for the tSVD estimating left-heart enhancement with the hybrid model data. The horizontal, dashed blue line represents mean (a) Root Mean Square Error (b) Percent Difference Maximum Enhancement (c) Enhancement Difference Index.

The impact of variable length test bolus enhancement data (20 to 40 seconds) on tSVD estimator performance are presented in **Figure 43**. The data are average values taken across all

20 subjects at each test bolus enhancement vector length. No noise was added to the test bolus enhancement data for these experiments.

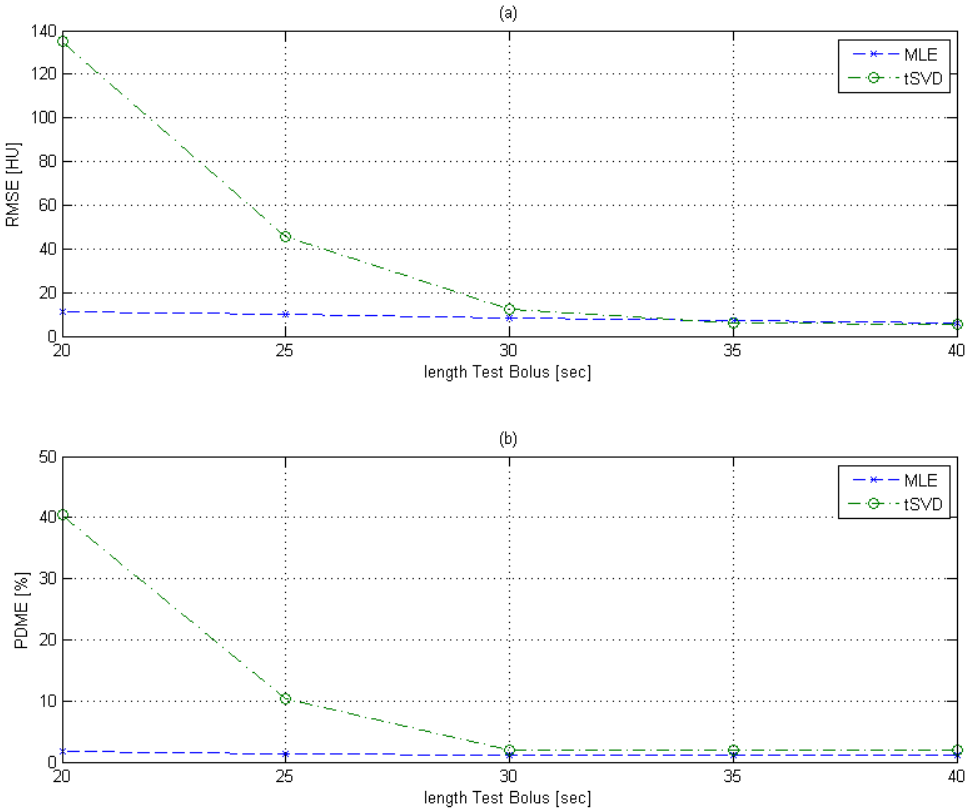

Figure 43 Hybrid model simulation results comparing the performance of the MLE and tSVD estimation methodologies as the length of the test bolus vectors ranged from 20 to 40 seconds . In all simulations, there was no additive noise present on the test bolus data.(a) RMSE results (b) PDME results

The performance of the tSVD estimator when the test bolus enhancement data were corrupted with AWGN is presented in **Figure 44**. Twenty simulations were performed using the

demographic data from the clinical data set. Test bolus vectors were truncated at 35 seconds for all the simulations. Additive Gaussian noise with standard deviations of 0,.1,.25,.5,1.0,2.5,5.0,10 and 20 HU were added to the test bolus data for each block of 20 subjects. The average RMSE values for the tSVD and MLE estimators are plotted together in the figure. Note that when the additive noise was greater than 2.5 HU, the MLE performed better. For low levels of additive noise (.1, .2, .5, and 1.0 HU sigma), the tSVD performed slightly better.

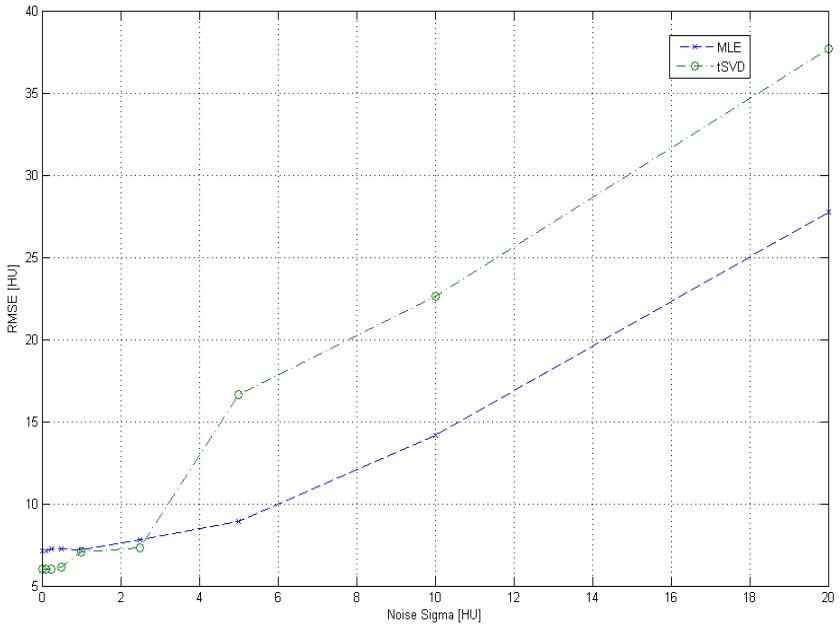

Figure 44 Simulation results for test bolus length of 35 seconds but when AWGN (sigma) added to the test bolus data varied from 0 to 20 HU. Each data point is the mean of 20 simulated subjects using the hybrid model.

5.2.4 Clinical data results

Comparative results for the tSVD and MLE methodologies, using the clinical data as the source of the test bolus and diagnostic enhancement data, are given in **Figure 45**. The MLE estimation technique produced enhancement estimates with lower RMSE, PDME and EDI in 14/20, 13/20, and 13/20 subjects, respetively. Summary results for the three performance metrics RMSE, PDME, and EDI were (mean +/- SD): 49.1+/-24.7 HU, 14.9+/-10.5 %, and 13.6+/-9.6%. Plots for all 20 simulations are presented in Appendix D.

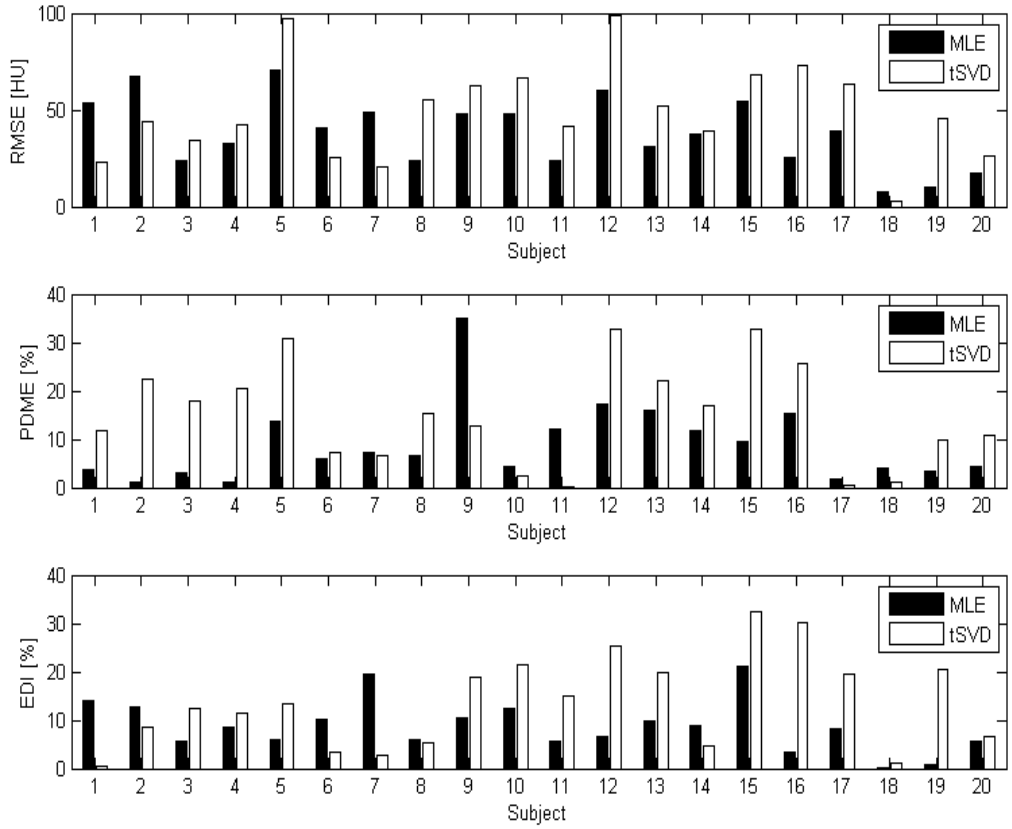

Figure 45 Results from the two estimation methodologies, MLE and tSVD, using the clinical data set test bolus vectors and diagnostic enhancement data (a) RMSE (b) PDME (c) EDI

The box and whisker plot in **Figure 46** show that the MLE method produced lower RMSE, PDME and EDI across the 20 subjects, but the differences were not statistically significant. It is apparent from the box-whisker plot that the estimated enhancements using tSVD resulted in wider variability around the median. Mann-Whitney U tests on the three sets of metrics reveals a significant difference only for the PDME results ($p<.05$).

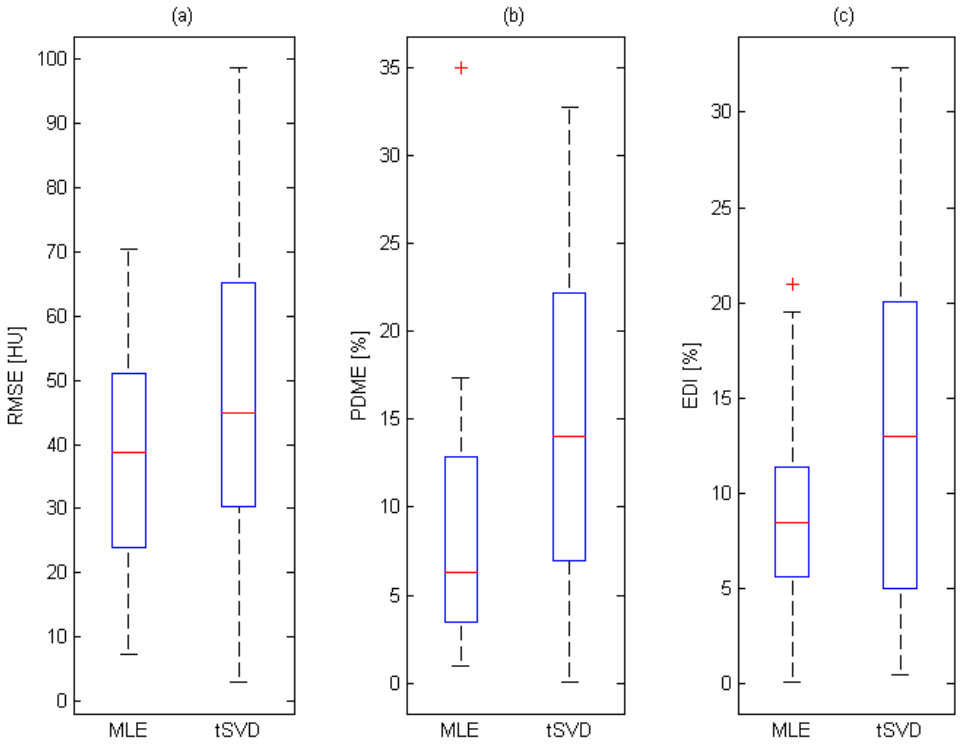

Figure 46 Box and whisker plots comparing the two estimation techniques using the clinical data set as the basis of comparison. (a) RMSE (b) PDME (c) EDI

In some cases, however, statistical significance for all three metrics was demonstrated between the two methods. Subjects 5, 12, and 19 had significantly greater mean RMSE and PDME with tSVD than MLE ($p<.05$, Sign-Rank test). These subjects showed the greatest discrepancy between the two data-driven estimation techniques.

5.3 DISCUSSION

The results indicate that the MLE method is superior to the tSVD method for predicting patient-specific contrast enhancement, especially when considering the constraints and practicalities of actual clinical practice. Specifically, the MLE is more robust to changes in test bolus enhancement data vector lengths, it has favorable noise rejection characteristics, and it provides parametric estimates of physiologic variables that could have utility in quantifying the status of the patient (eg: cardiac output estimation). If test bolus enhancement data are available that extend several seconds beyond the peak of contrast enhancement, then the tSVD and MLE methods perform similarly. In clinical practice, however, it is difficult to ensure that data acquisition during the test bolus scan will routinely contain data points after the peak is achieved.

Whereas the tSVD appears to have superior noise immunity for low levels of AWGN, the MLE has better noise immunity when the test bolus data are corrupted with large values of AWGN. The tSVD has a main advantage in that only one TEC curve is required for estimation and it is computationally less burdensome. However, the optimization within the MLE was performed in seconds using a Pentium III (not exceptional hardware) and widely available numerical methods. It is worth noting that the order of the system matrix computed via the truncated SVD is similar to the total order of the estimated MLE system.

Parametric bias and variance were favorable using the MLE. Visualization of the solution space also revealed well defined minima, albeit they were long and broad in some instances. There is evidence, therefore, to support that the cost function used in the MLE are adequate for computing the required parametric estimations for patient-specific contrast enhancement

prediction based on the performance metrics when the hybrid model simulation data tested the MLE method.

Some of the poor concordance between predicted and clinical data can be attributed to noisy and/or incomplete test bolus TECs from the clinical data set. The large error for subject 15 in both the MLE and tSVD experiments can be directly attributed to an incomplete test bolus curve. Subject 15's TEC is plotted in **Figure 47**. Peak enhancement values in the pulmonary artery and ascending aorta were not captured. Despite these missing features, the MLE was still able to produce a contrast enhancement with morphology not too dissimilar from the clinical data, albeit shifted in time (see Figure 72 in Appendix B). The three performance metrics using the tSVD on this subject, however, were all well above the sample mean, illustrating the impact of limited test bolus data on the tSVD's performance. The TECs for the entire test bolus clinical set are presented in Appendix E.

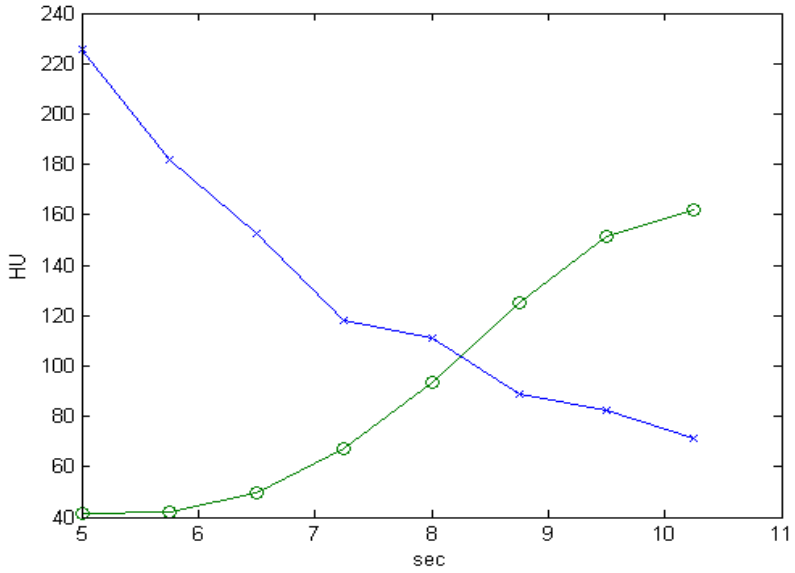

Figure 47 Test bolus for Subject 15 in the clinical data set. The curved marked with the "x"'s is the pulmonary artery TEC and the curve annotated with "o"'s is the ascending aorta TEC.

The second worst EDI score for the MLE outcome was for subject seven. Inspection of the diagnostic enhancement data and the predicted enhancement profile shows that the enhancement prediction tracks the diagnostic, clinical data but is offset by 40-80 HU. Perhaps the baseline attenuation for this subject was lower than 50 HU.

Subject five had the highest RMSE error for the MLE data. There is general agreement between the predicted contrast enhancement and the clinical data for this subject, but the predicted enhancement profile has an upslope that starts several seconds too early. Perhaps the test bolus data were improperly timed or the clinical data set scan delay was improperly recorded. The highest RMSE results with the tSVD predictions were seen with subjects 5, 12, and 16. Subject 15 had the worst performance for all three metrics, attributable to the poor test bolus data for that subject.

In general, the clinical scan data used in this chapter are not ideal for testing the identification methods because they were generated with diagnostic injection protocols having different flow rates from the test bolus injection protocol. As discussed in Chapter 4, injection flow rates alter the peripheral compartment flow rate. The dynamics for the model made by fitting the test bolus at one flow rate during the test bolus injection and scan can be slightly different for a diagnostic injection with a different flow rate. An ideal diagnostic injection protocol for comparing the identification methods would be similar to the one used with the hybrid model comparisons in this chapter – a fixed flow rate and same volume for all patients. Future clinical validation experiments using the techniques developed in this dissertation should be cognizant of this limitation and preferentially design experiments in which the test bolus and diagnostic bolus use the same flow rate.

The method by which the diagnostic enhancement data were generated must also be considered a limitation of the analyses because the TECs were not generated from a single-level scan at the same level from which the timing bolus TEC was constructed. Rather, the data were constructed from the spatiotemporal distribution of contrast in the aorta. The generation of the enhancement data from the helical data set could lead to unanticipated error and variability. Examination of the error bars on the diagnostic scan TECs in the plots of Appendix C shows the variability in the data (mostly due to the selection of thin-slice CT data for these analyses). Unfortunately, the ideal validation scenario in which a single level scan is performed at the ascending aorta during the diagnostic injection is not feasible with humans due to the excess radiation and contrast material the subjects would be exposed to. For these reasons, animal and phantom models are needed to validate contrast prediction models and contrast protocol generation techniques. Animal testing can be expensive, so a validated and realistic

cardiovascular phantom that mimics the transport and distribution of contrast material has much value.

Because the data-driven identification estimation techniques use data derived from the system (using a test bolus), they should produce greater prediction accuracy. As expected, the prediction error in subjects 6, 8 and 12, who had the greatest prediction errors with the hybrid model as shown in Chapter 4, decreased because the estimators rely upon image data acquired from the subjects. With a larger clinical data set, a statistically significant reduction in prediction error could be realized.

Whereas the MLE method was deemed a superior approach when two TECs were available, consideration must be made in a clinical algorithm when two ROIs can not be placed or when the data from the first ROI is corrupted. It is anticipated, therefore, that a clinical algorithm should use the tSVD as a secondary approach for estimating contrast enhancement in the scenario just mentioned. Some classification logic will be needed to determine whether the TEC data are adequate for use by the MLE technique.

6.0 PATIENT SPECIFIC CONTRAST PROTOCOL GENERATION

In the previous chapters, patient specific and data-driven techniques for identifying and predicting contrast pharmacokinetics in the human cardio-vascular system were developed. The goal of this research is not only to predict contrast enhancement, but to provide a method to compute an injection protocol that achieves prospectively chosen enhancement targets for an individual patient and procedure while using a minimal volume of contrast material. This chapter presents the methodology for computing individualized injection protocols for contrast-enhanced, cardiothoracic CT Angiography. The method was tested using the hybrid PBPK model developed in Chapter 4 as a surrogate for human data.

6.1 PROTCOL GENERATION ALGORITHM

The problem is posed as a non-linear minimization problem, with a non-negativity constraint placed on the input function. A distinct difference between the approach developed here and previously published efforts to compute individualized contrast protocols is that an effort is not made to force the predicted contrast enhancement to a specific trapezoidal function. In both Bae and Fleishmann's approaches, a contrast injection protocol was derived that attempted to achieve a constant, uniform contrast enhancement throughout the duration of the scan. An unfavorable

effect of their approaches is that excess control energy (contrast volume) was exerted in order to achieve the uniform peak enhancement as compared to attempting to focus on achieving peak enhancement.

When Bae and Fleischmann published their approaches for optimal contrast protocol computation, typical acquisition times for CTA scans ranged between 20-40 seconds. With the current generation of CT scanners, the acquisition window for CTA data rarely exceeds 10 seconds. It is less important, with very short scan acquisitions, to design injection protocols that minimize or prevent skewed, peaked enhancement profiles. Rather, a modern injection protocol generation technique should attempt to ensure that the scan occurs during the peak contrast enhancement and that a sufficient contrast enhancement is achieved at the start of data acquisition and at the end of the scan acquisition. The scan durations for the clinical data set used in the comparisons in Chapters 4 and 5 averaged 10 seconds. Those data were collected in 2006 and 2007. In the past 2 years, CT technology has advanced such that those scan times are now longer than the typical scan duration.

The goals of CTA contrast enhancement, and thus those guiding the protocol generation methodology in this research, are graphically depicted in **Figure 48**. A hybrid PBPK model simulation produced the contrast enhancement profile shown in the figure. The vertical lines represent a 4 second CTA acquisition window – a scan duration typical with contemporary CT scanners. The scan is timed so that it is positioned on the enhancement profile to ensure that peak contrast opacification is obtained during scan acquisition. At the start of scan acquisition (the scan delay) and at the end of the scan, the contrast attenuation is greater than 350 HU. If the scan duration was 8 seconds in this example and the desired enhancement target was 300 HU, then the goal would also have been satisfied by the injection profile assuming that the scan delay was

adjusted appropriately to ensure the scan started at 300HU. It is evident that an individual protocol generation algorithm should also compute an individual scan delay because the optimal scan acquisition time varies as a function of the injection protocol, the patient's hemodynamics and the selected contrast enhancement target.

The contrast enhancement level is a parameter that should be free for the radiologist to choose, and the appropriate enhancement target will depend upon the preferences of the radiologist dictated by the suspected pathology, and any procedural constraints. A general consensus has emerged that a minimum contrast enhancement of 250 HU is acceptable to differentiate vasculature lumen from plaques, thrombus and other pathophysiology during cardio-thoracic CTA [60]. At coronary artery CTA, Cademartiri et al. recently demonstrated an increased sensitivity for detecting accurate coronary stenoses when coronary contrast enhancement is greater than 320 HU [61]. In certain instances, when a patient has renal insufficiency or disease, a lower enhancement level may be tolerated if that means the contrast volume is minimized to help prevent or mitigate renal damage.

Regardless of the precise clinical motivation, a rational and patient-specific contrast protocol generation algorithm should provide the ability to prospectively target a contrast enhancement level for an individual patient. The algorithm should then attempt to achieve a desired maximum contrast enhancement and a minimum enhancement throughout the entire scan duration.

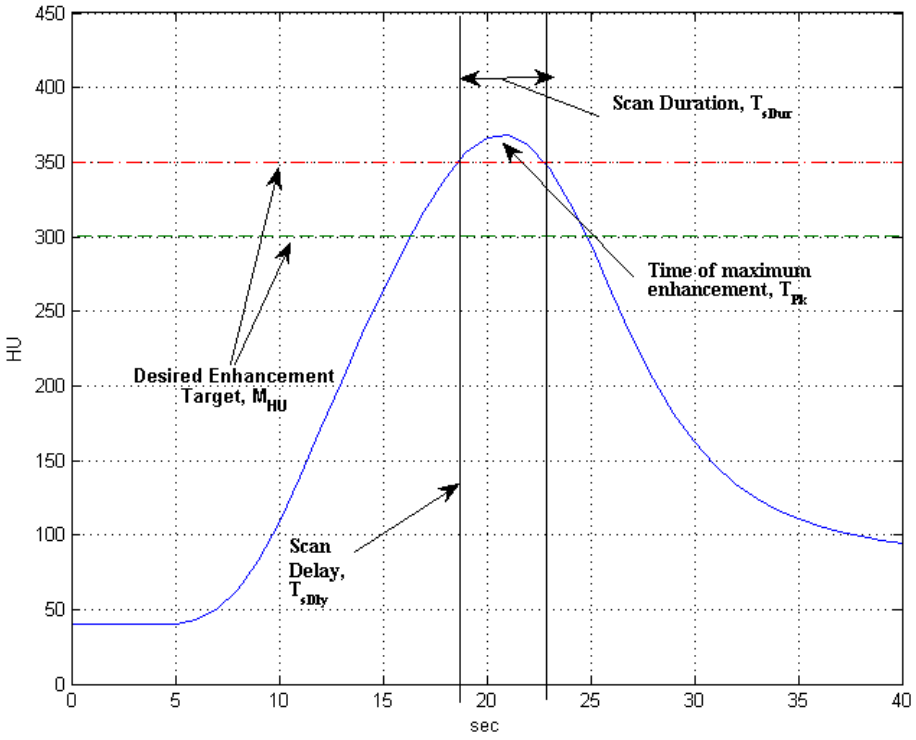

Figure 48 Depiction of the desired outcome from individualized protocol generation. The solid, curved line is a contrast enhancement profile computed with the hybrid PK model, the vertical lines represent the CT scan acquisition window and the dashed horizontal lines represent desired enhancement levels. The nomenclature within the labels coincide to the terms in equation (6.1)

6.1.1 Cost Function Formulation

Important considerations and requirements of a rational contrast protocol generation algorithm were discussed in the previous section. To achieve those goals, a cost function is presented that is the central component of the proposed contrast protocol generation algorithm. The cost function is minimized via numerical optimization. The result of the minimization is an injection protocol with the minimum flow rate and injection duration sufficient to minimize the cost. The cost function used by the contrast protocol algorithm is a function of $\hat{y}_{LH}(n)$, the predicted contrast enhancement in the Left Heart compartment generated by the data-driven, estimation methods developed in Chapter 5. It is:

$$J_{Prot} = \left|\hat{y}_{LH}(T_{sDly}) - M_{HU}\right| + \left|\hat{y}_{LH}(T_{sDly} + T_{sDur}) - M_{HU}\right| + \left|\hat{y}_{LH}(T_{Pk}) - M_{HU} + 50\right| \tag{6.1}$$

where T_{sDly} is the scan delay of the CT study as computed by the protocol generation algorithm, T_{sDur} is the scan duration of the CTA acquisition, T_{Pk} is the time of maximum contrast enhancement, and M_{HU} is the desired target enhancement level. All of the parameters are identified in **Figure 48**. Fifty HU is added to the peak target enhancement recognizing that the contrast enhancement will be peaked and no efforts are made to flatten the enhancement profile (as was done by Fleishcmann and Hittmair). Fifty HU was chosen as the target because two sections of aortic vasculature differing in contrast enhancement of 50 HU are typically not

clinically relevant[2]. Because the simulations and computations are performed in discrete time, the time parameters (T_{sDur}, T_{sDly}, and T_{Pk}) in the cost function are discrete time values. A non-quadratic cost function was chosen because of the success using the absolute value formulation in the [42], but also because the preliminary investigations of the cost function surface revealed that a quadratic form resulted in a much smoother topology near the minima. Furthermore, none of the three terms in the cost function weight any heavier than any other term.

Recall that the predicted Left Heart enhancement is a function of the parameter vectors and the contrast injection:

$$\hat{y}_{LH}(n) = f\ \ \hat{\theta}_{He1D}, \hat{\theta}_{He2D}, u_{inj}(n) \tag{6.2}$$

and the input function for the predicted enhancement , $\hat{y}_{LH}$ is a pulse:

$$u_{inj}(n) = Q_{inj} C_{inj} \left[u(n) - u(n - T_{inj}) \right] \tag{6.3}$$

The cost function defined in equation (6.1) was used and validated by Kalafut et al. in [42] . Its last term penalizes deviations of enhancement greater than 50 HU above the target enhancement level and is added into the cost function to prevent the situation in which the target HU is achieved but the peak is much higher than necessary (and using, therefore, more contrast than necessary to achieve the target goals).

[2] Personal correspondence, UJ Schoepf MD

Put within context of the injection protocol generation, the minimization procedure is stated as:

$$\underset{\phi \in \phi_{min}, \phi_{max}}{\arg \min} J_{Prot}(\phi) \tag{6.4}$$

where the arguments in the vector, ϕ, are the flow rate of the injection protocol ($\hat{Q}_{inj}$) and the duration of the injection ($\hat{T}_{inj}$),

$$\phi = \left[\hat{Q}_{inj}, \hat{T}_{inj} \right] \tag{6.5}$$

which parameterize the input function, equation (6.3).

The minimization is bounded because upper and lower limits are placed on the injection flow rate and injection duration. The obvious lower constraint is non-negativity, but the upper limits are problem specific. For example, the maximum flow rate may be determined as a function of the intravenous catheter's inner diameter or the preference of the nursing staff. The maximum injection duration is a function of the maximum volume of contrast available in the syringe. Because the upper limit of flow rate and volume are dictated by clinical constraints and are user-configurable, the upper limit of the injection duration is the maximum volume divided by the minimum flow rate. The lower flow rate limit is set to 3 ml/s and the minimum injection duration is eight seconds. Injections at flow rates less than 3 ml/s are not appropriate for CTA

because they likely result in enhancements less than 250 HU for the majority of patients. Injection durations less than eight seconds at the lowest flow rate of 3 ml/s also may result in contrast volumes equivalent to the test bolus.

6.1.1.1 Visualization of the cost function The presence of local minima and discontinuities in the cost function should be investigated prior to conducting numerical experiments and to that end, a few surface plots of the cost function given by equation (6.1) were generated using simulated contrast enhancement data created with the hybrid PBPK model. The parameters of the input function ranged from 2 to 7 ml/s (for Qinj) in .1 ml/s increments and from 6 to 22 seconds in .5 second increments. Subject 6's demographic data from the clinical data set were used to generate contrast enhancement predictions, $y_{LH}(n)$, at each pair of injection flow rate and duration. The contrast enhancement targets and scan durations used to generate plots of the cost function space were 250HU, 350 HU target and 2 and 8 seconds respectively. These values represent typical upper and lower limits based on current CT scanning technology and clinical preferences. Three dimensional surface plots of the four cases are presented in Figure 49 and 2D projections of the solution space are presented as contour plots in **Figure 50**.

Inspection of the cost function surfaces show that even for one patient there is a wide variety in the morphology of the solution space as the procedural parameters vary. The 8 second scans display two minima but a well-defined global minimum. For the 2 second scan duration cases, the global minimum is distinct, but it lies in a long trough indicating potential difficulties for a numerical solver to reach the true global minimum. The long trough indicates there may be multiple pairs of injection durations and flow rates that can satisfy the target criterion (achieving the desire target contrast enhancement for an interval equal to the scan duration). These findings

influenced the development of the protocol generation methodology described in the next section.

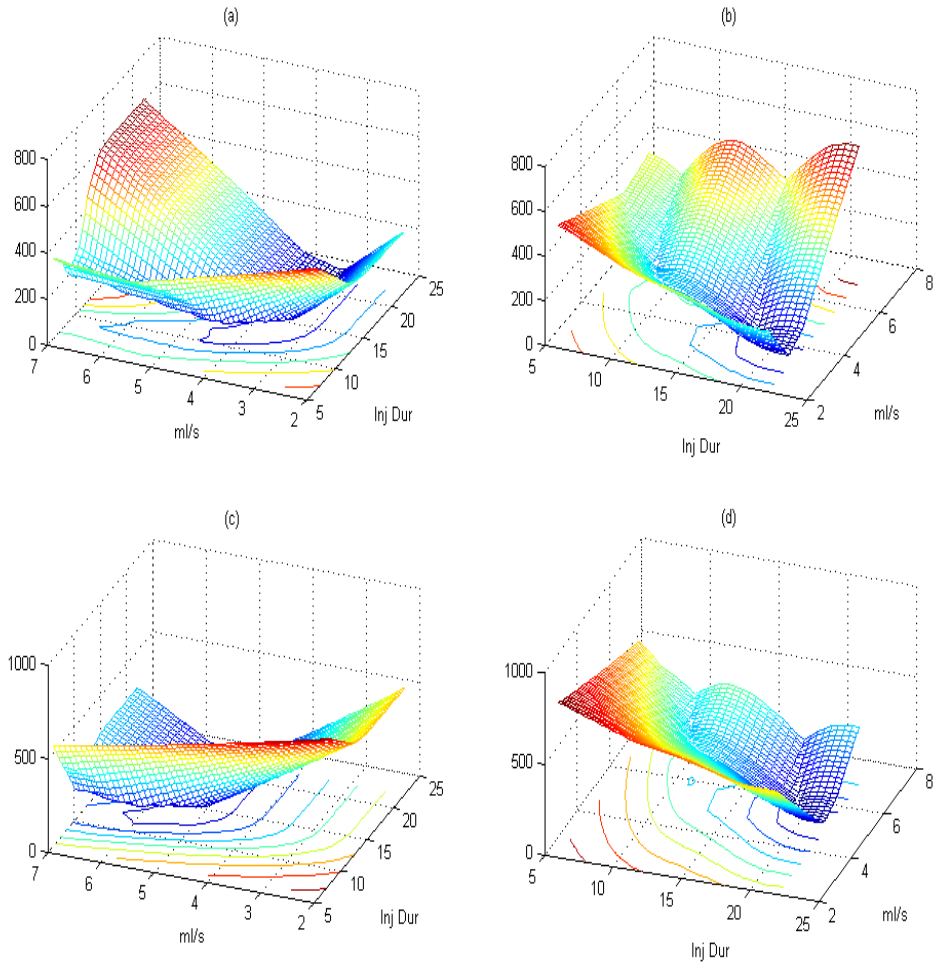

Figure 49 3D surface plots of the proposed cost function (6.1) using simulation data and different procedure characteristics.(a) Cost function for subject 6 with a 250 HU target and a 2 second scan duration (b) Subject 6 cost function with a 250 HU target and a 8 second scan duration (c) Subject 6 cost function with a 350 HU target and a 2 second scan duration (d) Subject 6 cost function with a 350 HU target and 8 second scan duration

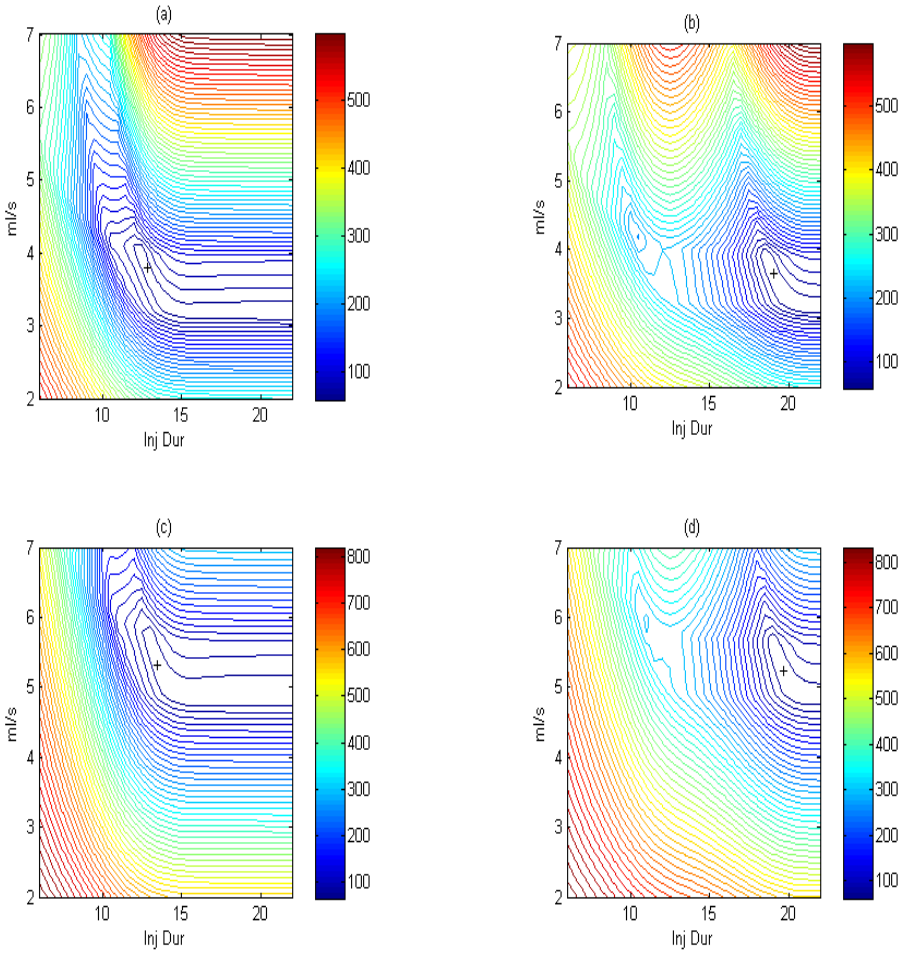

Figure 50 2D Contour plots of cost function for subject 6 simulated data and the proposed cost function, (6.1). The cross indicates the true minimum of each projection. (a) Cost function for subject 6 with a 250 HU target and a 2 second scan duration (b) Subject 6 cost function with a 250 HU target and a 8 second scan duration (c) Subject 6 cost function with a 350 HU target and a 2 second scan duration (d) Subject 6 cost function with a 350 HU target and 8 second scan duration

6.1.2 Protocol Generation Algorithm

As previously discussed, a robust contrast protocol generation algorithm should adapt to each subject and scan duration, allow a radiologist to select desired contrast enhancement targets, and ensure these targets are met at the beginning and end of the scan acquisition. It should also compute a patient-specific scan delay, satisfy the requirements within the parameter constraints of lower and upper bounds, and minimize the total volume of contrast. To achieve these goals, a numerical minimization scheme was developed using the cost function defined in (6.1) and (6.4) with an iterative procedure that adapts initial conditions and upper parameter bounds (when possible) and then tests the solution against the target enhancement goals. Implicit to the protocol generation technique is the use of a timing bolus to generate a patient-specific estimate of contrast enhancement. The general steps of the algorithm are:

1. Inject the patient with a test bolus
2. Process the timing bolus scan data to generate a patient-specific model of contrast enhancement (using the techniques in Chapter 5) using initial conditions in u_{inj} Q_{inj}^{*}, T_{inj}^{*}
3. Given the desired target enhancement levels (HU) and scan duration, compute an injection protocol with a flow rate and duration that satisfies (6.4)

Some parameters in the cost function (6.1) are determined by the preference of the radiologist (target contrast enhancement, M_{HU}) and the procedure (scan duration, T_{sDur}, maximum Volume, V_{max} and flow rate, Q_{max}) while the time of maximum contrast enhancement (T_{Pk}) is determined by the predicted contrast enhancement and the input function, $u_{inj}(n)$.

Consideration must be given to the parameterization of T_{sDly} because it is not easily defined by the radiologist or scanner operator. It is the time on the upslope of contrast enhancement ($\hat{y}_{LH}^{Diag}(n)$) when scan acquisition should commence and is a function of the time to maximum enhancement of the test bolus enhancement, $y_{LH}^{Test}(n)$, measured in the left heart compartment (aorta).

Because the test bolus has shorter injection duration than the full diagnostic injection, the time to reach maximum test bolus contrast enhancement should not be the time to start scan acquisition during the diagnostic scan. It is common practice to compute the scan delay for the diagnostic scan as the time of maximum enhancement from the test bolus TEC plus an offset term, T_{Offset}. In the prior work of Kalafut et al. [41], T_{Offset} was 4 or 6 seconds based on the duration of the scan. For short scans, a longer offset time is used in an attempt to position the short scan window on the peak of contrast enhancement. When the scan is long, the scan should start earlier to help ensure the peak and the target threshold values fit inside the scan window. Because the results in [41] were favorable using this scan timing approach, it was adapted for the current work and is expressed as:

$$T_{sDly} = T_{Pk}^{Test} + T_{Offset} \tag{6.6}$$

where T_{Pk}^{Test} is the peak time of the test bolus TEC. T_{Offset} is four seconds when the scan duration is longer than or equal to four seconds, and is six seconds for scan durations shorter than four seconds. A detailed algorithmic description is presented in **Table 16**.

Table 16 Protocol Generation Algorithm

Begin A: ESTIMATE PATIENT MODEL

1. Use techniques in Chapter 5 based on test bolus data, $y_{LH}^{Test}(n)$ and $y_{RH}^{Test}(n)$ if using MLE technique
2. Compute and store, T_{Pk}^{Test} from $y_{LH}^{Test}(n)$

End A

Begin B: COMPUTE CONTRAST PROTOCOL

1. Get and store: M_{HU}, T_{sDur},V_{Max},Q_{Max}
2. Set upper and lower limits on the parameter vector
   1. $\phi_{min} = \begin{bmatrix} 3 & 8 \end{bmatrix}$
   2. $\phi_{max} = \begin{bmatrix} Q_{max} & \frac{V_{max}}{Q_{min}} \end{bmatrix}$
3. Initialize T_{Offset} and φ
   1. **If** $T_{sDur} \geq 4$ sec
   2. $T_{Offset} = 4$ sec
   3. $\phi_0 = \begin{bmatrix} 4.5 & 15 \end{bmatrix}$
   4. **else**
   5. $T_{Offset} = 6$ sec
   6. $\phi_0 = \begin{bmatrix} 5 & 13 \end{bmatrix}$
   7. **end If**
   8. m =0
   9.
4. **while** targetMet != **true**
   1. run minimization - (6.4) until convergence
      - **i.** update $\phi = \begin{bmatrix} \hat{Q}_{inj} & \hat{T}_{inj} \end{bmatrix}$
   2. compute estimated enhancement using estimated patient model $\{\theta_{He1D},\theta_{He2D}\}$ or h_{est} and $u_{inj}(t)$ with $\phi = \begin{bmatrix} \hat{Q}_{inj} & \hat{T}_{inj} \end{bmatrix}$
   3. Find t_i s.t. $\hat{y}_{LH}^{Diag}(t_i) \geq M_{HU}$
   4. Compute T_D, time $\geq M_{HU}$ from t_i
   5. **If** $T_D \geq T_{sDur}$
      - **i.** update: $T_{sDly} = t_1$, the first element of t_i
      - **ii.** targetMet = **true**
   6. **else**
      - **i.** increment m

ii. If $m \leq 5$
    1. update: $\hat{T}_{inj} = \hat{T}_{inj} + 1$
iii. Elseif $m > 5$ & $m \leq 7$
    1. If $T_{offset} == 6$
        a. $T_{offset} = 4$
    2. elseif $T_{offset} == 4$
        a. $T_{offset} = 2$
    3. end If
iv. else
    1. *Can't satisfy constraints*
    2. targetMet = true
v. end If

7. end If
8. end While

END B

V_{Max} is the maximum upper bound constraint for the minimization and is selected by the radiologist. Q_{max} is the maximum flow rate for the individual patient dictated by venous access or IV catheter gauge. Both Q_{max} and V_{max} determine the upper constraint on the minimization routine.

6.2 NUMERICAL EXPERIMENTS AND RESULTS

A comparison with prior published results was made by implementing the Fleischmann and Hittmair algorithm and using test bolus enhancement data published in [9] as the input and output data. The same test bolus enhancement data was also used by the protocol generation algorithm in **Table 16**, and the contrast protocols generated with both methods were compared.

Validation of the protocol generation algorithm presented here was performed using the same 20 simulated data sets created with the hybrid model in Chapters 4 and 5. Multiple combinations of scan durations and target enhancements defined the procedure data. The generated injection protocols from the numerical minimization and protocol algorithm were used as inputs for hybrid PK model simulations for each subject. The outcome was deemed successful if the contrast enhancement profile generated by the algorithm exceeded the target enhancement (M_{HU}) for the duration of the scan, T_{sDur}.

The algorithm was implemented and executed in MATLAB (R2008b) using the Optimization toolbox function fmincon as the numerical optimization method. The fmincon function performs nonlinear, constrained optimization as a Sequential Quadratic Programming (SQP) problem. SQP techniques break the larger problem into smaller, Quadratic Programming (QP) subproblems at each iteration of the solver. The method uses a line-search technique (an approximation of the Hessian is made at each iteration and a quasi-Newton method updates the Lagrangian) and a merit function to solve each subproblem. More details of the solver may be found in [62].

The solver specific constraints were: convergence tolerance on the parameters (TolX) = 1E-4, convergence tolerance on the function (TolFun) = 1E-4, minimum increment for the finite difference subroutine (DiffMinChange) = .01, maximum increment for the finite difference subroutine (DiffMaxChange) = 2.0, and the maximum number of function evaluations at each iteration was 400. The maximum number of iterations (maxIter)was set at 100.

6.2.1 Comparison to Fleischmann and Hittmair

An implementation of (2.13) through (2.18) was made in MATLAB using the published test bolus enhancement data (as numerically tabulated in an Appendix of [9]) and desired enhancement levels. The test bolus-enhancement response from a human subject (enhancement values reported in [9]) is presented in **Figure 51** and was used to generate contrast protocols. The test bolus enhancement response is typical of short bolus injections measured at the descending aorta by a CT scanner. The desired enhancement was defined as a level of 200 HU starting at the peak of the test bolus enhancement. An increasing ramp ranging from 0 to 200 HU and a decreasing ramp from 200 HU to 0 were added to the leading and trailing edges of the desired enhancement profile to generate a trapezoidal enhancement profile. The slope of the leading and trailing ramps matched those from [9].

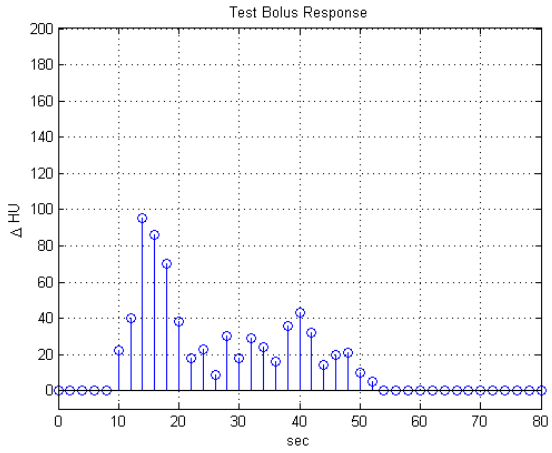

Figure 51 Sample test bolus response measured in a subject in the descending aorta as presented in [9]

Figure 52 presents computed injection protocols using the Fleischmann/Hittmair technique. **Figure 52**-A shows the raw protocol computed by the algorithm. The injection protocol is negative in sections and exceeds flow rates commonly employed, especially when viscous (13 –20 cPoise), high Iodine concentration contrast agents are administered. **Figure 52**-B is the same computed protocol, but with negative flow rates truncated to zero. **Figure 52**-*C* and *D* present the computed protocol with the maximum flow rate set at 7 ml/s (arbitrarily). Protocols *C* and *D* truncate the input protocol at different sample points as explained below.

The time to peak enhancement in the test bolus enhancement of **Figure 51** is 14 seconds and the transport delay, or contrast propagation time, for the contrast to arrive in the vessel (ascending aorta) is approximately 8-10 seconds. The contrast propagation time limits the contribution of contrast in the injection protocol for samples less than 10 seconds prior to the end of the scan. The protocol in **Figure 52**-C is truncated at 34 seconds whereas *D* is truncated at 32 seconds.

A trapezoidal, numerical integration was used to compute the total volume of contrast in each injection and the volumes are annotated in **Figure 52** A-D. These contrast volumes were computed to serve as a basis of comparison to the techniques presented in this dissertation. The total contrast volume decreased as the protocols were modified, but there is clearly arbitrariness in the approach taken to generate these results [9]. Fleischmann and Hittmair do not propose an optimization algorithm to minimize the contrast volume.

Predicted enhancement profiles using the estimated impulse response from Fourier deconvolution (using Fleischmann and Hittmair's technique) and the computed protocols of **Figure 52** are shown in **Figure 53** A-D The smallest residual between predicted and desired enhancement is for protocol A and the most for protocol D.

A contrast protocol was also created, using the same test bolus and procedure data, with the algorithm described in **Table 16**. Because only one test bolus curve is presented in [9], the tSVD methodology was used to identify the patient model. The resulting contrast enhancement curve, superimposed on the desired 30 second scan duration, is shown in **Figure 54**. The contrast volume computed by the algorithm, to achieve the desired enhancement target was 114.9 ml, at a flow rate of 4.1 ml/s. The volume is 20 ml less than that of the lowest volume prediction from the Fleischmann-Hittmair algorithm (**Figure 52**-D) and doesn't require modulation of the flow rate over time which could lead to undesired contrast bolus broadening in the peripheral vasculature.

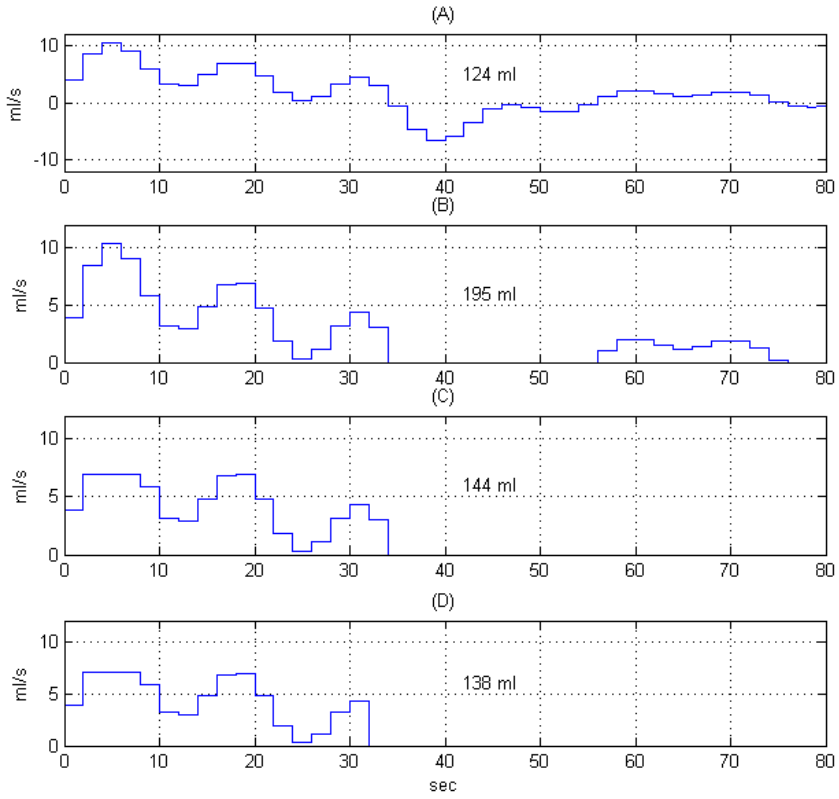

Figure 52 Computed injection protocols using the Fourier deconvolution method described in [9],Ts=2 sec/image. The total contrast volume of the injection is listed in each subfigure. (A) Raw protocol. Because the injection flow rate is allowed to be negative, the total contrast volume is lower than B-D. (B) Non-negative protocol (C) Non-negative protocol clamped at 7ml/s and injection commands at time > 34 sec removed (D) Same protocol as C but samples post 32 seconds removed.

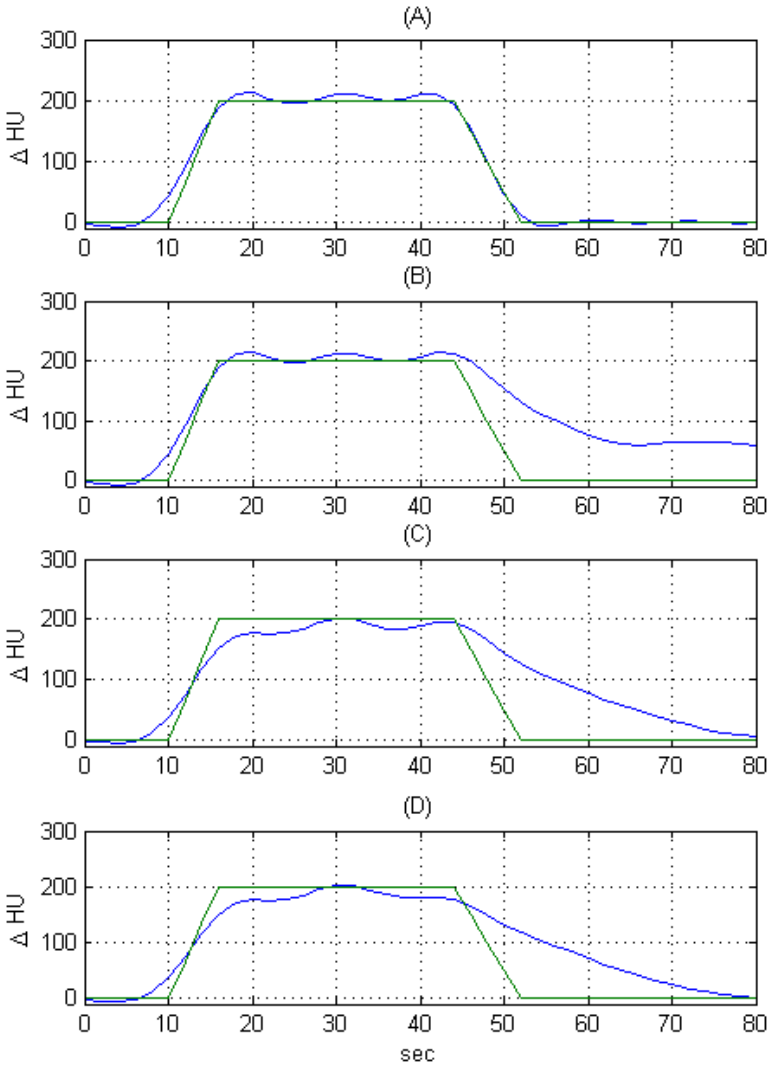

Figure 53 Predicted (blue) and desired (green) enhancement levels generated with the injection protocols presented in (A) Ideal enhancement profile using the raw protocol (B) Enhancement generated with non-negative injection protocol (C) Enhancement when non-negative injection is clamped to 7ml/s and injection is not allowed post 34 seconds (D) Enhancement profile as in C but with samples ignored after 32 seconds.

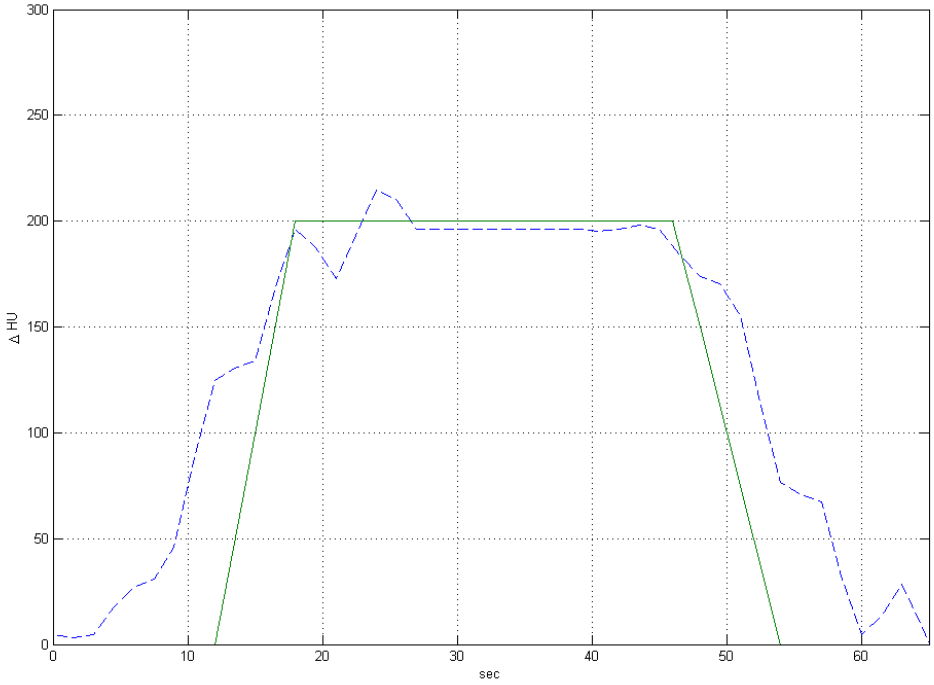

Figure 54 Comparative result between desired enhancement profile(solid line) and the predicted enhancement using the protocol generation algorithm in Table 18 (dashed line). A contrast volume of 115 ml and a flow rate of 4.1 ml/s was computed by the algorithm to generate the enhancement profile shown in the figure. The desired scan duration was 30 seconds.

6.2.2 Hybrid PBPK Model Simulations and Results

The protocol generation algorithm was tested under realistic conditions using 20 simulated data sets generated with the hybrid PBPK model. Subject demographic (height, weight, sex, age) data were identical to those from the retrospective clinical data set used in previous chapters. The physiologic parameter relationships defined in **Table 1- Table 2** were used to set the parameters of the hybrid model for the simulation runs. For each subject, the model was executed (simulation sample period = .01 sec/sample) with a 20 ml test bolus (with a 40 ml saline flush phase) at 5 ml/s as an input function and the corresponding test bolus TECs ($y_{RH}^{Test}[n]$, $y_{LH}^{Test}[n]$) were down-sampled. To better resemble clinical test bolus TECs, the vectors were windowed at 5 seconds (relative to the origin) and truncated at 25 seconds. Also, zero-mean AWGN with standard deviation of 1 HU was added to both TECs.

After the test-bolus enhancement curves were generated, they were used as the input and output data for the MLE algorithm developed in Chapter 5.1. The parameterized patient-specific model parameters ($\hat{\theta}_{He1D}, \hat{\theta}_{He2D}$) were used by the protocol generation algorithm defined in **Table 16**. For a protocol generation algorithm to be effective, it must accommodate different procedure specific parameters and constraints. Therefore, the simulated data were used to generate injection protocols under a combination of procedure settings. All 20 subjects were simulated and tested with desired target enhancements (M_{HU}) of 250 HU, 300 HU and 350 HU which span the range of minimally accepted vessel contrast enhancements [63] considered acceptable for cardiothoracic CTA [61]. At each enhancement target value, experiments were conducted at scan durations of 2, 4 and 8 seconds. These ranges of scan durations are typically encountered when

performing cardiothoracic CTA scanning procedures with modern MDCT scanners (64, 128, 256, 320 slice and dual-source). The maximum flow rate, Q_{max}, was 7 ml/s and the maximum volume, V_{max}, was 150 ml for all subjects. The minimum flow rate in all experiments was 3 ml/s and the minimum injection duration was set to 8 seconds. These values were chosen because it is generally accepted that CTA below 3 ml/s is not feasible and contrast bolus durations less than 8 seconds result in smaller than desired bolus volumes at the minimum flow rate of 3 ml/s (21 ml, for example).

The performance of the protocol generation algorithm was assessed by using the computed injection protocol as an input signal to the hybrid PK model. Upon simulation of the model with the calculated injection protocol, the duration of enhancement greater than the desired M_{HU} was recorded. The enhancement durations were compared to the scan duration for each experimental set and success was defined as enhancement greater than the target for the specified scan duration. Because of rounding errors (mostly introduced by the downsampling of the TECs to 1 sec/sample) and other random effects, acceptability was extended to scan duration plus/minus .5 seconds. A flowchart of the experimental configuration is presented in **Figure 55**.

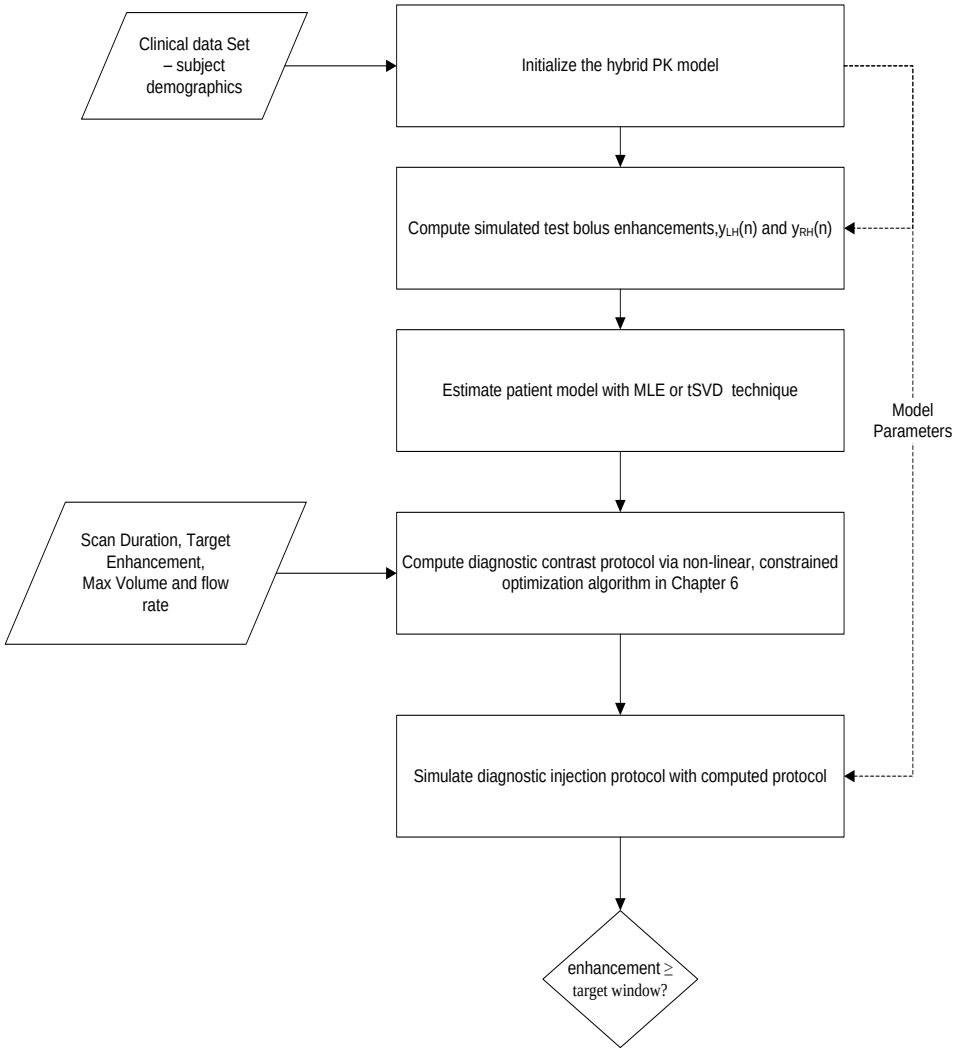

Figure 55 Illustration of protocol generation validation experiments.

An example of a typical result from the experimental data set is shown in **Figure 56**. In this instance (subject 8 from the clinical data set), the scan duration was 4 seconds and M_{HU} was 300 HU. The algorithm computed a diagnostic injection protocol of 4.52 ml/s for 15 seconds (67.8 ml of contrast) and resulted in a hybrid model TEC exceeding the target enhancement for the scan duration.

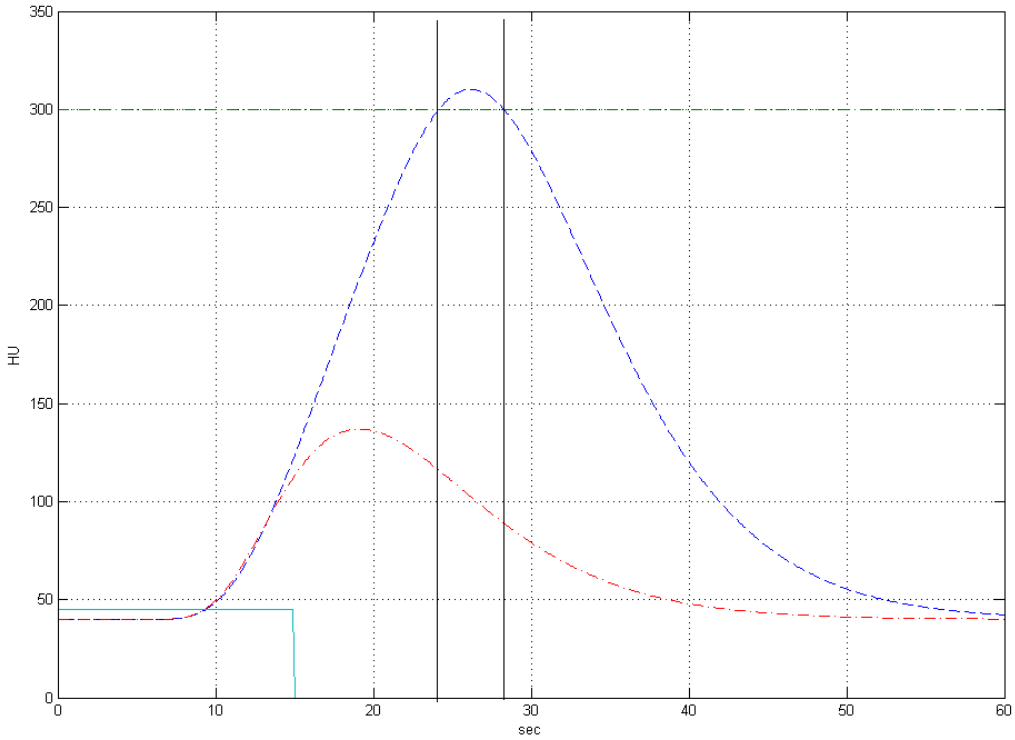

Figure 56 Hybrid model simulation result using Subject 8 data and injection protocol computed with methods presented in this chapter. The dot-dashed TEC (peaking at ~ 130 HU) is the Left Heart test bolus enhancement curve. The dashed TEC was generated with the injection protocol (flow rate 4.52 ml/s. 67.8 ml, 15 sec), visualized by the solid rectangle at the bottom left of the figure (flow rate multiplied by 10). The dot-dashed horizontal line intersecting the top of the diagnostic TEC is the target enhancement M_{HU} of 300 HU. The two solid, vertical lines represent the scan duration window, starting at T_{sDly} computed by the algorithm and lasting for 4 seconds.

Two summary plots displaying time exceeding the target enhancement, M_{HU}, across the 20 simulated subjects are presented in **Figure 57** and **Figure 58**.

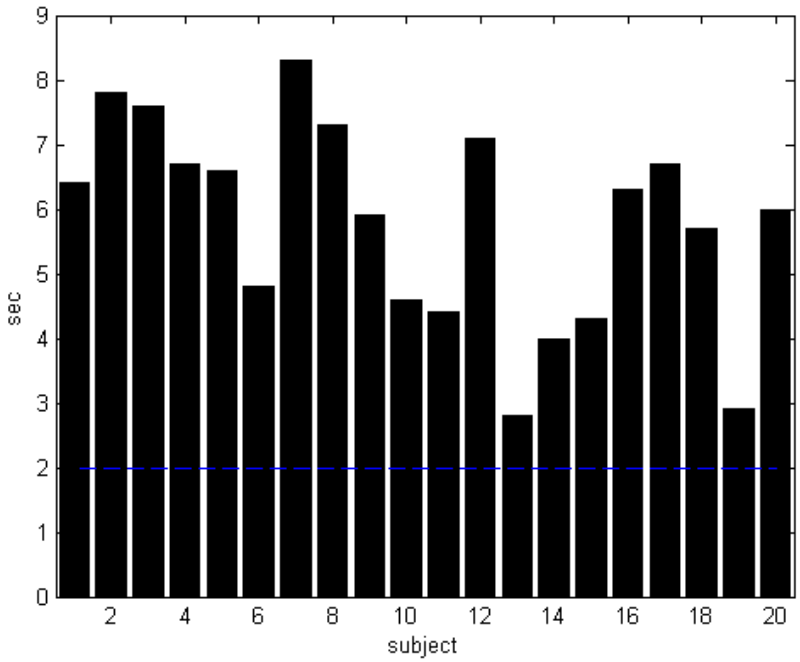

Figure 57 Enhancement values greater than the 350 HU target for the scan duration plotted for all 20 simulated subjects. The horizontal, dashed line at 2 seconds is the scan duration for all runs.

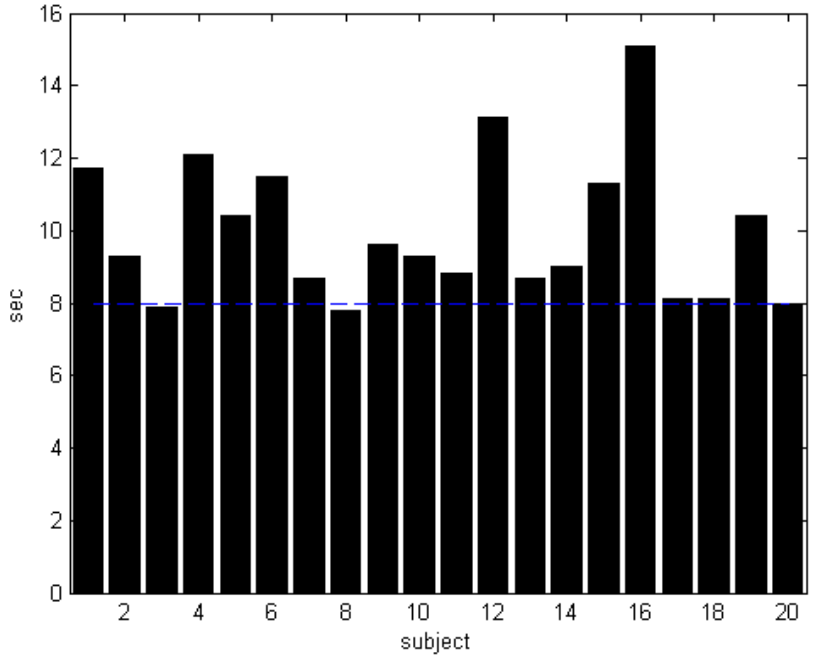

Figure 58 Enhancement values greater than the 250 HU target for the scan duration plotted for all 20 simulated subjects. The horizontal, dashed line at 8 seconds is the scan duration for all runs.

In both figures, the horizontal dashed line represents the scan duration for the particular experiment. In **Figure 57**, the scan duration was 2 seconds and the target enhancement was 350 HU. For all 20 subjects, the enhancement exceeded M_{HU} for the scan duration (starting at the computed scan delay, T_{sDly}).

Figure 58 shows the results of all twenty subjects tested when the scan duration was 8 seconds and M_{HU} was 250 HU. In this experiment, two subjects had resulting enhancement times slightly less than the target (subject 3 – 7.8 seconds, subject 8 – 7.6 seconds), but were within the tolerance stipulated. The other subjects had resulting enhancement curves greater than or equal to the scan duration and, in some instances, with excess enhancement sample time. Compared to

the two second scan duration and 350 HU target results, however, it appears that the optimization resulted in more efficient (minimum flow rate and injection duration) protocols. Tabulated results for all the experiments, including summary statistics of the computed diagnostic injection protocols (flow rates, volumes) are shown in **Table 17**.

Table 17 Summary results from protocol generation experiments. Each row represents 20 simulations of the hybrid PK model at the procedure targets defined in the first two columns.

Targets		*Injection Protocol Statistics (350 mgI/ml)*			*Summary Output Criteria*	
MHU [HU]	**Scan Duration [sec]**	**Mean Vol [ml]**	**Mean Flow [ml/s]**	**Mean Dur [sec]**	**Mean t > scan Dur [sec]**	**n > scan Dur & MHU**
350	2 sec	69.1	5.16	13.4	5.8	20
350	4 sec	69.3	5.26	13.2	6.2	20
350	8 sec	76.0	4.75	16.0	8.1	20
300	2 sec	54.3	5.28	10.3	5.5	20
300	4 sec	55.1	4.78	11.5	5.8	20
300	8 sec	62.8	4.15	15.1	8.3	20
250	2 sec	43.6	4.91	8.9	9.9	20
250	4 sec	43.8	4.37	10.0	6.3	20
250	8 sec	53.7	3.59	15.0	8.6	20

In all of the experimental cases, the non-linear optimizer found a feasible solution and converged to a solution. The average execution time for each subject's estimation and protocol optimization was 5.6 +/- 1.2 seconds (Pentium III PC, windows XPPro, 2 GB RAM).

6.3 DISCUSSION

Testing of the protocol generation algorithm using the hybrid PK model validated the technique as robust across different patient types and procedure settings. The results in **Table 17** reveal

trends consistent with contrast enhancement principles. For example, the injection duration and contrast volume increase as scan durations increase for each target enhancement group. Also, as the scan durations decrease, the computed flow rates increase, which is expected because with short acquisitions, the scan duration should be positioned near the peak of contrast enhancement. One can achieve greater peak enhancement by injecting with a short duration at a high flow rate.

In the results shown in **Figure 57**, the target enhancement was exceeded by a few seconds in all cases. These results could indicate that for short scan durations, the cost function might be modified to result in shorter injection duration. Also, for short scan durations, the positioning of the scan duration on the enhancement curve could be reconsidered. For example, the T_{sDly} could be set as the T_{pk} minus one half of the scan duration. This approach will not produce ideal results, however, when scan times are 8 seconds or longer because the TEC morphology tends to become skewed (to the right) for longer injection durations.

7.0 CARDIOVASCULAR FLOW PHANTOM

This chapter presents a physical, circulatory model designed to mimic the transport and distribution of radiographic contrast material through the mammalian circulatory system. The primary features of the model (or phantom) are: it recreates hemodynamic conditions in ranges similar to humans, it allows for the injection of contrast material, it is radio-opaque and it can be used both in the laboratory (using near-IR dye) and in a CT scanner. The phantom was used to test the methods developed in Chapters 5 and 6, and the results are reported here.

An overview of the phantom is presented followed by characterization study results demonstrating performance equivalency between use in a CT scanner and when near Infrared sensors in the laboratory measured dye injected through the phantom. Finally the results from prospective experiments validating the contrast prediction and protocol generation algorithms (chapters 5 and 6), performed in the laboratory, are presented.

7.1 BACKGROUND

Awai et al. published a feasibility study using a custom circulation phantom [16] to demonstrate and validate basic principles of contrast medium injection. Their model did not contain a separate pulmonary circulation system with physiological venous and arterial pressures, did not

mimic the delicate anatomy of the coronary artery tree, did not simulate the pulsatile nature of the heart, and did not provide a means to interface with a scanner's ECG triggering system. The Awai phantom also did not mimic physiologic hemodynamic parameters such as diastolic and systolic blood pressure. Repeated injections of contrast demonstrated that the model was adequate to replicate the contrast enhancement pattern of the abdominal aorta at CTA [16], however.

To better characterize the dynamics of early-phase contrast enhancement in the cardiothoracic vasculature, to improve upon the work of Awai, and to validate the novel, patient specific contrast protocol generation method developed in Chapter 6, a new flow phantom was developed. The following list enumerates the phantom's characteristics:

- configurable cardiac output, heart rate, stroke volume, blood volume
- accurate transport delays of the injected bolus
- accurate dilution of the contrast media through the cardiopulmonary circuit
- the ability to interface an ECG signal to the scanner
- accurate motion of the coronary tree
- pressures and flow rates within the physiologic realm and responsive to changes in the driving function
- pulsatile blood flow and heart rate

Details of the phantom have been presented by Kalafut et al in [64] and published by Behrendt et al. in [65], but a summary of the phantom and design is presented in the next section. Experiments conducted for this dissertation are then presented in subsequent sections.

7.2 PHANTOM TOPOLOGY/STRUCTURE

The flow phantom consists of a lung and a body circulation with an anatomically accurate replica of the aortic arch, the coronary arteries, and the thoracic aorta. Other components of the phantom include connecting tubes emulating the systemic vasculature, a water filled acrylic container, pressure and flow meters and a height-adjustable setup of the fill and drain compartment for adjusting the arterial and the venous pressure to different values.

A pulsatile Harvard medical heart pump (BS4, Harvard Apparatus, Holliston Mass) acts as the system's heart. The pump can be configured to deliver stroke volumes of 15 to 100 ml, heart rates from 10 to 100 bpm, and systolic/diastolic ratios from 35% to 50% full cycle. The pump was designed to safely administer blood or a blood emulant (like a glycerin and water mixture), but distilled water was chosen as the blood emulant in this research because of the large size of the vessels and the interest in modeling the macroscopic behavior of the contrast media's convective transport.

The pump was modified to generate a trigger signal at the end of full piston displacement. A micro-switch drives a MOSFET circuit that intercepts the ECG signal on a commercial ECG simulator (ECG Plus, Bio-Tek Inc., Winooski, Vermont USA). This circuit entrains the ECG rhythm to the pump – including an R-R interval to match the Harvard pump's duty cycle. The drive circuits of the ECG simulator were not modified so that standard 3 or 5 lead ECG sets from the scanner could record the synthetic ECG signal. The ECG trace is used by the scanner when scanning structures that move with the cardiac cycle and is used in the retrospective reconstruction of the cardiac data sets.

An off the shelf, silicone coronary tree model (Elastrat Model T-S-N-002, Shelley Medical Inc., London, Ontario Canada) emulates the human cardiovascular anatomy. It is the structure within the black box of Figure 59. The cardiovascular model includes a compliant, ascending aorta and arch, and the left and right coronary arteries. An additional silicone tube emulates the thoracic aorta. An image of the phantom system is in Figure 59.

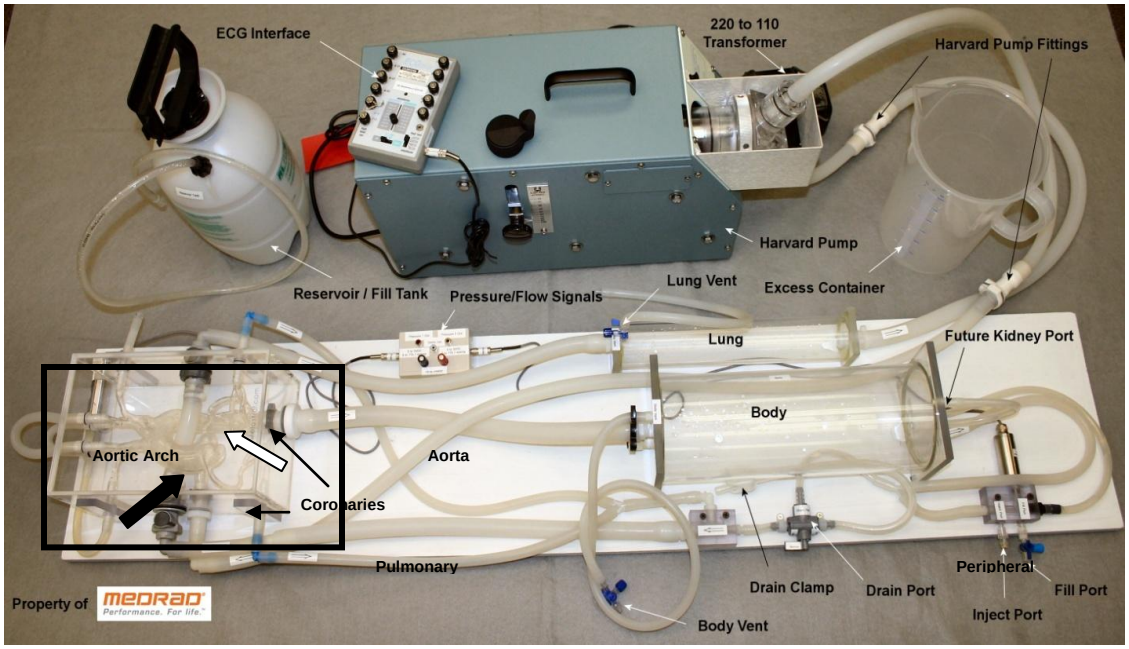

Figure 59 Picture of the cardiovascular phantom system and labels annotating the various sections of the model. The thick white arrow (with black edges) points to the pulmonary trunk structure fabricated for the phantom and the thick black arrow points to the thoracic aorta model.

The standard coronary and aortic arch model developed by Shelley Medical was modified to allow a pulmonary artery to cross the cardiac anatomy (thick white arrow in Figure 59 and Figure 60) to enable the acquisition of single-level, axial scans mimicking the contrast enhancement pattern at the pulmonary trunk in the human vascular system. Figure 60 displays an

axial CT image acquired with a 64 slice MSCT scanner (VCT, General Electric Healthcare, UK) displaying the pulmonary artery in relation to the emulated ascending and descending aorta. This configuration is essential when developing and testing contrast protocol injection techniques requiring TEC information from the pulmonary vasculature and the aorta, as with the MLE methodology for estimating patient specific contrast propagation models. To mimic the X-Ray absorption of the chest, distilled water filled the Plexiglas chamber holding the aortic arch and coronary vasculature.

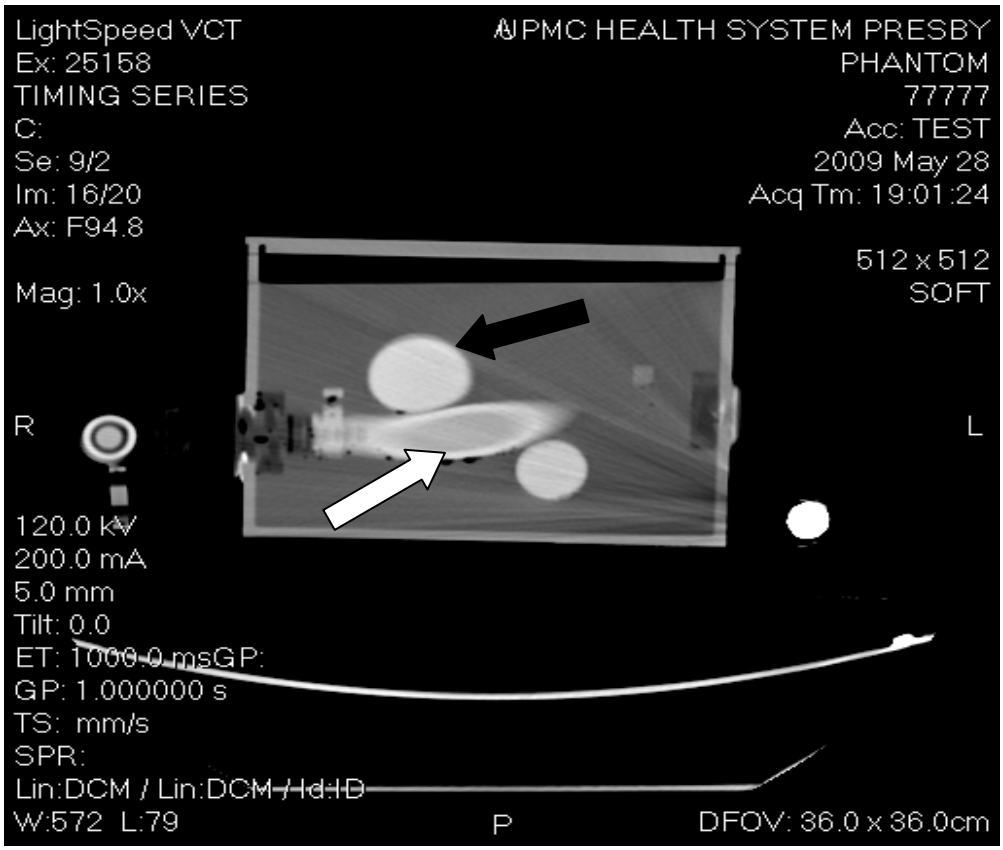

Figure 60 CT cross section of the phantom showing the ascending aorta (black arrow) and the pulmonary trunk (white arrow).

Contrast medium (or emulant) is administered into the phantom through an injection port via a commercially available i.v. catheter (size 18 G) and is transported through a peripheral venous compartment, consisting of tubing more compliant than that used in other parts of the phantom. The water and the contrast medium then circulate through the simulated pulmonary artery, the heart pump, the lung compartment, the aortic arch compartment (including the coronary arteries with direct reflow into the pulmonary system), the descending aorta compartment, and lastly the body compartment. The contrast and water mixture then recirculates back through the model. A diagram of the main compartments included in the model and the corresponding fluid volumes is given in Figure 61. The coronary arteries are configured to drain into a location proximal to the Pulmonary Vascular compartment similar to how the coronary arteries actually drain into the right heart via the coronary sinus in mammalian hearts. The total volume through the coronary artery return circuit, however, is less than 100 ml.

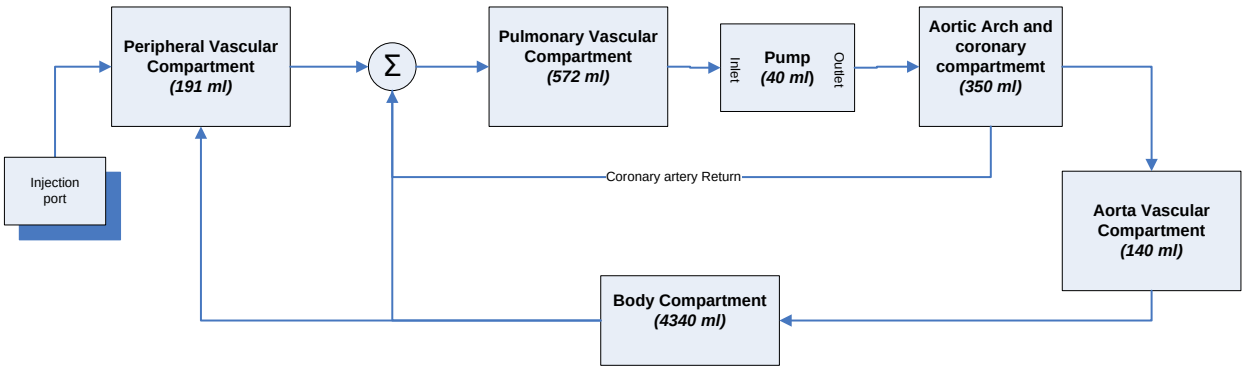

Figure 61 Topology of the cardiovascular phantom. The fluid volume in each compartment is annotated in each block.

To control the inlet pressure at the injection site, the injection port was placed on a lab stand. The variable height of the injection port above the phantom and the introduction of compliant tubing between the injection port and the inlet of the pump allows for control of the venous pressure. The pressure was set at physiological values with a mean venous pressure of 15 mmHg and an arterial pressure of 125/75 mmHg for all experiments.

The phantom is instrumented with two pressure transducers (Omega pressure transducers, PX35D, Omega Inc, Stamford Connecticut USA). One transducer is placed in the low pressure portion of the model, and the second transducer is located in the high pressure region. Instrumentation of the phantom's flow rate is made by in-line, ultrasonic transducers (Transonic Inc., New York USA). The pressures and flow-rates are continuously monitored and acquired using LabView (NIDAQ, National Instruments, Austin Texas USA) Data Acquisition hardware and software during experiments.

To reduce the necessity of requiring a CT scanner while testing protocol generation and identification concepts, custom-engineered and built near Infrared (nIR) sensors were used to measure the concentration of an X-Ray contrast agent emulant. The contrast emulant used is a water soluble nIR dye, a prototype dye manufactured by Fuji Fillm Inc., provided in sample quantities. The sensors consist of an LED and phototransistor pair that resides in an enclosure through which a tubular segment of the model passes. nIR photons pass axially through the tubing and are measured by the phototransistor on the opposite side.

Attenuation of the photons by the water and nIR mixture flowing through the tube is described mathematically by the Beer-Lambert law, which states that the transmission of light through material has a logarithmic dependence on the product of the absorption coefficient and the path-length of the light. For substances in liquid, the absorbance coefficient is the product of

the molar absorptivity and the concentration of the species. Due to this relationship, the concentration of the nIR at locations in the phantom model can be calculated by transforming the voltage of the phototransistor opposite from the nIR LED. One sensor pair is clamped onto a tube just proximal to the pulmonary vascular segment and another is clamped onto a tube segment proximal to the aortic arch compartment. The outputs from these sensors provide analogues to the X-Ray TECs measured by a CT scanner in the pulmonary artery and aortic segments of the phantom.

7.3 EXPERIMENTAL METHODS

Several experiments were designed and conducted to characterize the behavior of the contrast agent distribution through the phantom, to demonstrate equivalence between TEC generation via the nIR dye methodology and data measured from a CT scanner, and to provide validation of the methods developed in Chapters 5 and 6.

7.3.1 Phantom Linearity Validation

X-Ray contrast bolus morphology and transport through the phantom was investigated via several injection and imaging experiments designed and conducted with a 64 Slice CT scanner (Lightspeed 64 VCT, GE Healthcare, Chalfont U.K.). Bae et al [7] demonstrated the linear time

invariant properties of contrast pharmacokinetics with respect to injection duration. It is expected that for a linear system, the contrast enhancement pattern resulting from an injection of a long duration (measured at one-level in the vasculature) should be a linear superposition of injections with shorter durations.

The linearity experiments performed by Bae with pigs were replicated with the phantom via bolus injections using a power injector (Stellant D, MEDRAD Inc, Pittsburgh PA USA) and measurement of the resulting enhancement pattern at a fixed level in the model (the pulmonary trunk). Bolus injections of iopromide 370mgI/ml (Ultravist 370, Bayer Schering Pharmaceutical, Berlin Germany) lasting 5, 10 , 15 and 20 seconds were injected at a flow rate of 4 ml/s. The pump generated a cardiac output of 4.5 L/min (heart-rate of 60 bpm, stroke volume of 75 ml). Scan acquisition started 5 seconds after the beginning of contrast delivery and lasted for 45 seconds. TECs were manually created by a custom program in MATLAB that opened the CT scanner DICOM data. Offline analysis of the image data consisted of drawing a 1 cm ROI over the phantom's "ascending aorta", and software extracted the intensity average at each image. The TEC was constructed by combing the resulting data points into one vector per image data set.

7.3.2 Demonstration of equivalence between CT and nIR Injections

Before using the phantom and the nIR dye and sensors to validate the methods developed in this dissertation, equivalency testing of the nIR sensors was performed. The goal of the experimentation was to compare the phantom response after injection of nIR dye to TECs measured with a CT scanner and X-Ray contrast, using identical injection protocols (flow rates and volumes of the contrast) and pump settings.

The CT experiments were conducted on a 64 slice CT scanner (Lightspeed 64 VCT, General Electric Healthcare, Chalfont U.K.) at the University of Pittsburgh Medical Center. Contrast with a concentration of 370 mgI/ml (Ultravist, Bayer Schering Pharmaceuticals, Berlin) was used in the CT experiments. Twenty milliliters of contrast were injected into the phantom through an 18 Ga peripheral IV catheter at a flow rate of 4 ml/s and followed with a 20 ml saline flush with a CT power injector (Stellant D, MEDRAD Inc., Pittsburgh PA). Three injections were performed and TECs were obtained from a ROI placed on the ascending aorta of the phantom. The average of the three TECs was used to compare against the lab/nIR data.

Calibration of the nIR sensors was performed prior to comparing the CT experimental data with the nIR data. A stock solution of the nIR dye (Fuji Film) was prepared in a concentration of 10mg of dye per ml of distilled water. Eight aliquodts, made from a 5 cm section of phantom tubing with plugs on both sides, were filled with diluted nIR in the following concentrations: .016 mg/ml, .032 mg/ml, .063 mg/ml, .125 mg/ml, .250 mg/ml, .500 mg/ml, 1.00 mg/ml and 2.00 mg/ml. Voltages from the phototransistor circuit were recorded while the nIR LED diode (sourced at 10mA) was energized over 5 second measurement blocks. The nIR concentration values, along with 0 mg/ml concentration solution and a blocked light beam, were plotted against the mean voltages measurements. The resulting concentration versus voltage curve was the calibration curve used to convert sensor voltage readings into concentration units for the equivalence experiments and the other laboratory experiments described below.

TECs were constructed using the operational curve generated during the calibration step and voltages recorded after three, 20 ml injections of 1mg/ml nIR dye (followed by 40 ml of saline) at 4 ml/s using a CT power injector (Stellant D, MEDRAD Inc., Pittsburgh PA). The sensors were positioned on the pulmonary vascular compartment proximal to the aortic arch

compartment as previously described. For all experiments, the Harvard pump was set to generate a cardiac output of 4.5 L/min (50 bpm, 90ml stroke volume) through the phantom. Five liters of water was added to the phantom and refreshed between each injection experiment. An average enhancement profile was compute across the three injections and compared to the mean TEC measured with the CT scanner. Quantitative and qualitative comparisons of the data were made.

7.3.3 Contrast Enhancement Model Prediction Validation

The phantom was used to validate the data-driven methodology for predicting contrast enhancement using test bolus data. The ability of the tSVD method to predict enhancement using a 20 ml test bolus was tested by comparing predicted outputs against enhancement data measured in the phantom for 40ml, 60 ml, and 80 ml injections (1mg/ml dye used for all injections and a 20 ml saline flush followed all injections). In preliminary investigations, it was determined that a reliable pulmonary artery TEC could not be consistently measured with the nIR sensor. It was decided, therefore, to restrict the testing in this section to the tSVD method. The protocol generation algorithm is independent of the methodology used to identify the contrast dynamics so using the tSVD was justified. The injection flow rate was 4 ml/s for all the injections. The same power injector used in the previous experiment injected the nIR dye into the phantom through an 18 Ga catheter. The pump generated a cardiac output of 4.5 L/min, and 5.0 L of water filled the phantom. Between each experiment, the water was cleared of nIR dye and refreshed. Calculation of the RMSE between the predicted and measured data at each injection volume were computed and reported.

7.3.4 Patient Specific Contrast Protocol Creation Validation

The last set of experiments were designed to test the ability of the protocol generation algorithm developed in Chapter 6, independent of hemodynamics, to create injection protocols that achieve preset enhancement targets over a specified scan duration. In these experiments, different patients were approximated by varying the pump cardiac output and blood volume in the phantom.

In the first three experiments, the protocol generation algorithm's ability to produce desired enhancement targets on three different simulated patients was tested. In each case, TECs in the ascending aorta were recorded after the injection of a 20 ml test bolus followed by 40 ml of saline, injected at 4ml/s. The TEC data were processed by the protocol described in Chapter 6 (the tSVD method used to predict the enhancement) using a desired target enhancement of .07 mg/ml for 2 seconds. Because HU values reflect the concentration of the Iodine in the vasculature, the concentration of the nIR in the phantom was chosen as the target goal in these experiments, absent an equivalent HU measurement scale for the nIR sensors. In between each experimental run, the fluid in the phantom was exchanged with fresh water.

In the next three experiments, the cardiac output of the phantom and the desired targets varied for each case. These experiments were conducted to demonstrate the ability of the protocol generation algorithm to generate a desired enhancement independent of the patient cardiac function and when the desired enhancement targets and scan duration targets varied. Table 18 presents the configuration settings of the phantom for the protocol generation validation experiments.

Table 18 Phantom settings during the protocol generation validation experiments – set 1

Simulated Patient	Heart Rate [min^{-1}]	Stroke Volume [ml]	Cardiac Output [L/min]	Blood Volume [L]	Desired Target Concentration [mg/ml]	Desired Scan Duration [sec]
1	50	80	4.0	5.0	.07	6
2	50	70	3.5	4.5	.07	6
3	50	60	3.0	5.0	.07	6
4	55	80	4.4	5.0	.06	8
5	45	80	3.6	4.5	.08	4
6	50	60	3.0	5.0	.07	6

7.4 RESULTS

The data collected from the experiments are presented in this section. **Figure 62** shows the contrast enhancement response of the phantom (as measured with a CT scanner and 370 mgI/ml contrast) for increased injection bolus durations. The additive effect of the enhancement profile as a function of the injection duration is appreciated by inspection. As the injection duration increases, the time of maximum contrast enhancement also increases. These response data demonstrate the same features as Bae et al. measured in the porcine models under similar injection conditions [4]

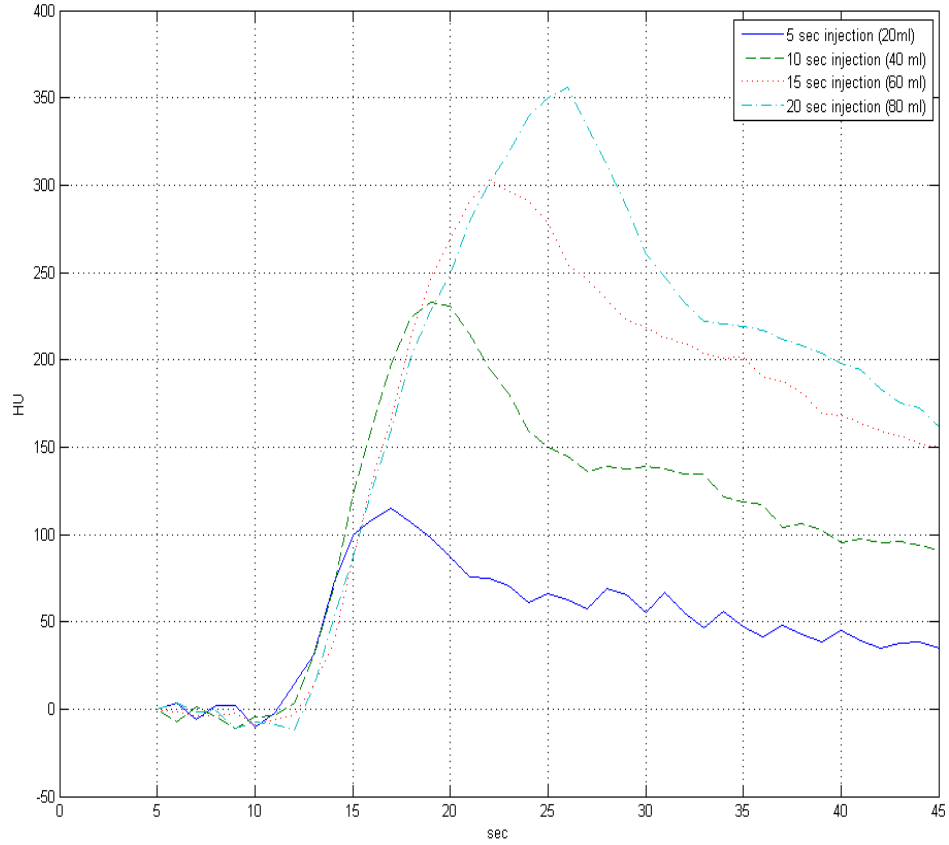

Figure 62 Plot displaying additive linearity response of phantom when injected with contrast material and measured with a CT scanner

The results from the equivalency experiments are presented in **Figure 63** and **Figure 64**. In **Figure 63**, the three TECs recorded by the aortic inlet nIR sensor are superimposed with the mean TEC of those three injections at 4 ml/s (20 ml, 1 mg/ml). All three injections produced similar TECs as evident by the overlap of all the curves and the mean.

Figure 64. presents the mean of the three TECs generated by the CT scanner along with the mean TEC from the nIR sensors (aortic compartment used to generate the data in both cases).

The power injector injected the same volume at the same flow rate for the lab and CT experiments. The pump was also set to the same values for both experiments. Each curve was normalized by its own maximum value. The absolute magnitude comparison is not of particular relevance for this experiment, but rather the width of the enhancement curve and the arrival time are of interest. The mean TECs are very similar in width and arrival, with the exception of the CT TEC's initial upslope enhancement being slightly more concave than the nIR data.

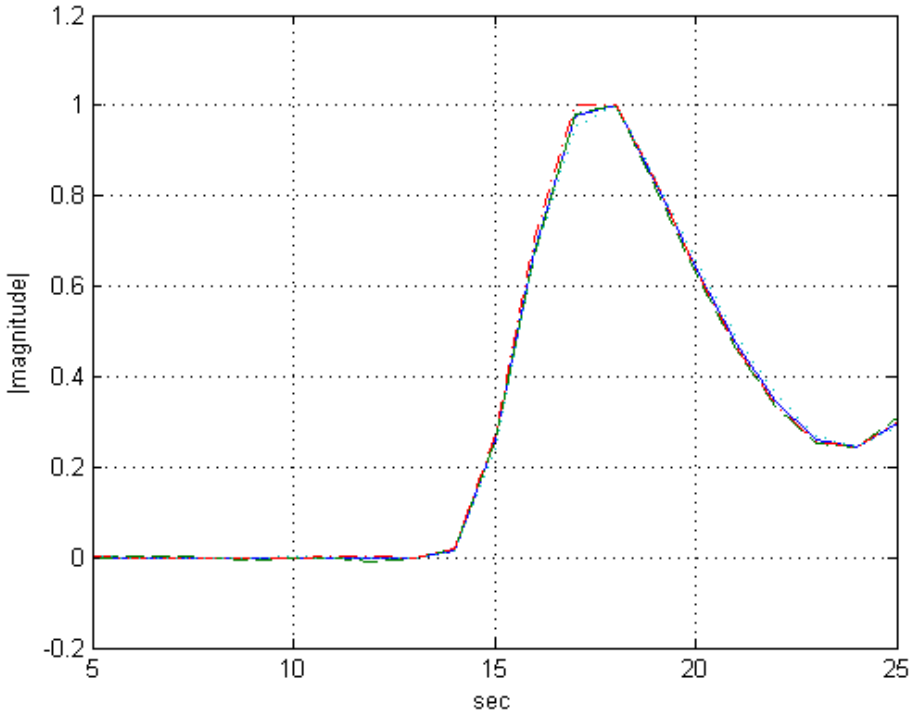

Figure 63 Plot of the mean (solid line) and curves from three separate injections of 20 ml nIR dye into the phantom in the laboratory

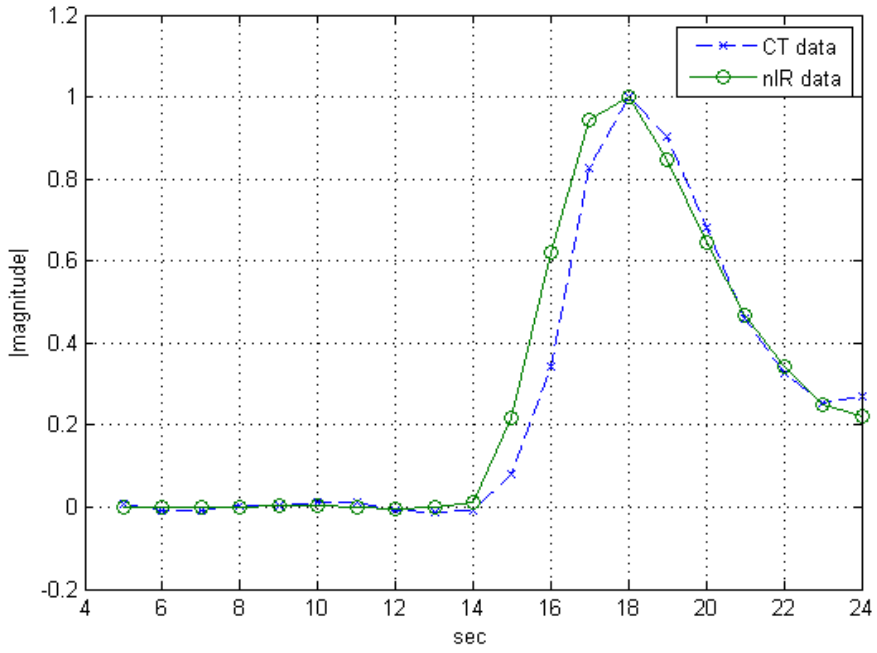

Figure 64 Plot of mean response from three injections of nIR dye (20 ml at 4 ml/s) in the lab to results measured with a CT scanner after injection of 20 ml of 370 mgI/ml contast at 4ml/s. The hemodynamic settings of the pump and phantom were identical for all experiments.

Results from the experiments testing the tSVD method's ability to predict arbitrary injection profiles based on test bolus data are displayed in **Figure 65**. There was good agreement between the predicted TEC and the curve measured in the phantom for all injections. The RMSE for the 20 ml experiment was .0003, for the 40 ml experiment it was .0027, for the 60 ml experiment it was .0029 and .0009 for the 80 ml injection.

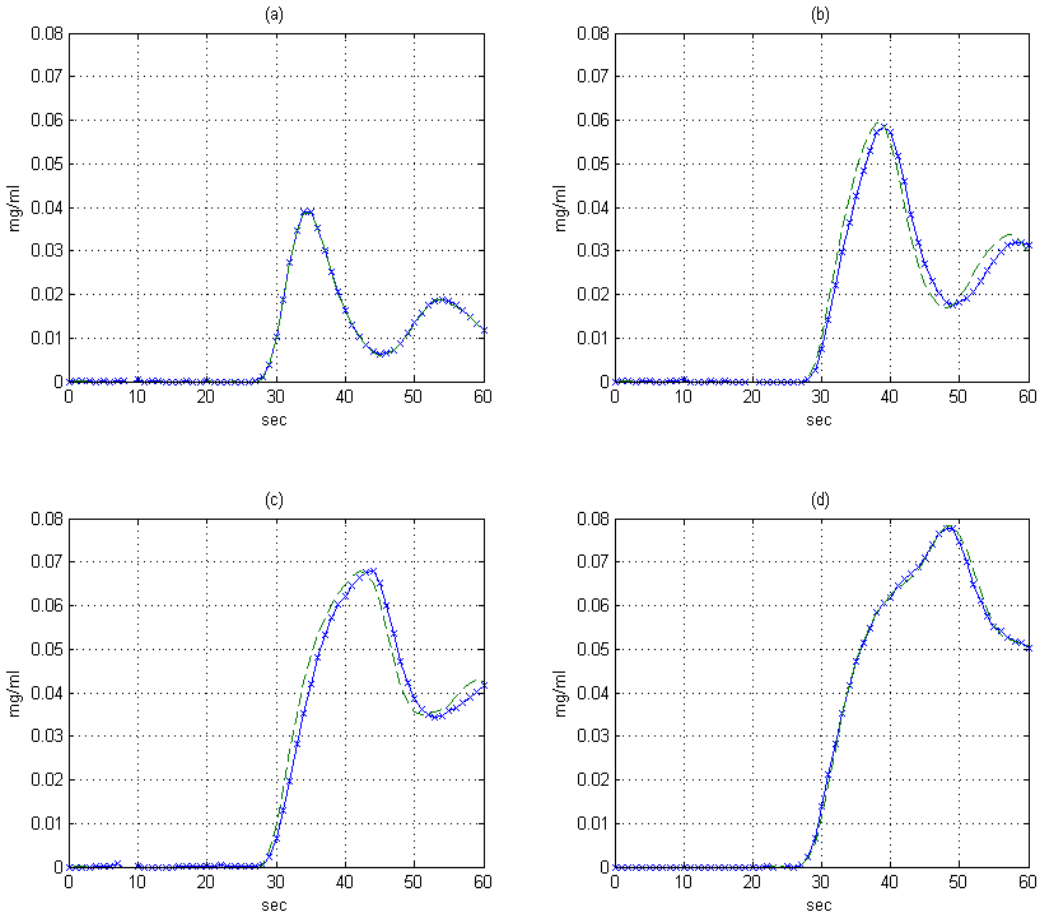

Figure 65 Results of phantom experiments testing the tSVD method to predict contrast enhancement. In each subplot, the measured data are annotated by x's connected with a solid line(x-), and the predicted enhancements are plotted with a dashed line (--). The flow rate was 4ml/s for all injection and the nIR dye had a concentration of 1mg/ml in the syringe. (a) predicted and measured aortic enhancement for 20 ml injection (b) predicted and measured aortic enhancement for 40 ml injection (c) predicted and measured aortic enhancement for 60 ml injection (d) predicted and measured aortic enhancement for 80 ml injection.

Tabulated results of the experiments validating the patient specific protocol generation algorithm are presented below. The computed flow rate and volume of the diagnostic injection to achieve the desired enhancement target over the desired scan duration are given. Also presented in the table is a binary response (yes or no) indicating if the enhancement TEC produced by the injection protocol achieved the specified goal for that experiment (the desired enhancement target for the duration of the scan).

Table 19 Results from the experiments in set 1. The parenthetical values in the "Goal Achievement" column are the desired enhancement target and the scan duration.

Experiment #	Computed Flow Rate [ml/s]	Computed Volume [ml]	Goal Achievement?
1	5.1	66	Yes (.07,4)
2	4.7	61	Yes (.07,4)
3	4.9	64	Yes(.07,4)
4	5.0	65	Yes (.06,8)
5	4.0	60	Yes (.08,4)
6	4.8	72	Yes(.07,6)

The results for experiments 1-3 are given in **Figure 66**. The measured enhancement in the aorta matched the predicted enhancements very well. The protocols computed by the generation algorithm resulted in enhancement exceeding or equaling the target in all three instances. **Figure 67** presents the results for experiments 4-6. The computed protocols resulted in measured enhancements that exceeded the goal in each instance.

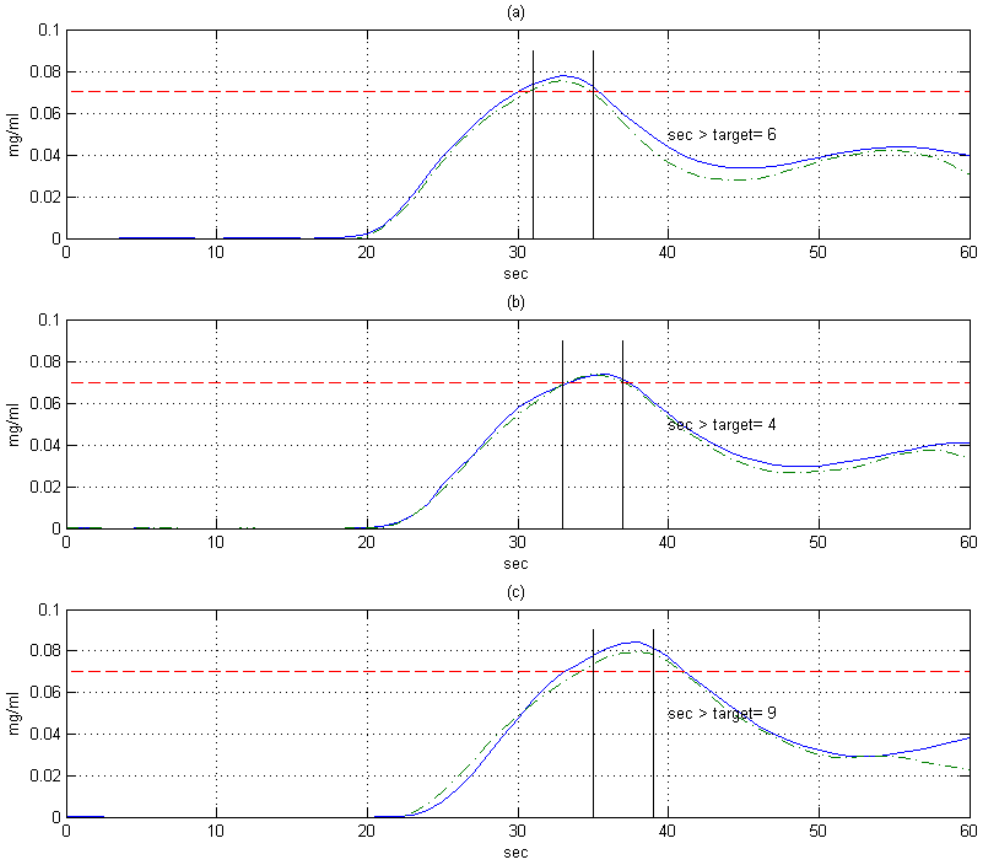

Figure 66 Predicted (dashed curve) and measured TECs (solid curves) from injections into the phantom for experiments 1 -3. The vertical lines in each subplot indicate the scan duration window, starting at the scan delay value computed by the algorithm. The horizontal dashed line indicates the desired enhancement target for the experiment. The text annotation (sec > target = x) in each subplot presents the duration of each curve greater than the target enhancement (a) experiment 1 results (b) experiment 2 results (c) experiment 3 results.

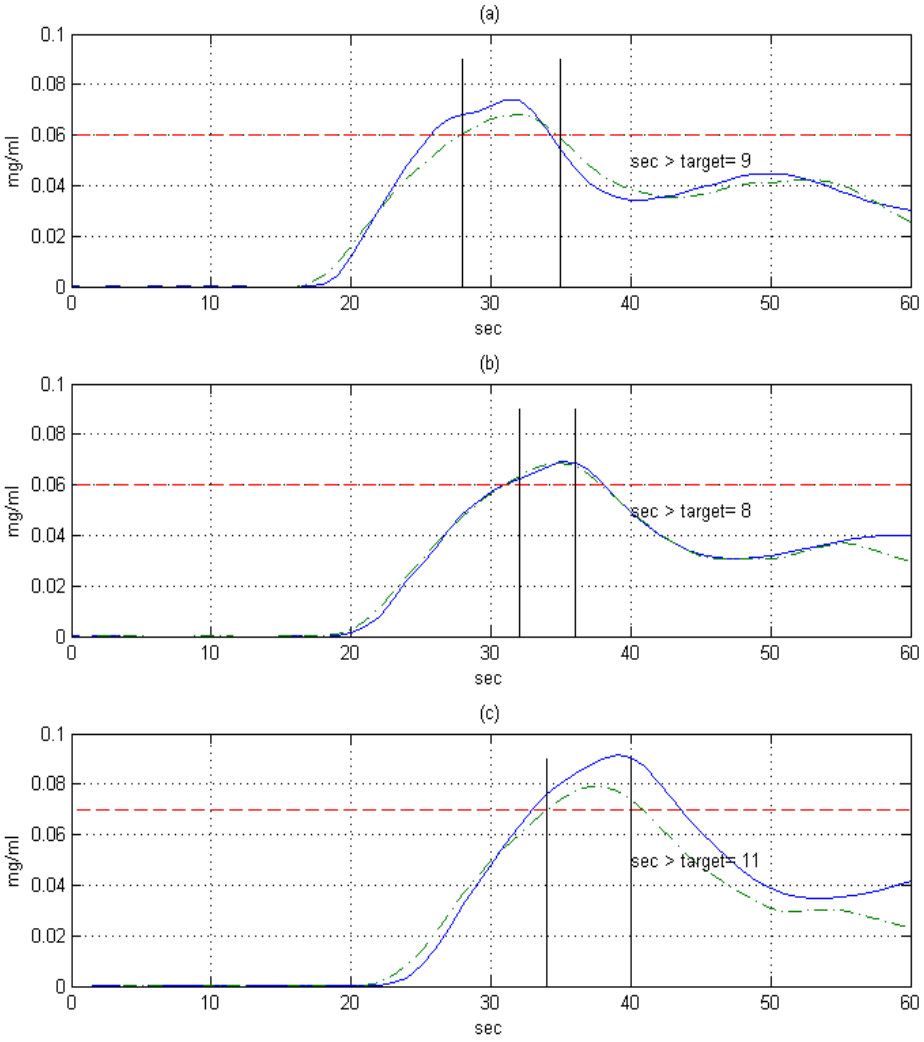

Figure 67 Predicted (dashed curve) and measured TECs (solid curves) from injections into the phantom for experiments 4-6. The vertical lines in each subplot indicate the scan duration window, starting at the scan delay value computed by the algorithm. The horizontal dashed line indicates the desired enhancement target for the experiment. The text annotation (sec > target = x) in each subplot presents the duration of each curve greater than the target enhancement (a) experiment 4 results (b) experiment 5 results (c) experiment 6 results.

7.5 DISCUSSION

In this chapter, a cardiovascular flow phantom for validating contrast enhancement prediction techniques was presented. In addition to several characterization experiments, the phantom was used to validate the contrast enhancement prediction methodology described in Chapter 5 and the patient specific contrast protocol generation algorithm described in Chapter 6. CT scanning of the phantom after injection of X-Ray contrast material with increasing injection durations generated enhancement profiles similar to those measured in a porcine model by Bae et al. A trend of increasing time to maximum contrast enhancement was noted, similar to the trend recorded in pig models and also reported in human studies by Awai et al [8].

The nIR sensors and dye were shown to replicate the behavior of a CT scanner and contrast system, thus allowing the phantom to be injected and measurements to be made in the lab. The laboratory testing reduced the need to test the developed patient specific contrast enhancement methods on an actual CT scanner. A practical limitation of clinical CT scanners is the ability to export the test bolus TEC during a procedure to a computer system capable of executing the algorithms developed in this research. The test bolus scan data used throughout this research were all obtained "offline", after the test bolus scan was performed and the scanner operator saved the TECs to a fixed hard drive within the scanner. Because of this limitation, the laboratory setup was critical for testing the algorithms in a physical simulator.

The tSVD method was used to validate the data-driven methodology for predicting contrast enhancement because long segments of the TEC could be measured. It was chosen because of limitations in the sensor characterization and measurements in the pulmonary trunk. Once those limitations are overcome, it is expected that the MLE methodology for predicting the

contrast enhancement in the phantom will be applicable and should be undertaken in future work. Because of the sensor limitation, validation of the protocol generation algorithm was also performed using the tSVD method to identify the patient model. As mentioned, the protocol generation algorithm functions independently of the method used to estimate the contrast enhancement dynamics so it is not expected that its performance, in the phantom, will differ when the MLE method is perfected with the phantom.

8.0 CONCLUSION

Four primary contributions are presented in this dissertation. 1) A new Physiologically Based Pharmacokinetic model (hybrid model) for X-Ray contrast medium that is a hybrid of Bae et al.'s PBPK model and Wada and Ward's PBPK model of alfentanil propagation. 2) Data-driven techniques for predicting contrast enhancement on a per-patient basis were developed. 3) A novel algorithm for computing patient specific contrast protocols based on the data-driven predictions of contrast enhancement was developed. 4) A cardiovascular flow phantom for testing and validating contrast prediction and protocol generation methods was constructed and used.

A few features of the hybrid PBPK model differentiate it from the Bae model. The hybrid model incorporates a non-linear saturation term in the peripheral venous compartment, it models the transport of contrast through the various compartments with configurable transport delay terms, and it enables the modeling of the saline flush phase commonly used during CTA imaging procedures. The hybrid model also has a reduced number of states as compared to the Bae model. Comparisons between the output of the hybrid model and the Bae model were favorable because lower prediction errors were measured by using the hybrid model, although most of the differences were not statistically significant. In certain cases, the hybrid model outperformed the Bae model when clinical data were used to compare the performance of both models.

Comparison of the two data-driven contrast enhancement methods revealed the MLE was more robust to real-life considerations encountered in the clinic. Specifically, the MLE can better predict contrast enhancement when shorter segments of test-bolus enhancement data are available. The tSVD method, however, only requires the placement of one ROI and is potentially less computationally burdensome. Maximum likelihood estimation was successfully used in identifying the reduced order PBPK model developed to enable patient-specific contrast enhancement predictions. Comparison tests using the hybrid model and retrospective clinical data demonstrated that the MLE was superior to the tSVD. The results are encouraging and suggest that a larger, prospective study using clinical data collection is warranted. As mentioned during the discussion of Chapter 5, a clinical algorithm should consider both data-driven techniques for estimating patient-specific contrast enhancement because there will be situations in which two TECs can not be generated from a test bolus injection. In these cases, assuming the Left Heart TEC is available, the algorithm should attempt to generate the contrast enhancement prediction using the tSVD method.

Using the data-driven contrast enhancement prediction methods, the protocol generation algorithm successfully generated contrast enhancement profiles across a range of procedures and patient variables. The hybrid PBPK model was used to validate the protocol generation algorithm. For short scan durations, it appears that the algorithm could be further optimized so as to reduce the volume of contrast needed to achieve the goals based on the results in **Figure 57**. In all of these short scan duration cases, the enhancement exceeded the target scan duration by at least 2 seconds, indicating further refinement could be possible.

The cardiovascular flow phantom developed for this research [64, 65], was shown to replicate the propagation of contrast material. The methods for predicting contrast enhancement

and generating patient-specific contrast protocols were validated using the phantom and nIR dye. The sensing mechanism and the phantom itself can serve as a useful platform to conduct future experiments requiring multiple injections and scanning and it can reduce the cost and complexity associated with performing feasibility studies on animals and humans.

The primary goal of this research was the creation of patient-specific methods to predict contrast enhancement in humans based on test bolus data and then to compute contrast protocols specific to the patient and the specific procedure. Numerical and physical phantoms were developed and used to test these methods. Validation results, using the phantom, were encouraging and suggest that human, clinical studies are warranted. It is anticipated that the methods can be adopted for other imaging modalities in which exogenous contrast material is intravenously infused into the patient.

8.1 PROPOSED CLINICAL VALIDATION

Validation of the contrast prediction techniques in Chapter 5 can be accomplished by a prospective study in which a test bolus determines the scan timing. TECs should be generated on the pulmonary artery and ascending aorta and saved for off-line analysis. The diagnostic contrast bolus should be injected at the same flow rate as used during the test bolus injection and a fixed volume of contrast should be used in all the subjects. A sample size of at least 30 patients is suggested.

To generate the diagnostic contrast enhancement profile for each subject, the axial CT data should be reconstructed in 5 or 10 mm slices and saved in an offline repository for subsequent analysis using the auto-segmentation software described in Chapter 4. In addition to the imaging data, patient demographics should be recorded for each subject (weight, height, sex, and age). The demographic data will be used to parameterize the hybrid model. Comparisons between the actual enhancement data in the aorta to the hybrid model prediction and between the enhancement data and predictions using the MLE and tSVD methods will be made using the three performance metrics used throughout the dissertation (RMSE, PDME, and EDI). It is expected that the prediction errors, using the prospective data, will be at least equivalent to the results produced in Chapters 4 and 5 (for the hybrid and data-driven prediction methods). Because the imaging data will be used in exploratory research, Institutional Review Board review will be mandated as will informed consent from the subjects.

Assuming positive outcomes from the previous study, the second prospective investigation should be conducted to test the contrast protocol generation in a clinical setting. In order to conduct this prospective study, a data exchange mechanism between the CT scanner and the injection system will need to be perfected. The CT software can process the TECs from ROIs on the image set and then transfer the data to the injection system (or an intermediary gateway PC) for processing and protocol generation. The resulting contrast protocol can then be automatically transferred to the injection system User Interface. Another option is for the scanner operator to transmit the test bolus enhancement imagery to the gateway PC, and an application will process the data and generate TECs for the pulmonary and ascending aorta.

When the software acquires the TECs, the contrast protocol generation algorithm will compute injection protocols based on constraints chosen by the Principal Investigator and

potentially by the technologist operating the scanner. The resulting contrast protocol will be reviewed by the technologist prior to injecting into the subject (and reviewed by the PI if necessary). The resulting diagnostic scan data will be saved and analyzed as described above. Specific endpoints for this study will be achievement of contrast enhancement in the aorta to the desired target enhancement lasting for the duration of the scan.

8.2 ADDITIONAL APPLICATIONS

The methods developed here for patient-specific, contrast enhancement CT of the cardiothoracic vasculature also has applicability to other anatomical regions of the body. In particular, peripheral arterial angiography of the leg arteries is challenging due to the acquisition speed of modern CT scanners. In many instances, the scanner must be slowed to account for the physiologic processes transporting the contrast bolus through the vasculature. Typically patients needing peripheral arterial CTA studies are also diabetic or have other renal insufficiencies and are potentially susceptible to kidney injury due to large volumes of contrast media. Therefore, computing a minimum volume of contrast dose in the patients is also very important.

Another clinical indication in which this research can be adopted is neurological CT imaging. A short bolus of contrast, precisely and individually timed, is critical for CTA of the brain arteries. It is important in these studies to synchronize the scan prior to contrast filling the veins of the head.

There is the opportunity to apply the hybrid model in predictive contrast enhancement scenarios in which a test bolus is not administered. Some radiologists prefer bolus tracking software over the test bolus methodology to synchronize the acquisition of the scan with the arrival of contrast. In these cases, the hybrid model (assuming the patient demographic data are available) could be used to determine, *a priori*, a contrast injection protocol to achieve desired targets in an iterative fashion. The drawback to this method is that true hemodynamic status of the patient is not available when constructing the contrast protocol. Also, due to the transport delays in contrast propagation through the cardiopulmonary circuit, once the bolus is injected there is no "control" that can be exerted over the bolus for a particular patient. However, using the model in this open-loop approach is still superior to dosing without any consideration of the patient's habitus or physiology. A more intriguing approach is to use the hybrid model and the data collected during the scanner's bolus tracking acquisition in a Model Predictive Control framework. To enable this research, however, close collaboration with the scanner manufacturers is required.

Gadolinium-based (Gd) contrast agents are routinely delivered during MRI examinations to provide enhanced visualization of arterial and venous structures (MR Angiography). The methods developed in this dissertation can be modified for MR applications, while recognizing that the relationship between signal intensity and blood-plasma concentration of the Gd contrast agent is not linear as it is with CT contrast agents.

9.0 SPECIFIC CONTRIBUTIONS BY THE AUTHOR

This section presents the original work and, where applicable, publications, generated by the author during the development of this dissertation.

- **A novel, PBPK model** and structure for describing the distribution of iodinated contrast in the human circulatory system.
- **Data-drive methods for predicting patient-specific contrast enhancement at thoracic CT Angiography**. The statistical methodologies were adapted from techniques in the literature (truncated SVD, maximum likelihood estimation) and the numerical methods were library functions provided by commercial software (MATLAB).The novel contribution, however, is the synthesis and application of these methods for the CTA contrast enhancement application.
- **A contrast protocol generation algorithm that considers clinical and patient constraints in its formulation.** The cost-function used in the optimization step was presented in an IEEE conference proceedings [42]:
    - *Kalafut JF, Kemper CA, Suryani P, Schoepf U. A personalized and optimal approach for dosing contrast material at coronary computed tomography angiography. Conf Proc IEEE Eng Med Biol Soc. 2009;2009:3521-4.*

- **A novel, physiologically realistic flow phantom**. The phantom was designed by JF Kalafut and constructed (under the direction of JF Kalafut) by Dave Reilly and Michael Yanniello (MEDRAD Inc. employees). The cardiovascular flow phantom has been presented in 2 forums – the 2008 European Congress of Radiology conference [64] and in an *Investigative Radiology* manuscript [65]. JF Kalafut was the lead author in the conference presentation. The imaging studies were performed at the Ohio State University Medical Center following a protocol developed by Kalafut. Kalafut was third author in the journal article because the experimental imaging protocol was designed and conducted by the physicians (first 2 authors).

    - *Kalafut, J.F., Kemper C.A., and Sammett S.. An anthropomorphic, cardiovascular flow phantom for CT contrast and imaging protocol optimization. in European Congress Radiology. 2008. Vienna Austria: ESR.*
    - *Behrendt FF, Bruners P, Kalafut J, Mahnken AH, Keil S, Plumhans C, Das M, Stanzel S, Wildberger JE, Pfeffer J, Günther RW, Mühlenbruch G. Introduction of a dedicated circulation phantom for comprehensive in vitro analysis of intravascular contrast material application. Invest Radiol. 2008Oct;43(10):729-36.*

Other relevant articles and presentations listed as author:

1. Numburi, U.D., et al., *Patient-specific contrast injection protocols for cardiovascular multidetector row computed tomography.* J Comput Assist Tomogr, 2007. **31**(2): p. 281-9. (4th author)
2. Seifarth, H., et al., *Introduction of an individually optimized protocol for the injection of contrast medium for coronary CT angiography.* Eur Radiol, 2009. **19**(10): p. 2373-82 (3rd author, but technical/algorithmic principle author)
3. Suryani P., et al. *A Computerized Prediction Model for Individualized, Patient-Based Contrast Dosing at Dual-Source Coronary CT Angiography* in *Radiological Society North America*. 2007. Chicago Illinois: RSNA. (2nd author)
4. Deible C., et al, *A Clinical Evaluation of an automated software program for patient-specific contrast injection during chest CTA to exclude pulmonary embolism*, in *Society Thoracic Radiology*. 2007, STR: Charleston SC. (4th author)

APPENDIX A

APPENDIX A MLE METHODOLOGY DETAILS

The methodology to construct a patient-specific, prediction of contrast enhancement in the left heart structures using Maximum Likelihood Estimation is summarized here A prerequisite for this technique is the availability of TEC data derived from CT measurements (simulated or actual) in the pulmonary trunk ($y_{RH}^{Test}(t)$) and the ascending aorta ($y_{LH}^{Test}(t)$) after delivery of a test bolus of contrast , uTest(t). Because the data are sampled according to the temporal resolution dictated by instrumentation constraints, the data are discrete and are expressed as $y_{RH}^{Test}(n) = y_{RH}^{Test} \; tk\Delta$, $y_{LH}^{Test}(n) = y_{LH}^{Test} \; tk\Delta$ and uTest(n)=Qinj(n)Cinj[u(n)-u(n-Ninj)] where k is an integer, index parameter, Δ is the sample period of the data, and Ninj is the duration of the test bolus injection in integer sample periods. $\hat{\theta}_{He2D}$ is estimated using the measured test bolus data $y_{RH}^{Test}(n)$ and $y_{LH}^{Test}(n)$. $\hat{\theta}_{He1D}$ is estimated using $y_{RH}^{Test}(n)$ and uTest(n). Prediction of an arbitrary injection (uDiag(n)) is based upon the serial cascade of the two system He1D and He2D (populated with the parameter estimates $\hat{\theta}_{He1D}$ and $\hat{\theta}_{He1D}$ estimated with the test bolus injection data). Metrics comparing the performance of the identification method are based upon the

simulated or clinical, contrast enhancement data in left heart structures. A detailed explanation of the algorithm is in Table 20.

Table 20 General algorithm for predicting enhancement using MLE

Set initial estimates for the parameter estimates by randomly picking parameter values, θ_{He1D}^{*} θ_{He2D}^{*}, within +/- 25% of the midpoint values in Table 8.:

Begin A

1. Acquire $y_{LH}^{Test}(n), y_{RH}^{Test}(n)$ (simulated or clinical) based upon a test injection, $u_{Test}(n)$
2. Perform Maximum Likelihood Estimation to derive parameter estimates θ_{He1D} and θ_{He2D} using (5.11) and (5.12).
3. Estimate $\hat{y}_{LH}^{Test}(n) = f_{He1D+He2D}\ \hat{\theta}_{He1D}, \hat{\theta}_{He2D}, u_{Test}(n)$ by serially cascading (5.9) and (5.10).
4. Compute the Root Mean Square error between $\hat{y}_{LH}^{Test}(n)$ and $y_{LH}^{Test}(n)$

end A

*Repeat **A** 5 times. Select Initial conditions and parameter estimated that generated the smallest RMSE in step A.4*

Set θ_{He1D} θ_{He2D}

Begin B

5. Generate a predicted Left Heart structure enhancement signal for an arbitrary, diagnostic injection of drug $u_{Diag}(n)$ using the parameter estimates: $\hat{y}_{LH}^{Diag}(n) = f_{He1D+He2D}\ \hat{\theta}_{He1D}, \hat{\theta}_{He2D}, u_{Diag}(n)$
6. Compare the predicted enhancement, $\hat{y}_{LH}^{Diag}(n)$, against simulated or actual enhancement data, $y_{LH}^{Diag}(n)$ using RMSE, PDME and EDI metrics as defined in Chapter 4

end B

APPENDIX B

APPENDIX B HYBRID MODEL PREDICTIONS

In this appendix are plots of hybrid model and Bae model predictions against the clinical data set. In each of the simulations, the procedure specifics for each patient (contrast volume, flow rates, concentration) were used as inputs into the simulations. The patient demographics (height, weight, age and sex) were used to parameterize each simulation using the equations for cardiac output and blood volume presented in Chapter 4. The diagnostic contrast enhancement from the clinical CT data served as the basis of comparison. In each plot, the diagnostic CT data are indicated with "x"'s and start at the scan delay recorded for each subject in the clinical study.

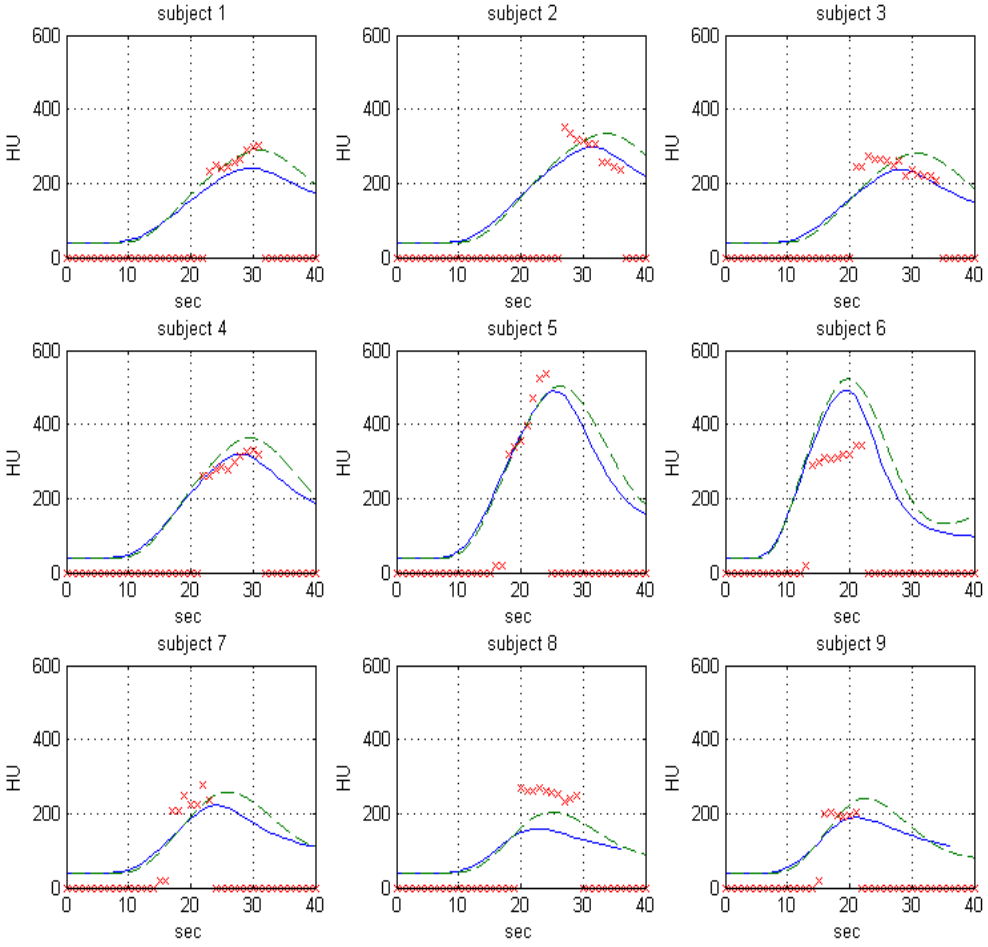

Figure 68 Hybrid model simulation outputs (dashed line) and Bae model simulation outputs (solid line) for subjects one through nine. In each plot, the CT diagnostic scan enhancement data are also plotted, indicated with "x"'s.

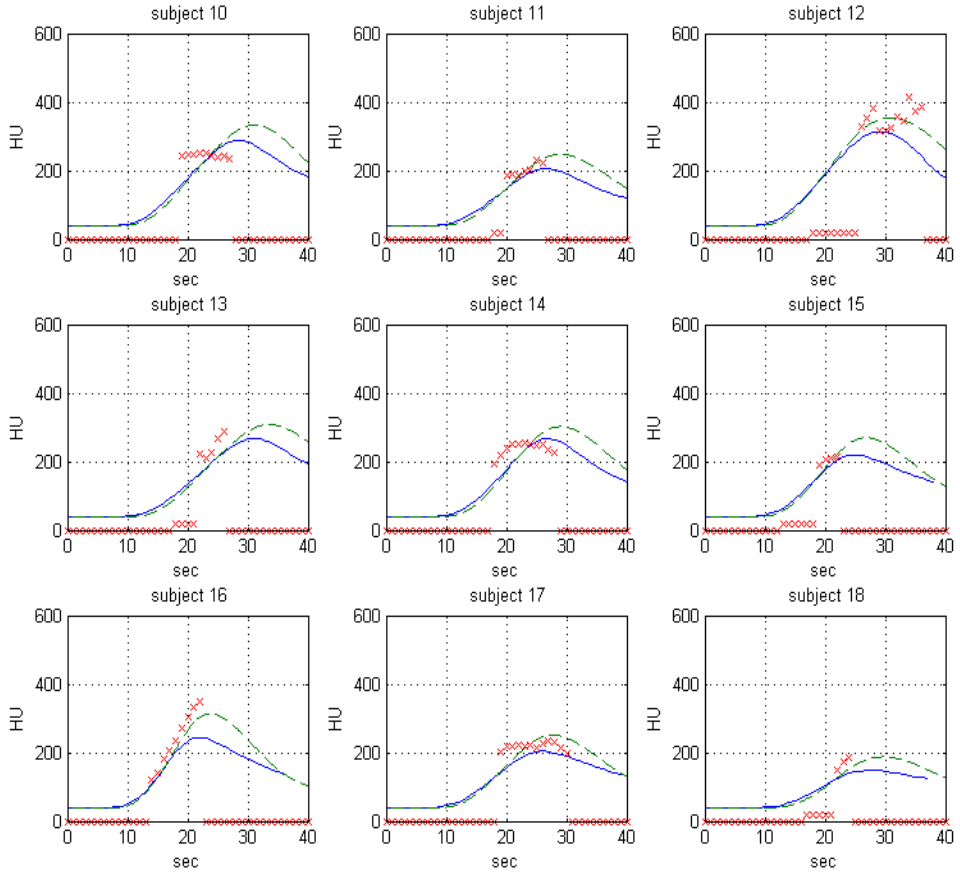

Figure 69 Hybrid model simulation outputs (dashed line) and Bae model simulation outputs (solid line) for subjects 10 through 18. In each plot, the CT diagnostic scan enhancement data are also plotted, indicated with "x"'s.

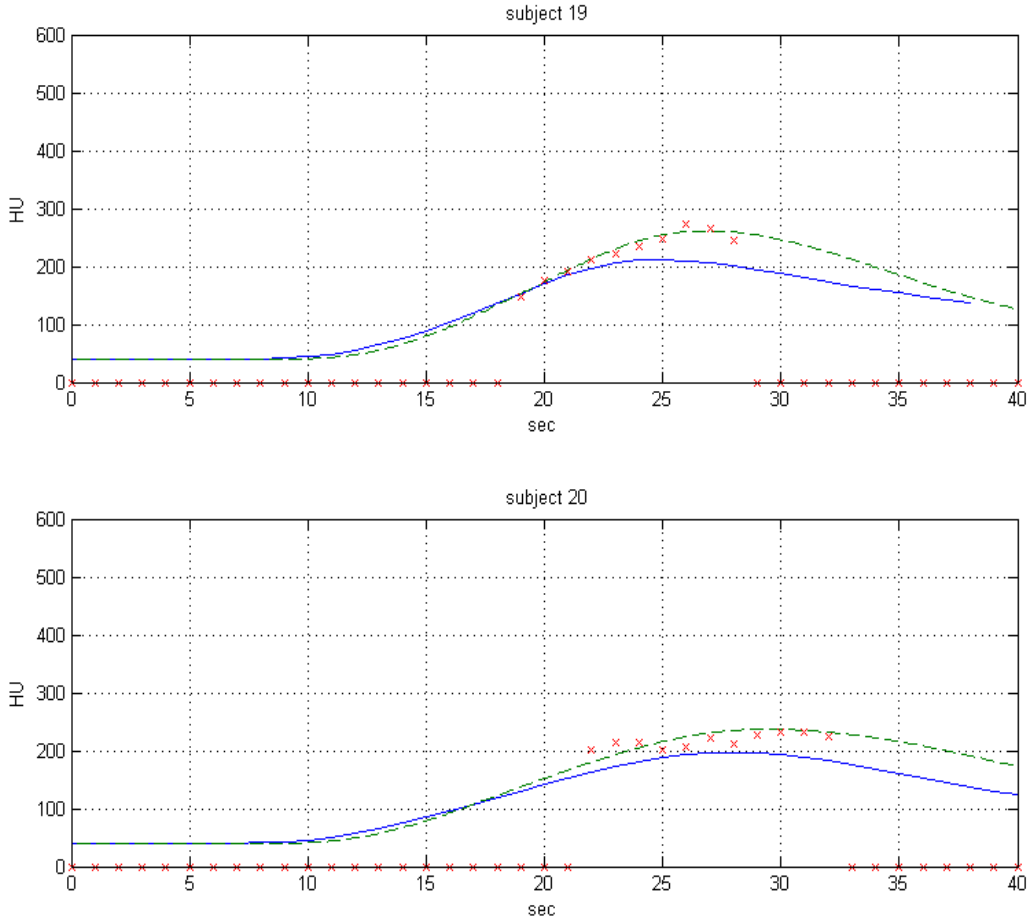

Figure 70 Hybrid model simulation outputs (dashed line) and Bae model simulation outputs (solid line) for subjects 19 and 20. In each plot, the CT diagnostic scan enhancement data are also plotted, indicated with "x"'s.

APPENDIX C

APPENDIX C PREDICTION OUTPUT MLE

The resulting predicted enhancement profiles for all 20 subjects using the MLE technique are presented in this appendix. Diagnostic scan enhancement data points at 600 HU indicate that portion of the diagnostic enhancement curve could not be extracted from the aorta due to motion artifact, contrast streaking, or anatomical deviation. The 600 HU values were not included in any of the calculations used to assess the performance of the estimators.

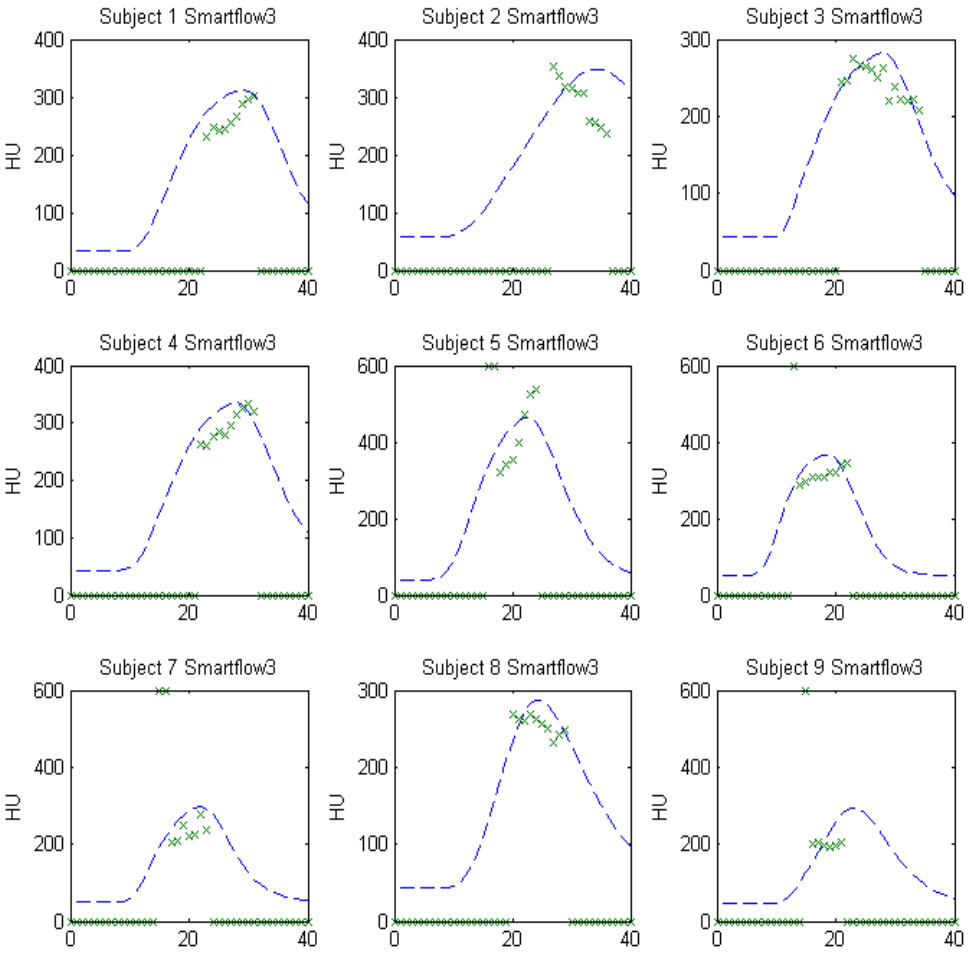

Figure 71 Predicted contrast enhancement (blue dotted lines) using the test bolus enhancement data from the clinical data set to parameterize the model The procedure data from the clinical study (contrast protocol, scan duration and delay) were applied to the identified model. The crosses are the clinical data from the diagnostic scan (enhancement measured in the aorta).

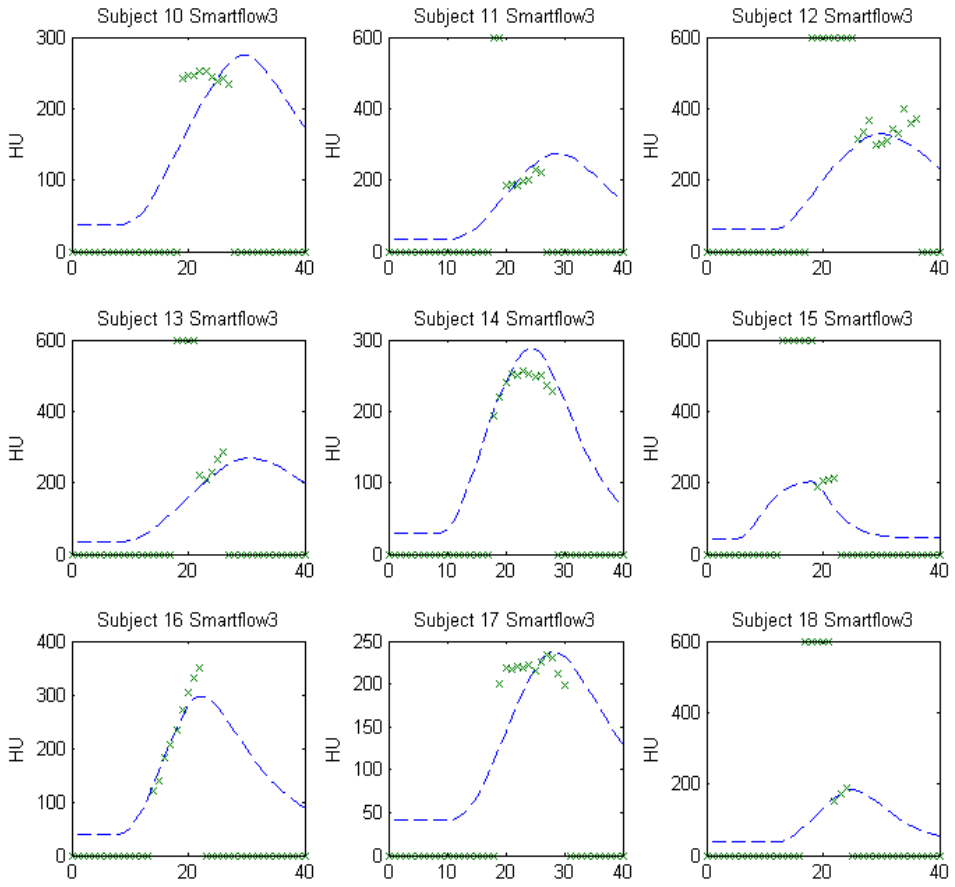

Figure 72 Predicted (subjects 10-18) contrast enhancement (blue dotted lines) using the test bolus enhancement data from the clinical data set to parameterize the model. The procedure data from the clinical study (contrast protocol, scan duration and delay) were applied to the identified model. The crosses are the clinical data from the diagnostic scan (enhancement measured in the aorta).

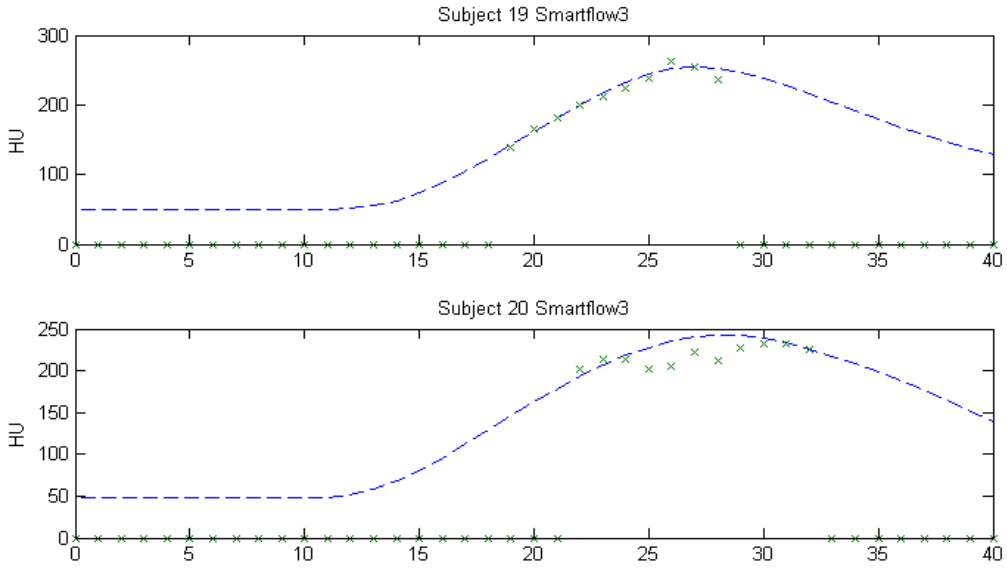

Figure 73 Predicted contrast (subjects 19 and 20) enhancement (blue dotted lines) using the test bolus enhancement data from the clinical data set to parameterize the model The procedure data from the clinical study (contrast protocol, scan duration and delay) were applied to the identified model. The crosses are the clinical data from the diagnostic scan (enhancement measured in the aorta).

APPENDIX D

APPENDIX D PREDICTION OUTPUT USING TRUNCATED SVD

The resulting predicted enhancement profiles for all 20 subjects using the tSVD technique are presented in this appendix. Diagnostic scan enhancement data points at 600 HU indicate that portion of the diagnostic enhancement curve could not be extracted from the aorta due to motion artifact, contrast streaking, or anatomical deviation. The 600 HU values were not included in any of the calculations used to assess the performance of the estimators.

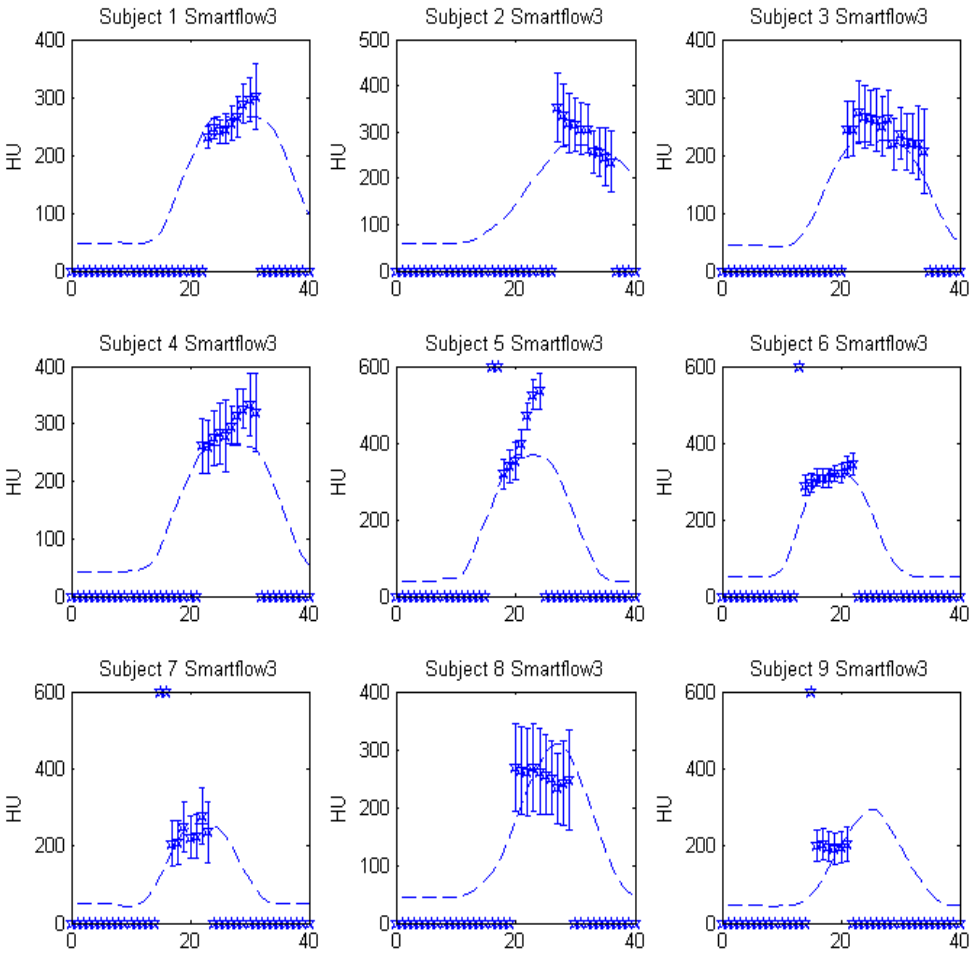

Figure 74 Predicted contrast (subjects 1 and 9) enhancement (blue dotted lines) using the test bolus enhancement data from the clinical data set to parameterize the model. The tSVD methodology provided the estimates. The procedure data from the clinical study (contrast protocol, scan duration and delay) were applied to the identified model. The crosses represent the clinical data from the diagnostic scan (enhancement measured in the aorta), with one standard-deviation error bars attached to each data point.

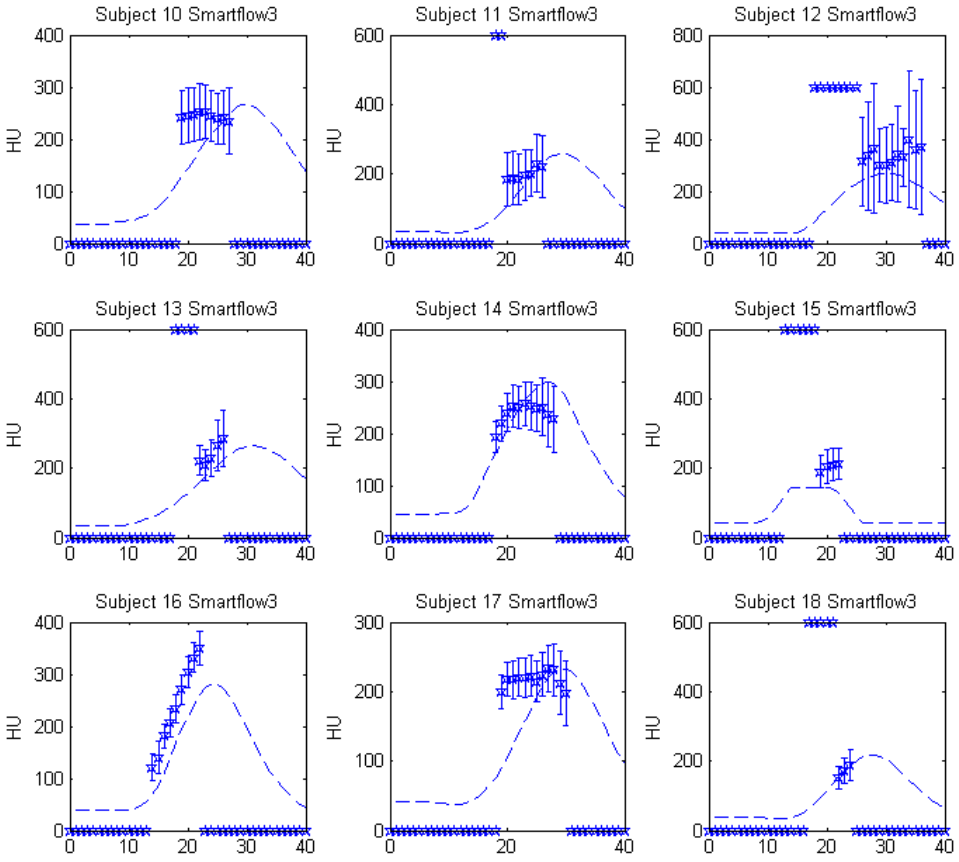

Figure 75 Predicted contrast (subjects 10 and 18) enhancement (blue dotted lines) using the test bolus enhancement data from the clinical data set to parameterize the model. The tSVD methodology provided the estimates. The procedure data from the clinical study (contrast protocol, scan duration and delay) were applied to the identified model. The crosses represent the clinical data from the diagnostic scan (enhancement measured in the aorta), with one standard-deviation error bars attached to each data point.

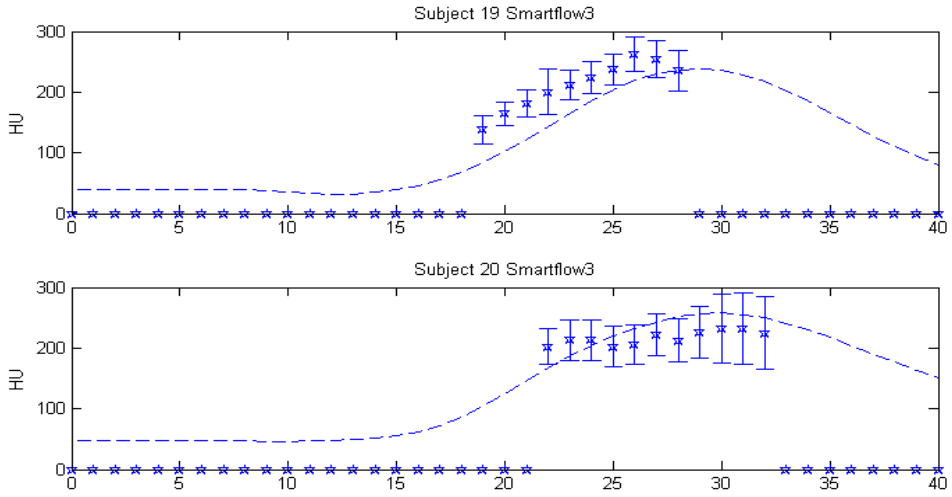

Figure 76 Predicted contrast (subjects 19 and 20) enhancement (blue dotted lines) using the test bolus enhancement data from the clinical data set to parameterize the model. The tSVD methodology provided the estimates. The procedure data from the clinical study (contrast protocol, scan duration and delay) were applied to the identified model. The crosses represent the clinical data from the diagnostic scan (enhancement measured in the aorta), with one standard-deviation error bars attached to each data point.

APPENDIX E

APPENDIX E CLINICAL TEST BOLUS TECS

The test bolus TECs for all 20 subjects used in Chapter 5 are presented below.

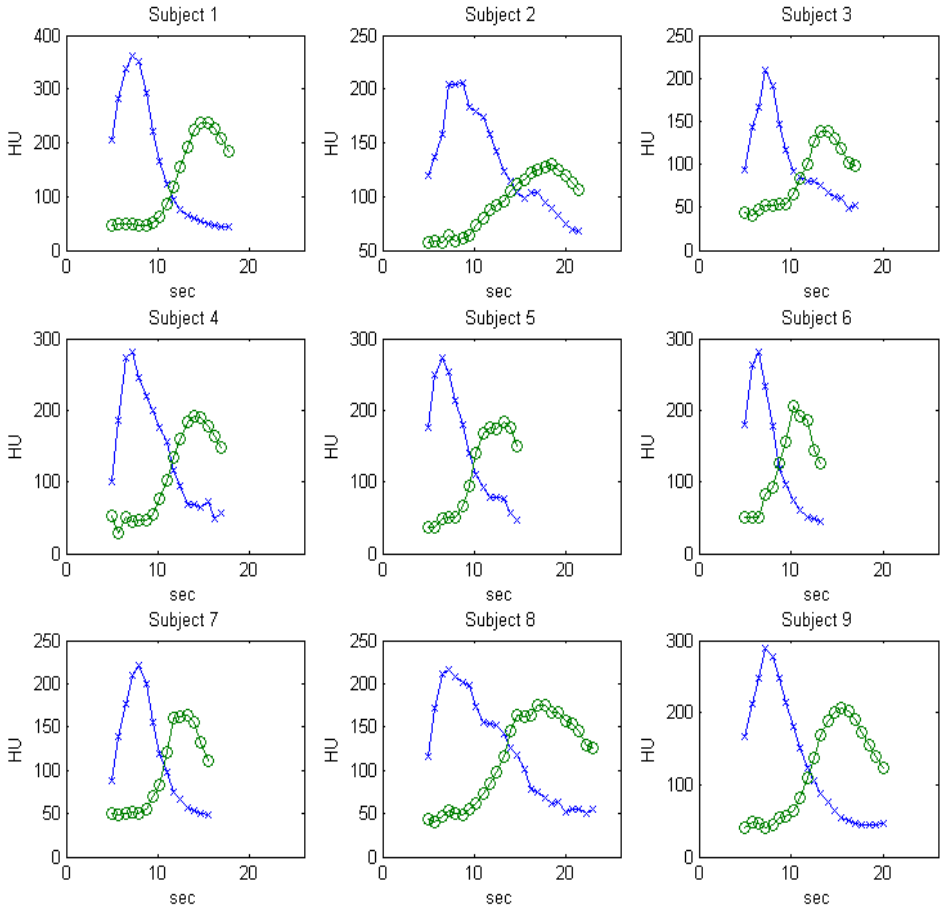

Figure 77 Clinical data - Time Enhancement Curves for subjects one through nine used by the methods developed and tested in chapter 5. The curves marked with the "'x"'s were measured in the pulmonary artery while the curves marked with "o"'s were measured in the ascending aorta. The end points for the TECs were determined by the scanner operator and were not controlled.

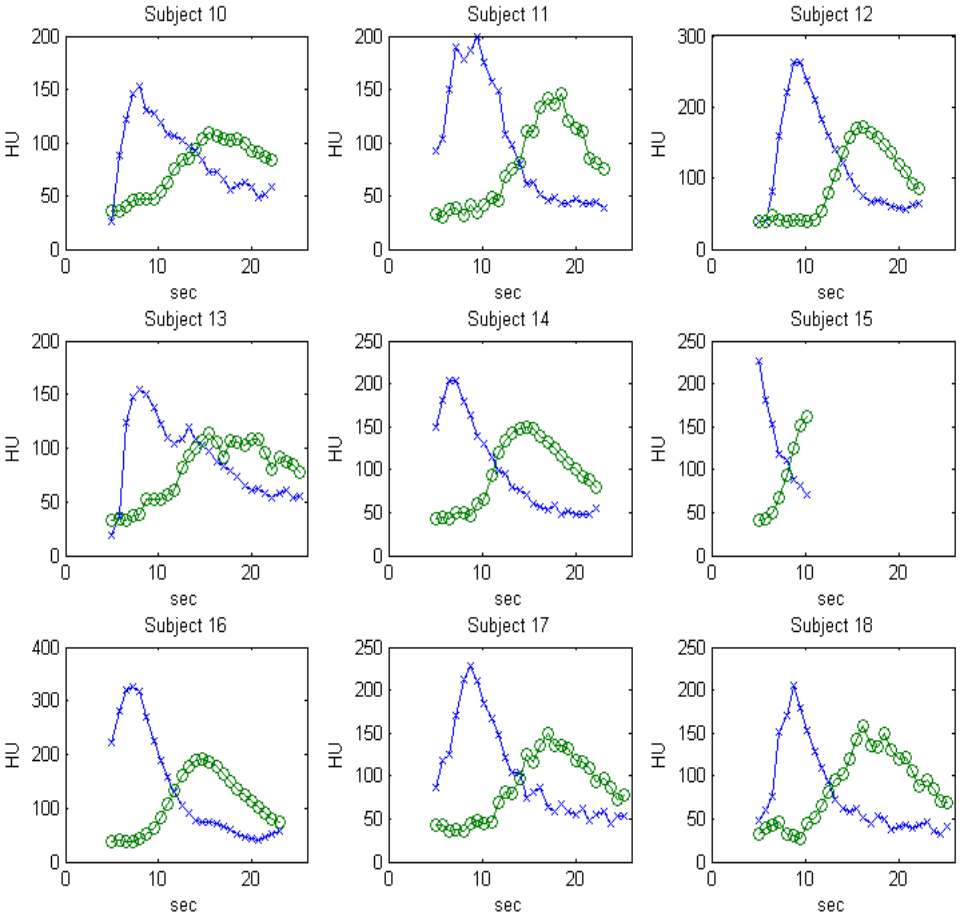

Figure 78 Clinical data - Time Enhancement Curves for subjects ten through eighteen used by the methods developed and tested in chapter 5. The curves marked with the "'x"'s were measured in the pulmonary artery while the curves marked with "o"'s were measured in the ascending aorta. The end points for the TECs were determined by the scanner operator and were not controlled.

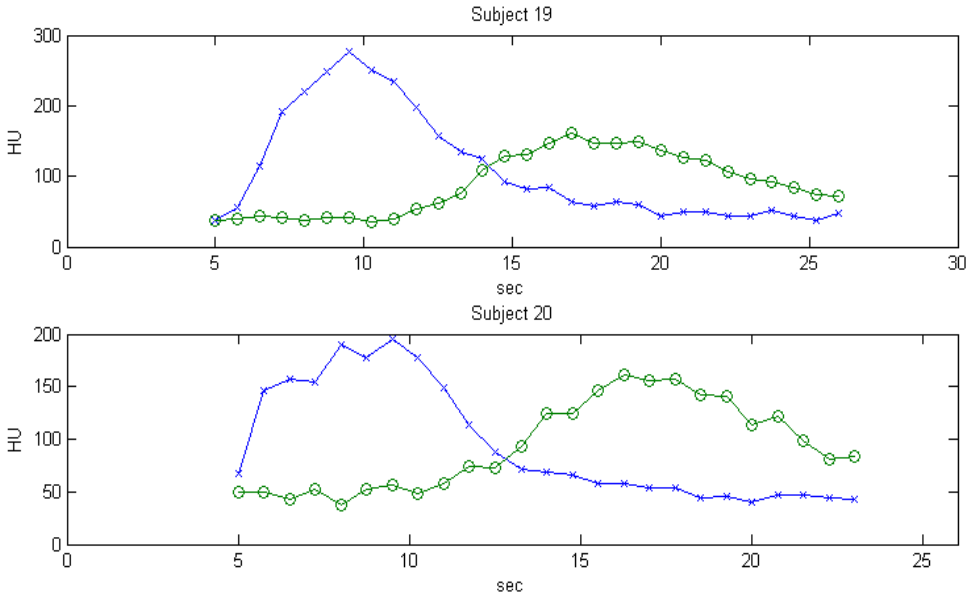

Figure 79 Clinical data - Time Enhancement Curves for subjects 19 and 20 used by the methods developed and tested in chapter 5. The curves marked with the "'x"'s were measured in the pulmonary artery while the curves marked with "o"'s were measured in the ascending aorta. The end points for the TECs were determined by the scanner operator and were not controlled.

BIBLIOGRAPHY

1. Cademartiri, F., et al., *Parameters affecting bolus geometry in CTA: a review.* J Comput Assist Tomogr, 2002. **26**(4): p. 598-607.

2. Van Hoe, L., et al., *[Spiral CT angiography]*. J Belge Radiol, 1995. **78**(2): p. 114-7.

3. Bae, K.T., Tran, H. Q., *Methods for Injecting a Contrast Medium to Generate Prolonged Uniform Vascular Enhancement*, in *US Patent 6,055,985*. 2000.

4. Bae, K.T., *Peak contrast enhancement in CT and MR angiography: when does it occur and why? Pharmacokinetic study in a porcine model.* Radiology, 2003. **227**(3): p. 809-16.

5. Bae, K.T., J.P. Heiken, and J.A. Brink, *Aortic and hepatic peak enhancement at CT: effect of contrast medium injection rate--pharmacokinetic analysis and experimental porcine model.* Radiology, 1998. **206**(2): p. 455-64.

6. Bae, K.T., J.P. Heiken, and J.A. Brink, *Aortic and hepatic contrast medium enhancement at CT. Part I. Prediction with a computer model.* Radiology, 1998. **207**(3): p. 647-55.

7. Bae, K.T., H.Q. Tran, and J.P. Heiken, *Uniform vascular contrast enhancement and reduced contrast medium volume achieved by using exponentially decelerated contrast material injection method.* Radiology, 2004. **231**(3): p. 732-6.

8. Awai, K., K. Hiraishi, and S. Hori, *Effect of contrast material injection duration and rate on aortic peak time and peak enhancement at dynamic CT involving injection protocol with dose tailored to patient weight.* Radiology, 2004. **230**(1): p. 142-50.

9. Fleischmann, D. and K. Hittmair, *Mathematical analysis of arterial enhancement and optimization of bolus geometry for CT angiography using the discrete fourier transform.* J Comput Assist Tomogr, 1999. **23**(3): p. 474-84.

10. Blomley, M.J. and P. Dawson, *Bolus dynamics: theoretical and experimental aspects.* Br J Radiol, 1997. **70**(832): p. 351-9.

11. Auler, M.A., et al., *Saline chasing technique with dual-syringe injector systems for multi-detector row computed tomographic angiography: rationale, indications, and protocols.* Curr Probl Diagn Radiol, 2006. **35**(1): p. 1-11.

12. Speck, U., et al., *Paradigms and perspectives in contrast media research.* Acad Radiol, 2002. **9 Suppl 2**: p. S392-7.

13. Marcus, C.D., et al., *Carotid arterial stenosis: evaluation at CT angiography with the volume-rendering technique.* Radiology, 1999. **211**(3): p. 775-80.

14. Fleischmann, D., *Present and future trends in multiple detector-row CT applications: CT angiography.* Eur Radiol, 2002. **12 Suppl 2**: p. S11-5.

15. Haage, P., et al., *Reduction of contrast material dose and artifacts by a saline flush using a double power injector in helical CT of the thorax.* AJR Am J Roentgenol, 2000. **174**(4): p. 1049-53.

16. Awai, K., et al., *Simulation of aortic peak enhancement on MDCT using a contrast material flow phantom: feasibility study.* AJR Am J Roentgenol, 2006. **186**(2): p. 379-85.

17. Lee, C.H., et al., *CTA Contrast Enhancement of the Aorta and Pulmonary Artery.* Invest Radiol, 2007. **42**: p. 486-490.

18. Cademartiri, F., et al., *Sixteen-row multislice computed tomography: basic concepts, protocols, and enhanced clinical applications.* Semin Ultrasound CT MR, 2004. **25**(1): p. 2-16.

19. Dawson, P. and M. Blomley, *The value of mathematical modelling in understanding contrast enhancement in CT with particular reference to the detection of hypovascular liver metastases.* Eur J Radiol, 2002. **41**(3): p. 222-36.

20. Awai, K. and S. Hori, *Effect of contrast injection protocol with dose tailored to patient weight and fixed injection duration on aortic and hepatic enhancement at multidetector-row helical CT.* Eur Radiol, 2003. **13**(9): p. 2155-60.

21. Yamashita, Y., et al., *Abdominal helical CT: evaluation of optimal doses of intravenous contrast material--a prospective randomized study.* Radiology, 2000. **216**(3): p. 718-23.

22. Blomley, M.J. and P. Dawson, *Contrast agent pharmacokinetics revisited: II. Computer-aided analysis.* Acad Radiol, 1996. **3 Suppl 2**: p. S264-7.

23. Gerlowski, L.E. and R.K. Jain, *Physiologically based pharmacokinetic modeling: principles and applications.* J Pharm Sci, 1983. **72**(10): p. 1103-27.

24. Reddy, M. and R.S. Yang, *Physiologically Based Pharmacokinetic Modeling:Science and Applications*. 2005: Wiley-Interscience. 420.

25. Rowland, M., L. Balant, and C. Peck, *Physiologically based pharmacokinetics in drug development and regulatory science: a workshop report (Georgetown University, Washington, DC, May 29-30, 2002).* AAPS PharmSci, 2004. **6**(1): p. E6.

26. Rao, R.R., et al., *Control of a nonsquare drug infusion system: A simulation study.* Biotechnol Prog, 1999. **15**(3): p. 556-64.

27. Held, C.M. and R.J. Roy, *Multiple drug hemodynamic control by means of a supervisory-fuzzy rule-based adaptive control system: validation on a model.* IEEE Trans Biomed Eng, 1995. **42**(4): p. 371-85.

28. Jacobs, J.R., *Algorithm for optimal linear model-based control with application to pharmacokinetic model-driven drug delivery.* IEEE Trans Biomed Eng, 1990. **37**(1): p. 107-9.

29. Glen, J.B., *The development of 'Diprifusor': a TCI system for propofol.* Anaesthesia, 1998. **53 Suppl 1**: p. 13-21.

30. Gentilini, A., et al., *A new paradigm for the closed-loop intraoperative administration of analgesics in humans.* IEEE Trans Biomed Eng, 2002. **49**(4): p. 289-99.

31. Krause, W., *Application of pharmacokinetics to computed tomography: injection rates and schemes: mono-, bi-, or multiphasic?* Invest Radiol, 1996. **31**(2): p. 91-100.

32. Ledzewicz, U. and H. Schattler, *Optimal controls for a model with pharmacokinetics maximizing bone marrow in cancer chemotherapy.* Math Biosci, 2007. **206**(2): p. 320-42.

33. Bae, K.T., H.Q. Tran, and J.P. Heiken, *Multiphasic injection method for uniform prolonged vascular enhancement at CT angiography: pharmacokinetic analysis and experimental porcine model.* Radiology, 2000. **216**(3): p. 872-80.

34. Wada, D.R. and D.S. Ward, *The hybrid model: a new pharmacokinetic model for computer-controlled infusion pumps.* IEEE Trans Biomed Eng, 1994. **41**(2): p. 134-42.

35. Wada, D.R. and D.S. Ward, *Open loop control of multiple drug effects in anesthesia.* IEEE Trans Biomed Eng, 1995. **42**(7): p. 666-77.

36. Fleischmann, D., et al., *Improved uniformity of aortic enhancement with customized contrast medium injection protocols at CT angiography.* Radiology, 2000. **214**(2): p. 363-71.

37. Hittmair, K. and D. Fleischmann, *Accuracy of predicting and controlling time-dependent aortic enhancement from a test bolus injection.* J Comput Assist Tomogr, 2001. **25**(2): p. 287-94.

38. Numburi, U., et al. *Modelling of contrast enhancement for cardiac multi-detector row CT*. in *Imaging Systems and Techniques, 2005. IEEE International Workshop on*. 2005.

39. Numburi, U.D., et al., *Patient-specific contrast injection protocols for cardiovascular multidetector row computed tomography.* J Comput Assist Tomogr, 2007. **31**(2): p. 281-9.

40. Kalafut, J.F. and D. Mishler, *Devices, Systems and Method for Fluid Delivery*. 2005: WPO.

41. Seifarth, H., et al., *Introduction of an individually optimized protocol for the injection of contrast medium for coronary CT angiography.* Eur Radiol, 2009. **19**(10): p. 2373-82.

42. Kalafut, J.F., et al., *A personalized and optimal approach for dosing contrast material at coronary computed tomography angiography.* Conf Proc IEEE Eng Med Biol Soc, 2009. **1**: p. 3521-4.

43. Mahnken, A.H., et al., *Measurement of cardiac output from a test-bolus injection in multislice computed tomography.* Eur Radiol, 2003. **13**(11): p. 2498-504.

44. Mahnken, A.H., et al., *Determination of cardiac output with multislice spiral computed tomography: a validation study.* Invest Radiol, 2004. **39**(8): p. 451-4.

45. Ostergaard, L., et al., *High resolution measurement of cerebral blood flow using intravascular tracer bolus passages. Part I: Mathematical approach and statistical analysis.* Magn Reson Med, 1996. **36**(5): p. 715-25.

46. Ostergaard, L., et al., *High resolution measurement of cerebral blood flow using intravascular tracer bolus passages. Part II: Experimental comparison and preliminary results.* Magn Reson Med, 1996. **36**(5): p. 726-36.

47. Koh TS, W.X., Cheong LH, Lim CCT, *Assesment of Perfusion by Dynamic Contrast-Enhanced Imaging Using a Deconvolution Approach Based on Regression and Singular Value Decomposition.* IEEE Trans Med Imaging, 2004. **23**(12): p. 1532-1542.

48. Hansen, P.C., *The truncated SVD as a method for regularization.* BIT, 1987. **27**: p. 534-55.

49. Guyton, A., *Circulatory physiology:cardiac output and its regulation*. 1963, Philadelpha PA: Saunders.

50. Bae, K.T., J.P. Heiken, and J.A. Brink, *Aortic and hepatic contrast medium enhancement at CT. Part II. Effect of reduced cardiac output in a porcine model.* Radiology, 1998. **207**(3): p. 657-62.

51. Suryani P., et al. *A Computerized Prediction Model for Individualized, Patient-Based Contrast Dosing at Dual-Source Coronary CT Angiography* in *Radiological Society North America*. 2007. Chicago Illinois: RSNA.

52. Flegal, K.M., et al., *Prevalance and trends in obesity among US adults, 1999-2000.* JAMA, 2002. **288**: p. 4.

53. Bae, K.T., *Method of and apparatus for predicting computed tomography contrast enhancement*, in *US5583902*, USPTO, Editor. 1996, MEDRAD Inc: USA.

54. Ljung, L., *System Identificaiton for the User*. 2 ed. 1999, Upper Saddle River, NJ: Prentice-Hall. 603.

55. Kelm M.B, M.B.H., Nix O.,Zechmann C.M.,Hamprecht F.A, *Estimating kinetic parameter maps from dynamic contrast-enhanced MRI using spatial prior knowledge.* IEEE Tran Med Imaging, 2009. **28**(10): p. 13.

56. Lopata, R.G., et al., *On the identifiability of pharmacokinetic parameters in dynamic contrast-enhanced imaging.* Magn Reson Med, 2007. **58**(2): p. 425-9.

57. Lopata, R.G. and N.A. van Riel, *Identifiability analysis of the standard pharmacokinetic models in DCE MR imaging of tumours.* Conf Proc IEEE Eng Med Biol Soc, 2004. **2**: p. 1040-3.

58. Hansen, P.C., T.K. Jensen, and G. Rodriguez, *An adaptive pruning algorithm for the discrete L-curve criterion.* Journal of Comput and Appl Math, 2007. **198**: p. 9.

59. Hansen, P.C., *Regularization tools: a MATLAB package for anaysis and solution of discrete ill-posed problems.* Numer. Algorithms, 1994. **6**: p. 35.

60. Bae, K.T., *Optimization of Contrast Enhancement in Thoracic MDCT*. Radiol Clin N Am, 2010. **48**: p. 20.

61. Cademartiri, F., et al., *Influence of intra-coronary enhancement on diagnostic accuracy with 64-slice CT coronary angiography.* Eur Radiol, 2008. **18**(3): p. 576-83.

62. Coleman and Branch, *Optimization Toolbox for Use with MATLAB, User's Guide*, T. Mathworks, Editor. 2007.

63. Becker, C.R., et al., *Optimal contrast application for cardiac 4-detector-row computed tomography.* Invest Radiol, 2003. **38**(11): p. 690-4.

64. Kalafut, J.F., C.A. Kemper, and S. Sammett. *An anthropomorphic, cardiovascular flow phantom for CT contrast and imaging protocol optimization*. in *European Congress Radiology*. 2008. Vienna Austria: ESR.

65. Behrendt, F.F., et al., *Introduction of a dedicated circulation phantom for comprehensive in vitro analysis of intravascular contrast material application.* Invest Radiol, 2008. **43**(10): p. 729-36.